Modelling, Simulation and Multivariable Control of Plasma Etching of Silicon and Silicon Dioxide

by

Liang TAN, B.Sc(Hons), M.Eng.

School of Electronic Engineering,
Dublin City University,
Dublin 9, Ireland.

A thesis submitted to Dublin City University in Fulfilment
of the Requirements for the degree of

Doctor of Philosophy

Project Supervisors:

Dr David Cameron
Professor Charles McCorkell

1994

ACKNOWLEDGEMENTS

Dr David Cameron, I cannot remember how many times I went to your office and took much time out of your busy schedule to discuss my work. I wish to express my deepest sincere gratitude for your valuable guidance, advice and tuition especially in the course of setting up experimental instrumentation, doing lab work and the preparation of this dissertation. I would not have acquired such an in-depth knowledge without your enthusiasm and continual drive to increase my understanding of plasma techniques. I will forever be impressed by your integrity, ability and hard working style.

Professor Charles McCorkell, it is not to be imagined that I could have completed a PhD degree if you had not introduced me to this active field. I am greatly indebted to you for your invaluable guidance, stimulating advice, the preparation of this thesis and continuous support through all stages of my academic work. I would like to give you a special word of appreciation and gratitude for your time, financial support, encouragement and for affording me the opportunity to pursue this work.

Dr Anthony Holohan, I would like to give you thanks for your enthusiasm, valuable guidance and helpful comments.

Mum and Dad, I owe a lot to you over the past 28 years, but especially over the past five. It was difficult for me to communicate with you so far away by the phone calls in which I so readily unloaded my current burdens. Things are a lot different now than when I left home, but I feel the same love and support I always have. Thank you. Also, I would like to thank my wife, Ching, who has provided understanding throughout my work. She has been patient to let me spend large amounts of time working both at the university and at home.

Mr David Condell, what can I say ? One chapter belongs to you, and it really ties things together. I've never forgot to thank you for your help throughout my five years research work in DCU and friendship during my stay there. As the rest of you, both present and past, you made it fun and interesting.

Special thanks also to Ms Breda McManus, Ms Valerie Hogg, John Whelan, Liam Meany, Conor Maguire, Paul Wogan, Peter McGorman and Stephen Neville for your help, information discussions and a great deal of fun and laughter. Throughout the course of the research, I have benefited from inspirational discussions with Professor John Carroll, Dr Patrick McNally and Dr Hugh McCabe. I am grateful to the workshop staff, Mr Ian Williams, Mr Tommy Walsh and Mr Martin Johnson who helped me to make the experimental devices. I would like to offer my thanks to Cambridge Control Limited in the UK for your informative discussions.

I also want to recognise the help and insight I have received from my friends and fellow postgraduates : Prijaca Naser, Dr Ziaul Karim, Michael Murphy, Stephen Daniels, Martin Hayes, Fiona Murray, Barbara Molloy, Jennifer Bruton, Declan Bates, Adrijan Baric, Tang Wenhui, Pran Kanai Saha, Rowshan Hafiz, Shafiqul Islam and many others who have helped me along my way. I wish you all the best of luck in completing your graduate work and excelling in your professional careers.

It is always difficult to thank all those that have made an experience rewarding. I am sorry if anyone gets left out, but that will be just one more mistake in a long line of them.

MODELLING, SIMULATION AND MULTIVARIABLE CONTROL OF PLASMA ETCHING OF SILICON AND SILICON DIOXIDE

Liang Tan
Dublin City University

Supervising Professors: David Cameron, Charles McCorkell

ABSTRACT

Plasma etching has been used extensively in the microelectronics industry for integrated circuit fabrication. However, the optimisation of this process is quite challenging because the plasma etching process is complex and not fully understood. An experimental and theoretical study of the etching characteristics of silicon (Si) and silicon dioxide (SiO_2) in a sulphur hexafluoride (SF_6) with Argon is reported. The selected manipulated variables or inputs are radio-frequency (RF) discharge power density, chamber pressure and gas component ratios. The semi-outputs or process variables are the relative percent concentration of plasma species: fluorine [F], [SF_x] ($x=3 \rightarrow 6$) and the electric field to pressure ratio E/p. The outputs or performance variables are Si and SiO_2 etch rates and (centre-to-edge) etching uniformity.

The etch rates of silicon and silicon dioxide in SF_6/Ar plasma are statistically investigated based on the effects of different settings of the manipulated variables. Optical emission spectrometry and laser interferometry have been employed to monitor spectral emission and etch rate in real time for plasma diagnostics, endpoint detection, and process control. The results obtained from this study have shown that etching Si and SiO_2 in SF_6/Ar leads to higher etch rates in comparison to other reported systems. Variations in optical parameters associated with manipulated conditions, such as RF power density etc., have been studied over a limited parameter space to obtain their effects on the etch rates of Si and SiO_2.

A dynamic mass balance has been employed to construct a comprehensive reactor model for a basic study of plasma etching of Si and SiO_2 with SF_6/Ar. The model includes diffusion and convection of molecular fragments in a duct geometry,

which is estimated by using an effective diffusion length which takes surface reflection into account. Electron impact dissociation and ionisation reactions which depend on the electric field and gas density are the dominant sources of active species generation. Fluorine atom generation is also described by dissociative chemisorption. Fundamental plasma parameters such as electron density and electric field are estimated from impedance measurements in designed experiments under the various operating conditions. Results presented show relatively good agreement between the model predictions and the experimental data.

Using regression analysis a steady-state model which relates the manipulated conditions to both the process and performance quantities has been developed. Optical emission spectroscopy and laser interferometry (both non-intrusive technologies) are again employed in order to maintain the integrity of the etching environment. This information can be used to find correlations and also feed into the model to track proper operating conditions. It is found that a fast, uniform Si and SiO_2 etch rate could be achieved in the SF_6/Argon process by using high RF power density, low pressure, high SF_6/Ar ratio. Correlations are developed to directly relate inputs, semi-outputs and outputs in the SF_6/Ar system. Response surface methodology (RSM) is used as a basis for further modelling of the non-linear plasma etching process. Results presented in this study compare favourably with the known discharge characteristics, some interpretations of the etching and discharge mechanism and also the comprehensive reactor model.

The singular value decomposition (SVD) technique has been applied to determine the pairings between performance quantities, process and manipulated variables. The non-intrusive techniques are also used for dynamic measures of interaction and are found to very rarely change the variable pairings. Step tests are run to determine process variable time constants for use in dynamic process simulation. The SVD pairings with input and output structural compensators designed by using the SVD technique form a multi input-multi output (MIMO) decoupled control system. The robust multivariable control system analysis based on structured uncertainties of inputs and outputs has been formulated as a "block diagonal bounded perturbation" problem (BDBP). The solution to this problem involves the structured singular value (SSV), a generalisation of the singular value decomposition, which is useful for robust multivariable control analysis since the model uncertainty due to the non-linear behaviour of the plasma etching is highly structured. The robust stability and performance properties of the system subject to disturbances and structured perturbations are developed.

Results presented show that the closed loop transient responses for SVD pairings with the structurally compensated MIMO control strategies are typically much faster than the conventional scheme. Both of the control strategies satisfy the robustness requirements but the robust stability of conventional control is worse for multiplicative input uncertainties and the structurally compensated scheme is less sensitive to input perturbations.

DECLARATION

In accordance with the regulations of the University, I hereby declare that this thesis, which I now submit for the assessment on the programme of work and study leading to the award of PhD, is entirely of my own work under the supervisions of Dr David Cameron and Professor Charles McCorkell and has not been submitted as an excise to any other universities and to the extent that such work has been cited and acknowledged within the text of my work.

____

Liang TAN
1994

DEDICATION

Dedicated to my parents, my wife Ching and my son Jeffrey.

TABLE OF CONTENTS

	PAGE
ACKNOWLEDGEMENTS	i
ABSTRACT	iii
LIST OF TABLES	xii
LIST OF FIGURES	xiii
LIST OF ABBREVIATIONS	xvii
NOMENCLATURE	xviii

CHAPTER 1 INTRODUCTION

1.1	Introduction	1
1.2	Preview of this Dissertation	2
1.3	Properties of Plasma	4
1.4	Review of Plasma Etching Processes	7
1.5	Plasma Etching of Si and SiO_2	9
1.6	Response Surface Methodology	16
1.7	Review of Process Control and Optimisation	18
1.8	Research Objectives and Summary	19

CHAPTER 2 EXPERIMENTAL DESIGN AND PROCEDURES

2.1	Equipment Description	22
	2.1.1 Plasma Etching Reactor	22
	2.1.2 Optical Emission Spectrometer	27
	2.1.3 Laser Interferometry	29
2.2	Experimental Procedures	31
	2.2.1 Reactor Preparation	31

2.2.2 Sample Preparation 32
2.2.3 Data Acquisition 33
2.3 Composite Design of Experiments 33
2.3.1 Variable Screening 33
2.3.2 Etch Rate Tests 34
2.3.3 Steady State Tests 37
2.3.4 Dynamic Tests 42

CHAPTER 3 COMPREHENSIVE REACTOR MODELLING STUDIES

3.1 Introduction 43
3.2 Theories of Impedance and Actinometry 44
3.3 Effects of Discharge Power and Electron Density on Etch Rates of Si and SiO_2 46
3.4 Comprehensive Reactor Modelling 48
3.5 Results and Discussion 51
3.6 Conclusions 55

CHAPTER 4 MULTIVARIABLE REGRESSION ANALYSIS AND MODELLING

4.1 Introduction 81
4.2 Selection of Process Variables 82
4.3 Multivariable Regression Analysis and Modelling 83
4.3.1 Development of Regression Model 84
4.3.2 Analysis of Manipulated/Process Variable Correlations 88
4.3.3 Analysis of Manipulated/Performance Variable Correlations 96
4.3.4 Analysis of Process/Performance Variable Correlations 108
4.4 Comparison with Comprehensive Reactor Model 111
4.5 Discussion and Conclusions 120

CHAPTER 5 DECOUPLING MULTIVARIABLE CONTROL SYSTEM DESIGN

5.1 Introduction 121
5.2 Effects of Process Scaling 122
5.3 Multivariable Dynamic Interaction Analysis 124
5.4 Decoupling Multivariable Control Strategy 129
5.4.1 Design of a Structural Compensator 129
5.4.2 Set-point Compensation and Disturbance Analysis 132
5.4.3 Controller Tuning 133
5.5 Simulation Results and Discussion 135
5.6 Performance Variable Analysis 136
5.7 Conclusions 138

CHAPTER 6 ROBUST MULTIVARIABLE CONTROL SYSTEM DESIGN

6.1 Introduction 146
6.2 Desirable Multivariable Feedback Properties 147
6.2.1 Setpoint Tracking 148
6.2.2 Measurement Noise Rejection 148
6.2.3 Disturbance Rejection 149
6.3 Multivariable Control System Analysis Based on Unstructured Uncertainty 150
6.3.1 Characterisation of Uncertainty 150
6.3.2 Robustness with Respect to Stability 153
6.3.3 Robustness with Respect to Performance 155
6.3.4 Applications of Unstructured Uncertainty 155
6.4 Multivariable Control System Analysis Based on Structured Uncertainty 159
6.4.1 The Block Diagonal Bounded Perturbation Problem 159
6.4.2 General Development of the Structured Singular Value 162
6.4.3 Characterisation and Computation of SSV 163

6.5 A General Framework for Multivariable Control System Design Under Uncertainty 164
6.5.1 Nominal Performance 165
6.5.2 Robust Stability 166
6.5.3 Robust Performance 166
6.6 Robust Multivariable Plasma Etching Control Based on Structured Uncertainty 166
6.7 Simulation Results and Discussion 171
6.8 Conclusions 172

CHAPTER 7 CONCLUSIONS AND RECOMMENDATIONS

7.1 Conclusions 178
7.2 Recommendations for Further Work 180

APPENDIX I.

Review of Published Models 183

APPENDIX II.

Derivation of Finite Element Equations 193

APPENDIX III.

Related Issues of Structured Singular Value Decomposition 199

APPENDIX IV.

Characterization of Stray Impedance 205

REFERENCES 207

LIST OF TABLES

1.1 Gas solid systems for plasma etching used in microelectronics industry 13

2.1 Calibration Lines for Optical Emission Spectrometer 28

2.2 2^3 Design and Variable Levels for Etch Rate Experiments 36

2.3 Composite Design Matrix for Steady State Experiments 40

2.4 Manipulated Variable Levels for Composite Design 41

3.1 Range of Process Manipulated Variables Used in the Comprehensive Reactor Model 56

3.2 Main Gas Phase and Surface Reactions for Plasma Etching of Silicon and SiO_2 in SF_6 57

3.3 Parameters Used in the Comprehensive Reactor Model 58

4.1 Time Constants (minutes) for the SF_6/Ar System 87

4.2 Steady State Gain for the SF_6/Ar System 88

4.3 Coefficients of Response of Process Variables to Manipulated Variables for the SF_6/Ar System 91

4.4 Coefficients of Response of Performance Variables to Manipulated Variables for the SF_6/Ar System 98

4.5 Coefficients of Response of Performance Variables to Process Variables for the SF_6/Ar System 110

5.1 IMC Tuning Constants for the Structurally Compensated MIMO Control of the SF_6/Ar plasma etching process. 135

6.1 Process Uncertainty Relationships 152

6.2 Robust Tuning Parameters for Plasma Etching System 172

I.1 Summary of Models Presented in Literature 184

IV Impedance Measurements of the Chamber without Discharge 206

LIST OF FIGURES

Figure 1.01	Schematic of two parallel electrodes glow discharge process	5
Figure 1.02	Fundamental principle of plasma etching of silicon in CF_4	5
Figure 1.03	Type of plasma reactors :(a) barrel reactor, (b) plasma mode reactor, (c) reactive ion etching reactor, (d) triode mode reactor	10
Figure 1.04	Microwave downstream plasma etching reactor [11]	11
Figure 1.05	The role of ion-enhanced surface reaction in determining the directionality of etching [11]	15
Figure 2.01	Cross section of etch chamber showing the structure of a parallel plate etcher, which is designed for this work	24
Figure 2.02	The data acquisition and control signal design for real-time computer control system for SF_6/Argon plasma etching system	25
Figure 2.03	Schematic of electric circuit model plasma	26
Figure 3.01	The structure of comprehensive model for plasma etching	49
Figure 3.02	Electron density on RF discharge power density on Si wafer	59
Figure 3.03	Electron density on RF discharge power density on SiO_2 wafer	60
Figure 3.04	Dependence of Si etch rate on RF discharge power density	61
Figure 3.05	Dependence of SiO_2 etch rate on RF discharge power density	62
Figure 3.06	Dependence of etch rate on relative fluorine atom emission	63
Figure 3.07	Dependence of half peak to peak voltage on RF discharge power density on Si wafer	64
Figure 3.08	Dependence of half peak to peak voltage on RF discharge power density on SiO_2 wafer	65
Figure 3.09	Dependence of rate constant of dissociation on E/p in SF_6 Plasma [71]	66
Figure 3.10	Electron density vs. electrodes spacing on Si wafer	67
Figure 3.11	Electron density vs. electrodes spacing on SiO_2 wafer	68
Figure 3.12	The electric field to pressure ratio on chamber pressure under various RF discharge power densities on Si wafer	69
Figure 3.13	The electric field to pressure ratio on chamber pressure under various RF discharge power densities on SiO_2 wafer	70
Figure 3.14	Si etch rate distribution under various SF_6 flow rates	71
Figure 3.15	SiO_2 etch rate distribution under various SF_6 flow rates	72
Figure 3.16	Contour plot of etch rate (nm/min) over a Si wafer	73
Figure 3.17	Contour plot of etch rate (nm/min) over a Si wafer	74

Figure 4.16 Plots of E/p as a function of pressure using Si wafer 115
Figure 4.17 Si etch rate (nm/min) on chamber pressure in SF_6/Ar system 116
Figure 4.18 SiO_2 etch rate (nm/min) on chamber pressure in SF_6/Ar system 117
Figure 4.19 Si etch rate (nm/min) on RF power density in SF_6/Ar system 118
Figure 4.20 SiO_2 etch rate (nm/min) on RF power density in SF_6/Ar system 119
Figure 5.01 Dynamic System with Scaling 123
Figure 5.02 Input-Output Block Diagram of a Multivariable Process 125
Figure 5.03 MIMO Control Loops for a 2x2 Process 126
Figure 5.04 Geometrical Interpretation of SVD 128
Figure 5.05 SVD Structural Compensation 130
Figure 5.06 Rearrangement of Block Diagram for System with Input and Output Compensation 131
Figure 5.07 SVD Pairing with Structurally Compensated Decoupling MIMO Controller Structure for the SF_6/Ar Plasma Etching System 134
Figure 5.08 Singular Values for Structurally Compensated Plasma Etching System 140
Figure 5.09 SF_6/Ar Plasma Etching System Closed Loop Response to Step Change in [F]. 1,4=[F]; 2,5=[SF_x]; 3,6=[E/p]. 141
Figure 5.10 SF_6/Ar Plasma Etching System Closed Loop Response to Step Change in [SF_x]. 1,4=[F]; 2,5=[SF_x]; 3,6=[E/p]. 142
Figure 5.11 SF_6/Ar Plasma Etching System Closed Loop Response to Step Change in [E/p]. 1,4=[F]; 2,5=[SF_x]; 3,6=[E/p]. 143
Figure 5.12 SF_6/Ar Plasma Etching System Closed Loop Response for a 15% Increase in RF Power Density. 1,4=[F]; 2,5=[SF_x]; 3,6=[E/p]. 144
Figure 5.13 SF_6/Ar Plasma Etching System Closed Loop Response for a 15% Increase in SF_6 Flow Rate. 1,4=[F]; 2,5=[SF_x]; 3,6=[E/p]. 145
Figure 6.01 General Multivariable Feedback Control System 148
Figure 6.02 Process Uncertainty Relationships 151
Figure 6.03 Equivalent Plots for Robust Stability with Respect to Output Perturbations 154
Figure 6.04 Output Uncertainty Bound (Equation (6.3-2)) for the Plasma Etching System 157
Figure 6.05 Transient Response for the Plasma Etching System 158
Figure 6.06 Feedback Control System with Input and Output Multiplicative Perturbations 160
Figure 6.07 Equivalent Representation of Figure 6.06 160
Figure 6.08 Rearrangement of Figure 6.07 160
Figure 6.09 The Block Diagonal Bounded Perturbation Representation 161

Figure 3.18 Si etch rate on chamber pressure in SF_6/Ar system 75
Figure 3.19 SiO_2 etch rate on chamber pressure in SF_6/Ar system 76
Figure 3.20 Si etch rate distribution on electron density 77
Figure 3.21 SiO_2 etch rate distribution on electron density 78
Figure 3.22 Si etch rate distribution under various electrodes spacing 79
Figure 3.23 SiO_2 etch rate distribution under various electrodes spacing 80
Figure 4.00 The appearance of the highest wave length line of fluorine as a function of time 87
Figure 4.01 Relative fluorine concentration (Arb.Unit) as a function of RF discharge power density and pressure using Si wafer 92
Figure 4.02 Relative SF_x concentration (Arb.Unit) as a function of RF discharge power density and pressure using Si wafer 93
Figure 4.03 Plots of E/p (volt/cm.mtorr) as a function of RF discharge power density and pressure using Si wafer 94
Figure 4.04 Plots of E/p (volt/cm.mtorr) as a function of RF power density and SF_6 flow rate using Si wafer 95
Figure 4.05 Si etch rate (nm/min) as a function of RF power density and pressure 99
Figure 4.06 SiO_2 etch rate (nm/min) as a function of RF power density and pressure 100
Figure 4.07 Si etch rate (nm/min) as a function of RF power density and SF_6 flow rate 101
Figure 4.08 SiO_2 etch rate (nm/min) as a function of RF power density and SF_6 flow rate 102
Figure 4.09 Si etch rate (nm/min) as a function of pressure and SF_6 flow rate 103
Figure 4.10 SiO_2 etch rate (nm/min) as a function of pressure and SF_6 flow rate 104
Figure 4.11 Si Anisotropy as a function of RF power density and pressure 105
Figure 4.12 Si uniformity as a function of RF power density and pressure 106
Figure 4.13 SiO_2 uniformity as a function of RF power density and pressure 107
Figure 4.14 Relative fluorine concentration as a function of pressure using Si wafer 113
Figure 4.15 Relative $[SF_x]$ concentration as a function of pressure using Si wafer 114

Figure 6.10 General BDBP Diagram 164
Figure 6.11 General BDBP Diagram with Control Absorbed into the Structure 165
Figure 6.12 Input and Output Multiplicative Uncertainties for Structurally Compensated MIMO and Conventional Control 168
Figure 6.13 Additive Process Uncertainty Characterisation for Plasma Etching Process Control 170
Figure 6.14 Maximum Singular Value and μ with Structurally Compensated MIMO and Conventional Controllers 174
Figure 6.15 Input Uncertainty Bound for the Plasma Etching System 175
Figure 6.16 Output Uncertainty Bound for the Plasma Etching System 176
Figure 6.17 Perturbation Responses of μ-synthesis Controllers for the Plasma Etching Plant with Uncertainties 177
Figure I.1 Dimension Representation 183

LIST OF ABBREVIATIONS

Ar	Argon
BDBP	Block diagonal bounded perturbation
CCD	Camera formation
CF_4	Carbon tetra fluoride
F	Fluorine molecule
IMC	Internal model control
MIMO	Multivariable input-multivariable output
MVSISO	Multivariable variable single input-single output
RF	Radio-frequency
RSM	Response surface methodology
Si	Silicon
SiO_2	Silicon Dioxide
SF_6	Sulphur hexafluoride
SF_x	Radicals of SF_6 ($x = 3 \rightarrow 6$)
SVD	Singular value decomposition
SSV	Structured singular value
UV	Ultraviolet

NOMENCLATURE

A, A_{eff}	the electrode area, cm^2
C_s	the sheath capacitance, F
d	the electrode spacing, cm
d'	input disturbance
D_i	the diffusivity, cm^2/sec
D_j	the diffusivity, cm^2/sec
e	the charge of an electron, 1.602×10^{-19} columb
e'	output disturbance
E/p	the electric field to the pressure ratio in the bulk plasma, volt/cm·mtorr
f	the electron energy distribution function
F	the external force per unit mass on an electron, cm/sec^{-2}
F	the process model absorbed controller G_c (in Chapter 6)
G	a general m x n complex matrix
G_c	the controller function
G_m	the nominal plant
G_p	the real plant
i	the measured peak current, columb/sec
k	the rate constant
K	the steady state gain the first-order plant transfer function.
K_i	rate constant of ion-assisted etching, cm^3/sec
K_{ij}	process steady state gains
K_{1-7}	the rate constants, cm^3/sec
k_B	the Boltsman constant
K_c,	the PI tuning constant gain
l_{aij}	the uncertainty in the i, j element of the process gain matrix
l_i	the input uncertainty
l_o	the output uncertainty
L	the reactor dimension, cm
m	the mass of electron, g
M	the SF_6 molecule, g/mole
M	the process structure model (in Chapter 6)
M^*	the excited state of M, cm^{-3}
N	a non reactive radical or molecule, cm^{-3}

n	the refractive index of the top layer
n	the measured fluorine atom concentration, cm^{-3}
n_e	the electron density, cm^{-3}
N_i	the mole concentration of species i, cm^{-3}
p	the gas pressure, mtorr
P	the etching product of SiF_4
q	the rank of the steady-state gain matrix
r	the reactor dimensions, cm
R	the plasma resistance, Ω
R_i, R_j	the SF_x and F radicals, cm^{-3}
$R_{i\rho}$	the electron impact dissociation reaction, cm^{-3}
R^2	coefficient of fit of regression equation
S	a surface molecule of Si and SiO_2
T_e	the electron temperature, °K
T_{ij}	process time constants
U	the left singular matrix (m x m)
U_k	the kth column of the left singular matrices
V_r	the gas velocity, cm/sec
V	the right singular matrix (n x n). (in Chapter 5)
V	the measured peak voltage, volt (in Chapter 3)
V_j	the reaction rates. ($cm^{-3}sec^{-1}$) (in p.p.47)
V_k	the kth column of the right singular matrices
w	the width of the reactor, cm
W	a third body for radicals recombinations
W	weighting matrix (in Chapter 6)
x_i	regression equation independent variable
Y	regression equation dependent variable
Z	impedance, ohm
∇_r	gradient operations in configuration
∇_v	gradient operations in velocity space

GREEK

α	star point level in composite experimental design
α_1	the dimensionless constant coefficient
β_1	the dimensionless constant coefficient
β_i	coefficient on independent variable x_i in regression equation
Δ	the block diagonal perturbation matrix
λ	characteristic diffusion length, cm. (in Chapter 2)
λ	the IMC filter constant = the closed-loop time constant. (in Chapter 5)
θ	the measured phase angle between the voltage and the current wave forms, degree
ε_e	the electron energy
σ_i	the singular values
$\sigma(\varepsilon_e)$	a collision cross section for a particular electron energy
σ_k	the kth singular value
σ^*	the maximum singular value
Σ	the singular value matrix (n x n)
ρ	the density
τ	the steady state time constant of the first-order plant transfer function.
τ_I	the PI tuning time constant
τ_{ij},	process time delay constants
μ	the structured singular value
μ_e	the electron mobility which is inversely proportional to the gas pressure, $cm^2 \cdot torr/V \cdot sec$
ω	the angular frequency, (rad)/sec
υ	the thermal velocity of fluorine, cm/sec
γ	the recombination probability
$\beta_{i\rho}$	the stoichiometric coefficient of the species
Φ	the dimensionless Thiele modulus

CHAPTER 1 INTRODUCTION

1.1 Introduction

Recent advances in silicon integrated circuit technology and pattern delineation processes in particular, have placed an increasing emphasis on thin film etching techniques. Chemical etching in thin-film technology plays a prominent role in both the preparation and the utilisation of thin films. Regardless of the method of film deposition or formation, the substrate must first be suitably prepared, either by removal of work damaged surface layers or by creating a relief structure of specific geometry. In the first case, chemical polish etching is usually the method of choice; in the second case, structural etching is required. Once a thin film has been deposited, chemical etching is often used for films [1].

As circuit dimension decreases further, conventional liquid phase chemical etching is no longer a feasible means for pattern transfer. Several limitations of wet etching, such as isotropic etching, loss of resist adhesion and prevention of liquid penetrating into submicron features by surface tension, prohibit its use for submicron integrated circuit fabrication. Accordingly, there has been a growing trend toward the use of gas phase plasma etching methods, which inherently have better resolution and cleanness.

Integrated circuit fabrication usually involves many repetitive steps, such as deposition, photolithography, and etching of thin films. Very large Scale Integration (VLSI) and Ultra Large Scale Integration (ULSI) systems need submicron features, strict shape and dimension control. Etching is one of the most important step in the fabrication process. Plasma etching is advantageous over wet etching because of its anisotropical etching capability, cleanness, reduced consumption of chemicals, compatibility with process automation and precise pattern transfer capability. The directionality of etching profiles becomes more important as the circuits dimension shrinks further to the submicron level.

Plasma etching employs a glow discharge to generate active species such as atoms or free radicals from a relatively inert molecular gas. The discharge is usually excited by a radio frequency or microwave discharge which supplies

energy which ionises and dissociates the gas. A schematic of such a discharge is shown in Figure 1.01. The central portion of the discharge is a plasma, while the regions between the plasma and the electrodes are known as sheaths. The sheaths result from the different velocities of the ions and the electrons. The plasma region is a weakly ionised gas of approximately equal numbers of positively and negatively charged particles [1 - 8].

Although etching processes are widely used in industry, the general understanding of these processes is poor, and process optimisation is difficult. The ability to etch fine lines, and the control of anisotropy, etching rate, uniformity and selectivity are obtained by experimental trial and error. Plasma chemistry is very complicated and many of the surface processes are not clearly understood. Moreover, investigations often are unable to define the basic parameters which are important in a given plasma process. For example, the flux and energy of ions and electrons impinging upon a given surface are uncertain. Furthermore, the types of neutral species and their concentrations in the gas phase are usually unknown. Additional problems for plasma etching processes include their inability to etch some materials, such as Cu and Pt, radiation damage to sensitive devices and corrosion by residual gases after etching [2][4][5].

1.2 Preview of this Dissertation

Since the plasma etching process is a complicated system, it is considered appropriate to provide the fundamental concepts of plasma chemistry and physics at the beginning of this thesis. Accordingly, a summary of those aspects of plasma chemistry and physics, plasma etching processes, response surface methodologies and process control and optimisation, are presented in Chapter 1.

The next chapter, provides background on the experimental equipment, procedures and the composite design of experiments followed in this study. A detailed description of the experimental techniques is also presented. Some theoretical background for the techniques is given for completeness. This is followed by a discussion of the experiments performed during each phase of the project and the basis for their design.

Chapter 3 deals with the chemical mechanisms of Si and SiO_2 etching in SF_6/Ar plasma. The comprehensive theoretical reactor modelling study and simulation of this process are presented in this Chapter, where an approximate approach for the analysis of reactor behaviour is preferred. Instead of concentrating on the microscopic information necessary for a complete theoretical understanding of the discharge, the electrical properties of the plasma including electron density, kinetic rate constants and effective electric field are characterized by impedance measurements. Specifically, experiments are conducted to determine the effects of RF power density on the relative concentration of fluorine atoms and etch rates of Si and SiO_2 by using optical emission spectroscopy and laser interferometry respectively. The theoretical predictions are compared with the experimental data and are discussed with particular emphasis on the influence of the various manipulated variables on the Si and SiO_2 etch rate distributions. Results are also compared with the regression modelling study, which are presented in Chapter 4.

Chapter 4 discusses the selection of process variables used to characterise the system. The non-intrusive measurement techniques are employed to estimate the relative plasma species concentrations, infer electron energy of the process, measure real-time etch rate, and maintain the integrity of the etching environment. Correlations with manipulated variables relating both process and performance variables based on the regression analysis are discussed in this chapter. Direct relationships between process and performance variables are developed and a steady-state regression model is given. Results are compared with a comprehensive theoretical reactor modelling study. A discussion of experiments to explore process dynamics and their importance in the control of the etching process conclude this chapter.

A decoupling multivariable control system is presented in Chapter 5. In this chapter, the SVD pairings with the input and output structurally compensated MIMO control scheme has been developed and compared with conventional control. The non-intrusive measurement and SVD techniques have been found to rarely change the variable pairings. Results presented in this chapter illustrate that the conventionally controlled system is very sensitive to disturbance direction, while the structurally compensated MIMO control strategy is directionally insensitive.

Chapter 6 presents a robust multivariable control scheme addressing control system design in the presence of uncertainty. Initial work involves robust stability with respect to unstructured uncertainty. A problem with this technique is that the

worst case may not occur for a particular process. This can result in a conservative control system design. Also, the case of multiple perturbations is not addressed with unstructured uncertainty procedures. This leads to the development of structured uncertainty techniques, which give the designer the ability to provide designs with better performance, for a given uncertainty norm. Results presented in this chapter illustrate that both of the SVD pairings with structurally compensated MIMO and conventional control strategies satisfies the robustness requirements but the robust stability of conventional control is worse for multiplicative input uncertainties and the structurally compensated scheme is less sensitive to input perturbations. The model uncertainty due to process non linearity is highly structured in the plasma etching process. The structured singular value is found very useful for robust multivariable control of plasma etching.

Conclusions from the research and recommendations for further study are presented in Chapter 7.

1.3 Properties of Plasma

A plasma is a partially ionised gas composed of equal numbers of positively and negatively charged species. The type of plasma of concern in this research is the abnormal negative glow discharge. It is characterised by weakly ionised gases, in which the fractional ionisation is on the order of 10^{-4} to 10^{-6}. The plasma is composed of species such as radicals, atoms, molecules, electrons and ions. The pressures at which the plasmas are sustained are typically between 10^{-3} torr to several torr and the gas temperature is usually near room temperature. A plasma can be sustained only if some external sources of energy is applied. Typically, either direct current or radio frequency sources of energy is applied. A plasma is said to be self-sustained if the applied field generates electrons and ions through ionisation processes at the same rate that electrons and ions are lost.

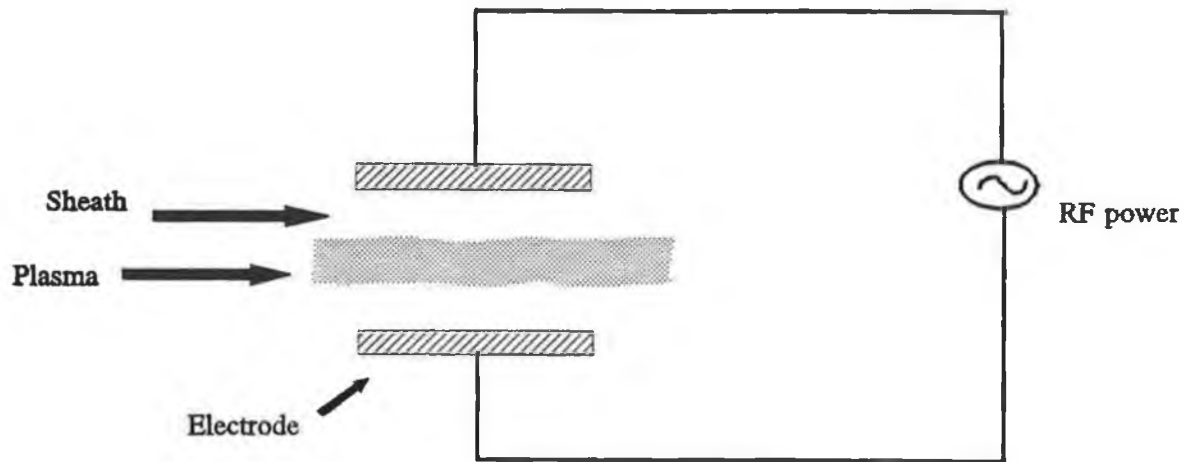

Fig 1.01 Schematic of two-parallel electrodes glow discharge process

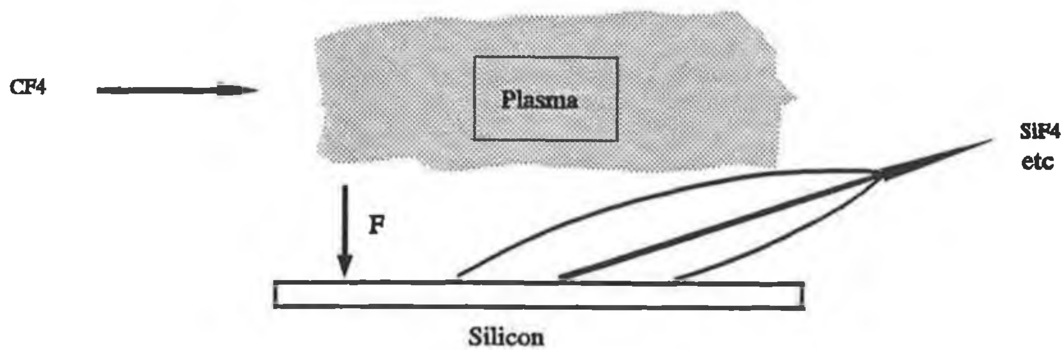

Fig 1.02 Fundamental principle of plasma etching of silicon in CF_4.

Collisions between electrons and heavy particles in a plasma are broadly classified as being elastic or inelastic. Elastic collisions involve the exchange of only kinetic energy between the participants. One of the important characteristics of glow discharges is the much higher average electron temperature compared to the neutral environmental temperature of the bulk. Electrons gain energy from the applied electric field and lose energy due to collisions with gas molecules. Electrons lose only a small fraction of their kinetic energy in the elastic collisions with heavy neutral species. Even after repeated elastic collisions, an electron may possess sufficient energy to ionise a molecule and produce an extra electron. The principal electron loss mechanism is diffusion to the walls of the reactor. When the rate of production of electrons equals their loss due to diffusion to the walls and other mechanisms, the gas is said to have broken down.

Another important physical-chemical mechanism is the action of the positive ion bombardment of the surface. The velocity of the electrons is higher than the velocities of ions near the surface and so the assumed plasma potential is usually positive with respect to the surface. Relatively small charge imbalance in the plasma causes substantial electric field to be formed in the sheath region near the surface.

The collisions of electrons and molecules may produce ionisation, dissociation, and excitation of the molecules. The collision rate of an electron striking a molecule is

$$r = k n_e n \quad ; \qquad \textbf{(1.2-1)}$$

where n_e and n are the concentrations of the electron and the molecules, respectively. The rate constant depends on the electron energy distribution $f(\varepsilon_e)$ according to [2]

$$k = \left(\frac{8}{\pi m}\right)^{1/2} (k_B T_e)^{-3/2} \int_0^{\infty} \varepsilon_e \sigma(\varepsilon_e) f(\varepsilon_e) d\varepsilon_e \quad ; \qquad \textbf{(1.2-2)}$$

where m is the mass of electron, k_B is the Boltzmann constant, T_e is the electron temperature, ε_e is the electron energy, and $\sigma(\varepsilon_e)$ is a collision cross section for a particular electron energy. The cross section represents the probability that the electron will collide with the species to form a product and it varies with the type of collision process. To calculate the rate constant for electron bombardment reactions the collision cross section must be known, however limited data are available, thus a quantitative modelling of plasma etching processes is difficult. The electron energy distribution function satisfies the Boltzmann equation which is the continuity equation in the glow discharge space [2].

$$\frac{\partial f}{\partial t} + v\nabla_r f + F\nabla_v f = \left(\frac{\partial f}{\partial t}\right)_{collisions} \quad ; \qquad (1.2\text{-}3)$$

The following descriptions are quoted from reference [2]. where f is the electron energy distribution function, F is the external force per unit mass on an electron, ∇_r and ∇_v are gradient operations in configuration and velocity space respectively. The first term on the left hand side of the Boltzmann equation gives the local variation of the distribution function with time. The second and the third terms on the left hand side of the continuity equation describe the local variation in f due to electrons diffusing in and out of the volume element under the applied fields. The term on the the right side of the continuity equation describes the mechanisms of binary collisions between electrons and molecules, ions and other electrons. At present, a general solution of the Boltzmann equation is impossible due to the complexity of the right hand side of equation, so it is customary to seek approximate solutions [2].

1.4 Review of Plasma Etching Processes

Plasma etching techniques have been considerably developed in the past few years in the microelectronics industry. The term plasma etching refers to plasma-assisted etching processes, in which the surface to be etched is placed on the ground electrode. The term reactive ion etching refers to a plasma-assisted etching processes, in which the surface to be etched is placed on the RF-powered electrode. It has long been observed that a molecular gas glow discharge can generate chemically active radicals. However, it was not until the last twenty years or so that glow discharges were used to provide active radicals for the etching of solid materials. The name plasma was first used by Langmuir [9] in his studies of glow discharges. RF discharge seems to have first been applied to semiconductor processing during the 1960s for the plasma stripping of thin films of photoresist polymer. This is a technique for the removal of photoresist materials which, being organic, consist primarily of carbon and hydrogen. Irving et al [10] invented the process of plasma etching for stripping polymer film, which exits today in a variety of forms. In the mid-1960s, this approach was extended to the etching of silicon and silicon dioxide using glow discharge of fluorine or chlorine-containing gases. Beginning in the 1970s, there has been a rapid growth in the use of reactive gas glow discharge for etching of solids. The motivation behind this growth is the need for directional etching processes in the microelectronics industry.

The most frequent applications are the etching of silicon and silicon dioxide in a discharge of CF_4 or SF_6 to form volatile SiF_4. The fundamental principle of plasma etching of Si is shown on Figure 1.02 (pp.3). The active species diffuse to the substrate where they react with the surface to produce volatile products. In most cases, plasma etching is carried out using a pressure higher than normally used for etching by ion sputtering, and etching occurs primarily by direct chemical reaction. In contrast to physical sputtering, plasma etching relies on the chemical reaction between the solid surface and the active species produced in the discharge. A good introduction to the topic of gas discharges used in the electronic materials processing is the book by Chapman [11], in which an extensive discussion of sputtering and etching discharges are included. Early work was performed with plasma etching equipment originally intended for stripping of polymer films. The so-called barrel systems are usually employed for this purpose and the surface to be etched is immersed in the glow discharge without applying an electrical bias. Consequently, isotropic etching profiles are usually obtained from barrel type etchers. Recognition of the importance of energetic ion bombardment in obtaining etching directionality led to the use of planar systems [12].

The ability to etch fine lines and anisotropic profiles, fast etching rates and high etching selectivity over the bottom layer are important properties which depend on the choice of process conditions. SF_6 has been frequently used for etching of silicon and silicon nitride in integrated circuits fabrication, as it offers fast silicon etching rates, high selectivity of Si over SiO_2, and carbon-free deposition.[13-22].

Pure SF_6 used for silicon etching gives fast isotropic etching which is mainly a result of the rapid spontaneous etching reaction of fluorine with silicon. SF_6 discharge has been studied in a wide variety of reactors. D'Agostino et al [23] found that using Ar Actinometry to relate the fluorine emission to fluorine concentration gave good agreement with fluorine concentration measured by titration. Thompson and Sawin [21] reported the response of polysilicon etching characteristics under various ranges of pressure, power, and gas flow rate in 13.56 MHz SF_6 discharges. Effects of Ar, N_2, H_2 and O_2 dilution in SF_6 gas and electrode materials contamination, loading effect, and magnetic confinement have been studied by Pinto et al [22]. The highest Si : SiO_2 selectivity obtained with quartz cathode is 18 : 1 for 100% SF_6 at 0.1 W/cm^2 power density level with magnetic confinement [22].

Several types of reactors, as shown on Figure 1.03, have been employed for dry etching in the microelectronics industry and they differ according to the relative role played by ion bombardment. In the barrel reactors, the wafers are immersed in the glow, virtually decoupled from the electrodes. The surface potential of these wafers is thus not very different from that of the surrounding plasma and so they are subjected only to weak ion bombardment. Often the barrel reactors are employed for photoresist stripping following pattern delineation. Planar diodes plasma-mode reactors have the wafers placed on the ground electrode and are subjected to low energy ion bombardment there. The plasma-mode reactors have electrodes of equal areas and consequently the sheath voltages at each electrodes are equal. This was confirmed by electrical measurements and by visual observation of the thickness of dark spaces formed at the sheaths [9]. The reactive ion etching reactors are essentially translated from sputtering systems. Wafers are placed on the powered electrode and the large area ratio of ground electrode to powered electrode results in an intense ion bombardment and anisotropic etching profiles. Triode plasma etching reactors are rather different from diode etchers. Since ion bombardment seems to be necessary for directional etching, the independent control of ion bombardment is fundamental in this design. Wafers are placed on a third electrode which is biased by a second electrical source and the ion bombardment energy is independently controlled by the bias of the third electrode. In order to avoid a direct ion damage, a downstream dry etcher, as shown in Figure 1.04, is an ideal design if microwave source is employed for the generation of high density reactive radicals which usually results in isotropic etching profiles [11][24].

After more than ten years of extensive studies, the major problem in the implementation of plasma etching is the complexity of process development and reactor scale up. Consequently, process development and scale-up can be a rather tedious, and time-consuming procedure.

1.5 Plasma Etching of Si and SiO_2

Plasma etching techniques are still quite new and not well understood, but this has not impeded their implementation. Only the etching of silicon materials in fluorine-based gases has been reasonably studied, and even in that system there are many unresolved questions, apparent aberrations, and disagreements on interpretation. Of the various reactor systems, the low pressure diode system is

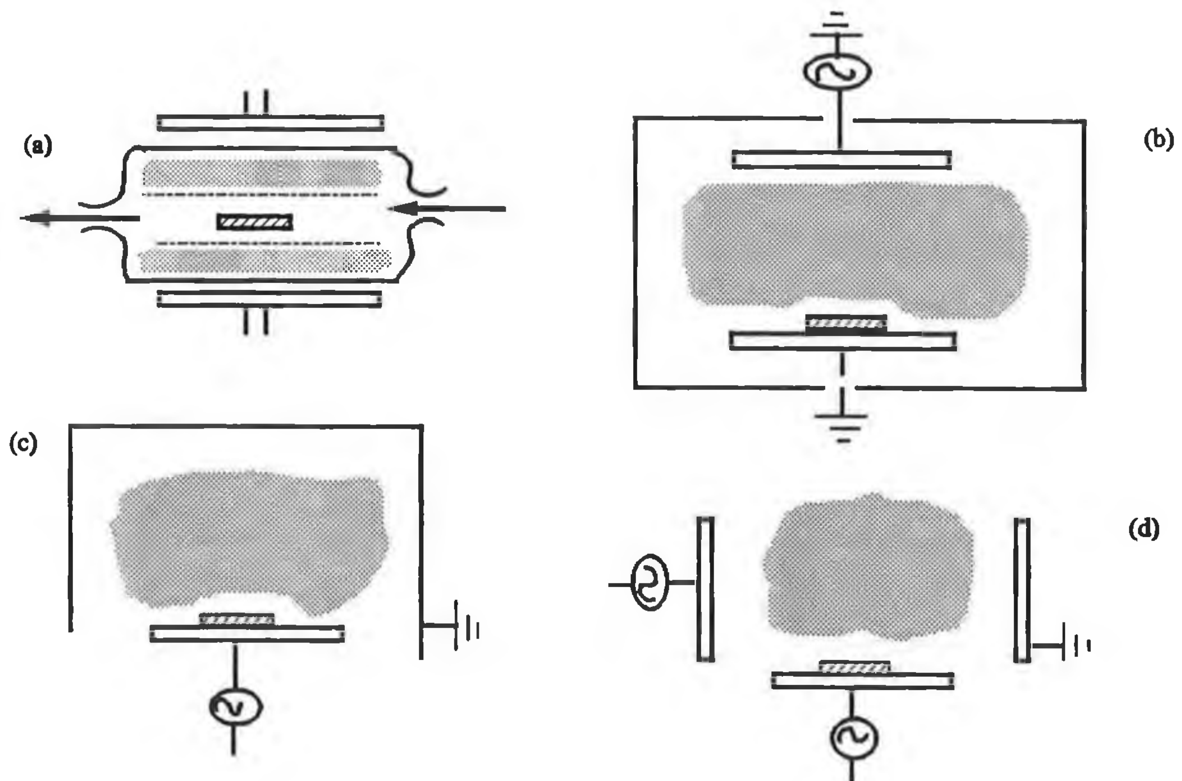

Fig 1.03 Type of plasma reactors: (a) barrel reactor, (b) plasma mode reactor, (c) reactive ion etching reactor, (d) triode mode reactor.

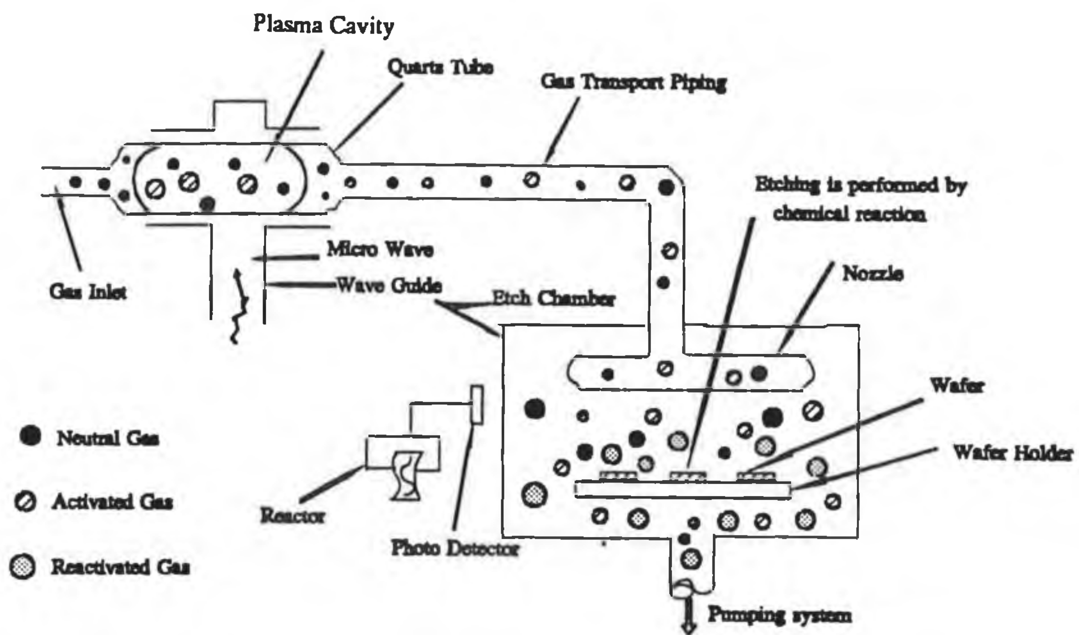

Fig 1.04 Microwave downstream plasma etching reactor [11]

probably the best understood, but that experience can always be extended to applications with more complex gases, and to reactor scale up.

It has long been recognised that atoms and radicals are far more chemically reactive than most molecules, however this principle was not extensively utilised in the etching of solids until the early 1960 when oxygen plasma became available for the etching of polymer films [10]. The chemistry produced in low pressure plasma by electrical discharge has been generally discussed by McTaggart [25]. For the past few years, the most popular fluorine-based gases used for plasma etching of Si are CF_4, SF_6, and NF_3. In 1975, Heinecke [26] found that silicon etching was favoured by a high fluorine density whereas SiO_2 etching required a fluorine-deficient plasma. His initial experiments showed that silicon etching was primarily a chemical process requiring reactive radicals while SiO_2 etching was more physical requiring ion bombardment to maintain the etching. He also concluded that fluorine was the main silicon etching in a CF_4 plasma.

Despite a decade of studies of plasma etching mechanisms, the difficulty in evaluating the various models for plasma etching lies in the fact that each model usually deals with only one specific etching aspect. In fact, plasma etching may have many aspects according to experimental conditions. The role of ion bombardment during etching and its interaction with adsorption, reaction and desorption were analysed in light of the various experimental results. Spontaneous etching of lateral walls, free of ion bombardment, resulted from the interaction of the solid surface with the thermally reactive neutral species to form volatile products [27]. The addition of O_2 to CF_4 plasma resulted in an increase of the silicon etching rate [28]. Mass spectrometry studies have identified the overall reaction products of silicon etching in a CF_4 / O_2 mixture. The dominant silicon product was silicon tetra fluoride, accompanied by carbon monoxide and dioxide, COF and COF_2 [27]. Substantial studies of optical emission spectroscopy of CF_4 + O_2 plasma have been performed by Kawata et. al [29][30]. The roles of oxygen during silicon etching by CF_4 plasma were identified as (i) the reaction of oxygen with carbon fluoride radicals to release extra fluorine atoms which increase the silicon etching rate and (ii) the competitive mechanisms between F atoms and O atoms on the silicon surface.

Table 1.1 Gas Solid Systems for Plasma Etching Used in Microelectronics Industry

Solid	Etch Gas	Product
Si, SiO_2	CF_4,SF_6, NF_3,CHF_3	SiF_4
Si	Cl_2, CCl_2F_2	$SiCl_4$
Al	BCl_3, CCl_4, Cl_2	Al_2Cl_6, $AlCl_3$
Organic Material, Polymer Film	O_2 $O_2 + CF_4$	CO, CO_2, H_2O CO, CO_2, HF
Refractory Metal (W,Mo,Ta...)	CF_4 , SF_6	WF_6, ...
GaAs, InP	Cl_2, BCl_3, CCl_2F_2	$GaCl_3$, $AsCl_5$

In many plasma etching systems, the etch rate decreases sharply as more surface area of the material to be etched is exposed to the plasma [31]. This phenomenon, called the loading effect, can be a serious problem in silicon etching as the etching rate increases dramatically towards the end of the etching. The loading effect in silicon etching results from having a limited supply of etching species to silicon to be etched. Mogab [31] has pointed out that the method to overcome the loading effect is to decrease the lifetime of the etching species. Alternatively, the loading effect can also be reduced by having an electrode constructed of the same material being etched so that the area of etched material remains roughly constant during the etching.

The impurities of the substrate to be etched also affect the etching rate [32]. The influence of the impurities on spontaneous etching appears to be determined by the structure of the SiF_X surface layer. Winters and Haarer [33] have shown that the influence of impurities on the spontaneous etching rate was small when the surface SiF_X layer was thin and much larger when the layer was thick, because the reaction probability of reactive species with surface silicon depends on the thickness of the SiF_X layer.

Finally, the effects of ion bombardment on the etching rate and profiles are briefly discussed. Winters and Coburn [34] found that XeF_2 gas could be used as a source of atomic fluorine. Figure 1.05 shows the role of ion bombardment in etching directionality and etching rate enhancement. Winters and Coburn [35][36] also observed that silicon could be spontaneously etched by fluorine atom without ion bombardment, with a reaction probability of 10^{-2}, which could be enhanced by simultaneous electron and ion bombardment. The rate of ion enhanced etching is greater than the sum of spontaneous etching and ion sputtering. The fact that ion bombardment is responsible for directional etching is reasonably accepted, however the way in which ion bombardment accelerates the etching rate is still under debate. All etching processes consist of three sequential steps: (i) adsorption of active species (ii) surface reaction (iii) products desorption [37]. The mechanism of acceleration depends on which of the steps is the rate determining step, which may vary from one system to another. The current disagreement results from insufficient studies of different systems.

Two different mechanisms have been proposed to explain the etching rate enhancement by ion bombardment. Winters and Coburns [34] believe that the primary mechanism responsible for ion enhanced etching is the ion bombardment

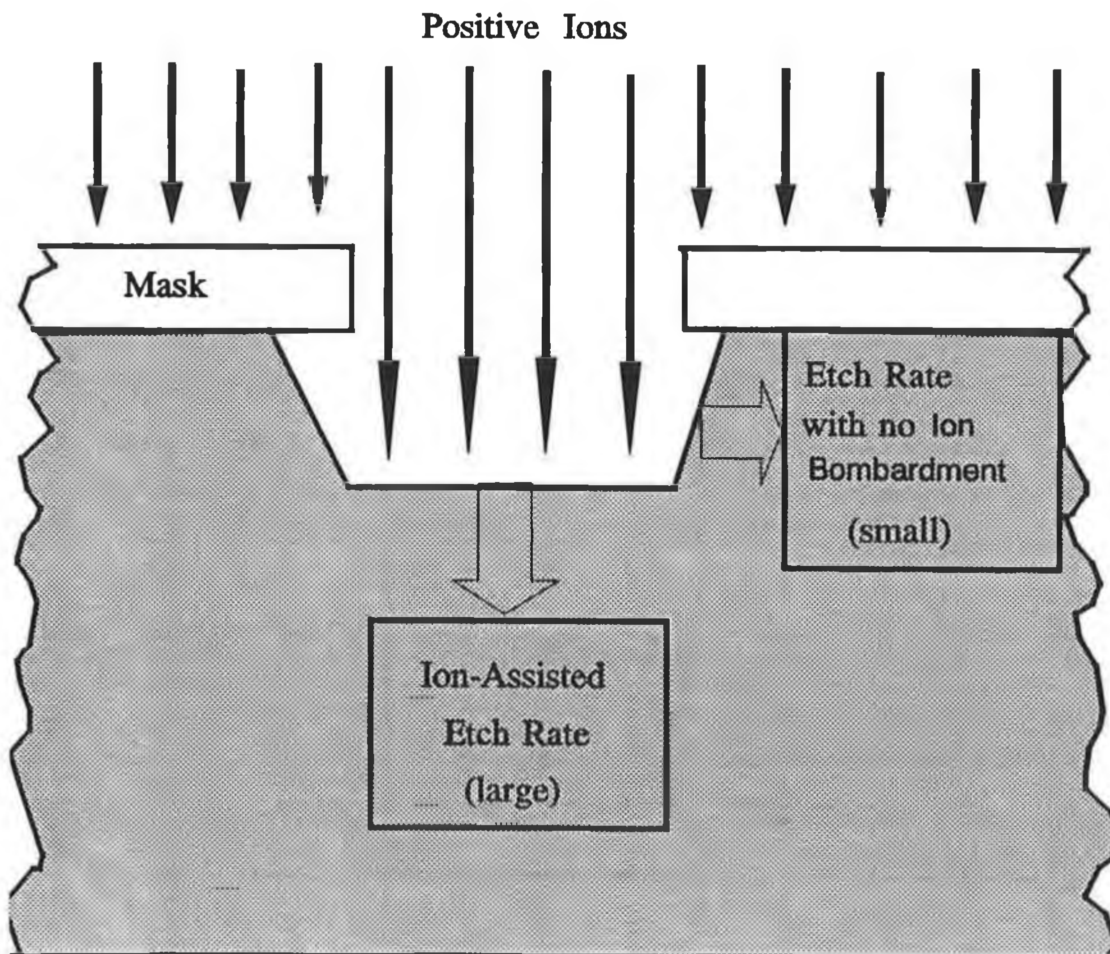

Fig 1.05 The role of ion-enhanced surface reaction in determining the directionality of etching [11]

induced gasification of the relatively stable layer of fluorinated silicon formed on the silicon surface. Two mechanisms have been proposed to explain the ion-enhanced desorption of silicon compounds: (i) chemical sputtering (ii) enhanced physical sputtering. Chemical sputtering implies that ion bombardment is supposed to induce a chemical reaction which produces weakly bound species that desorb from the surface [38]. Enhanced physical sputtering implies that the SiF_x species present on the silicon surface are not strongly bound to the silicon surface, so the enhanced desorption rate directly results from enhanced physical sputtering [34]. Pelletier [35] compared the different models of ion-enhanced desorption for the halogen based plasma etching of silicon. Donnelly and Flamm [36], however, suggested that enhanced etching is caused by energetic ion bombardment to produce lattice damage near the surface where impinging species react more rapidly. More experiments are needed to identify the right model and find out the limiting step during surface etching.

1.6 Response Surface Methodology

Response surface methodology (RSM), which represents an experimentally economic means of measuring the response to an empirical model of the system, is a classical statistical experimental design technique useful for characterizing complex processes. Using this technique defines a space within which the process might operate. The axes of the space are the factors (process variables) controlling, or likely to control, the process arranged perpendicularly (orthogonal) to each other. The limits of the axes are the physical limits allowed for the factor settings. The technique probes the surface and interior of this space systematically using an orthogonal array of factor settings (levels) in a design matrix. From the results of the experiments one builds regression models to predicts process results within that space. Box, Hunter, and Hunter [39] presented a good overview of RSM and its application to statistical analysis of experiments. The basis of RSM is the experimental design. The design must cover adequately the parameter space and allow construction of a model which adequately describes the process. Box and Draper [40] discussed the use of composite design as a means of handling second and higher-order designs with a reasonable number of experiments. A standard second-order factorial design for n variables required 3^n experiments. Box and Draper listed several designs which required significantly fewer experiments than

this. Hartley [41] claimed that his designs were the most compact and allow two-factor interactions to be modelled in addition to the second-order response.

The technique of response surface methodology has gained wider acceptance in the microelectronics industry recently. But only a few articles had appeared in the literature concerning microelectronics process development using RSM. Hamel [42] first used RSM to optimise a lift-off process, examining the effects of various process times and temperatures on a photoresist structure used in the lift-off process. Bergeron and Duncan [43] applied RSM to the plasma etching of polysilicon, by C_2F_5Cl/O_2 exploring the effects of the process parameters on anisotropy and selectivity of the etch to silicon dioxide and to photoresist. Both of these studies sought to develop an optimal set of process conditions through RSM. This application has become more popular since that time, particularly in the area of plasma etching. Riley [44] used RSM to develop a process for the etching of SiO_2 in a $CHF_3/C_2F_6/He$ mixture. Etch rate of silicon dioxide, polysilicon, and the oxide etch uniformity were measured as a function of input gas flow rate and chamber pressure. The resulting data were fit to a standard quadratic model and the process was optimised using a non-linear constrained optimisation algorithm. Fior et al [45] also studied etching of SiO_2, this time in CHF_3/SF_6, and optimised etch rate and selectivity as a function of power and inlet gas flow rates. A more general approach was taken by Daniel, et al. [46], who identified a process window for a single-wafer etcher. The etcher under study had run four processes for a year without problems, but began to experience difficulties in maintaining product specifications. A model of the parameter space was created using RSM and acceptable limits on product quality identified within this space. The added understanding of the process afforded through this study allowed them to combine the four original processes into one optimised process.

RSM is now coming to be used as a basis for further modelling of plasma etching processes. The empirical model developed through RSM is interpreted based on a theoretical model of the system. This was first used by Mocella, et al. [47] who used RSM to model the etching of polysilicon in CF_3Cl/Ar. A third-order model was fit using a seven-level, three-variable composite design requiring 37 runs. Etch rate of polysilicon was modelled as a function of power, pressure, and %Ar added. This was then compared to a plasma impedance model of the system (Sawin,et al., [48]). This work was extended to further measurements of the system as theoretical modelling continued (Allen, et al [49]). Response surface modelling included measurement of plasma bulk resistance, sheath capacitance, sheath voltage,

positive ion flux, and electron density as functions of the variables mentioned earlier. The correlated results were compared to the theoretical models developed (Allen and Sawin [50][51]). Thompson and Sawin also used RSM to study the etching of polysilicon in SF_6 discharges. Etch rate, E/p, electron density, fluorine atom concentration (determined by Actinometry), and ion flux were measured; power, pressure, and flow rate were the independent variables. Their results were compared to known discharge characteristics and some interpretations of etching and discharge mechanisms made based on these results. Response surface methodology provides a convenient, meaningful way to examine process data and draw conclusions concerning etch mechanisms. An extremely convenient method for interpreting the Taylor series regression models is contour plotting. Unlike a conventional graph which plots a response against a factor, this technique assigns a factor to each axis of the graph while holding any others at fixed values. The curves appearing on the graphs are lines of equal response, quite analogous to the contour intervals on a map.

1.7 Review of the Process Control and Optimisation

Process control has been widely discussed but not widely implemented in the microelectronics industry. Control structures and design for material production have been studied, see [52], but device production has remained outside the scope of most discussions. Atherton [53] looked at three separate control problems in the fabrication process: 1) overall control of the fabrication facility; 2) control of wafer movement within the facility; 3) control of individual process units. He attempted to define control terms for a process unit, describing manipulated variables as power, flow settings and electrode cooling fluid temperature. State variables according to Atherton include pressure, bias voltage, etch rate, wafer temperature, and plasma composition.

Jenson [54] has also addressed automation in the three areas described by [53] and stated reasons why advanced control algorithms have not been applied. The main reasons given for this are the lack of fundamental understanding (modelling) of the process units and the few device properties which can be measured on-line. Because of this most units are run open-loop which creates long feedback loops and measurement lag. Jenson used plasma etching as an example of the needs that must

be addressed in control of the device fabrication process, his main emphasis being on the need for process models. He suggested beginning with the application of multivariable control schemes to simple process models. McLaughlin [55] developed a control scheme for the plasma etching processes in the CF_4/O_2 and CF_4/H_2 based on statistical analysis. However, this method provides limitations to access to models that are computationally more amenable to the solution of immediate problems in the area of device manufacturing and process control.

Control of plasma etching reactors has been limited to endpoint detection schemes. Barna [56] advocated the use of an expert system applied to the endpoint trace of an etcher. Comparison of actual trace (on-line) to a normal trace held in memory was used to detect abnormalities in the etch and to assign causes to them wherever possible. A different approach than endpoint detection was taken by Bresnock et al [57]. They used adaptive algorithms to create and update a process model which was then used to control process variables such as actual power dissipated in the system and etching flow rates. Control of these variables was satisfactory, but their control system was effective only in controlling these process variables, not the process itself. No feed back on the etch quality was available, only etch rate through interferometry.

1.8 Research Objectives and Summary

The first objective of this research is to choose an etch chemistry suitable for study. Etching of Si and SiO_2 in SF_6/Ar plasma is selected as the etch system due to its frequency of use as an industrial process. Silicon is still the primary substrate for integrated circuits and silicon dioxide is used, for example, as a masking material for diffusion and ion implantation, and as gate material in MOS devices. The use of fluorine-based chemistry to etch these materials is common and relatively well-characterized. Fluorine chemistry is preferred over chlorine chemistry (CCl_4, Cl_2, etc.) for two reasons. Chlorine presents a greater problem due to difficulties with corrosion, particularly when used with aluminium, the masking material used in research. Secondly, several chlorides, such as aluminium chloride, are involatile and are thus difficult to remove from the etching reactor [5][6].

The next phase of research is concerned with selecting process and performance variables to characterise the system. RF power density, chamber pressure and SF_6 flow rate are selected as manipulated variables. In order to maintain the integrity of the etching environment, it was initially decided that the non-intrusive techniques, such as optical emission spectroscopy and laser interferometry, would be used for process variable measurement and real-time etch rate monitoring respectively. This provides a limitation as to which process variables could be studied and how they could be measured or inferred. These non-intrusive techniques are employed as a promising means for measuring the relative concentrations of plasma active species and etch rate respectively without perturbing the plasma chamber. Measurement of plasma species relative concentrations, [F], $[SF_x]$ (x=3-->6), and inference of the electron energy of system, the electric field to pressure ratio in the bulk plasma E/p, are chosen as process variables. Etch rates of Si and SiO_2 , uniformity of these etch processes and anisotropy are the measures of process performance variables.

The third objective of this work is to characterise the plasma chemistry and kinetics, to model the plasma etcher behaviour and to predict the magnitude and distribution of Si and SiO_2 etching in SF_6/Ar plasma under various ranges of manipulated conditions. In addition, a general computer simulation model which includes various chemical and physical mechanisms, is presented in order to predict the etched topography. Because of the great complexity of plasma systems, most of the previous modelling studies considered one particular aspect of the plasma. In this study, both theoretical and experimental approaches have been taken to explore the plasma etching process.

One of the important needs in microelectronics manufacturing is the improvement of the operating procedure in the unit operations used in the production of semiconductor devices. But the optimisation of the plasma etching process is quite challenging because of its complexity. The effects of ion bombardment on surface modification and surface chemistry are poorly understood. The large number of manipulated variables and their complex interaction often lead to non-optimal process performance quantities. Process development for these systems becomes a series of trial and error experiments. Plasma etching processes are time varying, highly non-linear and hard to characterise accurately. An alternative to this approach is an extensively designed experiment which determines optimal manipulated conditions, but generates little fundamental understanding. This approach also lacks the ability to accurately predict system behaviour outside

the experimental parameter space. Therefore, it is important to develop control system design techniques that are insensitive to model error. For these purposes, the manipulated variables have been selected as etching inputs to relate both the semi-output process variables and output performance variables using regression analysis and response surface methodology. Correlations are also developed between these variables. The step response method is employed to determine the process time constants. A steady-state regression model of this etch system is then developed based on composite design of experiments and comprehensive reactor theoretical modelling studies for control system simulation so that control strategies could be studied. Decoupling and robust multivariable control strategies are applied to the dynamic model to determine suitable variable pairings to minimise the process interactions for feedback control and necessary methods for achieving acceptable control system performance. In this work, both of SVD pairings with structurally compensated MIMO (multivariable input-multivariable output) and conventional control strategies satisfy the robustness requirements but the robust stability of conventional control is worse for multiplicative input uncertainties and the structurally compensated scheme is less sensitive to input perturbations. The closed loop transient responses for SVD pairings with the structural compensated MIMO control strategies are typically much faster than the conventional scheme. The model uncertainty due to process non linearity is highly structured in the plasma etching process. The structured singular value is found very useful for robust multivariable control of plasma etching.

CHAPTER 2 EXPERIMENTAL DESIGN AND PROCEDURES

2.1 Equipment Description

2.1.1 Plasma Etching Reactor

The reactor used for this study, as shown in Figure 2.01, is a parallel plate single wafer etcher. This etcher has a 12-inch diameter aluminium vacuum chamber with a mechanical pump, which provides a base pressure of approximately 10^{-3} torr before etching. Both anode and cathode are 6-inches diameter. Gases are introduced from a top gas pipe. Provisions are made to adjust the top plate so as to give a plate spacing that could be varied from 0 to 6 inch. The lower electrode was powered while the other was grounded to the reactor unit casing.

The process gas used in this research is sulphur hexafluoride (SF_6). In addition, argon (Ar) gas is used as actinometer for optical emission studies and the total actinometer flow rate could be kept at less than 4% of the etching flow rate. SF_6 and Ar gases are individually metered through the mass flow controllers (Tylan General Mass flow controller, Model FC 280-SA) and are then mixed before entering the reactor. Pressure control is achieved by controlling reactant flow rate. A Tylan Vacuum General pressure gauge (Capacitance Diaphragm Gauge, Model CMLB-11) is used to measure system pressure. The reactor is equipped with two ports suitable for optical emission spectroscopy and laser interferometry fitted with quartz viewports. A hole was drilled through the upper electrode for etch rate measurement through laser interferometry. The real-time installation of the plasma etching system is shown in Figure 2.02. The optical and laser system will be discussed in the later sections.

Set points for RF power, pressure, input gas flow rates, and process time can be entered and run manually. Changes in all of the process parameter set points can be made at any time during an experiment. A typical run proceeds as follows: wafers are placed on the lower electrode and the chamber is closed and the process begun. The system pumps down under the mechanical pump until the required pressure is

met (less than 10^{-2} mtorr in this research). At this time the each process gas is turned on. The pressure is allowed to stabilise for one minutes before the RF generator is turned on. The process time is calculated from when the RF generator is turned on. The end point detection of the process can be monitored by laser interferometry. At the end of the full process (i.e., all of individual etch steps on the same substrates), nitrogen can be bled into the system to purge it. The system is then allowed to come to atmosphere.

To estimate the time-averaged electrical properties of the plasma, such as spatial averaged electron density and effective electrical field, the impedance measurements and the electric circuit analogy are employed in this study [65][66]. The detailed analysis will be given in Chapter 3. The voltage is measured at the electrical feed through by a 100x voltage probe while the current is measured by a current monitor. The measured wave forms are stored on a digital oscilloscope. The stray capacitance is subtracted from the measurements according to an analogue circuit model, shown in Figure 2.03. The stray circuit elements are determined by measuring the impedance of the chamber and feed through in the absence of a plasma. The characterization and experimental data of the impedance measurements are presented in Appendix IV.The wafer temperature, which will be employed later to decide the reaction constant of fluorine atom with Si and SiO_2, is monitored with a temperature sensor. This information can be fed into modelling studies.

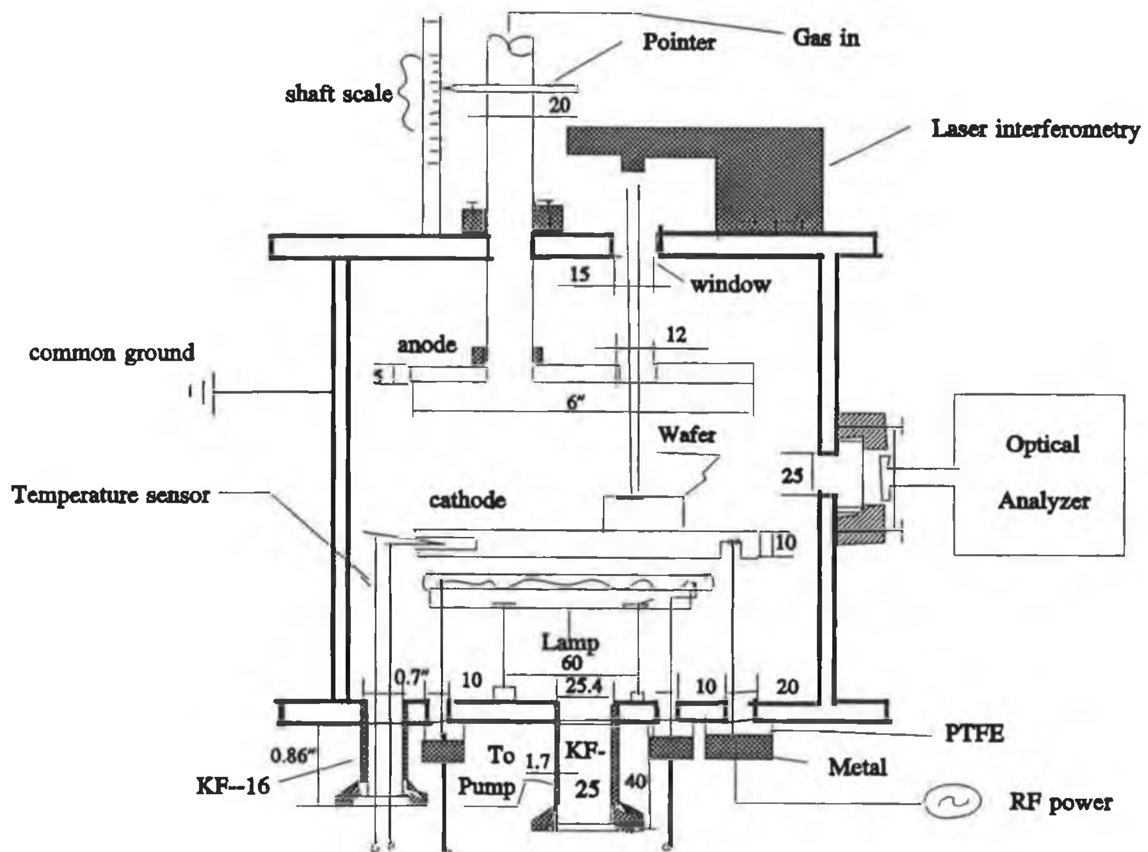

Figure 2.01 Cross section of etch chamber showing the structure of a parallel plate etcher, which is designed for this work.

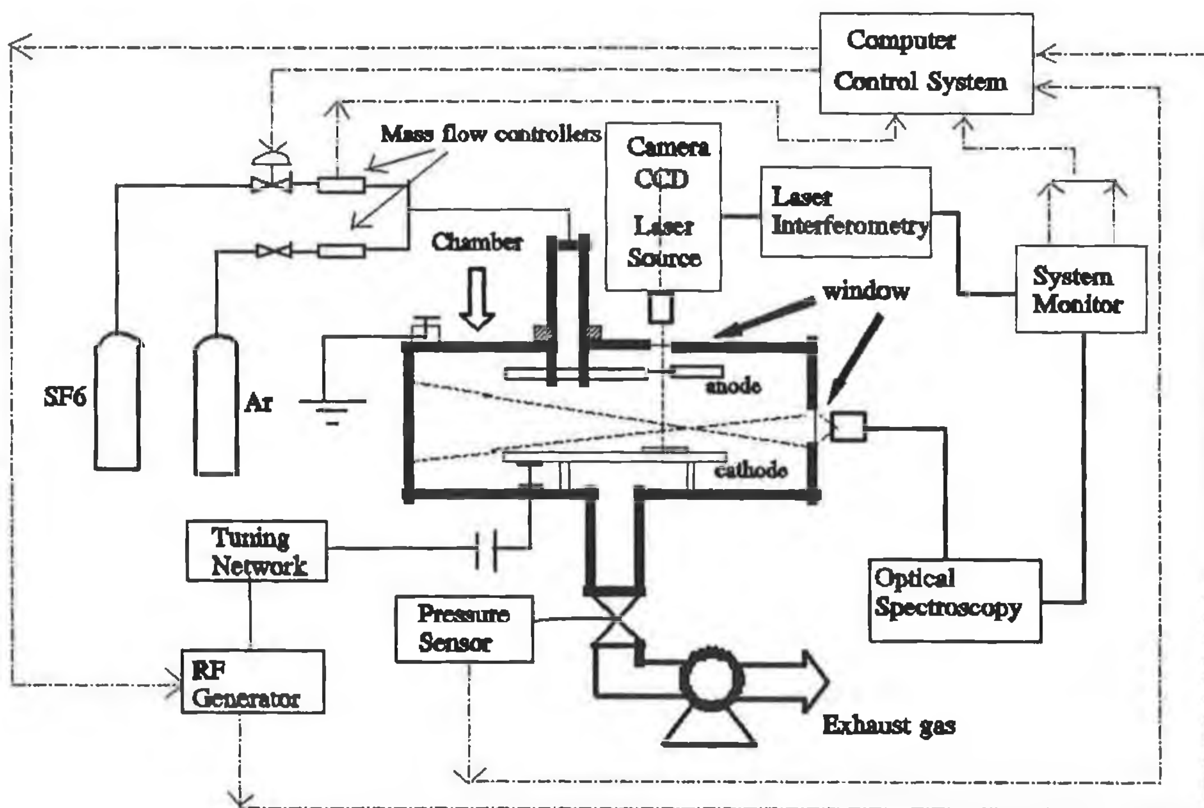

Figure 2.02 The Data Acquisition and Control Signal Design for Real-time Computer Control System for SF_6/Argon Plasma Etching Process

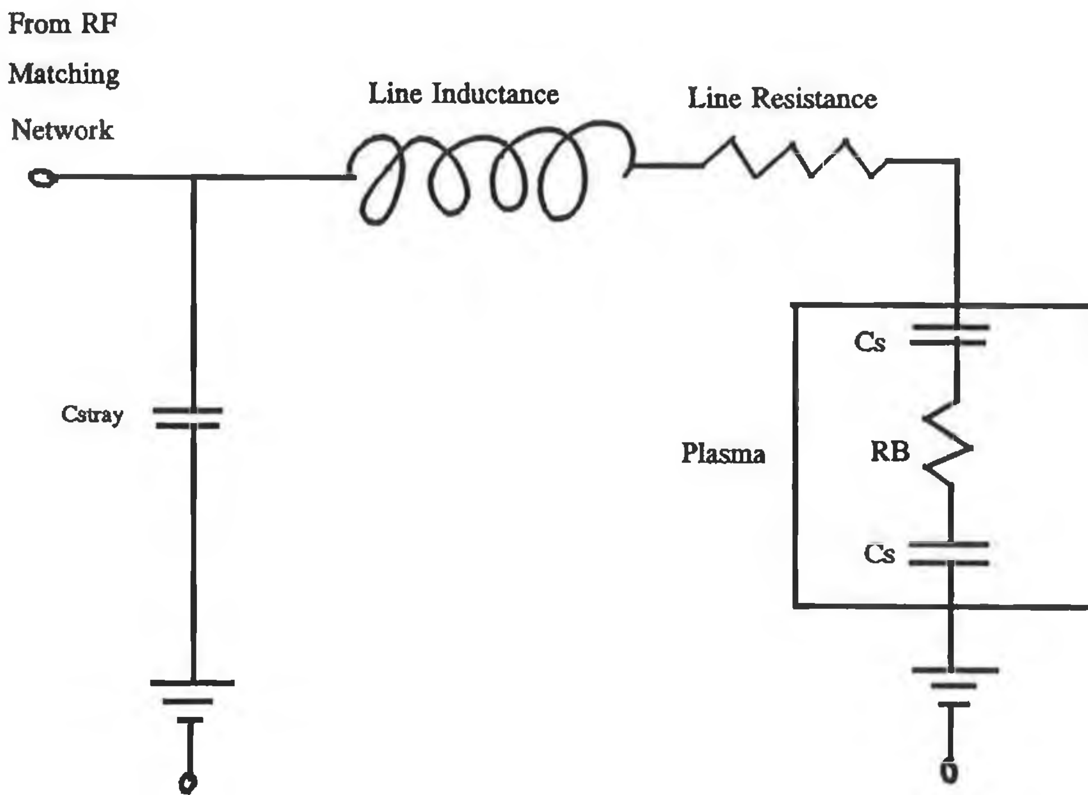

Figure 2.03 Schematic of electric circuit model plasma

2.1.2 Optical Emission Spectrometer

The optical spectrometer used in this research is a SOFIE DIGITWIN Dual Optical Monitoring instrument. This is a powerful spectral analysis tool for the control and verification of the plasma etching based on the emission spectroscopy of reactive plasma. The system monochromator can be adjusted for UV range (200-600 nm) or for visible range (500-900 nm). It analyses in real-time the evolution of the radiation emitted by atoms, molecules and ions energised by the free electrons of the plasma. The optical system is coupled to the plasma etching reactor through a fibre optical cable attached to the viewport mentioned earlier (See Figure 2.02). The optic emission sampled through a fibre optic represents a bulk value of species emissions in the plasma. Spatial resolution is not possible using a fibre optic alone. The system is calibrated through the use of gas plasma lamps with known spectra. A sample spectrum is taken from a lamp whose spectrum falls in the range of interest. As many seven spectral peaks may be used to calibrate the system. Table 2.1 lists the calibration wavelengths which may be used for each spectral region studied.

Optical emission spectroscopy is employed for in-situ monitoring of gas phase species in this work. The recorded spectra can be printed directly or stored on disk in ASCII format. The ASCII format is particularly useful since disks formatted by the optical system are IBM-compatible. This allows manipulation of the spectrum by user-supplied programming. The visible radiation from the plasma is sampled to obtain a spectrum of emission intensity versus wavelength. 4% Argon gas is added to the plasma and its emission is monitored at 750 nm, corresponding to the threshold energy for the excitation of fluorine atom species to their emitting state [59]. A linearly increasing Ar emission intensity with increasing Ar flow rate (concentration) is observed, in agreement with previous results [59]. The addition of the Ar gas to the feed does not affect the emission intensity of the other species present in plasma under different etching gases and conditions. all data shown in this work have been adjusted to their relative concentrations.

Table 2.1 Calibration Lines for Optical Emission Spectrometer

Variable Screening Experiments

250 - 370 nm	400 - 540 nm	530 - 670 nm	670 - 800 nm
295.4 (Hg)	404.5 (Hg)	546.1 (Hg)	671.7 (Hg)
296.7 (Hg)	435.8 (Hg)	577.0 (Hg)	696.5 (Ar)
334.1 (Hg)	507.3 (Hg)	603.0 (Ne)	727.3 (Ar)
365.0 (Hg)	540.0 (Hg)	626.7 (Ne)	750.4 (Ar)
	453.7 (Ne)	650.7 (Ne)	772.4 (Ar)
	470.8 (Ne)	671.7 (Ne)	801.5 (Ar)
	483.7 (Ne)		

2.1.3 Laser Interferometry

The etching rate measurements are performed by a laser interferometry system (SOFIE DIGITWIN instrument). The DIGITWIN laser system is equipped with a special designed solid state laser source including a CCD camera for imaging the laser impact on the sample during the process. A,X,Y table allows to adjust the right position during the process too. The detector of reflected signal is a photo multiplier which is linked to the laser head by a fibre optic.

The general principles of interferometric and reflectrometric phenomenon are described as follows : A laser beam is directed perpendicularly at a wafer coated with transparent layers, which are either to be etched or deposited. The different stacks of materials deposited and etched on the wafer which constitute the electronic devices, form interferometers. Due to changes of the refraction coefficient between the different layers, a complex reflecting system of standing waves occurs under the laser beam. According to the laws of wave composition, the resulting intensity varies as the thickness of the films decreases and increases over time. This intensity is measured and analysed by computers. Any change of the interferogram shape is then interpreted in function of the process evolution. The calculation of the derivative signal in relation to time of the interferogram provides complementary information concerning : a) the etch rate or deposition rate; b) the etching selectivity compared to the mask; c) the reactor uniformity. The detection of the etching completion is indicated by variations of the trace linked directly to : the ratio of unmasked area to the lit area not masked by resin; the selectivity between the layer being etched and the layer; the variation of the refraction coefficient at the etching completion.

The theory of multilayers reflectance is described in many books on optics. It is easy to show that the reflectance is a periodic function of thickness of the top layer (if it is not strongly absorbing), with one period corresponding to a thickness change d given by : $d = \lambda/2 \cdot n$;
where λ is the wavelength of the incident light, n is the refractive index of the top layer.

Therefore, the optical etch rate monitor signal repeats itself after etching about 215 nm (665.5 nm /1.47 /2) of silicon dioxide or about 81 nm (665.5 nm / 2/

3.9) of polysilicon, when using a semiconductor laser source. This is the periodicity which is widely used for optical etch rate monitoring.

Therefore, a general rule is that a layer which is an integral number of half-wavelengths thick will have the same optical effect as no layer at all. For example, if the oxide in a polysilicon/oxide/silicon structure is one wavelength thick, then the structure looks like polysilicon/silicon. Since heavily-doped polysilicon and lightly-doped silicon have nearly the same indices of refraction, the reflectance is practically independent of polysilicon thickness and cannot be used to monitor polysilicon etching. This undesirable effect has been observed experimentally [60].

Another interesting result, from the standpoint of practical application, is the total reflectance when two different areas on the wafer are etching at different rates. This is the case when part of the wafer surface is covered by a low etch rate resist and remaining area is to be etched at a higher rate. For each area, the reflected light has an amplitude and phase which depends upon the film structure of that area, and the light beam reflected from different areas will interfere with each other.

The overall effect of these two types of interference (among light reflected from different layers within an area and among light reflected from different areas) can be calculated by adding the complex reflection coefficients corresponding to etched area, and then taking the square amplitude of that sum. This model does not include diffraction at the step edges, but the contribution from this effect is expected to be small if the areas are large compared to λ.

Also, etch rate measurements can be determined off-line by measuring the loss of silicon with a stylus profilometer or ex-situ interferometer and dividing by the etch time. This technique is only employed to compare with the laser interferometry. Under different length of etching times, it is confirmed that the etch rate is not a function of time at this study.

2.2 Experimental Procedures

Experimental conditions for the manipulated variables are chosen such that data could be compared to model predictions in a convenient manner. In other words, variables are changed one variable at a time so that only a specific variable could be investigated. The exact method used to obtain data is presented next. A detailed discourse of reactor preparation is presented in order to demonstrate the condition of the reactor in each experiment. As will be discussed, the exact condition of the reactor is important to obtain repeatable data.

2.2.1 Reactor Preparation

The variable screening experiments are run in an empty reactor, so no particular preparation is required before an experiment is performed. However, prior to the beginning of experimentation and for changeover of gases, process lines are purged for cleanliness and safety. All process lines are flushed with SF_6. This is done to assure that no residual moisture remained in the lines.

Si and SiO_2 chips are used in both the steady state and dynamic experiments and it found that, in the SF_6/Ar plasma, material tended to deposit on reactor wall and surfaces. This noted most clearly as a linear decrease in optical emission with the number of experiments run. It is necessary to employ a cleaning step before each experiment when etchable material has been present in the reactor. The cleaning methods are tested by running several replicate experiments, each followed by the cleaning step of interest.

For every experiment, the following sequence followed :

(1) The reactor chamber is flushed with Argon.
(2) A pre-run is performed.
(3) The reactor is brought to atmosphere.
(4) Samples are prepared and loaded into reactor.
(5) The system is pumped down to base pressure.
(6) The feed gases are started.
(7) Pressure is adjusted.

(8) If pressure stabilised, the RF power is tuned on.
(9) RF power is turned off after the etching completion.
(10) The feed gases are stopped.
(11) The reactor is brought to atmosphere.
(12) The samples are removed for analysis.

The length of the experiment is determined by initial experimentation and also examination of etch rate monitoring by the laser interferometry. The dynamics of the etching processes are very fast and hard to know and control. In this work, the etching process is slowed down by reducing the initial manipulated conditions, such as RF power density in order to observe the real-time etch rate due to the limitation of the laser system and to obtain the enough time for process control. RF power condition for SiO_2 coated wafers etching is found higher than Si wafers for the same etch rate.

2.2.2 Sample Preparation

Unmasked and unpatterned Si (n-type) and SiO_2 (0.2 to 0.6 μm thermal oxide on n-type Si) wafers used in this research are supplied by the Electronic Materials Research Lab in DCU. Samples with exposed silicon are dipped in buffered hydrofluoric acid for approximately 10 seconds to remove native oxide from the silicon. They are then rinsed in distilled water and blown dry with nitrogen. This procedure is performed on each silicon sample just prior to the beginning of an experimental run to provide a clean and reproducible silicon surface for the etch process. In this work, most of experiments are run initially with no additional substrate heating. The wafers gain thermal energy due to impact of high energy ions and powered electrode. Because of the low pressure at which the etching reactor operates, there is negligible heat transfer between the gas and substrate [61]. Ion bombardment is assumed on the powered electrode while little on the grounded electrode[62][63]. The measurements are taken in the same plasma on powered electrode only.

2.2.3 Data Acquisition

No single acquisition system will be used to collect data from etch experiments for each manipulated variable and performance variable. Optical emission will be collected from each experiment stored on disk. Real-time etch rate is determined by a laser interferometry or measuring the etched depth of Si and SiO_2 wafers by a stylus profilometer. The same data is then be used to calculate etch centre-to-edge uniformity and anisotropy. Also anisotropy can be measured from scanning electron microscope photographs of regions of the etched wafers. The various instrumentation signals will be signal conditioned and interfaced to a IBM PC-486 based Personal Computer via Metrabyte DASH16 and DDA06 input/output cards. The DASH16 provides timers and D/A facilities and uses an industry standard (HI-674) 12 bit successive approximation converter with a 12 μs conversion time. All instrumentation signals will be filtered and interfaced in differential configuration which provided 90 dB common mode rejection and ± 10 V common mode range. The DDA06 provides 6 independent 12 bit D/A converters and 24 bits of digital I/O and are TTL/CMOS compatible.

2.3 Composite Design of Experiments

2.3.1 Variable Screening Tests

The primary purpose of these experiments is to evaluate the optical emission spectra for spectral peak identification and to determine which of these peaks would be satisfactory for monitoring in future experiments. No peaks corresponding to etch products are sought, so no etchable material is placed in the reactor. Each manipulated variable is studied separately and is varied incrementally from low to high value. The other manipulated variables are held constant during each experiment.

A second purpose of these experiments is to compare the results from our etching reactor and optical system with results obtained from previous studies to verify and improve these results and our experimental techniques. Some of the

results found in the references, such as Coburn and Chen [59], had been generated using one-variable-at-a-time experimentation, so this method is used.

As stated above, these experiments are run using an empty reactor. The optical system is first calibrated in the spectral range of interest. Three spectral ranges are needed to cover the entire region desired (200 - 900 nm), so each set of experiments is run in each range. The image intensifier is set so that the intensity of the largest peak throughout the set of experiments, i.e., through all experiments in a given spectral range, would be approximately 85% of detector saturation. Intensity is an arbitrary number, but care is taken that the scale for a set of experiments would be the same so that spectral lines could be clearly compared. For these experiments, the reactor is run in manual mode. The reactor is pumped down, process gas flows and chamber pressure are set and the system is allowed to stabilise for about one minute. The RF generator is then turned on. One minute is allowed for stabilisation, although it is generally noted that the time required to stabilise is much shorter. With the plasma still on, a change is made in the variable of interest and the system is again allowed to stabilise. A full spectrum is acquired at each set of process conditions. This process continues until all desired values of the variable are obtained. The RF generator and process gases are then turned off and the reactor is vented.

2.3.1 Etch Rate Tests

These experiments are run to determine suitable etch times for the steady-state experiments. SiO_2 sample partially covered by Si wafer are placed on the powered electrode surface. Process conditions are set prior to pump down with the process time for each experiment and the reactor is run in manual mode. The plasma is allowed to stabilise for one minute before the optical system begins acquiring spectrum, except in the case of the shortest etch time when the spectrum are begun 30 seconds into the run. Etch rate for the wafers is measured using the laser interferometry. These experiments are run using the spectral lines chosen from the variable screening tests. The lines fall into two distinct ranges, 260-400 nm and 650-800 nm. The optical system is calibrated as before and the spectrum mode of acquisition is chosen. This was done to save data space and for diagnostic purposes to allow monitoring of the plasma during the etch process. Once the etch is

completed and the chamber has come up to atmosphere, the wafers are removed and stored for later analysis.

The purpose of these experiments is to determine the amount of time required to generate a good etch profile in the SiO_2 samples without etching all the way through the 0.5 μm oxide layer. A factorial design as described in Box, Hunter [39][40] is used to design these experiments. A 2-level factorial design is chosen, capable of fitting a linear function to the data. Three manipulated variables are studied: RF power density, chamber pressure, and total SF_6 flow rate. The electrode spacing is set constant for each experiment. The 2^3 factorial design is shown along with the levels used for each manipulated variable in Table 2.2. The designs are randomised before being run.

Table 2.2 2^3 Design and Variable Levels for Etch Rate Experiments

x_1	x_2	x_3
+	+	+
+	+	-
+	-	+
+	-	-
-	+	+
-	+	-
-	-	+
-	-	-

SiO_2 Wafer	x_1 = RF power density	x_2 = pressure	x_3 = SF_6 flow rate
+	0.5 W/cm^2	300 mtorr	30 sccm
-	0.35 W/cm^2	200 mtorr	15 sccm

Si Wafer	x_1 = RF power density	x_2 = pressure	x_3 = SF_6 flow rate
+	0.25 W/cm^2	250 mtorr	30 sccm
-	0.15 W/cm^2	150 mtorr	15 sccm

Electrode spacing = 1.5 cm.

2.3.2 Steady State Tests

The purpose of these experiments is two-fold. First, the SF_6/Ar system has not been systematically explored through statistical experimental design, so it is necessary to provide regression model for this system. This could then be used to verify some of results of experimentation on this system found in the literature and compare with the comprehensive etching reactor model developed in Chapter 4. A second objective is to construct a steady state model of system for use in the later studies of process control and its application to plasma etching.

An experimental design is needed to cover the parameter space in a reasonable number of experiments. Under the steady state conditions, the etching process under investigation has four factors: RF power density, chamber pressure, SF_6 flow rate, electrodes spacing. Simple two-level factorial designs support linear or planar models. Since we desire to characterize any curvature present in a response, the study requires at least three levels of each factor so that a quadratic model of form [39]

$$Y = \beta_0 + \sum_{i=1}^{n} \beta_{ij} x_i^2 + \sum_{i<j}^{n} \beta_{ij} x_i x_j \quad ; \qquad \textbf{(2.3.2-1)}$$

could be fit to data. Using a factorial design this would require $3^4 = 81$ experiments for each system and would estimate all three and four factor interaction, quantities. Composite design allows these interactions to be neglected in the interest of decreasing the necessary number of experiments in a design. Box and Wilson [64] suggested using designs at two levels and adding "star" points to measure quadratic response. Star points are experiments run with the value of one variable at a high or low level while the other variables are held at central levels. This is in effect supplementing factorial design with one-factor-at-a-time experimentation. $2n+1$ points are added to a 2^n factorial design in this case, reducing (for a four-variable design) the number of experiments required to $2^4 + 2x4 + 1 = 25$ experiments for each system. Hartley [41] suggested using fractional factorial designs augmented with star points to further reduce the required number of experiments. In this case, however, judicious use must be made of the defining equation for the fractional replicate so that desired interactions are not lost. The equations obtained from the defining equation form "alias-sets", those whose effects are confounded (masked) by other effects in the design. Normally, defining equations are designed to keep main effects clear of two-factor interactions; however, this may leave one unable to

uniquely determine the coefficients on all two-factor interactions since they may be aliased with one another. Hartley [41] presented a theorem concerning how many and which coefficients may be estimated from a given design:

(a) In any composite design, in which no main effect is used as a defining contrast of the $(1/2^k)\ 2^n$ fractional replicate, it is always possible to estimate the following coefficients of the quadratic response surface (Equa. 2.3.2-1): all linear coefficients (b_i), all quadratic coefficients (b_{ij}), and the constant b_o; One of the product coefficients (b_{ij}) selected from each of the alias-sets.

(b) It is not possible to estimate more than one of the product coefficients (b_{ij}) from each alias-set.

The results of this theorem is that the largest number of coefficients of the quadratic response surface that can be determined from a given fractional replicate occurs when each alias-set is made up of at least one two-factor interaction. With this in mind, a half-fraction of a 2^4 factorial is suggested using the defining equation

$$x_1 = x_2 x_3 ; \qquad \textbf{(2.3.2-2)}$$

The following alias sets (in addition to the above definition) are obtained :

$$x_2 = x_1 x_3 ; \qquad \textbf{(2.3.2-3)}$$
$$x_3 = x_1 x_2 ; \qquad \textbf{(2.3.2-4)}$$
$$x_4 = x_1 x_2 x_3 x_4; \qquad \textbf{(2.3.2-5)}$$
$$x_1\ x_4 = x_2 x_3 x_4; \qquad \textbf{(2.3.2-6)}$$
$$x_2\ x_4 = x_1 x_3 x_4; \qquad \textbf{(2.3.2-7)}$$
$$x_3\ x_4 = x_1 x_2 x_4; \qquad \textbf{(2.3.2-8)}$$

This design allows all two-factor interactions to be estimated and the augmentation of the half-fraction with star points (plus a centre point) allows all main effects to be estimated as well. The total number of runs required is $2^{4-1} + 2x4 + 1 = 17$ runs. Additional replicate centre points are added for the estimation of experimental error bringing the number of runs for each design to 21. Table 2.3 and 2.4 list the experiments required for the composite design and the levels of manipulated variables used in this design. It should be noted that the design is symmetric about each factor so that each variable is examined equally in the resulting analysis. The star points are listed as $\pm\alpha$, taken to be 2 for these

experiments to insure rotatability of the design. A rotatable design is one in which the accuracy of the design results is a function only of the distance from the centre of the design, i.e., is not a function of the variable examined [39]. The design is randomised and run on the SF_6/Ar system.

Table 2.3 Composite Design Matrix for Steady State Experiments

x_1	x_2	x_3	x_4
+	-	-	-
-	+	-	-
-	-	+	-
+	+	+	-
+	-	-	+
-	+	-	+
-	-	+	+
+	+	+	+
0	0	0	0
$-\alpha$	0	0	0
$+\alpha$	0	0	0
0	$-\alpha$	0	0
0	$+\alpha$	0	0
0	0	$-\alpha$	0
0	0	$+\alpha$	0
0	0	0	$-\alpha$
0	0	0	$+\alpha$

Table 2.4 Manipulated Variable Levels for Composite Design

SiO_2 Wafer	x_1 = RF power density	x_2 = pressure	x_3 = SF_6 flow rate	x_4 = electrode spacing
+2	0.50 W/cm^2	300 mtorr	30 sccm	4.0 cm
+	0.45W/cm^2	250 mtorr	25 sccm	3.0 cm
0	0.40 W/cm^2	200 mtorr	20 sccm	2.0 cm
-	0.35 W/cm^2	150 mtorr	15 sccm	1.5 cm
-2	0.30 W/cm^2	100 mtorr	10 sccm	1.0 cm

Si Wafer	x_1 = RF power density	x_2 = pressure	x_3 = SF_6 flow rate	x_4 = electrode spacing
+2	0.25 W/cm^2	250 mtorr	30 sccm	4.0 cm
+	0.20W/cm^2	210 mtorr	25 sccm	3.0 cm
0	0.15 W/cm^2	170 mtorr	20 sccm	2.0 cm
-	0.10 W/cm^2	130 mtorr	15 sccm	1.5 cm
-2	0.05 W/cm^2	90 mtorr	10 sccm	1.0 cm

2.3.3 Dynamic Tests

These experiments are also run using the spectral lines determined earlier. Two spectral ranges are again required. A 10 minute process time is used. SiO_2 sample partially covered by Si are placed on the powered electrode surface. Initial process conditions are set, and the process is started. The optical system is calibrated as usual and the spectrum mode is selected. The laser interferometry is employed to monitor the real-time etch rate of the chips, which will be discarded after the run is completed.

Experiments to elucidate process dynamics involve step tests on the reactor. Each of manipulated variables is examined separately. Experiments are run with positive and negative step changes and responses of the process variables are measured indirectly for these steps. In addition, etch rate, as one of the performance variables, can be monitored on-line as one of outputs while others, such as anisotropy and uniformity, can be estimated off-line. Step tests are made from three base sets of conditions (the conditions and results will be discussed further in the chapter 4) with the same steps run at each set of conditions.

CHAPTER 3 COMPREHENSIVE REACTOR THEORETICAL MODELLING STUDY

3.1 Introduction

Although plasma etching has been widely used in the microelectronics industry for pattern replication, the optimisation of this process is quite challenging because of its complexity [1-8]. The ability to etch fine lines and anisotropic profiles, fast etching rates and high selectivity over bottom layer are important properties which depend on the choice of process conditions. The effects of ion bombardment on surface modification and surface chemistry are poorly understood. The large number of manipulated conditions and their complex interaction often lead to non-optimal process performance quantities. Process development for these systems becomes a series of trial and error experiments.

This chapter deals with the chemical mechanism of silicon and silicon dioxide etching in a SF_6/Ar plasma. Fluorine and chlorine chemistries are generally used in the etching of silicon, with fluorine chemistry the dominant of the two. SF_6 has been frequently used for etching of Si and SiO_2 in integrated circuits fabrication, as it offers fast silicon etch rates, high selectivity of Si over SiO_2. SF_6 discharge has been studied in a wide variety of reactors [14-19]. Mixed fluorine/SF_x chemistries and their effects on anisotropy by etching silicon in SF_6/Ar, have shown that etching processes which use unsaturated etchants lead to anisotropic etch profiles in this work. The main reason for the great use of fluorine chemistry in silicon etching is that atomic fluorine etches Si spontaneously. The volatile product from the etching of silicon in fluorine chemistry is SiF_x, however, there is much discussion as to the value or values of x. Atomic fluorine and probably all SF_x fragments are considered etching species in this study, but the only silicon-containing product of this etch is SiF_4. The relative fluorine and SF_x species density can be measured by the optical emission spectroscopy [73]. In any case, there is general agreement that the SiF_x product reacts with fluorine or fluorine-containing species in the gas phase to produce SiF_4, meaning that an overall balance would reveal the same (or almost so) consumption of F atoms from each of mechanisms. The etching characteristics of silicon in fluorine-based plasma can be varied by the addition of different chemical species to the etching

gas. The mechanism underlying the etching of silicon dioxide is still a subject of discussion despite much study in recent years. Questions remain as to the actual etching species and the role of ions, both as bombardment species and active etchants. It is now understood that atomic fluorine does etch SiO_2. SF_x radicals and/or ions are also presumed to be etchants of SiO_2, although the roles of these species are less well-known.

The analysis method of the dynamic mass balance has been employed to construct the comprehensive reactor model for simulating plasma etching of silicon and silicon dioxide with SF_6/Ar in this work. The model includes diffusion and convection of molecular fragments in a duct geometry, which could be estimated by using an effective diffusion length which takes surface reflection into account and increases as the surface reflection probability increases. Electron impact dissociation and ionisation reactions which depend on the electric field and gas density are the dominant sources of active species generation. Fluorine atom generation is also described by dissociative chemisorption. Fundamental plasma parameters such as electron density, electric field and rate constants are estimated from impedance measurements in a designed experiments under the various operating conditions in conjunction with the gas phase chemistry and mass transfer, to predict local etching across a Si or SiO_2 wafer. The effects of RF power density on the relative concentration of fluorine atoms and etch rates of Si and SiO_2 are determined by using optical emission spectroscopy and laser interferometry respectively. The addition of the Ar gas to the feed gas does not affect the emission intensity of the other species present in plasma under different etching gases and conditions. All data shown in this work have been adjusted to their relative concentrations. Results presented in this work show the relatively good agreement between the model predictions and the experimental data.

3.2 Theories of Impedance and Actinometry

To estimate the time-averaged electrical properties of the plasma, such as spatial averaged electron density and effective electrical field, the impedance measurements and the electric circuit analogy are employed in this study [65][66]. Thompson and Sawin [67] also investigated SF_6 electronegative discharge and successfully derived plasma characteristics from an equivalent electrical circuit.

Bletzinger and Flemming [68] measured the electrical properties of discharges over wide ranges of pressures and operating frequencies and correlated the electrical characteristics with a simple circuit model, as shown in Figure 2.03. The bulk of the plasma is primarily represented by a resistor and the sheaths are represented by capacitors. The primary sink for power dissipation is considered to be the resistor representing the electron impact processes in the bulk of the discharge. This circuit model was found to be quite accurate in the high discharge frequency and medium gas pressure range [49][65]. The plasma impedance Z is calculated from

$$Z = R - \frac{2j}{\omega C_s} = \frac{|V|}{|i|} \exp(i\theta) \; ; \qquad \textbf{(3.2-1)}$$

When a sinusoidal voltage is applied to this circuit, the plasma resistance, R, is given by

$$R = \frac{|V|}{|i|} \cos(\theta) \; ; \qquad \textbf{(3.2-2)}$$

where $|V|$ and $|i|$ are the amplitudes of the applied peak voltage and current respectively. θ is the measured phase angle between the voltage and the current wave forms, as discussed in Chapter 2. The capacitance of the sheath, C_s, is given by

$$\frac{2}{\omega C_s} = \frac{|V|}{|i|} \sin(\theta) \; ; \qquad \textbf{(3.2-3)}$$

where ω is the angular frequency. Assuming that the bulk of the current is carried by the electrons, and uniform electron density exists in entire plasma. The electron density (n_e) and electric field to the pressure ratio (E/p), can be estimated from the resistance of the plasma bulk as,

$$n_e = \frac{d}{Ae\mu_e R} \; ; \qquad \textbf{(3.2-4)}$$

$$E/p = R|i|(2pd)^{1/2} \; ; \qquad \textbf{(3.2-5)}$$

where d is the electrodes spacing, A is the electrode area, e is the charge of an electron, and μ_e is the electron mobility which is inversely proportional to the gas pressure p [69]. The electron mobility has been estimated from experimental measurements of electron drift velocities in SF_6 at an E/p of 50 - 200 V/cm-torr [69]. The electron mobility was found to vary inversely with the gas pressure p and the value of μ_p is $2x10^5$ cm^2·torr/V·sec [74].

A minimum number of experiments is done, according to the principle of composite design, as discussed in Chapter 2, in order to measure the impedance across the entire parameter space [39][75]. The range of parameters used is listed in Table 3.1. Some experiments are performed to interrogate the entire parameter space available which produces stable and well confined glow discharges. The detailed characterization and experimental data of stray impedance will be presented in Appendix IV.

Optical emission usually results from the inelastic electron impact on the ground state atoms and molecules which are excited and then decay back to the lower energy state, thus generating photo emission. The visible radiation from the plasma can be sampled to obtain a spectrum of emission intensity versus wavelength. The emission intensity is proportional to the ground state species concentration multiplied by an excitation efficiency factor. D'Agostino et al [16], and Coburn and Chen [59] have employed rare gas Actinometry in which a small concentration of a rare gas is added to the plasma to monitor the specific emission energy level. The energy level chosen should match the threshold energy for the excitation of the species of interest. The main assumption of this technique is that the direct electron impact excitation from the ground state is the primary excitation path for both species. Previous studies [16][59] have shown that the Actinometry method is in good agreement with the fluorine atom concentration measured by a titration method.

3.3 Effects of Discharge Power and Electron Density on Etch Rates of Si and SiO_2

Based on the present study and previous mass spectrometric study [69], it is postulated that the fluorine atoms are formed by electron collision with the SF_6 molecules and SF_X radicals. Radicals recombination has been found in many different glow discharge [70]. For any fixed set of conditions, an optimum power level is evident, above which a recombination reaction takes place, which reduces the number of active species. A chemical reaction model is proposed to describe the mechanism of plasma etching, especially the relationship between the electron density and etching rate. The following major reactions are assumed:

$$e + M \xrightarrow{K_1} M^* + e \quad ; \qquad \textbf{(3.3-1)}$$

$$\text{Generation Step}: \quad M^*\alpha_1 \xrightarrow{K_2} R_1 + N_1 \quad ; \qquad \textbf{(3.3-2)}$$

$$M^*(1-\alpha_1) \xrightarrow{K_2} R_2 + R_3 + N_2 \; ; \tag{3.3-3}$$

Etching Step : $$S + R_i \xrightarrow{K_3} P \; ; \tag{3.3-4}$$

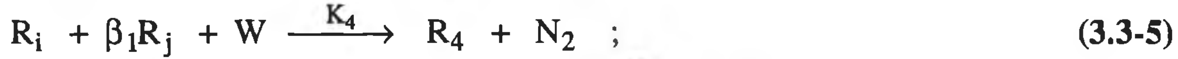

$$R_i + \beta_1 R_j + W \xrightarrow{K_4} R_4 + N_2 \; ; \tag{3.3-5}$$

Recombination Step : $$R_i + (1-\beta_1)R_j \xrightarrow{K_4} N_5 \; ; \tag{3.3-6}$$

where M is the SF_6 molecule, M^* is the excited state of M, R_i and R_j are the SF_x and F radicals, N is a non reactive radical or molecule, S is a surface molecule of Si or SiO_2, W is a third body and P is the etching product of SiF_4.

The values of α_1 and β_1 vary between zero and unity. The reaction rates V_j ($j=1\rightarrow4$) can be obtained from

$$V_1 = K_1 n_e [M] \; ; \tag{3.3-7}$$

$$V_2 = K_2 n_e [M^*] \; ; \tag{3.3-8}$$

$$V_3 = K_3 \sum R_i = K_3 R \; ; \tag{3.3-9}$$

$$V_4 = K_4 R^2 \; ; \tag{3.3-10}$$

where $R = \Sigma\, SF_x$ and α_1 and β_1 are assumed to be unity. Under a steady state assumption

$$\frac{d[M^*]}{dt} = V_1 - V_2 = 0 \; ; \tag{3.3-11}$$

$$\frac{dR}{dt} = V_2 - V_3 - V_4 = 0 \; ; \tag{3.3-12}$$

one obtains

$$K_4 R^2 + K_3 R - K_1 n_e [M] = 0 \; ; \tag{3.3-13}$$

from which the radical R can be obtained

$$R = -\frac{K_3}{2K_4} \left(\left(\frac{K_3}{2K_4}\right)^2 + \frac{K_1}{K_4} n_e [M] \right)^{1/2} \; ; \tag{3.3-14}$$

The etch rate, V_3, is obtained from equation (3.3-15)

$$V_3 = K_3 \left(\frac{K_1}{K_4} n_e [M] \right)^{1/2} \; ; \tag{3.3-15}$$

The rate constants K_3 and K_4 depend on the gas phase temperature and wafer surface temperature only, and their values are assumed constant in this study. K_1 is a function of the electron energy gained from the electrical field and consumed through electron and neutral particle collisions. For SF_6 glow discharge, Kline [71] has found that K_1 increases with the ratio of effective electric field to pressure.

Impedance measurements, as shown in Figure 3.07 and 3.08, show that the half of peak to peak voltage increases by only 7% under 0.05 to 0.25 W/cm^2 RF discharge power density on Si wafer, 10% under 0.25 to 0.50 W/cm^2 RF discharge power density on SiO_2 wafer respectively, so K_1 is fairly constant within the range of this study. From the Si and SiO_2 etch rates measurements, it is found that only small part of the SF_6 is consumed by silicon or SiO_2 etching, so the concentration of SF_6 is nearly constant in this study. Equation (3.3-15) shows that the etching rate is proportional to the square root of the electron density, i.e. discharge power density. Raman spectroscopy measurements by Hargis and Greenberg [72] reported strong recombination in SF_6 discharge. Their experimental results are in relatively good agreement with the proposed SF_6 discharge mechanism.

At low discharge power density, the concentration of R_i is small, the radicals recombination can be neglected, i.e., $V_4 = 0$, and the etching rate becomes

$$V_3 = V_1 = K_1 n_e [M] \quad ; \qquad \textbf{(3.3-16)}$$

Thus, at low discharge power density the etching rate is first order with respect to the electron density.

3.4 Comprehensive Reactor Modelling

The structure of the comprehensive reactor model, which includes two types of inputs, those of a fundamental nature such as diffusivities, mobility and ionisation coefficients, and those relating to the process manipulated variables such as radio-frequency (RF) power density, chamber pressure, SF_6 flow rate, electron temperature and reactor geometry, has been developed in Figure 3.01.

Based on this structure, the plasma physics can be modelled assuming that the composition of discharge is not altered. Parameters such as the electron density, electron energy, effective electrical field, ion flux, and the electric field to chamber pressure ratio(E/p), as discussed in section 3.2, can be obtained from impedance measurements.

The subsequent gas-phase reactions, transport, and surface reactions are proposed to describe the mechanism of plasma etching. It is well known that

plasma etching of silicon with fluorinated compounds is due primarily to free fluorine [16]. The only reaction product of Si and SiO_2 etching in SF_6 is SiF_4 and no other compounds could be found by downstream mass spectrometry [74]. The dominant neutral species of SF_6 plasma have been identified as free fluorine and sub fluorides of SF_6 [74][78]. In addition, the generation of fluorine by dissociative chemisorption of SF_5 and SF_3 to SF_4 and SF_2 is considered [79]. The dissociation of SF_6 is assumed to involve electron impact dissociation reactions of the form

$$e + SF_{x(g)} \xrightarrow{K_{7-x}} SF_{x-1(g)} + F_{(g)} \quad ; \; (x = 3 \rightarrow 6) \qquad \textbf{(3.4-1)}$$

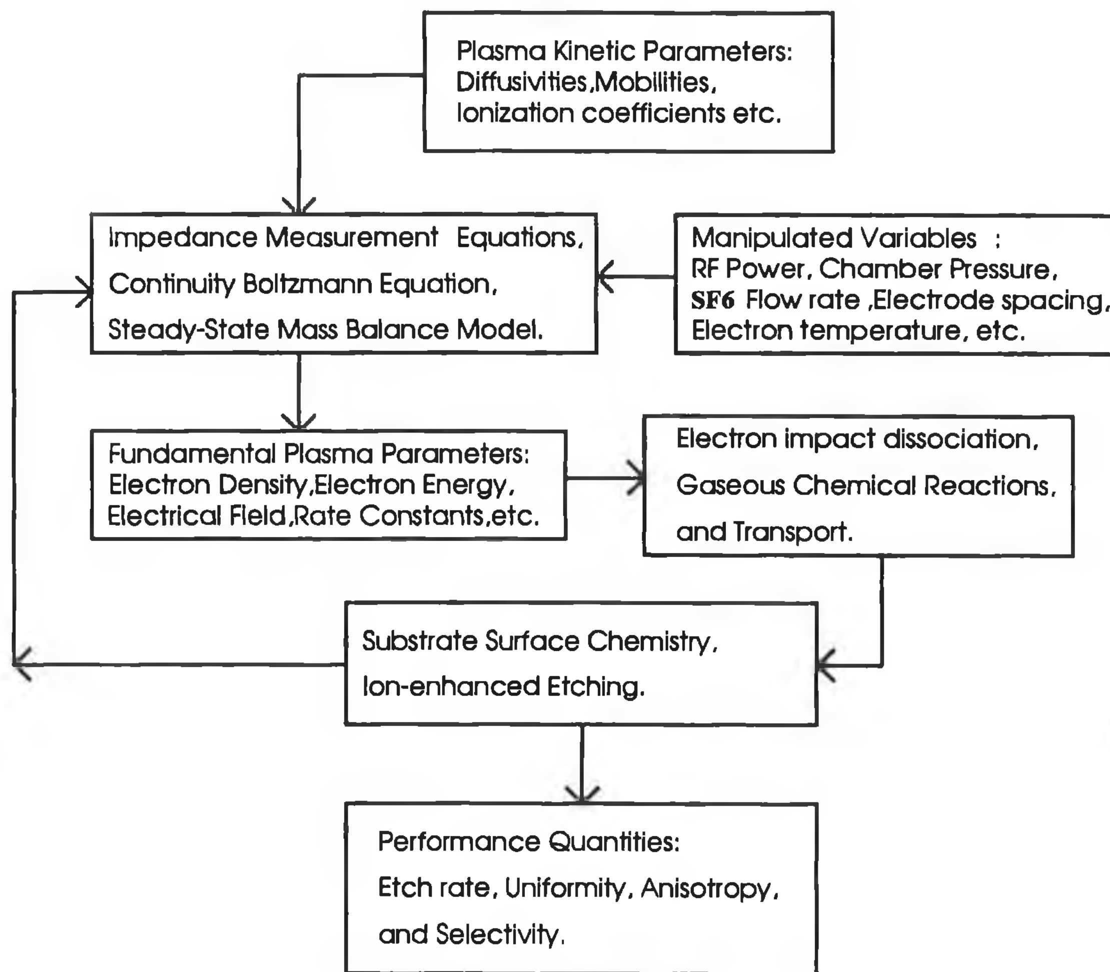

Figure 3.01 The Structure of Comprehensive Model for Plasma Etching

The rate constants for these reactions have to be calculated as a function of measured electric field and gas pressure [6]. The rate constant for etching of silicon and SiO_2 with fluorine atom, K_5, as listed in Table 3.2, can be obtained from ref. [77].

$$4F_{(g)} + Si \xrightarrow{K_5} SiF_4 \quad ; \qquad \textbf{(3.4-2)}$$

Fluorine atom recombination is also considered at the surface. The recombination probability of fluorine on metal surfaces is reported to be much large than on non-metal surfaces [80]. Without silicon wafer existing in reactor, the fluorine atom generation rate is equal to the recombination rate at electrode surface. The recombination probability, γ, of fluorine atoms on the stainless-steel electrodes can be estimated as [80]

$$\gamma\left(\frac{1}{4}\right)n\upsilon = K_1 n_e [SF_6]\frac{d}{2} \quad ; \qquad \textbf{(3.4-3)}$$

where n is the measured fluorine atom concentration at downstream with H_2 titration method [81], υ is the thermal velocity of fluorine, K_1, which is obtained from measured electrical properties and reference [6], is the rate constant for electron impact dissociation and d is the electrode spacing. Using equation (3.4-3), the recombination probability is estimated to be 2.6 x 10^{-4} in agreement, within a factor of ten, with the reported fluorine atom recombination probability of $10^{-5} \rightarrow 10^{-3}$ [80]. The first order surface recombination rate constant, which can be calculated from the recombination probability [80], is equal to 4.14 cm/sec. The calculated first-order recombination rate constant closes, within an order, to the measured recombination rate constant of SF_5 and F by Ryan and Plumb [76].

Because of the variations in the plasma composition caused by the electron impact dissociation, gas-phase chemistry, and surface reactions, the composition of the process can be significantly different from that which is assumed in the initial calculation of the plasma physics. To obtain a self-consistent solution, this procedure must be iterated until the plasma condition after the surface etching is the same as the initial composition used in the discharge calculation. The reactor pressure is considered constant and the gas velocity increases as the SF_6 dissociates. Under steady-state conditions and assuming a fully developed flow, a mass balance can be developed for $SF_{x=2\text{-}6}$, F, and SiF_4 in a manner similar to conventional chemical reactors :

$$\frac{\partial}{\partial r}\left(-rD_i\frac{\partial N_i}{\partial r}\right) - \frac{\partial}{\partial r}\left(rD_i\frac{\partial N_i}{\partial r} - V_r N_i\right) = r\sum_{\rho=1}^{M}\beta_{i\rho}R_{i\rho} ; \qquad \textbf{(3.4-4)}$$

where r is the reactor dimensions, $\beta_{i\rho}$ is the stoichiometric coefficient of the "i"th species for the "ρ"th electron impact dissociation reaction $R_{i\rho}$, N_i represents the mole concentration of species i, D_i is the diffusivity and V_r is the gas velocity. The left hand side of Equa(3.4-4) represents the diffusion and convection of fragments of SF_6 in the plasma. The right hand side of the Equa(3.4-4) represents the dissociation reactions which are assumed to be first order. Surface etching of silicon, silicon dioxide, and recombination of fluorine atom with SF_x radicals have the form $R_{i\rho}=K_\rho N_i(r,\rho)S(r,\rho)$. Gas phase radical recombination has been neglected [80][94]. Here $S(r,\rho) = 1.0$ at the place where surface reaction ρ occurs, and $S(r,\rho) = 0$ where reaction ρ does not occur. The equations can be solved by a finite difference algorithm with the following parameters [82]:
Reactor dimensions: Diameter w=35.5cm; L= 35.5 cm; Electrode spacing 2.0 cm;
Gas temperature : T=298°K;

Process parameters: Pressure=200mtorr; RF power density = 0.125W/cm^2 (for Si wafer), SF_6 flow rate=30 sccm +4%Ar; RF power density=0.35W/cm^2 (for SiO_2); Neutral species diffusivities D_i can be estimated by using an effective diffusion length which takes surface reflection into account and increases as the surface reflection probability increases [71]. Derivation and calculation of finite element equations are presented in Appendix II and also can be found in [82].

3.5 Results and Discussion

The following process manipulated variables and parameters are investigated: SF_6 gas flow rate, chamber pressure, RF discharge power density, and electrodes spacing. The range of manipulated variables and parameters is shown in Table 3.1 and the physical properties and dimensions used in the comprehensive reactor model are summarised in Table 3.3.

The electron densities, obtained from the impedance measurements, are shown in Figures 3.02 and 3.03 to be the first order with respect to the RF discharge power density, within our experimental ranges. Higher discharge power increases the gas ionisation and consequently results in a higher electron density. Figures 3.04 and 3.05 show that the effects of discharge power densities, from 0.05 to 0.25 W/cm^2 for Si, and 0.25 to 0.50 W/cm^2 for SiO_2 respectively, on the etch rates. These increase almost linearly with the discharge power density at

lower power. However, the slopes of the etch rates over discharge power density decrease gradually when the discharge power densities are larger than 0.20 W/cm^2 for Si, 0.35 W/cm^2 for SiO_2. The etch rate is enhanced at higher power densities where dissociation of SF_6 is increased, providing a greater number of SF_x and F atom radicals for reactions. In order to understand this interesting phenomenon, the optical system has been employed to obtain the optical emission spectrum of SF_6 plasma. From previously study [78] , the large amounts of fluorine atoms which have been observed in the plasma, indicate that fluorine atoms are one of the most important species contributing to silicon etching. By monitoring the relative intensity of fluorine to argon from optical emission under different discharge power densities, a linear dependence between the etch rate and the fluorine atoms emission intensity has been shown in Figure 3.06 [78]. The etch rate, as already pointed out in a previous study [83], faithfully follow the atomic fluorine concentration. This result seems indicate that, Si/F system exhibits a fluorine multilayers adsorption on silicon [84][85].

In this study the chemical reaction model has been employed to simulate the effects of discharge power on the etch rates of silicon and SiO_2 by SF_6 plasma. Under lower discharge power, the etch rates are first order with respect to the discharge power densities, and under higher discharge power the etch rates are proportional to the square root of discharge power densities. For SF_6 glow discharge, Kline [71] has found that K_1 increases with the ratio of effective electric field to pressure. Impedance measurements, as shown in Figures 3.07 and 3.08, show that the half of peak to peak voltage increases by only 5% and 8% under 0.10 to 0.25 W/cm^2 RF power density for Si, and 0.25 to 0.50 W/cm^2 for SiO_2 respectively, so K_1 is fairly constant within the range of this study. By analysing the experimental data according to the chemical reaction model, one can estimate the rate constants K_1 and K_4. As shown in Figure 3.09, K_1 is calculated to be 2.0×10^{-9} cm^3/s, which is close to the reported theoretical value [71]. The gas phase three body recombination rate constant K_4 is found to be equal to 1.25×10^{-31} cm^3/s. It is believed that the fundamental rate constants obtained from this study will be useful for the comprehensive reactor modelling studies.

The plasma measurements and visual observations indicate that the plasma is homogeneous and well-confined between the electrodes. The thickness of the sheaths is smaller than 0.5 mm for most experimental conditions. The electron density and E/p show small changes with gas flow rate. Electrode gap and RF power density are found to be the most significant parameters that affect electron

density and effective electric field. The responses of electron density to the electrode spacing are shown in Figures 3.10 and 3.11. The electron density increases with the electrodes spacing, which is in agreement with other observation [86]. As the pressure changes, electron densities remain nearly constant within our experimental range. A reduction in pressure always increases the electron energy and the value of E/p, as shown in Figures 3.12 and 3.13. A minimum is reached and E/p begins to rise as pressure is increased further. This is due to a decrease in electron density because of the increased probability of electron attachment reactions [5]. Finally, E/p shows a little reduction with increasing RF power density and very little change with gas flow rate.

The solution of the comprehensive model for the distribution of the etch rates along the central axis are plotted in Figures 3.14 and 3.15 under various SF_6 flow rate. Figures 3.16 and 3.17 show calculated etch rates contours for an entire wafer at 30 and 80 sccm flow rates of SF_6 respectively. At low flow rates, fluorine is depleted from the gas phase. At the high flow rates the local residence time of the gas decreases, and as a result, the local etch rate of Si increases as more SF_6 is dissociated along the reactor length.

The characteristic time of fluorine diffusion, L^2/D_i, is 0.5 sec and the characteristic time of the gas phase reaction, $1/K_1 n_e$, is 0.2 sec. On the other hand, at front side of wafer the residence time of the gas is 0.14 sec at 30 sccm SF_6 flow rate[88]. Therefore, the characteristic times of fluorine atoms diffusion and generation are longer than the residence time of the gas. Thus, under high flow rates, the etch rate is controlled by the gas residence time since the neutral species diffusion is slower than convection.

From impedance measurements, it is empirically known that increasing the gas pressure decreases the value of E/p, and consequently the etch rate decreases, and the etch rate distribution becomes more uniform at higher pressures. The dimensionless Thiele modulus Φ can be obtained from the dimensionless form of equation (3.4-4) [88]

$$\Phi^2 = \frac{L^2 K_i n_e}{D_j} ; \qquad \textbf{(3.5-1)}$$

The Thiele modulus can be physically interpreted as the ratio between the rate of gas phase electron bombardment dissociation and the rate of diffusion. Elementary consideration for achieving uniformity requires the absence of concentration

gradient, therefore the value of the Thiele modulus should be smaller than one for uniform etching to occur. As the pressure decreases from 500 mtorr to 100 mtorr, the Thiele modulus increases from 0.48 to 2.40 because the increasing rate of K_i is larger than the increasing rate of D_j, so better uniformity of etching can be obtained at higher pressures. Figures 3.18 and 3.19 show the effect of the pressure on the etch rate distribution. In this study, etch rates increase almost linearly with pressure, especially at lower power density for silicon and high power density for silicon dioxide. Our experiments are in the low pressure region of their pressure ranges where etch rates increase with pressure. This is consistent with our results. Raman spectroscopy measurements by Hargis and Greenberg [87] showed a significant dropping of the SF_6 dissociation by increasing pressure from 200 mtorr to 600 mtorr. The strong dependence on pressure is consistent with previous observations of the importance of recombination in SF_6 discharge kinetics [87].

Figures 3.20 and 3.21 show the linear increase in etch rate with average electron density. Increasing the discharge power normally increases the electron density, and consequently, dissociation occurs, giving rise to free fluorine. Figures 3.22 and 3.23 show the effects of the electrodes spacing on the etch rates distribution. Over the range of electrodes spacing studied, the resistance of the RF discharge decreases with increasing electrodes spacing. A likely explanation for this result, as mentioned earlier (see equations (3.2-4,5)), involves surface recombination of charged particles. Similar behaviour has been reported by Mlynko and Hess [86]. As the electrodes spacing decreases, the ratio of plasma volume to electrode area decreases resulting in a larger electron recombination probability at the surface of the electrode. Figures 3.22 and 3.23 indicate that the etch rates are usually higher under larger electrodes spacing.

3.6 Conclusions

Etch rates of Si and SiO_2 coated wafers in plasma discharge of SF_6 are measured and modelled as a function of SF_6 flow rate, pressure, RF discharge power density and electrodes spacing. Variations in these variables and parameters have been theoretically and experimentally investigated over a limited parameter space to obtain their effects on the etch rates, uniformities etc. Various etch rates distribution can be explained by the gas residence time and local loading effect. As the pressure changes, electron densities remain nearly constants in our

experimental range and lower etch rates can be obtained at lower pressure. It appears that mechanisms of dissociation and recombination are in competition, with dissociation being dominant at low pressure. Higher RF discharge power gives higher electron density and etch rate. The etch rates increase with electrodes gap due to the increase in electron density.

A comprehensive theoretical reactor model for plasma etching processes, which is described by a set of gas phase and substrate surface reaction equations and the corresponding species concentrations and rate constants, has been developed for the plasma etching with SF_6/Ar in order to predict the reactor behaviour for achieving a desired performance quantities. The generation of this model is a key step both to obtain a basic understanding of the dynamics involved as well as to develop a rational basis for etching process development.

Results presented in this chapter suggest that relatively simple model of plasma etching can be used to make quantitatively predictions and provide a basis for further regression modelling studies for the purpose of controlling the process. Some of the results are consistent with previous studies which can be found from literature. Generally, more uniform etching is achieved by increasing the gas pressure and decreasing the electric discharge power. The success of this overall model with particular emphasis on the comprehensive modelling of the plasma etching depends on accurate knowledge of fundamental electron collision cross sections, some of which are not known and are difficult to determine experimentally. Additional information concerning electron density distribution, electric field distribution, and surface recombination probability is needed for a more detailed modelling. The incorporation of such models with similar modules which describe the plasma and surface chemistry show promise in predictively modelling plasma processes. The development of predictive model has the potential for improving our ability to control and optimise plasma etching processes.

Table 3.1 Range of Process Manipulated Variables Used in the Comprehensive Reactor Model

Model I Using Si Wafer

Manipulated Variables	Range
Chamber Pressure	90-250 mtorr
RF Power Density	0.05-0.25 W/cm^2
SF_6 flow rate	10.0-30.0 sccm
Electrode spacing	1.0-4.0 cm

Model I Using SiO_2 Wafer

Manipulated Variables	Range
Chamber Pressure	100-300 mtorr
RF Power Density	0.30-0.50 W/cm^2
SF_6 flow rate	10.0-30.0 sccm
Electrode spacing	1.0-4.0 cm

Table 3.2 Main Gas Phase and Surface Reactions for Plasma Etching of Silicon and SiO_2 in SF_6

Gas phase reactions:	$e + SF_{x(g)} \xrightarrow{K_{7-x}} SF_{x-1(g)} + F_{(g)}$; $(x = 3 \rightarrow 6)$
Si wafer surface reactions: (Rate Limiting)	$SF_{x(g)} + \frac{1}{4} Si \xrightarrow{K_5} \frac{1}{4} SiF_{4(g)} + SF_{x-1(g)}$; $(x = 5 \rightarrow 3)$ $SiF_{x-1(g)} + F_{(g)} \xrightarrow{K_5} SiF_{x(g)}$; $(x = 1 \rightarrow 4)$
SiO_2 wafer surface reactions: (Rate Limiting)	$SF_{x(g)} + SiO_2 \xrightarrow{K_6} SiF_{4(g)} + SO_2 + SF_{x-1(g)}$; $(x = 5 \rightarrow 3)$ $SiF_{x-1(g)} + F_{(g)} \xrightarrow{K_6} SiF_{x(g)}$; $(x = 1 \rightarrow 4)$
On aluminium electrode surfaces:	$SF_{x(g)} \longrightarrow SF_{x(s)}$; $SF_{x-1(s)} + F_{(g)} \xrightarrow{K_7} SF_{x+1(g)}$; $(x = 2 \rightarrow 5)$

Table 3.3 Parameters Used in the Comprehensive Reactor Model

Reactor Dimension	w = 20.30 cm, L = 20.30 cm
Kinetic Parameters	K_1=K_2=K_3 =2.0 x 10^{-9} cm^3/s; [71] K_4= 1.25 x 10^{-31} cm^3/s ; K_5=25.0 x $(T_e/298.0)^{1/2}$ x exp(4.2-1253/T_e) cm/s;[77] K_6 = K_5 ; (experimental results) K_7 = 4.14 cm/s; [80]
Gas Temperature	T = 298 °K
Neutral Species Diffusivities	D_{SF_6} = 56.1 x (0.5/P_{torr}) cm^2/s D_{SF_5} = 61.0 x (0.5/P_{torr}) cm^2/s D_{SF_4} = 71.8 x (0.5/P_{torr}) cm^2/s D_{SF_3} = 87.7 x (0.5/P_{torr}) cm^2/s D_{SF_2} = 111.9 x (0.5/P_{torr}) cm^2/s) D_{SF} = 152.3 x (0.5/P_{torr}) cm^2/s D_F = 623.0 x (0.3/P_{torr}) cm^2/s D_{SiF_4}=75.0 x (0.5/P_{torr}) cm^2/s

The neutral species diffusivities can be obtained from the equation

D_i = rate constant x (0.5/P_{torr}) cm^2/s [71][77]

where

the rate constant = μ_p $[N_i](K_B T_e/e)$; [71]

μ_p = the electron mobility, $2x10^5$ $cm^2 \cdot torr/V \cdot sec$; [74]

$[N_i]$ = the mole concentration of species i;

K_B = Boltzman constant [2];

T_e = the electron temperature [2];

e = the charge of an electron, 1.602 x 10^{-9} columb.

The effective electrode field : $A_{eff} = \pi r^2 \approx 176.7$ cm^2.

The electrode diameter : 2r = 17.75 cm.

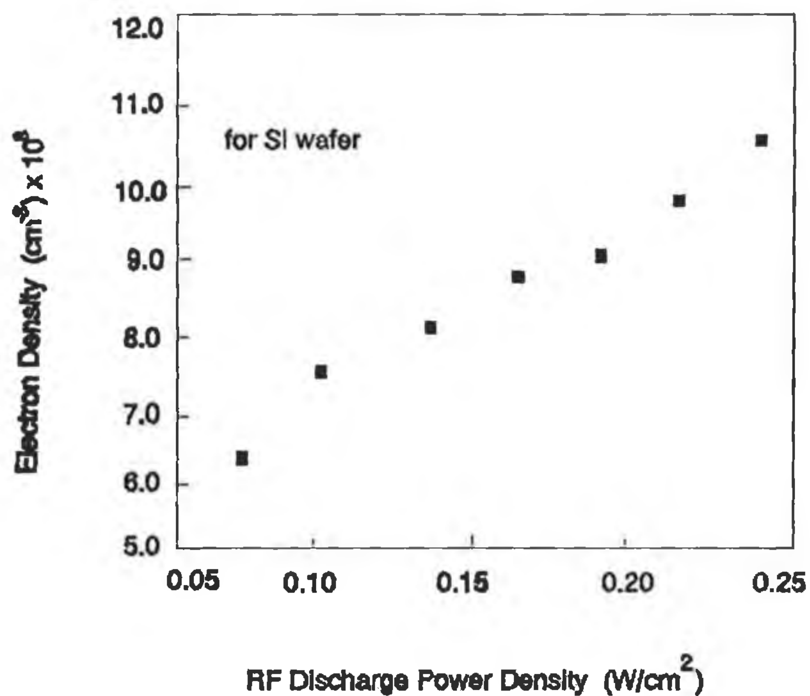

Figure 3.02 Electron Density on RF Discharge Power Density on **Si Wafer**

Electrode spacing = 2.0 cm,
Pressure = 200 mtorr,
SF_6 flow rate = 30 sccm + 4% Ar,
Etching gases: SF_6/Ar.
Results obtained from Eqn(3.2-4)

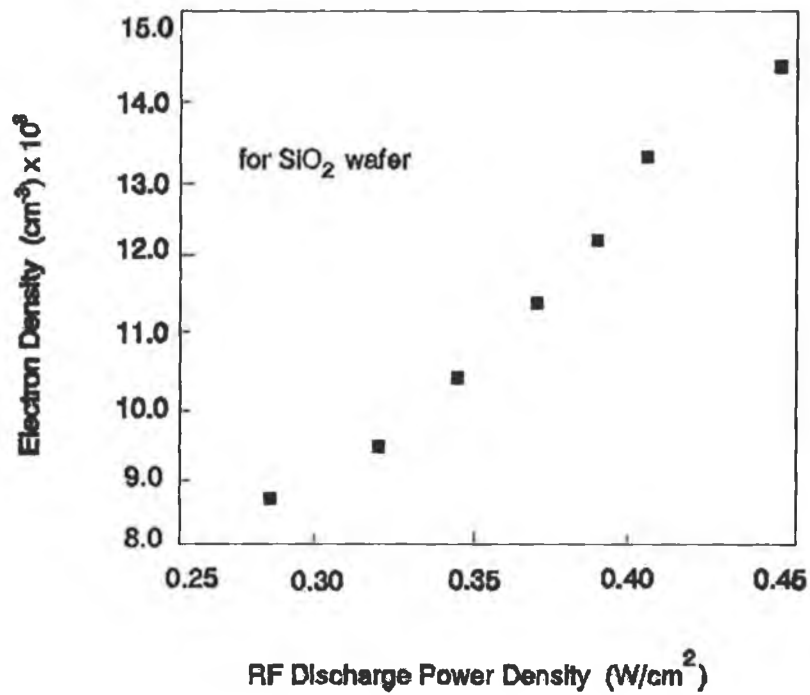

Figure 3.03 Electron Density on RF Discharge Power Density on SiO_2 Wafer

Electrode spacing = 2.0 cm,
Pressure = 250 mtorr,
SF_6 flow rate = 30 sccm + 4% Ar,
Etching gases: SF_6/Ar.
Simulation results obtained from Eqn(3.2-4)

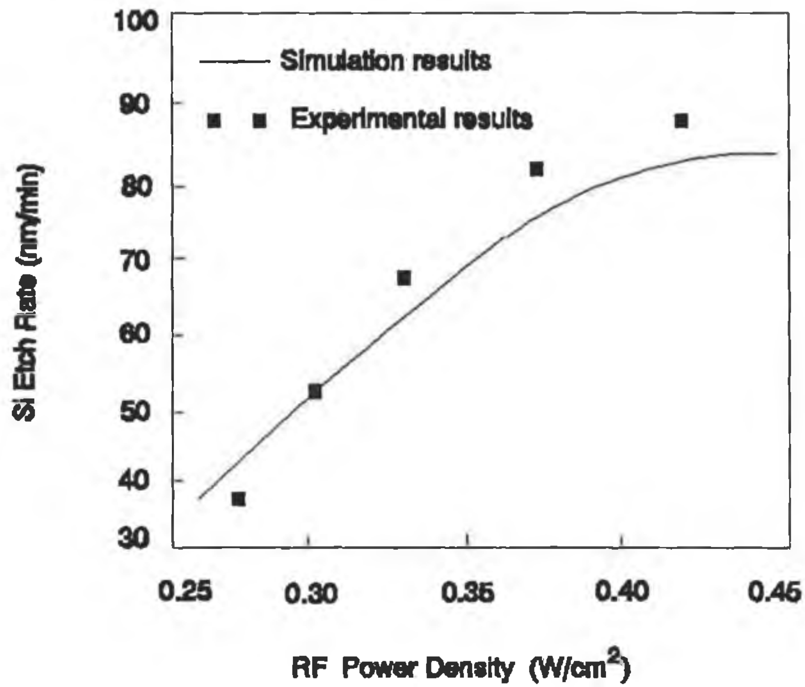

Figure 3.04 Dependence of Si Etch Rate on RF Discharge Power Density

Electrode spacing = 2.0 cm,
Pressure = 200 mtorr,
SF_6 flow rate = 30 sccm + 4% Ar,
Etching gases: SF_6/Ar.

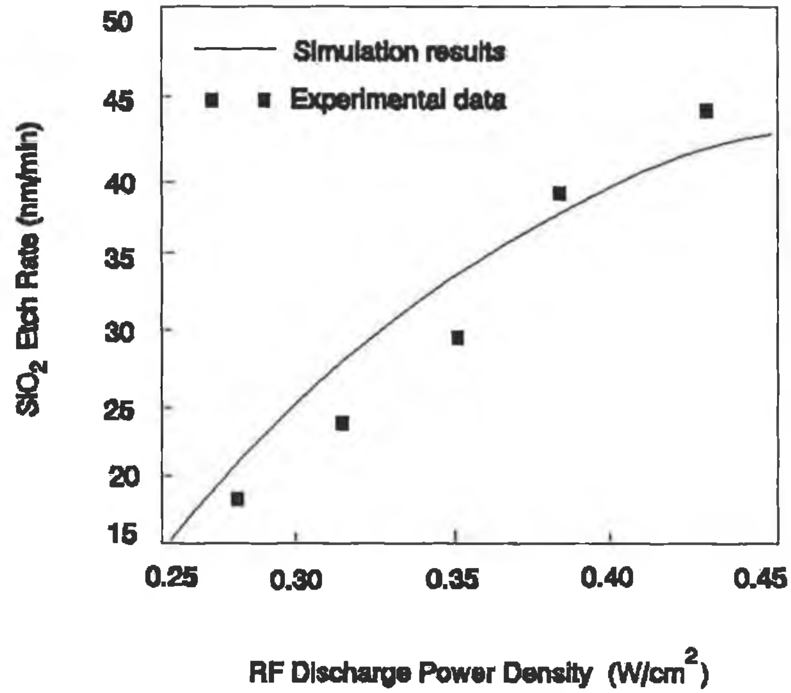

Figure 3.05 Dependence of SiO_2 Etch Rate on RF Discharge Power Density

Electrode spacing = 2.0 cm,
Pressure = 250 mtorr,
SF_6 flow rate = 30 sccm + 4% Ar,
Etching gases: SF_6/Ar.

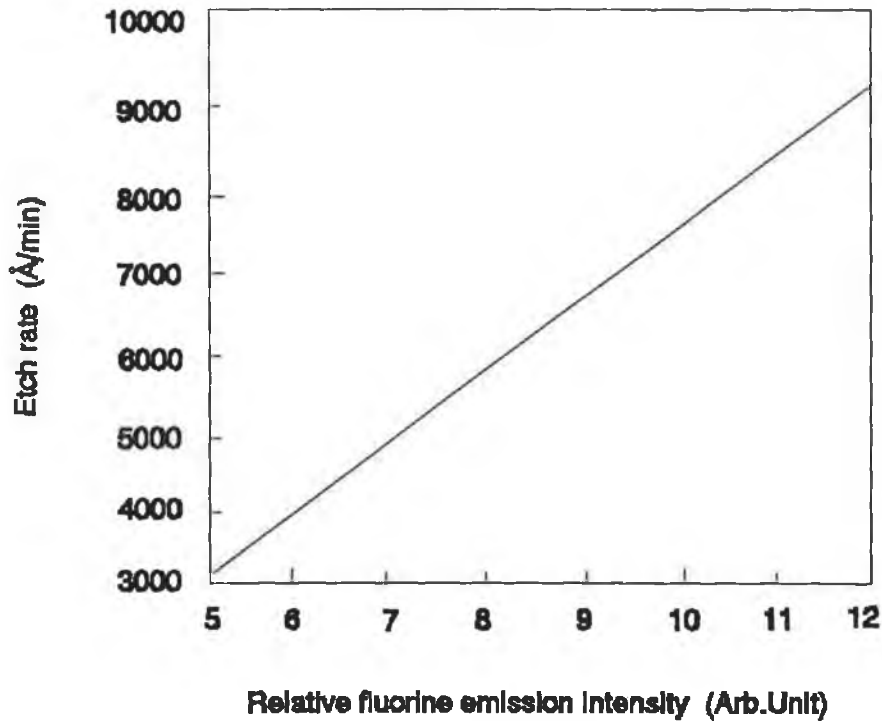

Figure 3.06 Dependence of Etch Rate on Relative Fluorine Atom Emission Intensity [78]

Electrode spacing = 2.0 cm,
Pressure = 250 mtorr,
SF_6 flow rate = 30 sccm + 4% Ar,
Etching gases: SF_6/Ar.

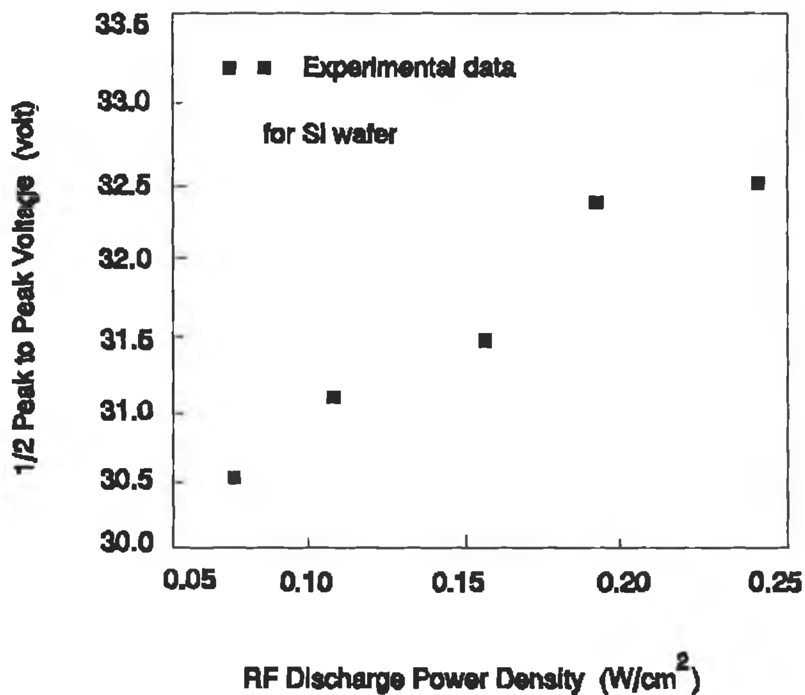

Figure 3.07 Dependence of Half Peak to Peak Voltage on RF Discharge Power Density on Si Wafer

Electrode spacing = 2.0 cm,
Pressure = 200 mtorr,
SF_6 flow rate = 30 sccm + 4% Ar,
Etching gases: SF_6/Ar.

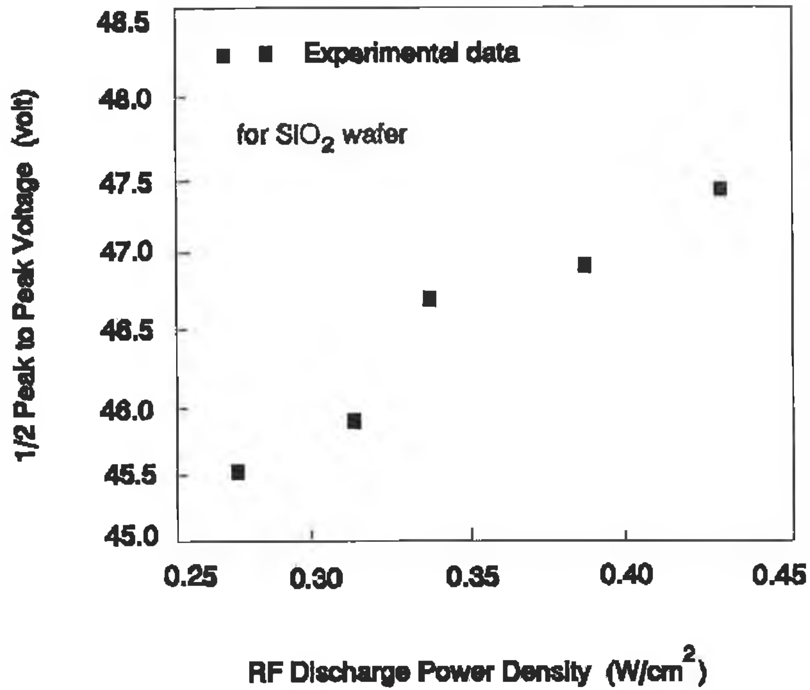

Figure 3.08 Dependence of Half Peak to Peak Voltage on RF Discharge Power Density on SiO_2 Wafer

Electrode spacing = 2.0 cm,
Pressure = 250 mtorr,
SF_6 flow rate = 30 sccm + 4% Ar,
Etching gases: SF_6/Ar.

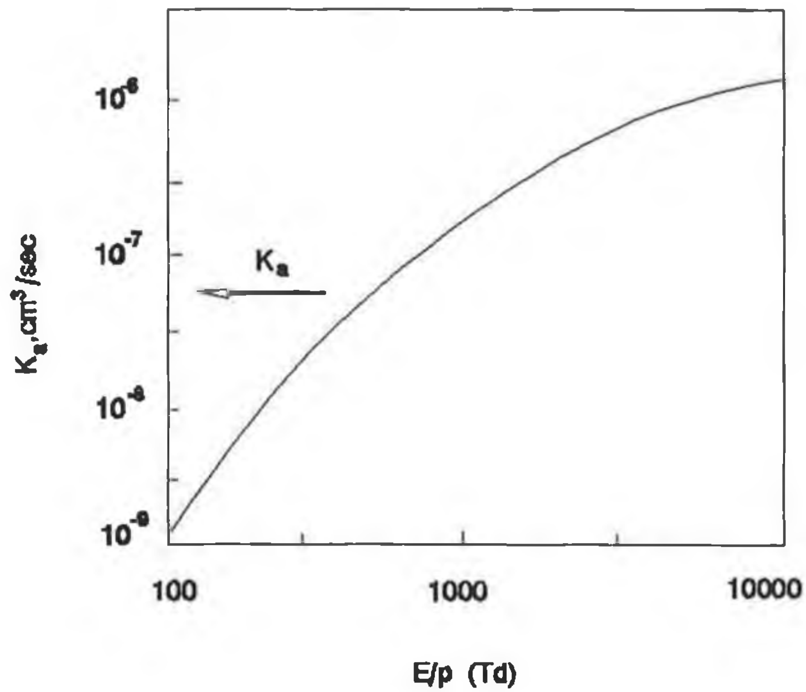

Figure 3.09 Dependence of Rate Constant of Dissociation on E/p in SF_6 Plasma [71]

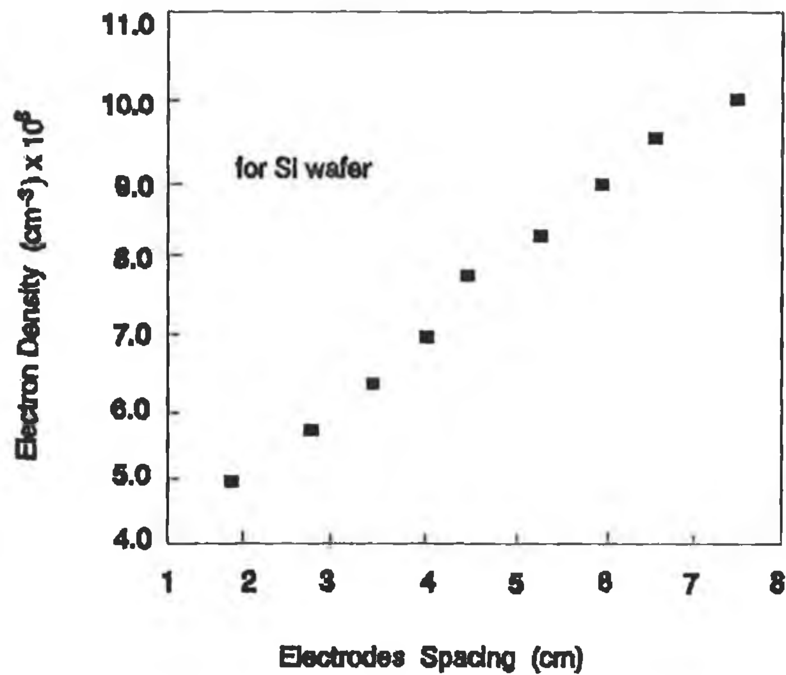

Figure 3.10 Electron Density vs. Electrodes Spacing on Si Wafer

RF power density = 0.17 W/cm^2,
Pressure = 200 mtorr, A=176.7 cm^2;
SF_6 flow rate = 30 sccm + 4% Ar,
Etching gases: SF_6/Ar.
Results obtained from Eqn.(3.2-4);
The measurements of Stray Impedance can be found from Appendix IV

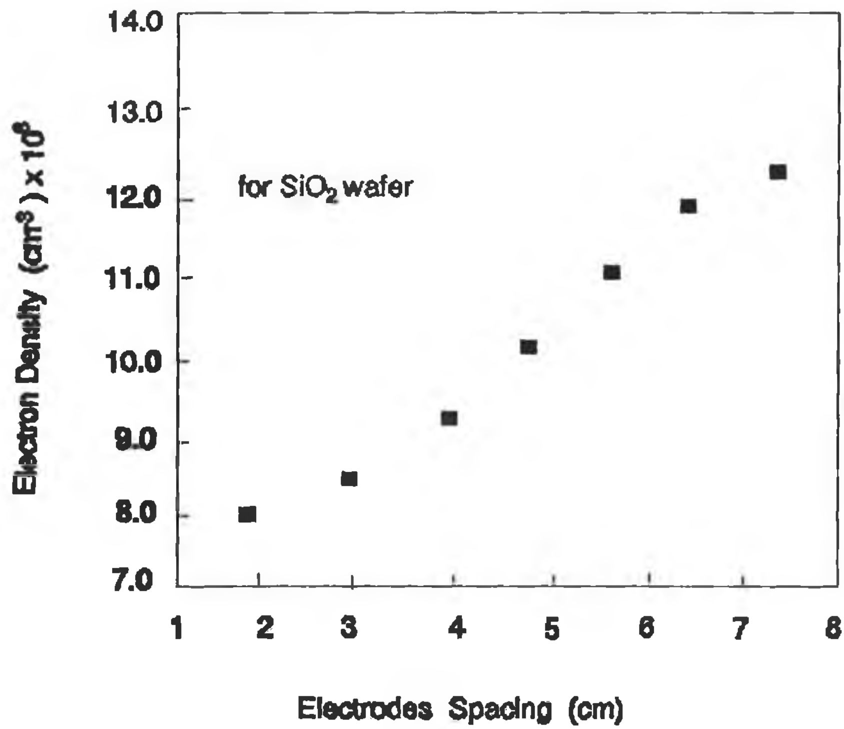

Figure 3.11 Electron Density vs. Electrodes Spacing on SiO_2 Wafer

RF power density = 0.35 W/cm^2,
Pressure = 250 mtorr,A=176.7 cm^2;
SF_6 flow rate = 30 sccm + 4% Ar,
Etching gases: SF_6/Ar.
Results obtained from Eqn(3.2-4) and Appendix IV

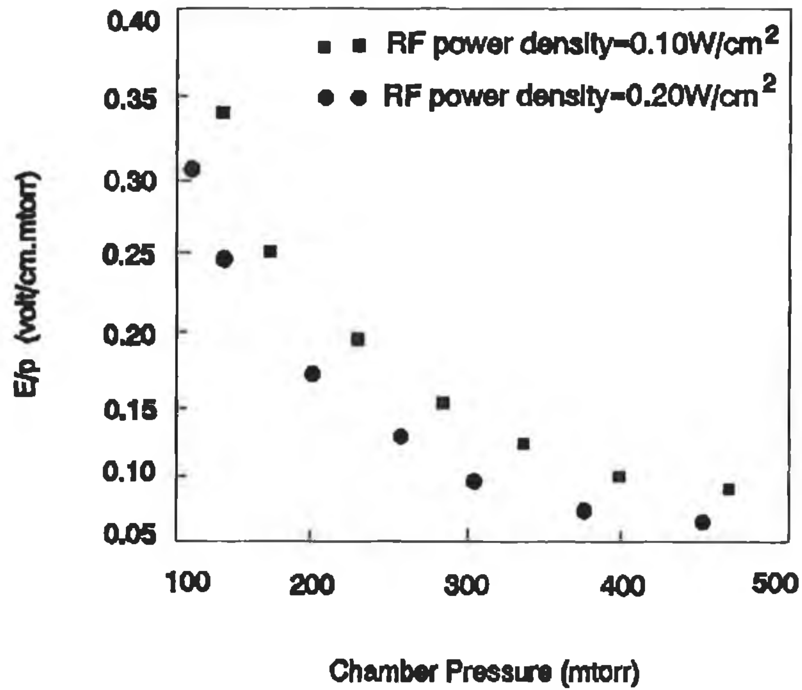

Figure 3.12 The Electric Field to Pressure Ratio on Chamber Pressure Under Various RF Discharge Power Densities on Si Wafer

Electrode spacing = 2.0 cm,
SF_6 flow rate = 30 sccm + 4% Ar,
Etching gases: SF_6/Ar.
Results obtained from Eqn.(3.2-5) and Appendix IV.

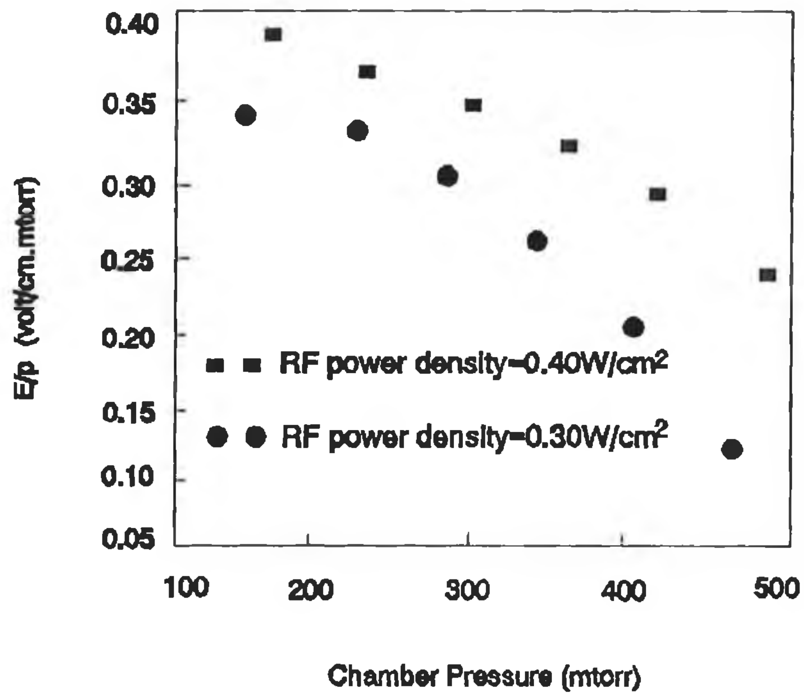

Figure 3.13 The Electric Field to Pressure Ratio on Chamber Pressure Under Various RF Discharge Power Densities on SiO_2 Wafer

Electrode spacing = 2.0 cm,
SF_6 flow rate = 30 sccm + 4% Ar,
Etching gases: SF_6/Ar.
Results obtained from Eqn(3.2-5) and Appendix IV

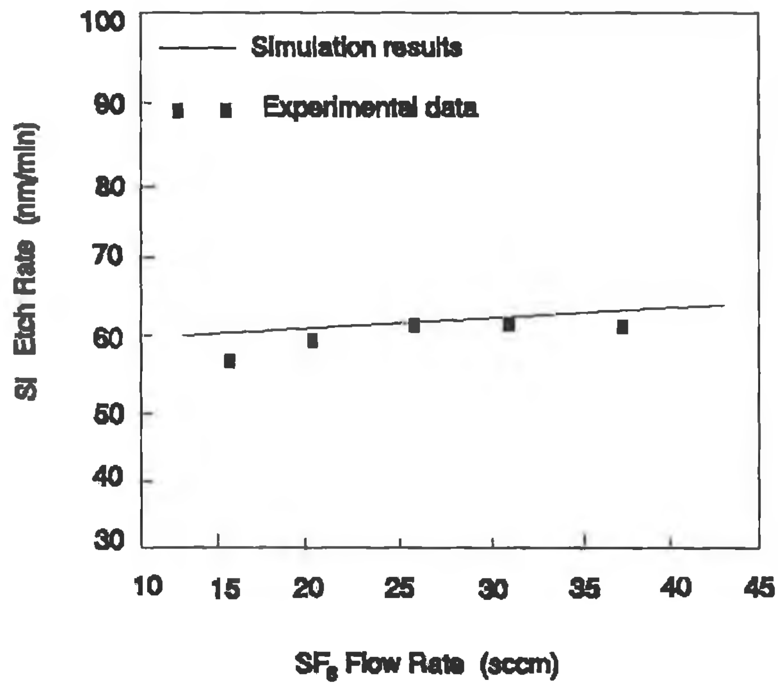

Figure 3.14 Si Etch Rate Distribution Under Various SF_6 Flow Rates

Electrode spacing = 2.0 cm,
RF power density = 0.15 W/cm^2 ,
Etching gases: SF_6 + 4% Ar,
Pressure = 200 mtorr.

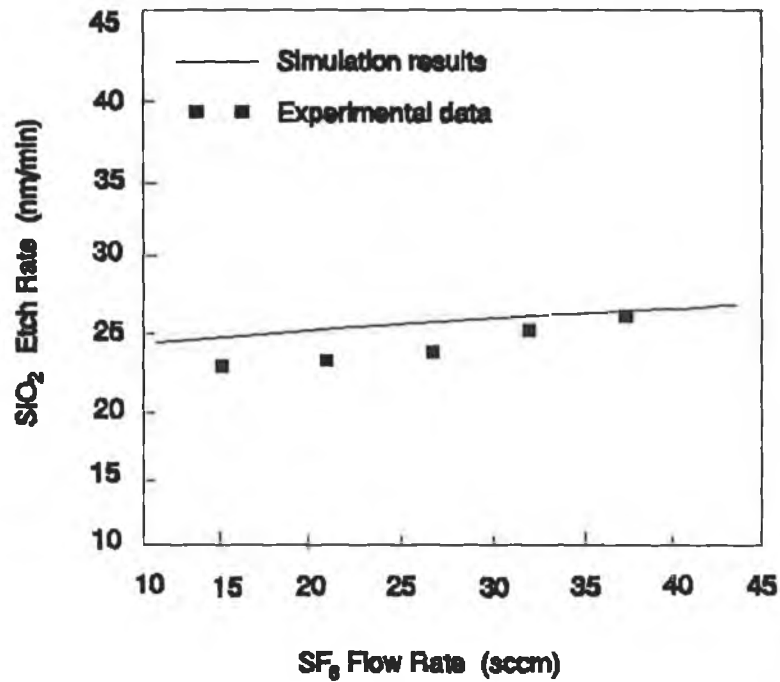

Figure 3.15 SiO_2 Etch Rate Distribution Under Various SF_6 Flow Rates

Electrode spacing = 2.0 cm,
RF power density = 0.35 W/cm^2 ,
Etching gases: SF_6 + 4% Ar,
Pressure = 250 mtorr.

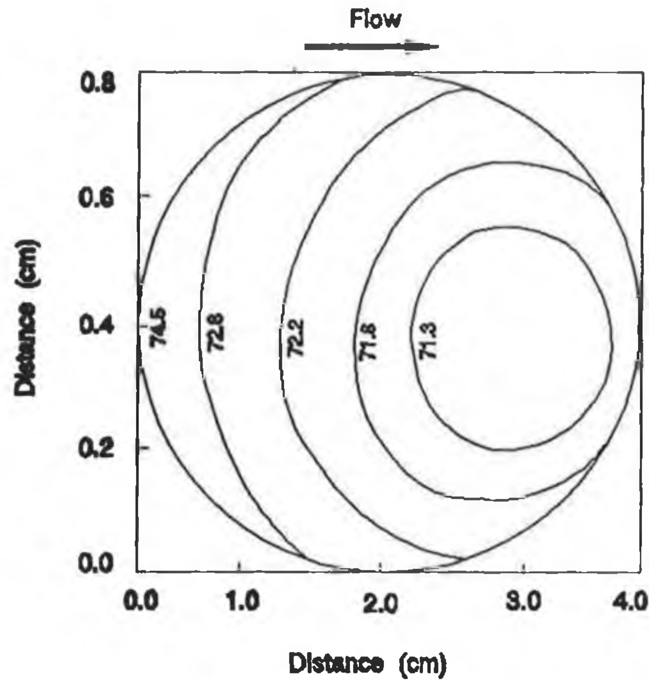

Figure 3.16 Contour Plot of Calculated Etch Rate (nm/min) over a Si wafer

Electrode spacing = 2.0 cm,
RF power density = 0.20 W/cm^2 ,
Etching gases: SF_6 + 4% Ar,
SF_6 flow rate = 30 sccm,
Pressure = 200 mtorr.

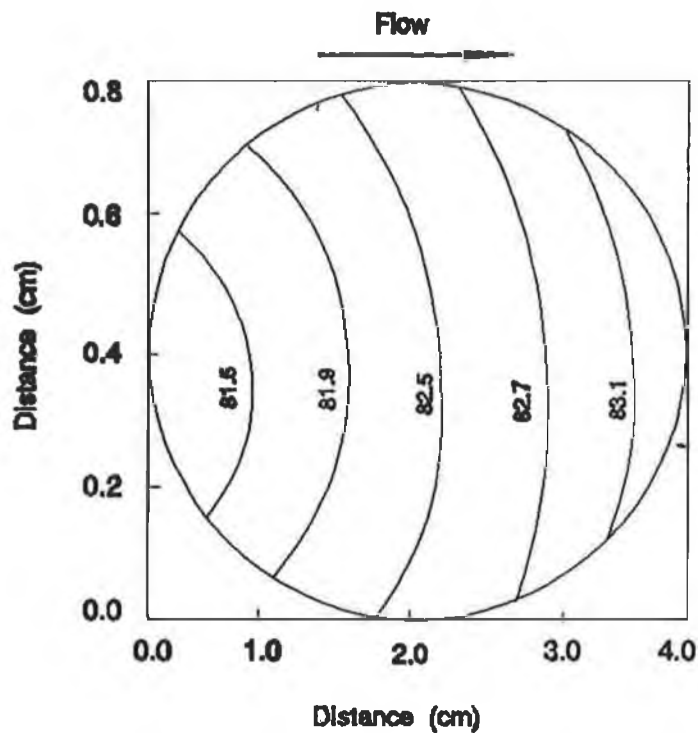

Figure 3.17 Contour Plot of Calculated Etch Rate (nm/min) over a Si wafer

Electrode spacing = 2.0 cm,
RF power density = 0.20 W/cm^2 ,
Etching gases: SF_6 + 4% Ar,
SF_6 flow rate = 80 sccm,
Pressure = 200 mtorr.

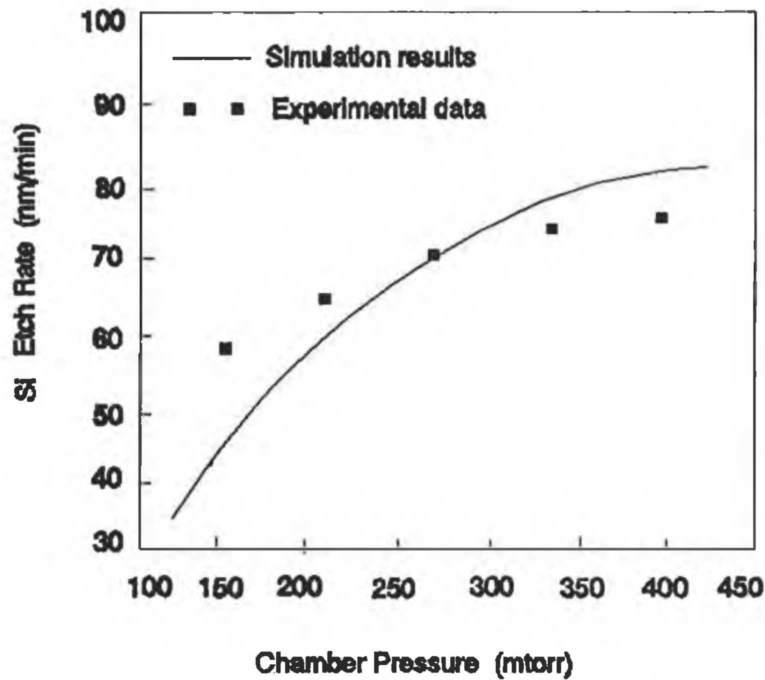

Figure 3.18 The effect of chamber pressure on Si etch rate in SF_6/Ar System

Electrode spacing = 2.0 cm,
RF power density = 0.20 W/cm^2 ,
Etching gases: SF_6 + 4% Ar,
SF_6 flow rate = 30 sccm,

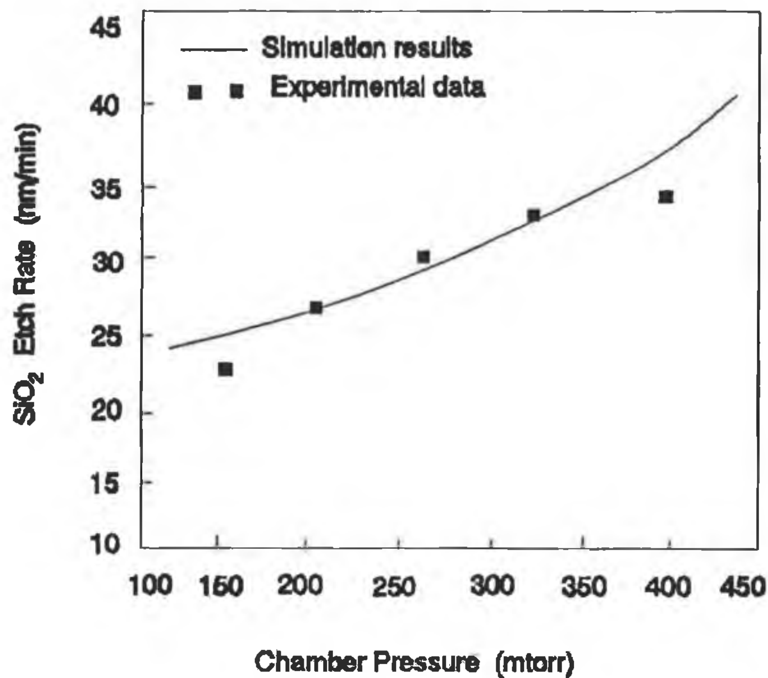

Figure 3.19 The effect of Chamber Pressure on SiO_2 Etch Rate in SF_6/Ar System

Electrode spacing = 2.0 cm,
RF power density = 0.35 W/cm^2 ,
Etching gases: SF_6 + 4% Ar,
SF_6 flow rate = 30 sccm,

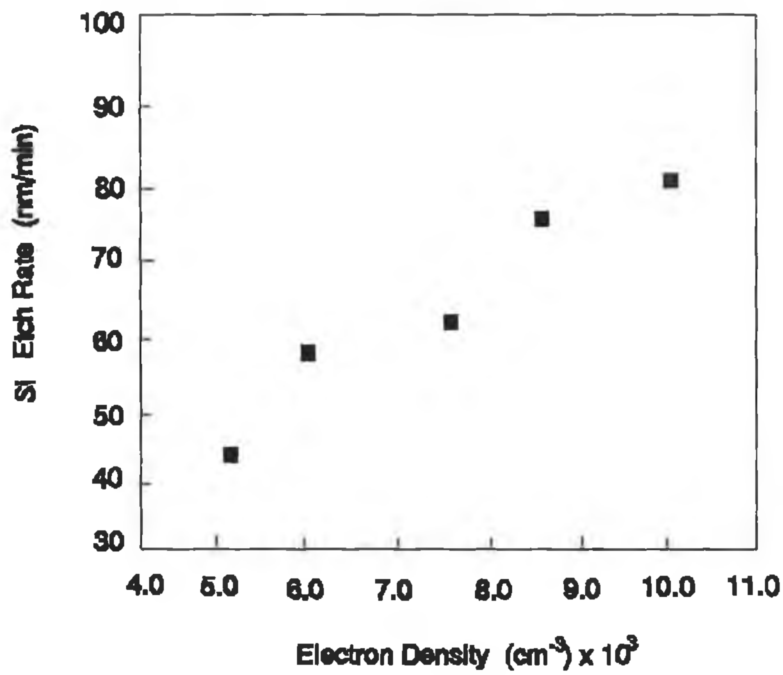

Figure 3.20 Si Etch Rate Distribution on Electron Density

Electrode spacing = 2.0 cm,
Etching gases: SF_6 + 4% Ar,
SF_6 flow rate = 30 sccm,
Pressure = 200 mtorr.

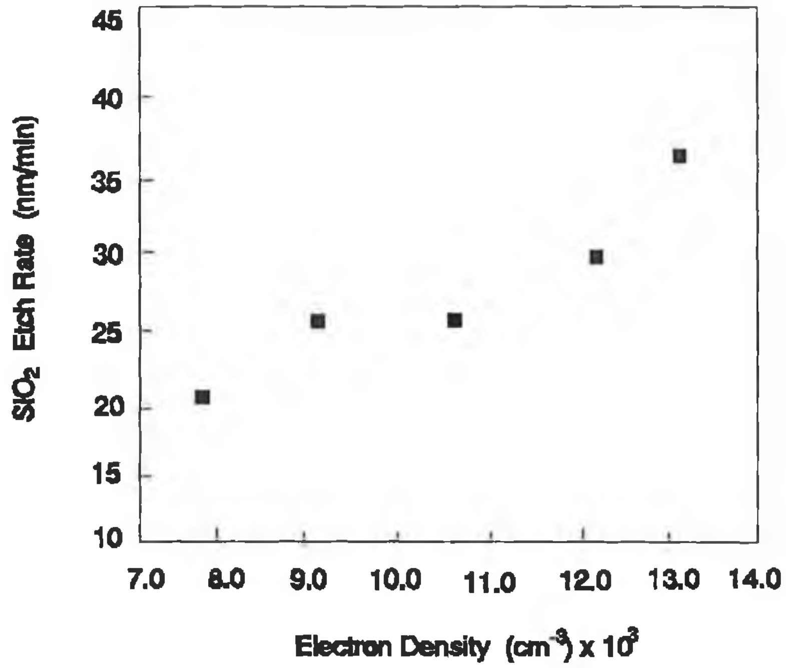

Figure 3.21 SiO_2 Etch Rate Distribution on Electron Density

Electrode spacing = 2.0 cm,
Etching gases: SF_6 + 4% Ar,
SF_6 flow rate = 30 sccm,
Pressure = 250 mtorr.

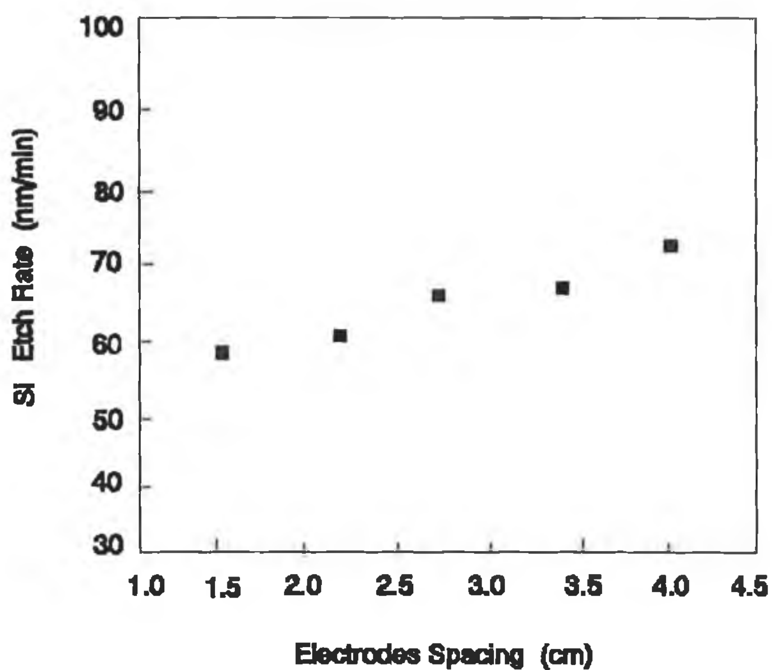

Figure 3.22 Si Etch Rate Distribution under Various Electrodes Spacing

RF power density = 0.17 W/cm^2 ,
Etching gases: SF_6 + 4% Ar,
SF_6 flow rate = 30 sccm,
Pressure = 200 mtorr.

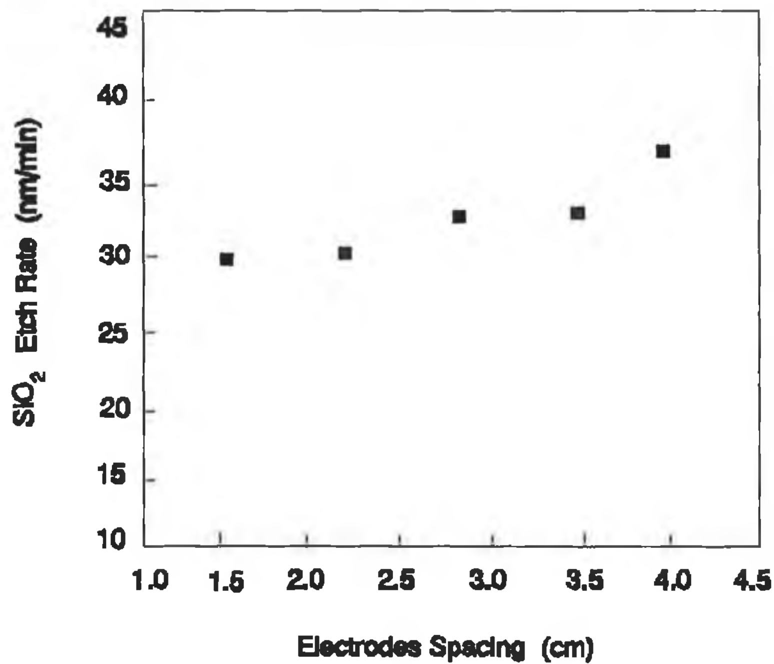

Figure 3.23 SiO_2 Etch Rate Distribution under Various Electrodes Spacing

RF power density = 0.35 W/cm^2 ,
Etching gases: SF_6 + 4% Ar,
SF_6 flow rate = 30 sccm,
Pressure = 250 mtorr.

CHAPTER 4 MULTIVARIABLE REGRESSION ANALYSIS AND MODELLING

4.1 Introduction

The comprehensive reactor model devised in this study describes the dynamics of the plasma etching process but would be difficult to apply in real-time control because of the complexity of the model structure. Thus, it is necessary to develop a relatively simple model suitable for control algorithm design.

This chapter is concerned with selecting process and performance variables to characterise the system structure. In order to maintain the integrity of the etching environment, it was decided initially that non-intrusive techniques, as discussed in Chapter 2, would be used for process variable estimation. This provides a limitation as to which process variables could be studied and how they could be estimated or inferred. Optical emission spectroscopy was chosen as a promising means of calculating the concentrations of plasma active species without perturbing the plasma chamber. Estimation of plasma species concentrations and inference of the electron energy of the system are chosen as process variables. Etch rate of silicon, uniformity and anisotropy of this etch process are the measures of process performance. In addition, some of the etching performance quantities on the SiO_2 wafer are included for completeness.

There have been many experimental and theoretical examinations of the processes explored in this research, but a comprehensive study which explores the etch phenomena using the statistical approach of experimental design and response surface methodology has not been made. This technique allows the many results produced in other research to be verified and unified in one set of experiments. The regression equations resulting from the composite experimental design and response surface analysis and the comprehensive reactor modelling studies allow two sets of correlations to be made directly. Results are then compared in a coherent fashion to the existing data which allows various etch mechanisms to be evaluated based on these results. The inputs, or factors, of this design are the manipulated variables, such as RF power density, chamber pressure and SF_6 flow rate, whose values can be set independently of one another. There are two distinct sets of outputs, the

values of the process variables and the values of the performance variables. The set of equations relating the manipulated variables to each of these forms a steady state regression model for the control system simulation of the SF_6/Ar plasma etching. Process dynamics for the manipulated variable-process variable relationships are then studied to complete the necessary process information.

4.2 Selection of Process Variables

One of the initial constraints of this research is that the monitoring techniques used be non-intrusive. This can be quite limiting in the measurement of plasma characteristics, but it is felt that sufficient information for control of a plasma etching reactor could be found from observation of the plasma without perturbing it. As a result of this restriction, we concentrate heavily on the use of optical emission spectrometry. The relative percent concentration of the plasma species could be estimated based on the different wave length distribution.

As discussed in Chapter 3, the etch rate of silicon is proportional to fluorine atom density. It is commonly suggested in the literature, and in our previous studies, that the highest wave length lines of fluorine and argon be used.

SF_{x-1} ($x=3 \rightarrow 6$) radicals have also been suggested as an etchant of Si and SiO_2 based on our previous plasma chemistry studies (see Table 3.2) [71], although the roles of these species are less well-known. The difficulty encountered here is in finding the specific value of x due to the limitation of our optical system. In this study, all molecule of SF_x are involved. From the gas phase and surface reaction equations the concentration of SF_x can be calculated. Thus $[SF_x]$ can be selected as a process variable.

Average electron energy is correlated with E/p, the electric field to pressure ratio, as discussed in Chapter 3. Zarowin et al [89], among others, have put forth this correlation and have likewise shown that E/p relates to ion energy, i.e. the degree of ion bombardment in the system. This is directly related, according to [89],

to the degree of anisotropy of an etch process. E/p can also be obtained from the equation (3.2-5) based on impedance measurements. So measurement of E/p is a useful choice as a process variable for the SF_6/Ar system.

In summary, process variables are chosen for the non-intrusive nature of their measurements, plasma impedance measurements, main gas phase and surface reaction analysis, and their relationships to process performance quantities.

4.3 Multivariable Regression Analysis and Modelling

The experimental designs are run as described in Chapter 2 and are based on some of data from Chapter 3. The data is analyzed using the stepwise regression routine in Matlab. A stepwise regression "builds" an algebraic regression equation by examining each available independent variable at each step and determines which variable contributes most to the regression equation by checking a user-specified entrance criterion, the F-to-enter value [90]. A partial F correlation is made on each available variable. The F test for each variable X_i is based on the ratio of the mean square of X_i to the mean square of the model residual with X_i in the model [40]. The variable with the highest partial F, if greater than the F-to-enter value, is added to the equation. Linear regression is used to determine the coefficient on each variable. Also at each step, the variables already in the regression equation are rechecked to see if they meet the F-to-remain criterion, also user specified. If any do not, they are removed from the regression equation. This process is continued until there are no more variables eligible for entry in the equation and all variables in the equation meet the F-to-remain requirements. An adjusted R^2 correlation of fit, normalised to the number of degrees of freedom in the equation, is calculated to determine the quality of fit of the resulting equation [90].

The nominal F-to-enter used in this study is 4, corresponding to a 95-99% significance level based on the number of degrees of freedom in the equation. This provides good results in all but a few of the correlations where an adequate fit could not be made with this requirement. In these cases, the F-to-enter requirement is relaxed to as low as 2, representing an approximately 90% significance level of the incoming variable. In this way, only variables which met this requirement of statistical significance are included in the regression equations. While statistical

significance does not imply causality, it does provide an initial screening of the independent variables. The regression equations can then be examined more easily with respect to a mechanistic understanding of the system and evaluated on this basis. Most of the process variables and many of the performance variables could be correlated to an adjusted R^2 of 0.85 or higher, allowing quantitative prediction of the variables behaviour within the range of study. Several more have adjusted R^2 coefficients of greater than 0.8, indicating a knowledge of trends in these areas but not allowing quantitative predictions.

The results of regressions will be shown in the following sections, the manipulated/process variable correlations and the manipulated/performance variable correlations and then the process/performance variable correlations. The results will be shown in the form of contour plots which allow the dependent variable to be viewed with respect to each two of the independent variables. This is necessary in order to view the two-factor interactions which the experimental designs are set up to reveal. Three-factor and higher order interactions are assumed to be negligible in this work, so contour plots should provide all of the necessary insight into the results. In each contour plot, the independent variables not shown are held at their centre point levels (see Table 2.4). The regression equations themselves can be developed in the following sections.

4.3.1 Development of Regression Model

One of the main objectives of this research is to develop control systems suitable for application to the plasma etching process. By developing regression equations relating the manipulated variables for this system to both the process and performance variables based on the composite experimental design and statistical analysis, a steady-state model of the etching process has been created as following:

$$\begin{bmatrix} Y_1 \\ \\ Y_2 \\ \\ Y_3 \end{bmatrix} = \begin{bmatrix} \frac{K_{11}e^{-\tau_{11}s}}{T_{11}S+1} & \frac{K_{12}e^{-\tau_{12}s}}{T_{12}S+1} & \frac{K_{13}e^{-\tau_{13}s}}{T_{13}S+1} \\ \\ \frac{K_{21}e^{-\tau_{21}s}}{T_{21}S+1} & \frac{K_{22}e^{-\tau_{22}s}}{T_{22}S+1} & \frac{K_{23}e^{-\tau_{23}s}}{T_{23}S+1} \\ \\ \frac{K_{31}e^{-\tau_{31}s}}{T_{31}S+1} & \frac{K_{32}e^{-\tau_{32}s}}{T_{32}S+1} & \frac{K_{33}e^{-\tau_{33}s}}{T_{33}S+1} \end{bmatrix} \cdot \begin{bmatrix} u_1 \\ \\ u_2 \\ \\ u_3 \end{bmatrix} ;$$

(4.3.1-1)

$$\begin{bmatrix} Y_1 \\ Y_2 \\ Y_3 \end{bmatrix} = \begin{bmatrix} [F] \\ [SFx] \\ [E/p] \end{bmatrix} ; \qquad \begin{bmatrix} u_1 \\ u_2 \\ u_3 \end{bmatrix} = \begin{bmatrix} \textit{Chamber}\text{ Pressure} \\ \text{RF Power Density} \\ SF_6 \text{ Flow Rate} \end{bmatrix} ;.$$

Where K_{ij}, $T_{i,j}$, τ_{ij}, are the process steady state gains, time constants and time delay constants respectively. This model can be used to determine an operating strategy for a process. First, performance criteria for the etch must be defined by setting desired values for the performance variables. The necessary levels of the manipulated variables are then calculated by means of the model relationships. It should be noted that some control strategies, i.e. relative gain array, can only be used for square system. So some choice have been made as to which performance variables are to be specified and which ones are less important for a given etch. Also, the manipulated variables are constrained to lie within the defined operating space for the model to be valid. Thus, an arbitrary set of operating conditions may not satisfy these constraints. Once these requirements have been met, the process could be run by setting the manipulated variables at the levels determined by the model, ignoring the process variables entirely. This is the common practice in plasma processing today. There are, however, flaws inherent in this method, It is not possible to measure all of the performance variables directly, so a feedback control system based on these variables cannot be used to react to varying etch conditions during a process or changing reactor conditions over an extended period of reactor use. This is the reason for inclusion of process variables in the reactor modelling studies. Given the levels of the manipulated set from the model, necessary levels of the process variables can be directly calculated, also through the model. Control of the process variable forms the basis of the process control system.

The regression equations were first scaled so that both inputs and outputs are on the same scale. This is necessary for proper application of SVD analysis or other control strategies, such as robust control etc., which are known to be scale-dependent. The resulting regression equations are scaled to lie in the specific range (i.e., -2 to 2), both inputs and outputs. These equations are non-linear, so it is necessary for them to be linearized for determination of the appropriate steady state gains. The equations are linearized about a point slightly away from the centre of the variable space. The linearization is performed not at the centre point since SF_6 flow rate appears only in interaction terms of the regressions and would not appear in a linearization about the centre point. This is due to the fact that the centre point of the variable space is scaled to zero, and interaction terms vanish under these circumstances. The steady state gain K_{ij} between output i and input j with all loops open can then be determined from these regression equations:

$$K_{ij} = \partial y_i / \partial u_j \Big|_{u_{k,\, k \neq j}} ; \qquad \textbf{(4.3.1-2)}$$

Dynamics within a plasma are known to be quite fast. Electrons react to the alternating current from the RF generator on a time scale similar to the plasma frequency in our case. Free radicals and ions respond more slowly than electrons due to their far greater mass, but the time scale for movement of material and chemical reactions in a plasma are short, on the order of fractions of a second to several seconds for typical processes. The actual time constants are not well known, but it is expected that these will be too small to be treated by a process control system. In most cases transients can be ignored and only steady states will be managed in a control system applied to a plasma etching reactor. However, some understanding of the relative magnitudes of these time constants is necessary for control system simulation and evaluation of potential control algorithms. It is with this in mind that the following experiments are run.

Step changes of ±0.05 W/cm^2, ± 50 mtorr, and ± 5 sccm are made to the plasma for RF power density, pressure and SF_6 flow rate respectively at steady state (see Tables 2.3,2.4). For these experiments the composite design techniques are also employed and only spectral variables are studied. Measurements of the plasma parameters employed in the comprehensive reactor model and the calculations of the process variables are made during these steps to estimate the time constants for the systems based on the spectral data, which are recorded at minimum acquisition time (1.0 sec), the closest approximation to real-time available. It is commonly suggested in the literature that the highest wave length lines of fluorine and argon be used. The

relative percent concentration of the plasma species [F] and [SF_x] could be estimated based on the different wave length distribution. As an example, the time constant for the pairing [F] -- RF power density can be obtained from the measurement of the time taken by the strongest wave length line of fluorine to reach 63.2% of its final value after an open-loop step is made (Fig.400). The time constants estimated here are not very accurate but they represent order of magnitude estimates. They are meant to show the relative differences between the responses of the process variables. The multivariable control analysis will be based on analysis of steady state process information, but time constants are added to reflect qualitative dynamics for the process studied.

The time constants estimated from the different step changes for the SF_6/Ar system can be found in Table 4.1. Numbers marked an asterisk(*) are not measured during the experimentation and are later estimated for use in the simulations. The steady state gains determined from the regression model can be found from Table 4.2. The time delay constants τ_{ij} are very much smaller than process time constants. Probably it could be ignored at first stage and studied later.

The steady state gains determined from these equations are combined with the time constants to create regression steady state model for the SF_6/Ar system.

Table 4.1 Time Constants (minutes) for the SF_6/Ar System

for Si wafer	RF Power Density	Pressure	SF_6 Flow Rate
[F]	0.20	0.40	0.40(*)
[SF_x]	0.12	0.40	0.40(*)
E/p	0.15(*)	0.40(*)	0.40(*)

Note: Numbers marked with an asterisk (*) are estimated from other constants in the system.

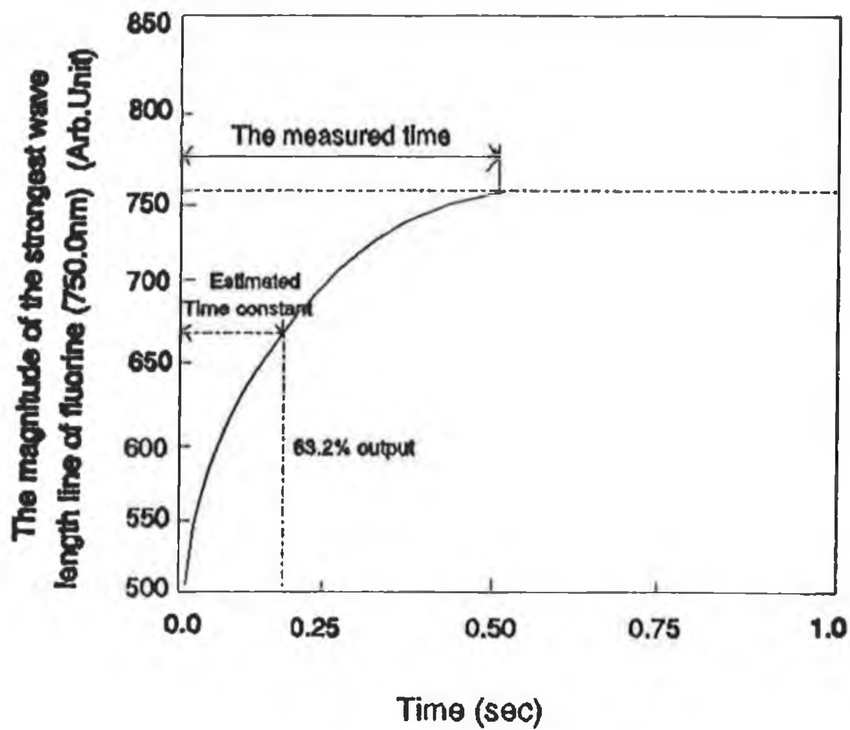

Figure 4.00 The magnitude of the strongest wave length line of fluorine as a function of the time

Electrode spacing = 2.0 cm,
RF power density = 0.17 W/cm^2,
SF_6 flow rate = 30 sccm,
Etching gases: SF_6 + 4% Ar.

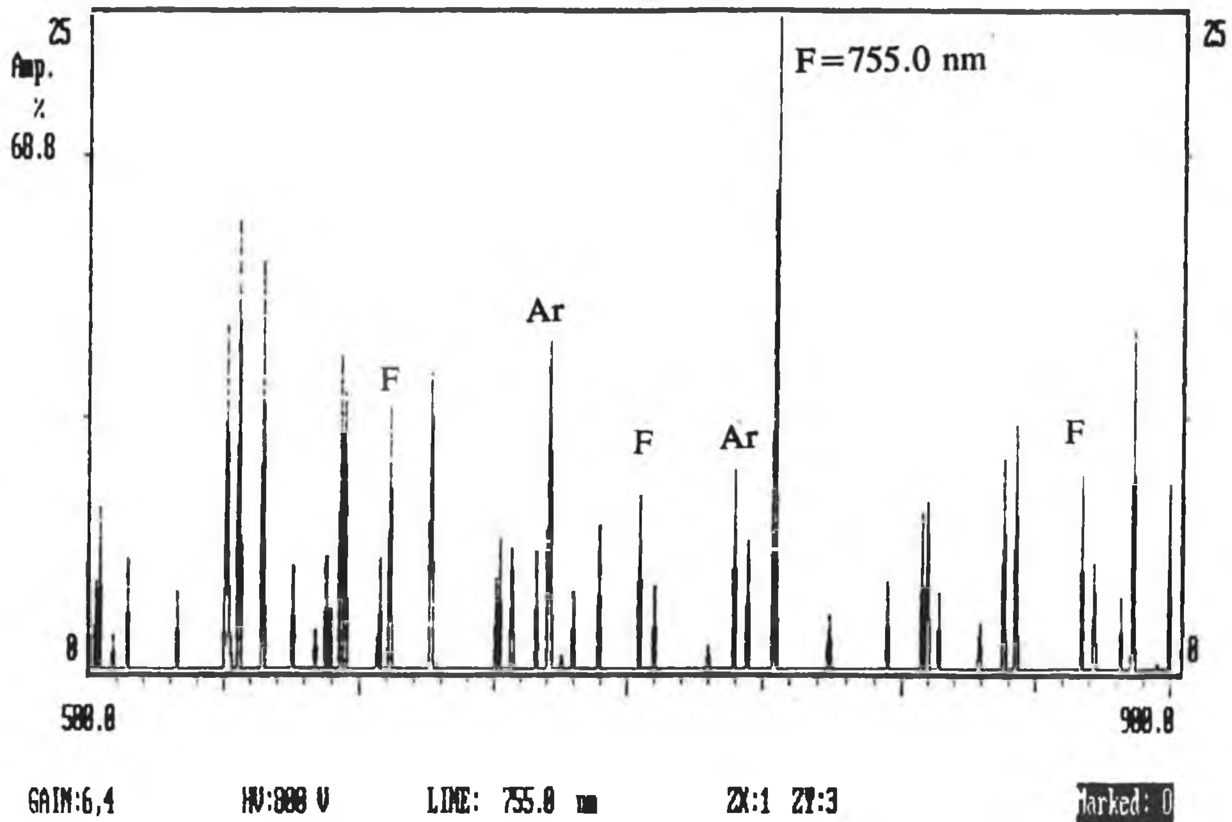

Figure 4.00_1 The optical emission spectrum of SF_6/Ar plasma

Electrode spacing = 2.0 cm,
RF power density = 0.17 W/cm^2,
SF_6 flow rate = 30 sccm,
Etching gases: SF_6 + 4% Ar.

Table 4.2 Steady State Gain for the SF_6/Ar System

for Si wafer	Pressure	RF Power Density	SF_6 Flow Rate
[F]	0.70	0.20	0.0 (*)
E/p	0.50	0.65	0.0 (*)
[SF_x]	0.90	0.9	1.5

(*) The reason is that the relative concentration of fluorine [F] and E/p are found to be insensitive to the changes of SF_6 flow rate within our operation contions.

4.3.2 Analysis of Manipulated/Process Variable Correlations

The process variables studied are [F], [SF_x], and E/p. The measurements of these plasma species have been described in section 4.2. Ar is used between 3% to 10% as actinometer for the measurements. The manipulated variables studied are RF power density, chamber pressure, SF_6 flow rate. RF power density is varied from 0.05 W/cm^2 to 0.25 W/cm^2 for Si. Similar steps can be performed for the SiO_2 wafer. Total system pressure is varied from 90 to 300 mtorr. The inlet gas composition is varied from 3% to 10% Ar in SF_6 for Actinometry purposes. The SF_6 flow rate is varied from 10 to 30 sccm. Electrodes spacing is varied from 4.0 cm to 1.0 cm. Several variables are held constant during the experimentation: electrode area, electrode material (stainless steel), excitation frequency, and wafer loading.

Fluorine atom concentration is found to be an increasing function of RF power density, pressure and flow rate. This is in general agreement with the results found from the literature. The atomic concentration showed a relative small, linear dependence on power in contrast to the sublinear dependence discussed in the Chapter 3 and [78]. This is due to the fact that the experimental design is created to

correlate linear and quadratic responses of the independent variables. The actual sublinear functionality is approximated linearly. A linear dependence on both of these variables is as expected from the variable screening results and estimated from the main gas phase and surface reactions model (Chapter 3) and found from the literature [78]. The variation in [F] with RF power density and pressure is shown in Figure 4.01. The adjusted R^2 for this equation is 0.90.

Relative [SF_x] concentration is found to be an increasing function of RF power density and pressure with a slight interaction between the two (Figure 4.02). The adjusted R^2 for this equation is 0.823. It is thought that the dissociation of SF_6 produces primarily atomic fluorine and SF_x, so the similarity in functionalities F and SF_x is not surprising. SF_x, like fluorine, shows an increase with pressure in the parameter space while its increase with power density is less than a factor of two. The interaction between RF power density and pressure is a result of the increasing electron energy with power density and species density with pressure. The same effect is noted in the case of fluorine but is masked in its significance by the other mechanisms.

The results of the E/p regression are found in Figures 4.03 and 4.04. The adjusted R^2 for this correlation is 0.890, a nice fit with good predictive capability. The plot of E/p versus RF power density and pressure agrees qualitatively with the results of Sawin [5]. E/p decreases markedly with pressure as electron energy is decreased due to increased electron density. A minimum is reached and E/p begins to rise as pressure is increased further. This is due to a decrease in electron density because of the increased probability of electron attachment reactions. The decrease in electron density corresponds to an increase in electron energy and hence in E/p. E/p is a much weaker function of RF power density [5]. According to our previous studies (Chapter 3), electron density should increase roughly linearly with RF power density and the electron energy should remain relatively constant, if electron-impact processes are the main source of power dissipation in the plasma.

An interesting effect is noted in the E/p versus RF power density and flow rate plot (Figure 4.04). At sufficiently low values of SF_6 flow rate, E/p shows a decrease with increasing power density whereas E/p increases with power density at higher flow rates. In the same manner, E/p decreases with increasing flow rate at low power density and increases at high power density. This phenomenon has not been previously studied, so the following mechanism is suggested. Low values of

flow rate represent a longer residence time of plasma species in the reactor and thus a smaller value of the characteristic diffusion length. As power density is increased at low flow rate, the probability of electron-molecule collisions increases due to the long residence time and electron energy is lost in this way. As flow rate increases and residence time decreases, the power dissipation favours an increase in electron energy over collisional losses. At low power density, an increase in flow rate causes an increase in characteristic diffusion length as residence time decreases. Sawin [5] has shown that E/p varies inversely with $P\lambda$, the product of pressure and characteristic diffusion length. At constant pressure, E/p becomes inversely proportional to λ so E/p will necessarily decrease. At high power levels, however, the competition of this loss mechanism with the decrease in collision probability as residence time decreases begins to favour the latter, and E/p increases with flow rate. The coefficients of response of process variables to manipulated variables for the SF_6/Ar system have been shown in Table 4.1.

Table 4.3 Coefficients of Response of Process Variables to Manipulated Variables for the SF_6/Ar System

For Si wafer	[F]	$[SF_x]$	[E/p]
Mean	14.305	0.077	0.801
RF power density, x_1	1.385	0.020	0.115
Pressure, x_2	5.352	0.025	-0.690
SF_6 flow rate, x_3	-----	-----	-----
x_1x_2	-----	0.003	0.003
x_1x_3	-----	-----	0.000
x_2x_3	-----	-----	-----
x_1^2	-----	-----	-30.0
x_2^2	-----	-----	383.0
x_3^2	-----	-----	-----
Adj. R^2	0.900	0.823	0.890

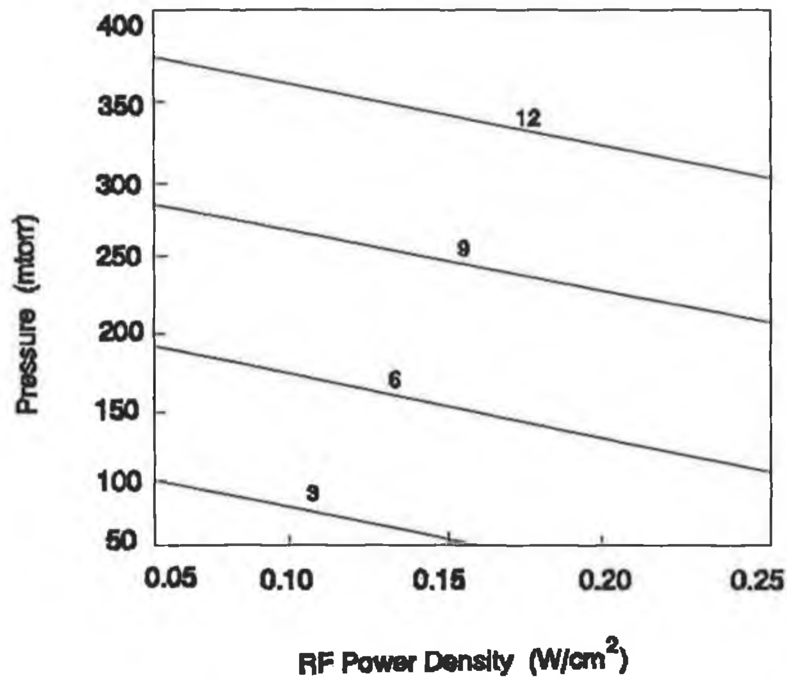

Figure 4.01 Calculated Relative Fluorine Concentration (Arb.Unit) as a Function of RF Power Density and Pressure Using Si Wafer

Electrode spacing = 2.0 cm,
SF_6 flow rate = 30 sccm + 4% Ar,
Etching gases: SF_6/Ar.

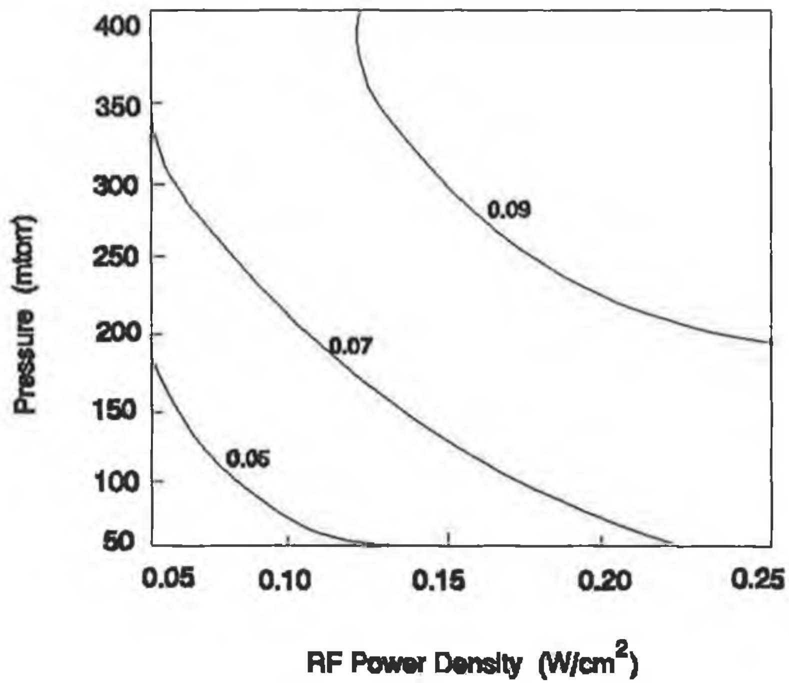

Figure 4.02 Calculated Relative SF_x Concentration (Arb.Unit) as a Function of RF Power Density and Pressure Using Si Wafer

Electrode spacing = 2.0 cm,
SF_6 flow rate = 30 sccm + 4% Ar,
Etching gases: SF_6/Ar.

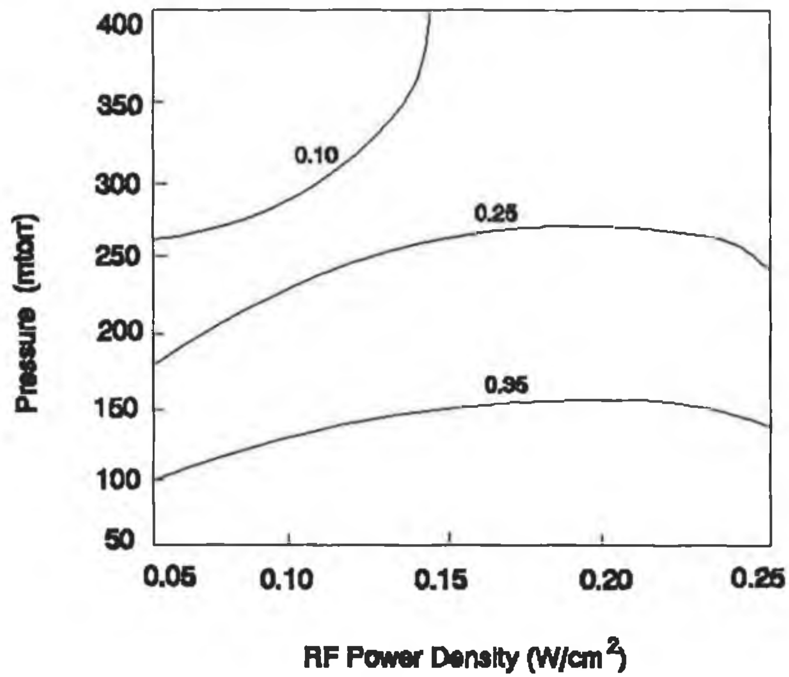

Figure 4.03 Plots of E/p (volt/cm.mtorr) as a Function of RF Power Density and Pressure Using Si Wafer

Electrode spacing = 2.0 cm,
SF_6 flow rate = 30 sccm + 4% Ar,
Etching gases: SF_6/Ar.

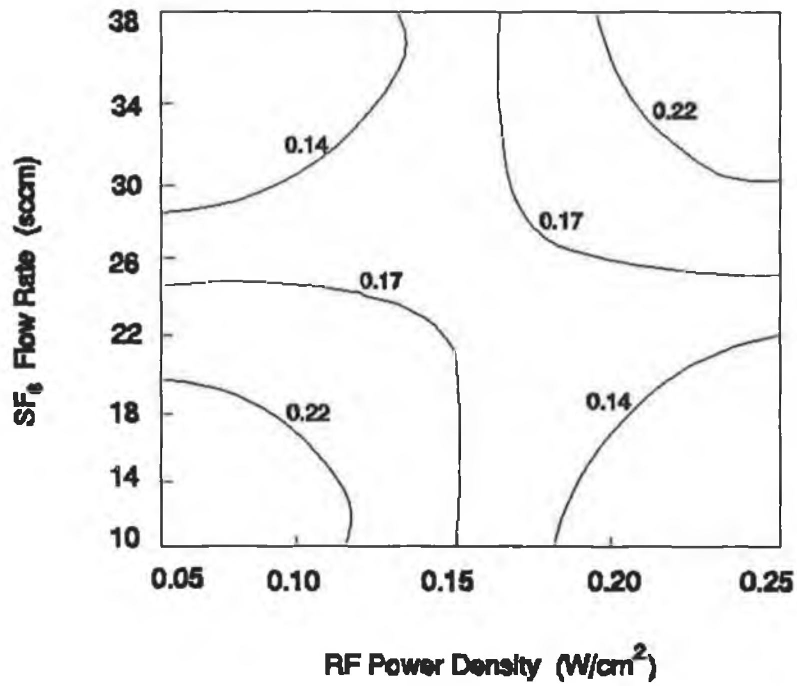

Figure 4.04 Plots of E/p (volt/cm.mtorr) as a Function of RF Power Density and SF_6 Flow Rate Using Si Wafer

Electrode spacing = 2.0 cm,
Pressure = 200 mtorr,
Etching gases: SF_6/Ar.

4.3.3 Analysis of Manipulated/Performance Variable Correlations

The performance variables studied for this system are Si etch rate, anisotropy, etch centre-to-edge uniformity. SiO_2 etch rate study is also involved. The manipulated and reactor variables are the same as those described in section 4.3.2.

Si and SiO_2 etch rates are found to be the function of RF power density, pressure and SF_6 flow rate, with an interaction between RF power density and SF_6 in Figures 4.05 to 4.10. The adjusted R^2 for Si etching is 0.70 indicating a significant lack of fit of the model for this response. An examination is made of the ratio of lack-of-fit to pure error for this equation, and the resulting F test shows the lack-of-fit to be significant (F=7.0, significant at 5%). Allen, et al [49][50] employed a cubic model to correlate etch rate to power, pressure, and percent argon in the etching of polysilicon and obtained a good fit. These facts together suggest that the quadratic model is not sufficient to completely track silicon etch rate; however, the quality of fit is sufficient to examine trends in etch rate, although the exact shape of the curve is not known. Si and SiO_2 etch rates are found to increase with RF power density, pressure, and SF_6 similarly to fluorine concentration, although RF power density is the most significant variable in the etch rate correlation, suggesting an ion-enhancement of the etch rate. The etch rate is enhanced further at higher powers where dissociation of SF_6 is increased, providing a greater number of SF_x radicals for reactions. The dependence of etch rate on pressure is more subtle. In this study, etch rates increase linearly with pressure both for Si and SiO_2. Allen et al [49][50] found a maximum in polysilicon etch rate with pressure, especially at lower power. Our experiments are in the low pressure region of their pressure range where etch rates increase with pressure. It appears that mechanisms of dissociation and recombination are in competition, with dissociation being dominant at low pressure. This is consistent with previous results in Chapter 3. Through response surface methodology we are able to present evidence to validate the mechanism in this etching process.

Silicon etching anisotropy shows a dependence on all manipulated variables, although the correlation is quite weak, with an adjusted R^2 of 0.49 (Figure 4.11). This means that predictive ability of the model is poor and trend analysis will be only approximate. The analysis of replicate experiments in this case shows a large spread in the data. The ratio of lack-of-fit to pure error is very low, showing that the problem is in the measurement of anisotropy, not the form of the model. Anisotropy

can be measured as line width loss in a test pattern on each material. The etch depth in silicon in SF_6/Ar system is greater than the initial line width, so a relatively isotropic etch would be impossible to measure, or at least subject to much error. However, the SF_6/Ar silicon etch is not expected to be highly anisotropic, so this variable is not considered to be of great importance. Its inclusion here is for completeness. The results of this analysis found from literature [49][50] are employed on this study. Anisotropy can be calculated by the following equation:

$$\text{Anisotropy} = 1 - \frac{\text{Line width before etch} - \text{Line width after etch}}{\text{Etch depth}} \quad ; \qquad \textbf{(4.3.3-1)}$$

by this definition, a completely anisotropic etch will have an anisotropy of 1 while a completely isotropic etch will have an anisotropy of 0. Pressure shows the largest effect on anisotropy. This is due to the fact that the only mechanism for anisotropy in the SF_6/Ar system is ion-enhanced etching. As the degree of ion bombardment decreases with increasing pressure, so does anisotropy. Anisotropy displays a maximum with RF power density. This is likely due to the competition between increasing fluorine concentration and increasing ion bombardment with RF power density. At low power, etching by fluorine (chemical etching) will be dominant as ion energy remains low. Increased ion bombardment will cause increased anisotropy as RF power density is raised. However, ion energy is less a function of RF power density than pressure, so as power density is raised further, the creation of atomic fluorine becomes dominant and the etch mechanism becomes more chemical than physical, decreasing the anisotropy.

Silicon etching uniformity is shown in Figures 4.12 to 4.13 as a function of the manipulated variables. The adjusted R^2 for this equation is 0.885, sufficient for trend analysis. Uniformity, as discussed in Chapter 3, is measured as the percent difference in etch rate between the centre and edge of the electrode, so a low value indicates good uniformity. The most significant variables to effect uniformity are RF power density and pressure. As can be seen, uniformity is improved with increasing RF power density and decreasing pressure. Also, uniformity improved with increasing SF_6 flow rate except at low power density. Although little has been said in literature concerning uniformity, two requirements are generally understood. A uniform electron density distribution in the reactor and uniform species concentrations across the electrode lead to better uniformity of an etch process. The trend of the results of the model are consistent with those concepts. The coefficients of response of performance variables to manipulated variables for SF_6/Ar system have been shown on Table 4.4.

Table 4.4 Coefficients of Response of Performance Variables to Manipulated Variables for the SF_6/Ar System

For Si wafer	Etch rate (nm/min)	Anisotropy	Uniformity
Mean	68.95	0.452	0.242
RF power density, x_1	18.70	------	-0.039
Pressure, x_2	7.202	-0.047	0.077
SF_6 flow rate, x_3	-----	-----	-----
x_1x_2	-----	-1.265	-----
x_1x_3	-----	-----	-0.045
x_2x_3	-----	-----	-----
x_1^2	-----	-0.019	-----
x_2^2	-----	-----	-0.019
x_3^2	-----	-----	-0.014
Adj. R^2	0.700	0.490	0.885

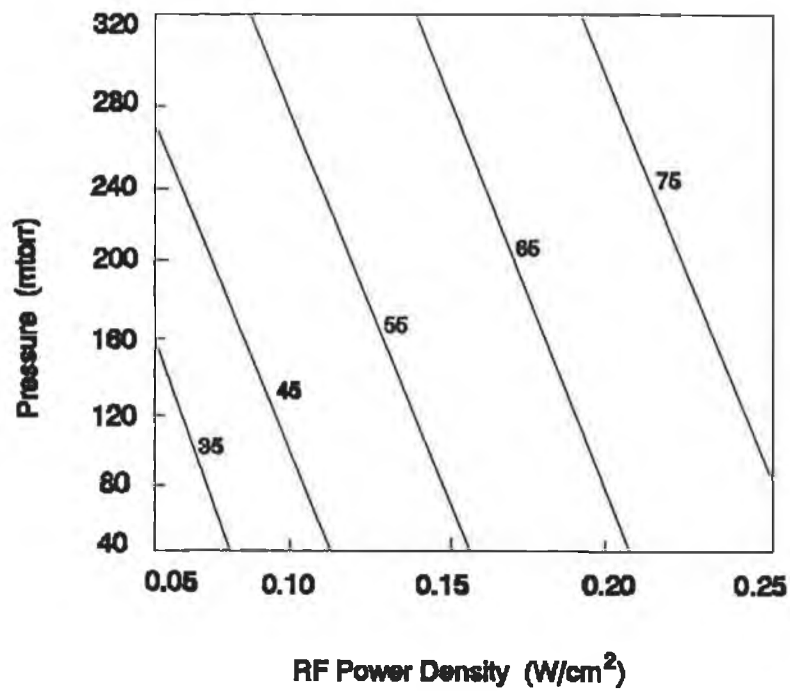

Figure 4.05 Si Etch Rate (nm/min) as a Function of RF Power Density and Pressure

Electrode spacing = 2.0 cm,
SF_6 flow rate = 30 sccm + 4% Ar,
Etching gases: SF_6/Ar.

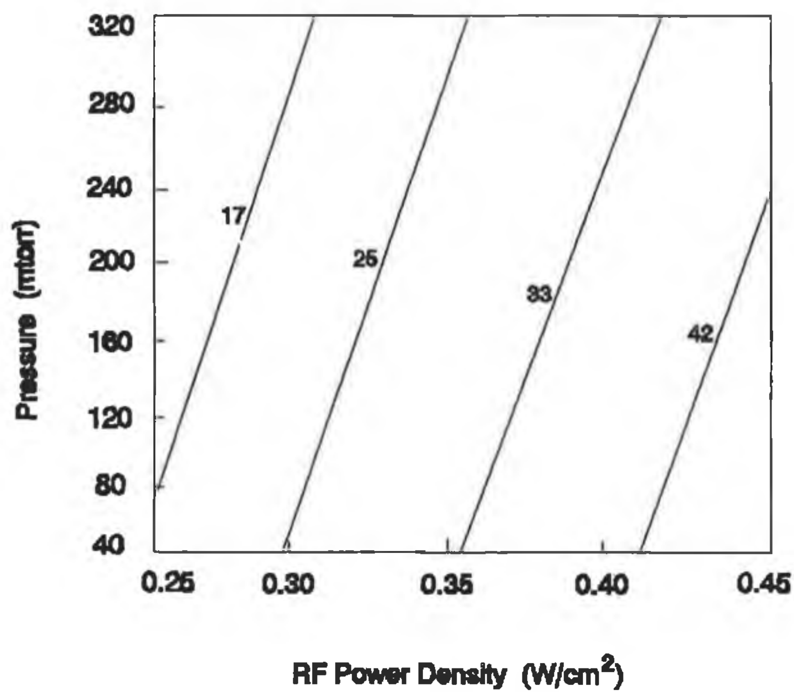

Figure 4.06 SiO_2 Etch Rate (nm/min) as a Function of RF Power Density and Pressure

Electrode spacing = 2.0 cm,
SF_6 flow rate = 30 sccm + 4% Ar,
Etching gases: SF_6/Ar.

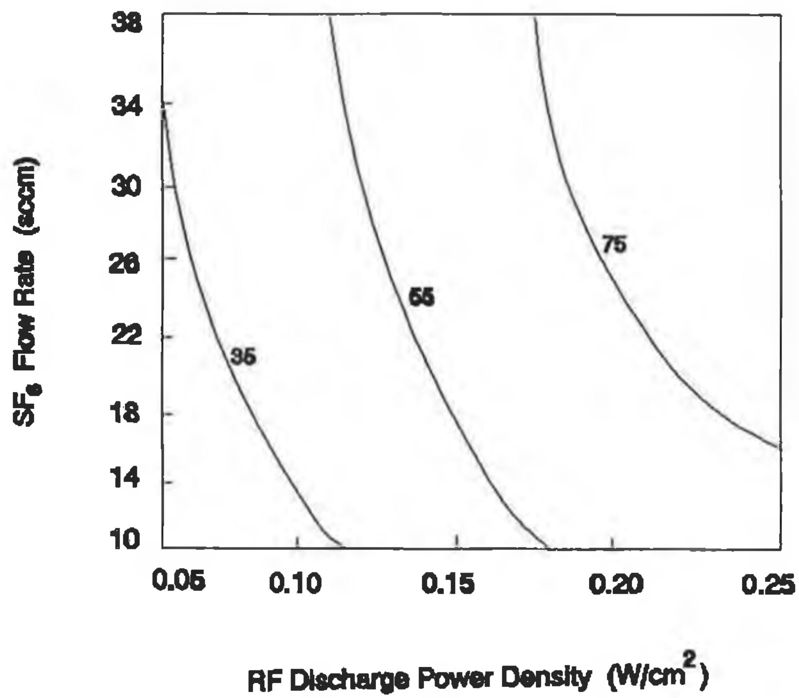

Figure 4.07 Si Etch Rate (nm/min) as a Function of RF Power Density and SF_6 Flow Rate

Electrode spacing = 2.0 cm,
Pressure = 200 mtorr,
Etching gases: SF_6 + 4% Ar.

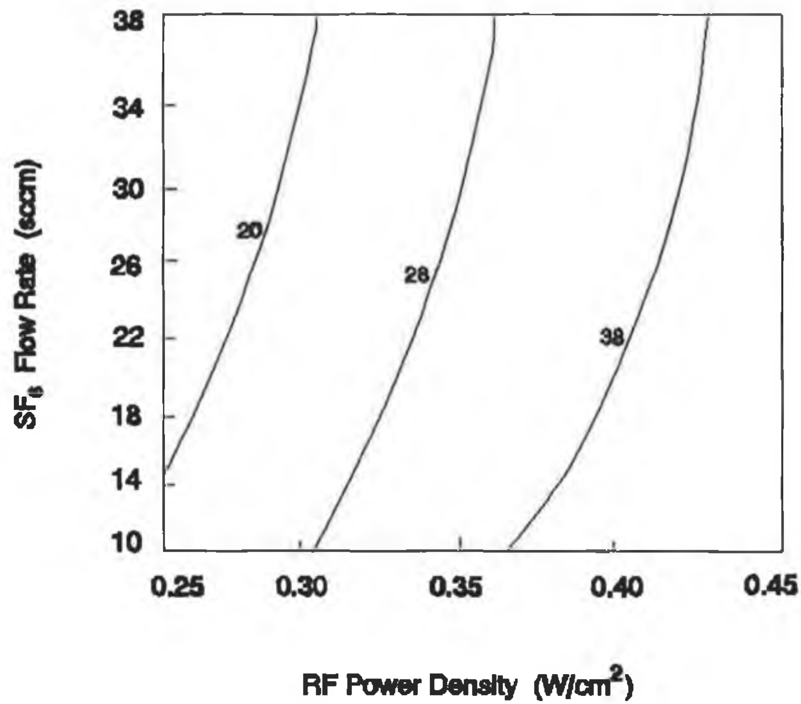

Figure 4.08 SiO_2 Etch Rate (nm/min) as a Function of RF Power Density and SF_6 Flow Rate

Electrode spacing = 2.0 cm,
Pressure = 250 mtorr,
Etching gases: SF_6 + 4% Ar.

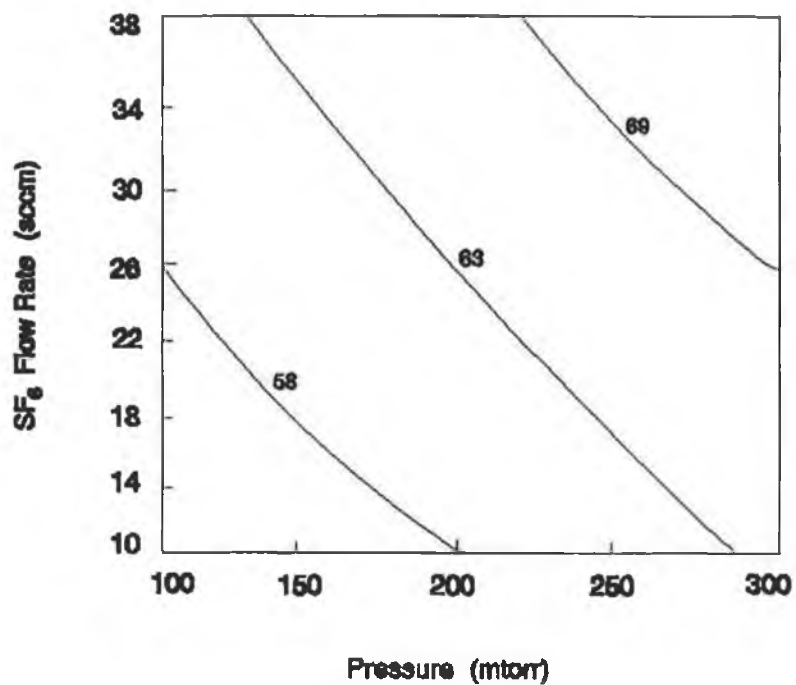

Figure 4.09 Si Etch Rate (nm/min) as a Function of Pressure and SF_6 Flow Rate

Electrode spacing = 2.0 cm,
RF power density = 0.17 W/cm^2,
Etching gases: SF_6 + 4% Ar.

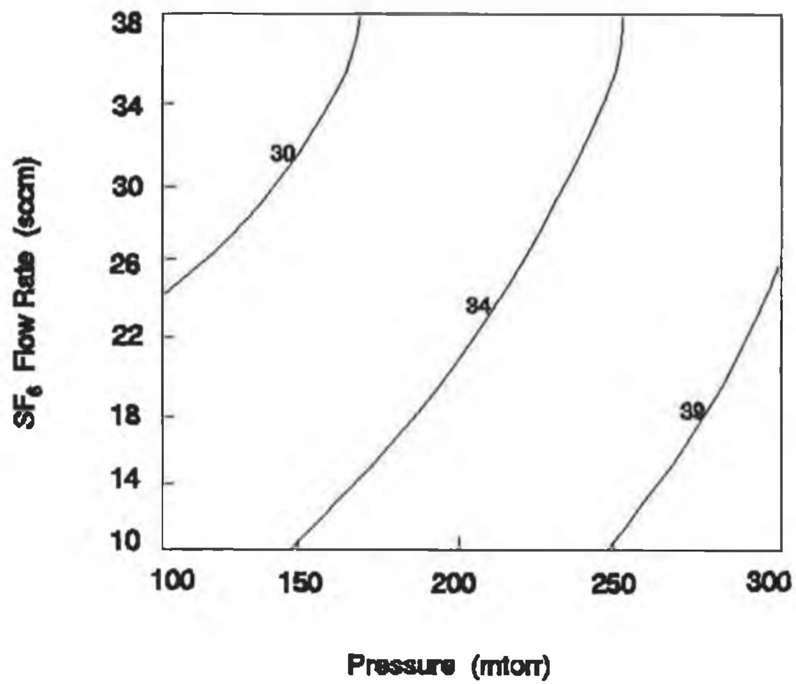

Figure 4.10 SiO_2 Etch Rate (nm/min) as a Function of Pressure and SF_6 Flow Rate

Electrode spacing = 2.0 cm,
RF power density = 0.35 W/cm^2,
Etching gases: SF_6 + 4% Ar.

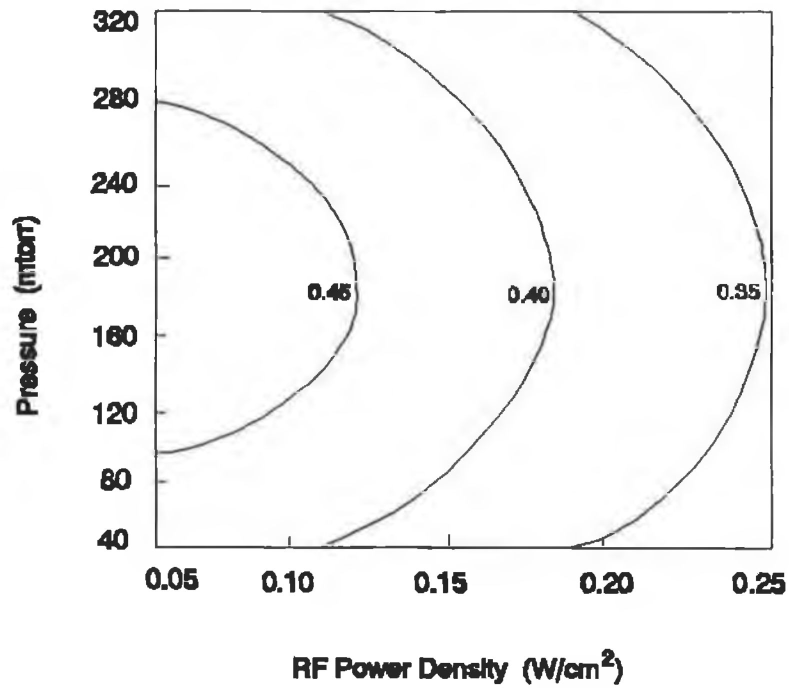

Figure 4.11 Si Anisotropy as a Function of RF Power Density and Pressure

Electrode spacing = 2.0 cm,
SF_6 flow rate = 30 sccm,
Etching gases: SF_6 + 4% Ar.

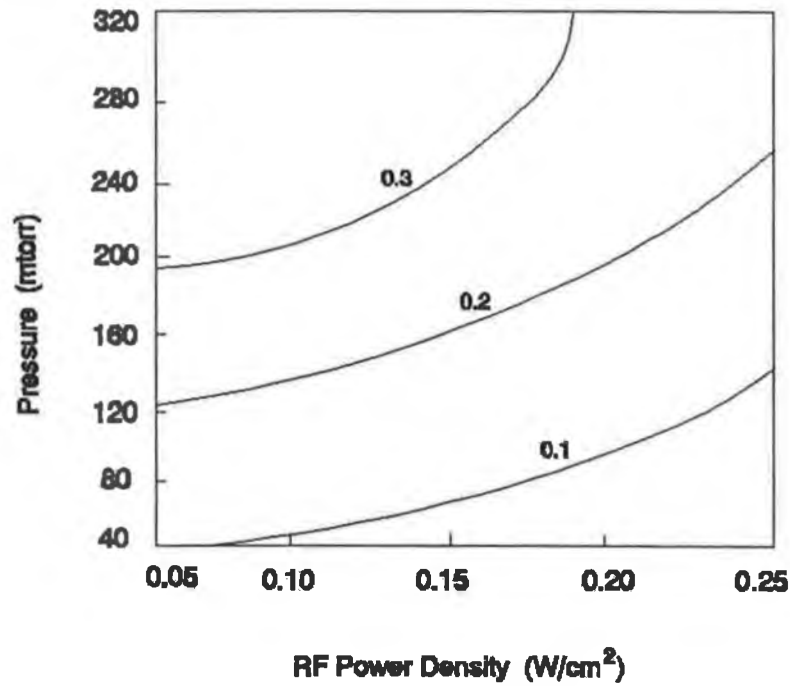

Figure 4.12 Si Uniformity as a Function of RF Power Density and Pressure

Electrode spacing = 2.0 cm,
SF_6 flow rate = 30 sccm,
Etching gases: SF_6 + 4% Ar.

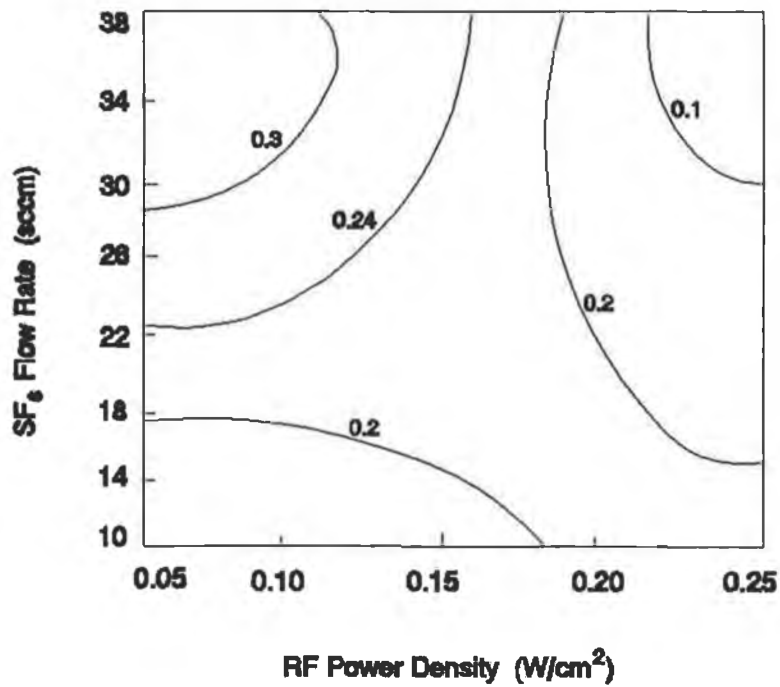

Figure 4.13 Si Uniformity as a Function of RF Power Density and SF_6 Flow Rate

Electrode spacing = 2.0 cm,
Pressure = 200 mtorr,
Etching gases: SF_6 + 4% Ar.

4.3.4 Analysis of Process/Performance Variable Correlations

In developing a control system, it is necessary to relate three sets of variables: inputs or manipulated variables, process variables, and outputs or performance variables. The requirement of a control system is to satisfy a performance index, in our case dictated by some optimisation of the levels of the plasma etching performance variables on Si wafer: etch rate, anisotropy, uniformity. The same technique employed in this study can be used for SiO_2 etching analysis. Most of variables cannot be measured on-line; thus it is necessary that the performance variables to be related to the process variables in some fashion. There is inherent in our composite experimental design an indirect relationship between these sets of variables through their respective relationships to the manipulated variables. This formulation, however, is not amenable to the application of a control system design theory such as relative gain analysis or singular value decomposition or robust control since they require steady state gain information for their use. It is necessary, then, to relate these variables directly through some means of correlation.

The stepwise regression function is chosen to create these correlations. It is recognised that the process and performance variables measured in original experiments and theoretical studies do not form an orthogonal experimental design; the variables are in fact not orthogonal. The stepwise algorithm, however, searches for correlations among the sets of variables and fits model parameters for these variables; this is felt probably to be sufficient for our requirements. In an orthogonal design, the significance of any term in a regression equation is independent of the other terms in the equation. In addition, the values of the process variables are not evenly spaced and correlations made from these may be skewed according to regions where the data is concentrated. The process variables are scaled in the same manner described for the manipulated variables earlier. Linear terms, quadratic terms, and all two-factor interactions are included as before.

The data are presented in tabular form for each system. Only those coefficients found to be statistically significant are included in the following table. These coefficients will be used to form the matrix of steady state gains for the control system analysis. It should be careful in the interpretation of this data, as it must be remembered in analysing these equations that correlation does not necessarily imply causation. Correlation between two variables may be due to a

direct relationship between the variables or an indirect relationship through another effect. This will be further studied.

The regression coefficients of the performance variables for this system are shown in Table 4.3. Silicon etch rate is found to correlate primarily with E/p. The correlation with E/p indicates that the etching of silicon is ion-enhanced. In fact, [SF_X] and [F] in this case describes similar occurrences in the system and thus both would tend to not be included in the same regression. The portion of the model described by [SF_X] is approximately the same as that described by [F], namely conditions where high fluorine concentration is favoured. It is clear that the model created using this analysis are not inherently mechanistic in nature. Fundamental modelling of the etch process studied on Chapter 3 is one of the basis of this analysis. In this part, it is desired to develop a method of selecting performance variables for initial specification of the etch. By examining the process/performance variable relationships directly, we can determine which pairings will be most effective for the proposed control system.

Silicon etching anisotropy correlated well with the process variables. The strongest functionalities for silicon anisotropy are fluorine concentration and E/p. Similar studies were carried by Bergeron et al, [43] and McLauglin et al, [55]. An increase in anisotropy with E/p is expected due to increased ion bombardment while decreased anisotropy with increasing fluorine concentration is due to the increasing contribution of the chemical mechanism [43][55].

Uniformity of etching is correlated well for silicon. In this discussion it should be remembered that increasing uniformity indicates a decrease in the value assigned to uniformity. Because this is defined as the fractional difference in etch rate between the centre and edge of the electrodes. The most significant variable in each case is E/p, and the etching uniformity of both species increases with increasing E/p. This is likely due to the non-uniform electron energy distribution which favours higher electron energies toward the outer edge of the electrode [67][71]. This in turn leads to greater production of fluorine (through greater dissociation of SF_6) and thus a higher chemical etch contribution at the outer edge, shown in the coefficient on [F] in correlation. Increasing E/p increases ion bombardment and thus mitigates the effect of this non-uniform distribution through an increase in the physical portion of the etch. Interestingly, silicon etching uniformity correlated with [SF_X]. SF_X tended to decrease silicon etch uniformity.

Table 4.3 Coefficients of Response of Performance Variables to Process Variables for the SF_6/Ar System

For Si wafer	Etch rate (nm/min)	Anisotropy	Uniformity
Mean	59.85	0.452	0.271
[F], x_1	-----	-0.077	0.035
[SF_x], x_2	-----	-----	0.077
E/p, x_3	15.98	0.025	-0.067
x_1x_2	7.290	-----	-----
x_1x_3	-10.65	-----	-----
x_2x_3	-----	-----	-----
x_1^2	-9.43	0.278	-----
x_2^2	-2.23	-----	-----
x_3^2	-----	-----	-----
Adj. R^2	0.857	0.690	0.879

4.4 Comparison with Comprehensive Reactor Model

The results of the regression analysis are compared in this section to the results from a comprehensive model of the etching of Si and SiO_2 in SF_6/Ar plasma studied in the Chapter 3. The comprehensive reactor model, which includes gas phase electron dissociation of SF_6, surface recombination and etching of Si and SiO_2, is isothermal with fully developed flow and the variable Si and SiO_2 loading is assumed to be uniformly distributed over the electrode. In addition, an assumption of uniform electron density distribution in the reactor is made.

It should be noted that the work on the comprehensive model is in its early stages and uses the different parameters for the theoretical modelling study, so exact quantitative agreement between the theoretical model and the regression analysis is not expected. The comparisons are made to examine trends predicted by the theoretical model and to determine if these trends are qualitatively correct. In addition, it must be remembered that the calculation of plasma species densities provides a relative indicator of the actual concentrations. Thus, the scale used in each plot of the regression model and comprehensive model determined plasma species density is arbitrary and the results should be compared based on gross trends. Etch rates are compared directly, but the comprehensive model assumes that the etch rate of silicon is directly proportional to the atomic fluorine. For comparison with our data, the comprehensive model is run at sets of conditions similar to those used in our regression modelling.

Figure 4.14 shows a sublinear dependence of fluorine concentration on pressure from the regression analysis whereas the comprehensive model determined a linear dependence. Fluorine concentration compared well with the model. The linear function is in better agreement with some elements at the literature [92]; however, the degree of non linearity in the fit is slight, so the fit to the data is good.

SF_X concentration displays a marked difference between the comprehensive model and regression model results. Figure 4.15 shows a peak in $[SF_X]$ with increasing pressure, presumably due to increased recombination reactions at higher pressure. This is found in the regression model, which shows $[SF_X]$ to be a monotonically increasing function of pressure.

The plasma measurements and visual observations indicate that the plasma is homogeneous and well-confined between the electrodes. The thickness of the sheaths is smaller than 0.5 mm for most experimental conditions. The electron density and E/p show small changes with gas flow rate. Electrode gap and RF power density are found to be the most significant parameters that affect electron density and effective electric field. Higher discharge RF power density increases the gas ionisation and consequently results in a higher electron density. As the pressure changes, electron densities remain nearly constant within our experimental range. A reduction in pressure always increases the electron energy and the value of E/p, as shown in Figure 4.16. Both results are in good agreement.

Etch rate displayed a sublinear dependence on pressure according to the theoretical model whereas the regression data support a sublinear dependence also (Figures 4.17 and 4.18). The shapes of the curves are different, but the values of etch rate differ between the results by a factor of two or more. The results are in good agreement at low pressure, but the slope of the theoretical model curve is greater than that found in regression modelling. The comprehensive model assumes etch rate is proportional to fluorine concentration, so it would seem that either the model over-predicts the increase in fluorine concentration with pressure or the regression results do not support the idea that etch rate is proportional to fluorine concentration alone. Figures 4.19 and 4.20 show that etch rates of Si and SiO_2 are increased with increasing RF power density, as discussed in Chapter 3, both on comprehensive reactor model and regression analysis respectively.

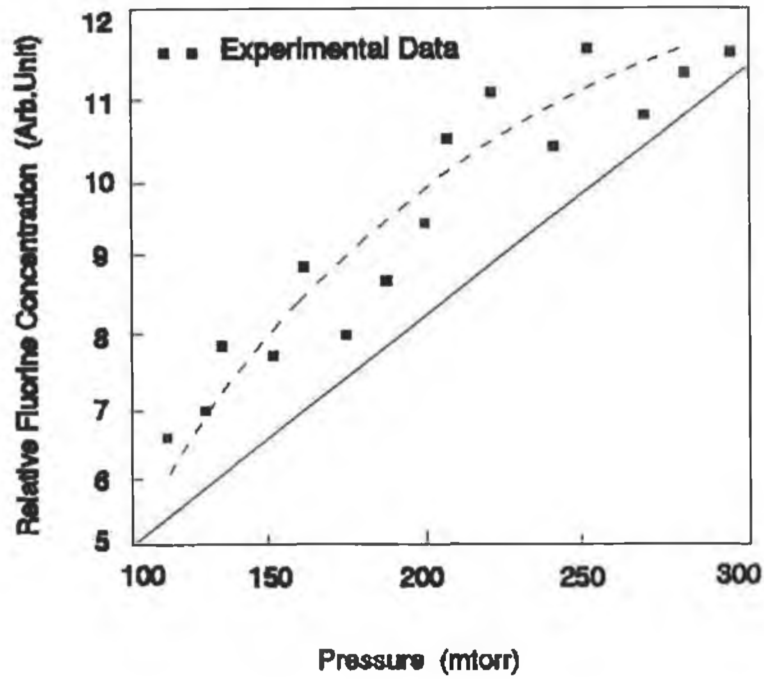

Figure 4.14 Relative Fluorine Concentration as a Function of Pressure Using Si Wafer

Electrode spacing = 2.0 cm,
RF power density = 0.17 W/cm^2,
SF_6 flow rate = 30 sccm,
Etching gases: SF_6 + 4% Ar.
———— Results from Comprehensive Model
-------------- Results from Regression Analysis

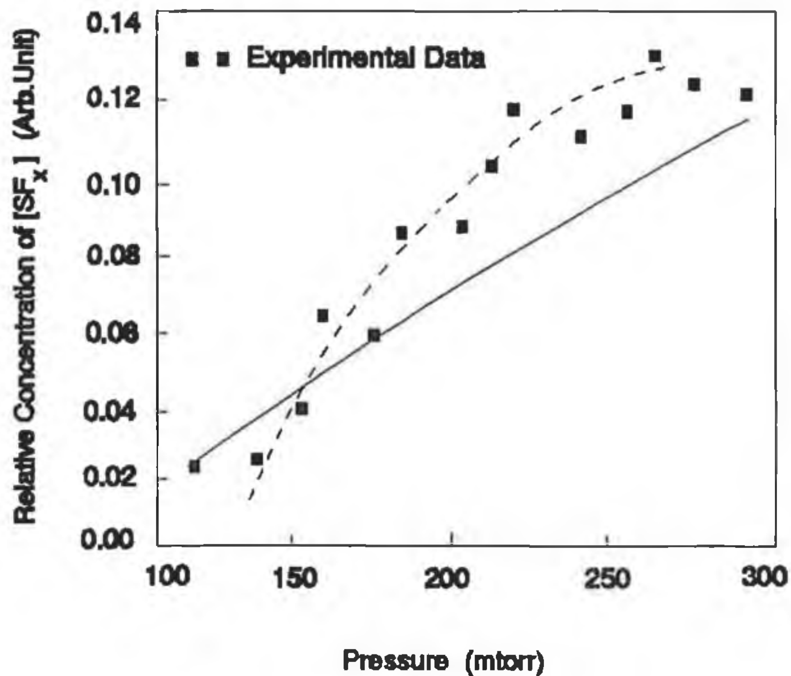

Figure 4.15 Relative [SF_x] Concentration as a Function of Pressure Using Si Wafer

Electrode spacing = 2.0 cm,
RF power density = 0.17 W/cm^2,
SF_6 flow rate = 30 sccm,
Etching gases: SF_6 + 4% Ar.
__________ Results from Comprehensive Model
-------------- Results from Regression Analysis

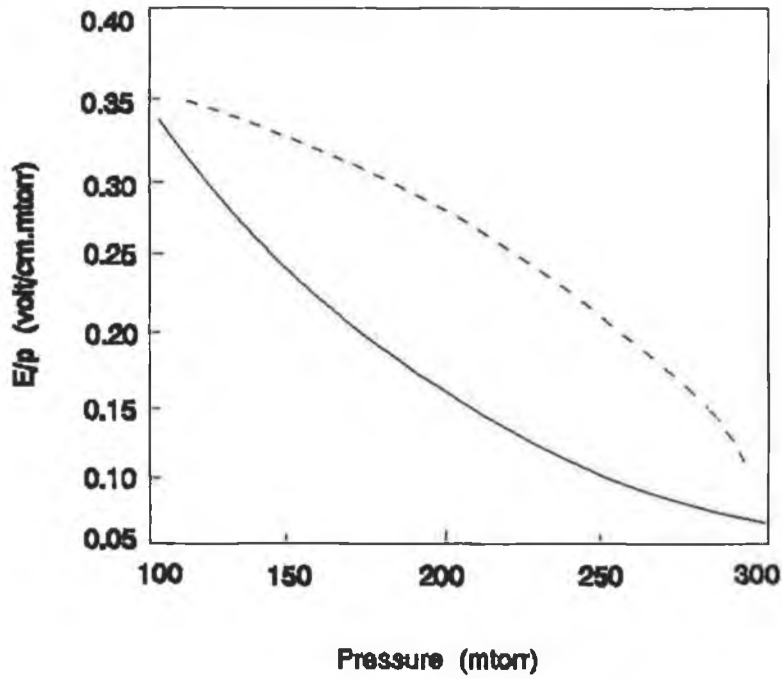

Figure 4.16 Plots of E/p as a Function of Pressure Using Si Wafer

Electrode spacing = 2.0 cm,
RF power density = 0.17 W/cm^2,
SF_6 flow rate = 30 sccm,
Etching gases: SF_6 + 4% Ar.
__________ Results from Comprehensive Model
-------------- Results from Regression Analysis

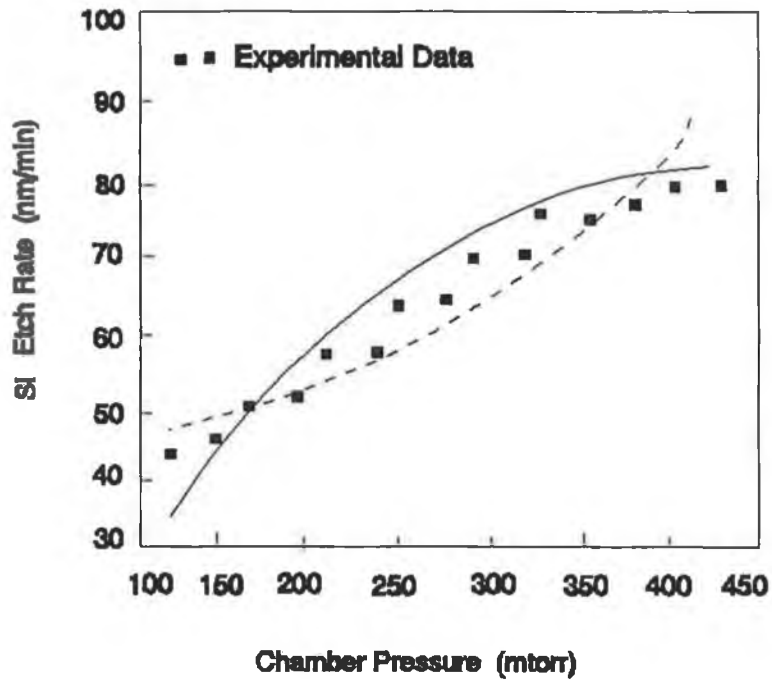

Figure 4.17 Si Etch Rate (nm/min) on Chamber Pressure in SF_6/Ar System

Electrode spacing = 2.0 cm,
RF power density = 0.17 W/cm^2 ,
Etching gases: SF_6 + 4% Ar,
SF_6 flow rate = 30 sccm,
__________ Results from Comprehensive Model
-------------- Results from Regression Analysis

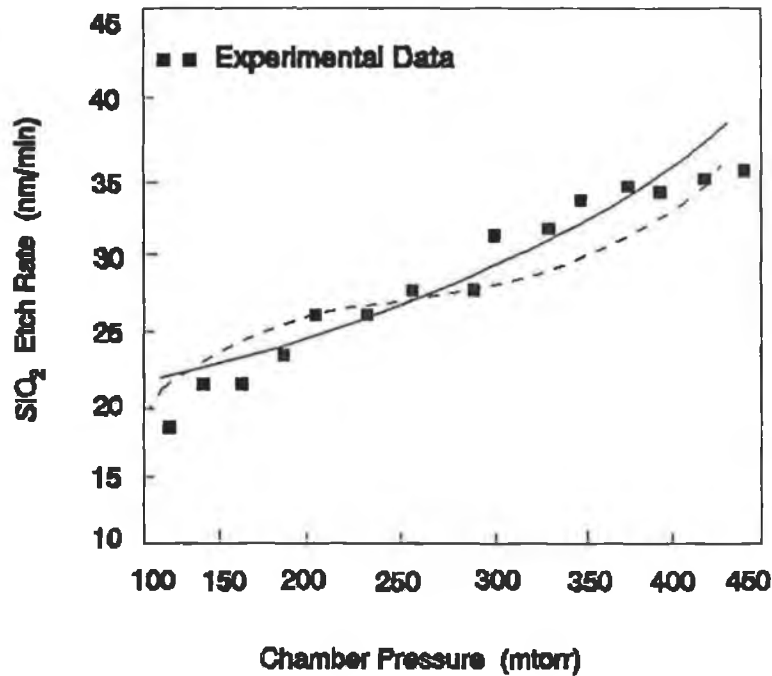

Figure 4.18 SiO_2 Etch Rate (nm/min) on Chamber Pressure in SF_6/Ar System

Electrode spacing = 2.0 cm,
RF power density = 0.34 W/cm^2 ,
Etching gases: SF_6 + 4% Ar,
SF_6 flow rate = 30 sccm,
__________ Results from Comprehensive Model
-------------- Results from Regression Analysis

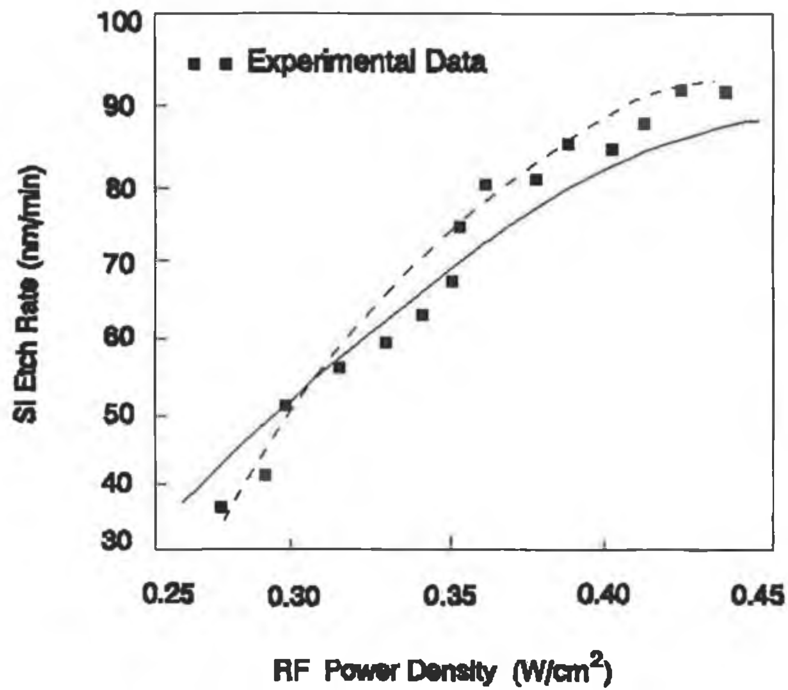

Figure 4.19 Si Etch Rate (nm/min) on RF Power Density in SF_6/Ar System

Electrode spacing = 2.0 cm,
Pressure = 150 mtorr,
Etching gases: SF_6 + 4% Ar,
SF_6 flow rate = 30 sccm,
________ Results from Comprehensive Model
-------------- Results from Regression Analysis

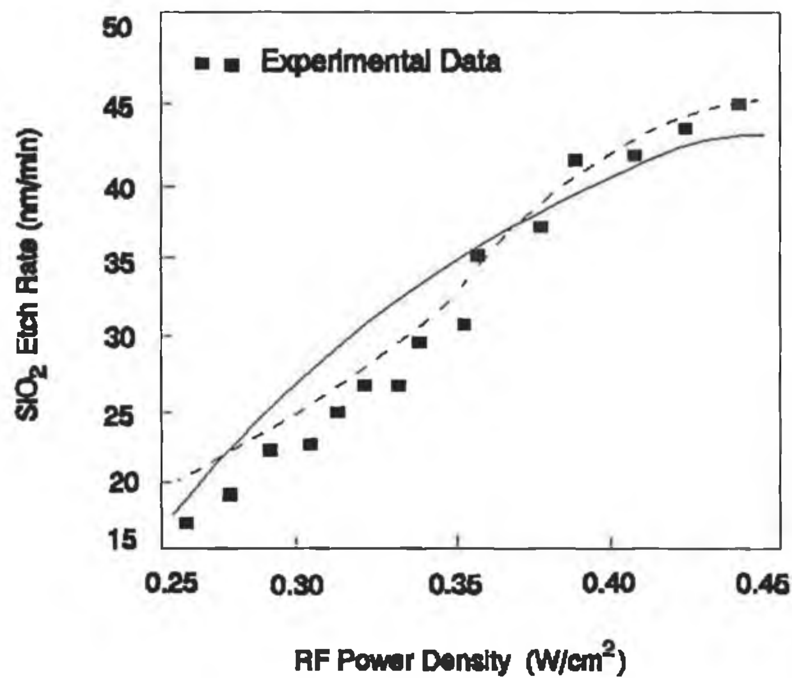

Figure 4.20 SiO_2 Etch Rate (nm/min) on RF Power Density in SF_6/Ar System

Electrode spacing = 2.0 cm,
Pressure = 200 mtorr,
Etching gases: SF_6 + 4% Ar,
SF_6 flow rate = 30 sccm,
——— Results from Comprehensive Model
-------------- Results from Regression Analysis

4.5 Discussion and Conclusions

The purpose of this part of research is to develop the steady-state regression model based on the composite experimental design and the comprehensive modelling studies for the control system design. The model is developed using regression analysis, along with the adjusted R^2 coefficients of fit. A quadratic model is used and found to adequately represent the data in a few cases.

All process variables are correlated to an adjusted $R^2 > 0.8$, indicating that the resulting model are adequate for trend analysis [93]. The steady-state model is evaluated using response surface methodology. The manipulated/performance variable correlations reveal the location of desirable operating conditions for our process. It is assumed that the fast, uniform Si and SiO_2 etching could be achieved in the SF_6/Ar system by high RF power density, low pressure, and high SF_6 flow rate. Silicon anisotropy is generally unimportant in the SF_6/Ar system since this process is normally used for etching of Si and SiO_2 in non-critical situations where anisotropy is not needed. The inclusion of anisotropy in this study is because of the completeness for the control.

Correlations are then developed to directly relate process and performance variables in this system. This is found to be important in process specification, yielding steady state gain matrices for these variables which could later be used to identify which performance variables should be used to specify set points for the process variables during performance development. Etch rate and uniformity are generally well correlated for the system, but anisotropy is not well-correlated. These results will be employed for control of this process.

Examination of contour plots of the manipulated/process and performance variable correlations indicates that our regression modelling results compared favourably with previous studies of this system. The results show similar functionalities in the regression analysis and the comprehensive model predictions.

Process dynamics are studied so that a qualitative understanding of the process variable time constants could be obtained. This is necessary for simulation and evaluation of further control system. The time constants for each system are measured from open-loop step tests run on the plasma etching reactor.

CHAPTER 5 DECOUPLING MULTIVARIABLE CONTROL SYSTEM DESIGN

5.1 Introduction

One of the main objectives of this project is to develop control systems suitable for the plasma etching process. The steady state regression model developed in Chapter 4 can be used to determine an operating strategy for the process. For the given set of performance variables, the corresponding manipulated variable levels are set by their model relationships. The process variable set points are then calculated through application of the regression model. The process variables with these set points are used for feedback in an inferential process control scheme. This methodology outlined to this point requires several issues to be addressed. It is clear that not all of the performance variables can be set independently, so criteria must be chosen to select the measures of performance for this process. It is also necessary to select pairings between the process variables both to manipulated and performance variables for minimising the interactions of the system variables.

A cornerstone of decoupling multivariable process control system development is the issue of pairing of input and output variables. The method of singular value decomposition (SVD) is used to determine these pairings. One of the major advantages of this method is that it can handle non-square systems and design the structural compensators for the control systems. The primary disadvantage is that the process system must be correctly scaled (i.e. all input and output variables should cover the same range). Thus, the physical scaling technique has been suggested for this purpose. It is possible that these analyses will provide different pairing selections, so process simulation must be used to evaluate the alternatives and recommend an algorithm for control of this system. In many cases processes can be adequately controlled by single input-single output controllers. In this work, the SVD pairings with the input and output structurally compensated multi input-multi output (MIMO) control scheme has been developed to compare with conventional control. These issues will be addressed in this chapter.

The general philosophy of the research is that the optimal control procedure be formulated in general terms that are not specific to the model of the SF_6/Ar plasma etching of Si and SiO_2 presented in Chapter 4. Instead it is intended that the control formulation be applicable to any plasma etching process whose behaviour can be accurately described by a steady state model. Since the model used to test the optimisation procedure is the SF_6/Ar model, the input and output variables are posed in terms of this model. To use the optimisation procedure on another model, it would be necessary to change the names of these variables and find the correlations between them to those of the new model. The goal is to show how optimisation can take advantage of the etch model's ability to predict behaviours (e.g., etch rate, uniformity, and anisotropy) to meet performance objectives while satisfying constraints. The design of control system assumes that the model accurately predict the behaviour, the results from open-loop optimisation may be erroneous, and the robustness of the multivariable control policy should be examined.

5.2 Effects of Process Scaling

Recently, there has been much discussion in the literature concerning the effects of process scaling. The singular value decomposition technique has been found to be sensitive to the scaling used [96]. Some model reduction techniques, such as the generalised structured dominance method [104], are sensitive to the process scaling. The purpose of this section is to review some of the suggested scaling procedures, and to emphasise the importance of scaling with respect to the physical range of the variables on the plasma etching regression model which was developed in Chapter 4.

Morari and co-workers [105] have suggested scaling the process to minimize the condition number. The condition number was used to identify the bounds for model/plant mismatch with respect to integral controllability. They reasoned that stability must be independent of scaling, therefore the least conservative scaling should be used (i.e. minimising the condition number). Process scaling is important for reasons other than integral controllability analysis. For example, SVD can be used to identify the sensitive states and input variables in a multivariable process [106]. When SVD is used for this variable selection, it is important that the process scaling have physical meaning. Bonvin and Mellichamp [104] developed the

equivalence factor scaling method to scale systems that have not been instrumented, and therefore the variable range is unknown. Their approach is to define an equivalence factor to express the accumulation terms in terms of a common variable. Each state is then multiplied by the appropriate equivalence factor. Once the states have been scaled, the inputs are scaled. The scaling factor for a particular input is the maximum of the absolute value of the input factor over all of the equations. Figure 5.01 shows a dynamic system with the state and input scaling matrices.

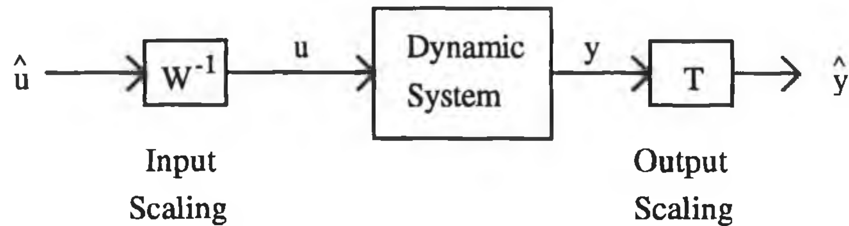

Figure 5.01 Dynamic System with Scaling

Bonvin and Mellichamp's [104] method is useful when no information on the range of the process variables is given. Our philosophy, however, is to allow the process engineer to use his physical insight to scale the process. In the plasma etching or deposition processes, the equipment design sets constraints on the manipulated conditions. For example, the process internal dynamics and performance quantities determine the minimum and maximum inputs.

The most useful method for process scaling is based on the physical range of the variables. From a simulation point of view, it is preferable to have the variables cover the same range, so that one can obtain a feel for the effect of each manipulated variable on each output variable. For many uses of the SVD technique it is necessary that the variables cover the same range. SVD can be used to determine the strongest input and output directions for a process.

$y = Gu$; **(5.2-1)**

$G = U \Sigma V^T$; **(5.2-2)**

where y = outputs : y_1 , y_2 ;

u = inputs : u_1, u_2 ;

U = left singular matrix (m x m);

Σ = singular value matrix (n x n);

V = right singular matrix (n x n).

Equation (5.2-2) can also be expressed in a dyadic expansion :

$$G = \sum_{k}^{q} \sigma_i U_i V_i^T \ ; \qquad \textbf{(5.2-3)}$$

An input vector in the direction of V_i is scaled by σ_i and is transformed into the output direction U_i. This is easily seen by using the dyadic expansion of G :

$$y = Gu = \sum_{k}^{q} \sigma_i U_i V_i^T u \ ; \qquad \textbf{(5.2-4)}$$

If the input variable vector, u, is in the direction of V_i, $V_i^T u = 1.0$ and $V_j^T u = 0.0$ ($i \neq j$), therefore

$$y = \sigma_i U_i (1.0) \ ; \qquad \textbf{(5.2-5)}$$

Considering a 2x2 process, a dyadic expansion of Equa (5.2-3) is

$$G = \sigma_1 U_1 V_1^T + \sigma_2 U_2 V_2^T \ ; \qquad \textbf{(5.2-6)}$$

If the input vector is unit length, in the V_1 direction, then

$$y = \sigma_1 U_1 \ ; \qquad \textbf{(5.2-7)}$$

indicating that the output vector length is σ_1 in the U_1 direction. The minimum length bound is when the input vector is in the V_2 direction. In this case

$$y = \sigma_2 U_2 \ ; \qquad \textbf{(5.2-8)}$$

or magnitude σ_2 in the U_2 direction.

If the manipulated variables u_1 and u_2 are not scaled to the same range, then no useful information can be obtained. The physical scaling technique has been found useful to the SF_6/Ar plasma etching process.

5.3 Multivariable Dynamic Interaction Analysis

The plasma etching process is a complex multi input- multi output (MIMO) system, where each input may affect each output of the process. The following questions constitute the essence for the design problem on the synthesis of multivariable plasma etching control system: Which variables should be controlled

and which should be measured in order to monitor completely the operation of a plant? Which inputs should be manipulated for effect control ? How should the output measurements be paired with the manipulates to form the control structure? This has commonly been referred to as interaction analysis. The simplest control scheme for a MIMO process is known as a multivariable single input-single output (MVSISO) control strategy. Figure 5.02 is an input-output block diagram of a multivariable process, where each input may affect each output of the process.

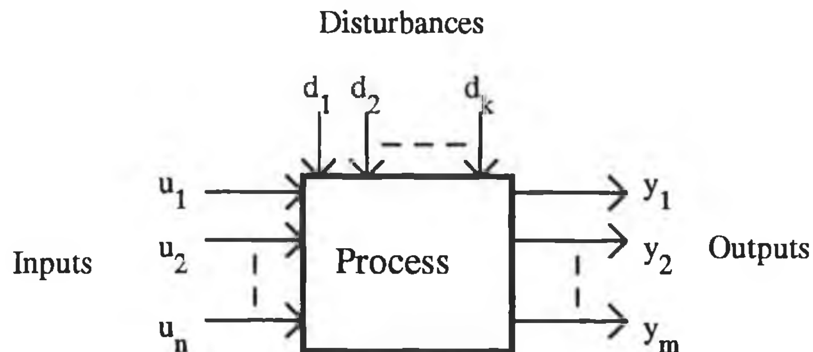

Figure 5.02 Input-Output Block Diagram of a Multivariable Process

When a MVSISO strategy is used, the primary question is "how do we select which output, y_i, will be paired with which input, u_i ?" Consider the simplest multivariable system, one with 2 inputs and 2 outputs.

$$\begin{bmatrix} y_1(s) \\ y_2(s) \end{bmatrix} = \begin{bmatrix} g_{11}(s) & g_{12}(s) \\ g_{21}(s) & g_{22}(s) \end{bmatrix} \begin{bmatrix} u_1(s) \\ u_2(s) \end{bmatrix} ; \qquad \textbf{(5.3-1)}$$

The control diagram for this 2 x 2 case, with the y_1-u_1 and y_2-u_2 pairing is shown in Figure 5.03. The potential problem with control loop interaction is shown by the following analysis: If a change in set point, $r_1(s)$, is made, the controller $g_{c1}(s)$ will cause a corresponding change in the input variable, $u_1(s)$. Since u_1 has an effect on both y_1 and y_2, both outputs will change. A change in output y_2 then causes a change in input variable u_2, through controller g_{c2}. Input u_2 also effects both y_1 and y_2, so we can see how a simple set point change in one variable has been propagated through both loops. The same type of analysis can be used when a disturbance enters the system.

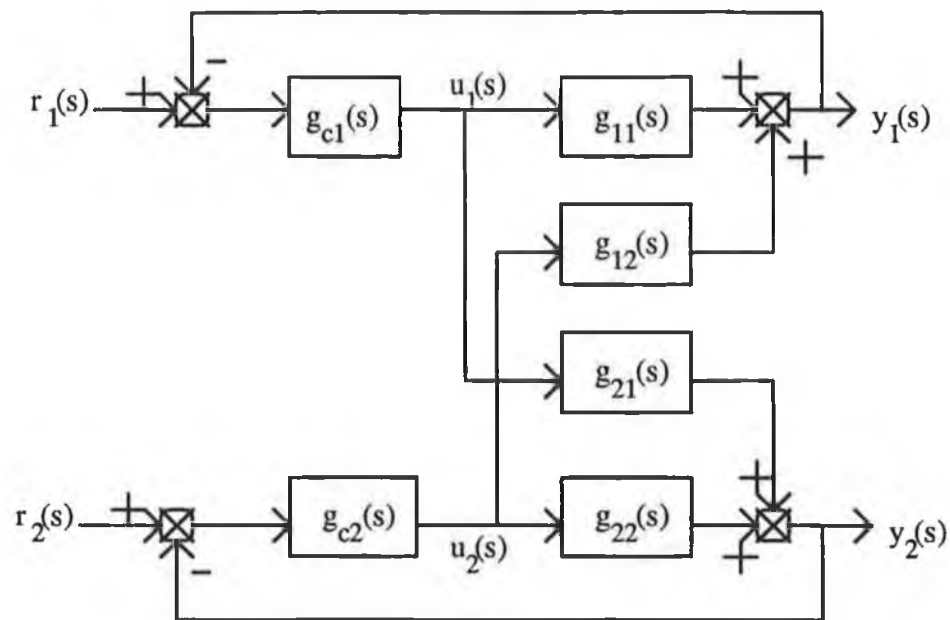

Figure 5.03 MIMO Control Loops for a 2x2 Process

Obviously, time domain simulations can be performed, and the controller tuned iteratively until an "acceptable" response is obtained. The same method could be performed on each possible pairing, with the final pairing based on the best response. With a 2x2 system, there are only 2 possible pairings, so this method is feasible, albeit time consuming. With a n x n system the number of possible pairings is n! We can see that a synthesis method, that would allow one to determine the best controller pairing a priori (without controller tuning) is desirable. This has been an active area of research in the past two decades. The most common methods that have been suggested are input decoupling and implicit decoupling [95]. In actual practice, these methods have not been effective because of the sensitivity to model error. The structural interaction analysis based on SVD has been used to determine variable pairings in this work [96]. Since the steady state model based on this method has been created to obtain much structural information.

The set of regression analysis equations relating the manipulated variables to each of the process and performance variables combines with the steady state process gains and time constants to form the steady state model for multivariable control of the SF_6/Ar etching system (Chapter 4). The relative concentration of F and E/p are found to be insensitive to the changes of SF_6 flow rate. Then terms I_{13} and I_{23} in the following scaled model can be designed to be 0.

$$\begin{bmatrix} [F] \\ \\ [E/p] \\ \\ [SF_x] \end{bmatrix} = \begin{bmatrix} \frac{0.70}{0.40S+1} & \frac{0.20}{0.20S+1} & 0 \\ \frac{0.50}{0.40S+1} & \frac{0.65}{0.15S+1} & 0 \\ \frac{0.90}{0.40S+1} & \frac{0.9}{0.12S+1} & \frac{15}{0.40S+1} \end{bmatrix} \begin{bmatrix} \text{Chamber Pressure} \\ \\ \text{RF Power Density} \\ \\ SF_6 \text{ Flow Rate} \end{bmatrix} ; \qquad \textbf{(5.3-2)}$$

One of the major advantages of SVD is that it requires only steady state gain information which has found use in control systems engineering. As discussed in the last section, the system must be correctly scaled (i.e. all input and output variables should cover the same range). Klema and Laub [103] gave a more complete treatment of the topic, so only a brief treatment will be given here. The SVD of a general m x n complex matrix was described in equation (5.2-2). The non-zero values of Σ, called the singular values of K, are the eigenvalues of G^TG. The number of non-zero values in Σ is the rank of G.

$$\Sigma = \begin{bmatrix} \Delta & 0.0 \\ 0.0 & 0.0 \end{bmatrix} \begin{matrix} q \\ m-q \end{matrix} ; \qquad \textbf{(5.3-3)}$$
$$\begin{matrix} q & n-q \end{matrix}$$

$q = \text{rank } G \leq \min(m,n)$,

Δ is a diagonal matrix of ordered singular values

$\sigma_1 \geq \sigma_2 \geq \cdots \geq \sigma_q > 0.0$;

U,V are unitary matrices, i.e. each column is orthogonal to every other column and of norm 1.0. Consider first the properties of a unitary matrix.

$U = [\ U_1\ U_2 \cdots U_m\ ]$; **(5.3-4)**

$V = [\ V_1\ V_2 \cdots V_n\ ]$; **(5.3-5)**

then

$U_i^TU_j = 0.0, \ i \neq j$; $\quad U_i^TU_j = 1.0, \ i=j$;

$V_i^TV_j = 0.0, \ i \neq j$; $\quad V_i^TV_j = 1.0, \ i=j$;

Additionally, the ratio of the largest to the smallest non-zero singular values is called the condition number of the matrix. The condition number is used to identify potential control problems for a process by showing the sensitivity of the process to changes in the matrix elements. A process which has a large condition number will be very sensitive to errors in the gains, and may be difficult to control.

$$\text{Condition number} = \frac{\text{Highest number in } \Sigma \text{ matrix}}{\text{Lowest number on the diagonal of } \Sigma \text{ matrix}} \; ; \qquad (5.3\text{-}6)$$

The SVD can be given the geometrical interpretation [96] shown in Figure 5.04.

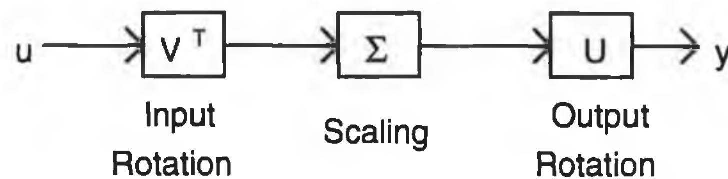

Figure 5.04 Geometrical Interpretation of SVD

The following dyadic expansion form of SVD is also used to determine suitable control loop pairings, the so-called natural loop pairings [96], in a plasma etching system.

$$\sum_{k=1.0}^{q} \sigma_k W_k \; ; \quad W_k = U_k V_k^T \; ; \qquad (5.3\text{-}7)$$

where q is the rank of the steady-state gain matrix
σ_k is the kth singular value
U_k is the kth column of the left singular matrices
V_k is the kth column of the right singular matrices

For each k, the y_i - u_i pairing is determined by the maximum element $|W_k|$. For the system (5.3-2) the SVD is:

$$U = \begin{bmatrix} 0.1281 & -0.6298 & 0.7661 \\ -0.0222 & -0.7741 & -0.6327 \\ -0.9915 & -0.0640 & 0.1131 \end{bmatrix};$$

$$\Sigma = \begin{bmatrix} 1.9827 & 0 & 0 \\ 0 & 1.0364 & 0 \\ 0 & 0 & 0.2591 \end{bmatrix};$$

$$V^T = \begin{bmatrix} 0.4897 & -0.7432 & 0.4558 \\ -0.4444 & -0.6626 & -0.6029 \\ -0.7501 & -0.0926 & 0.6648 \end{bmatrix};$$

Examination of the singular values reveals that the condition number is 1.9827/0.2591= 7.652, indicating a relatively well conditioned process because of the small condition number [91][97]. This suggests that this process is not very difficult to control. The rows of V^T map through the singular values in descending order, so that the first row maps through the largest singular value and last row maps through the minimum singular value. In addition, the rows of V^T are orthonormal (the squares of the elements sum to 1), so a large magnitude in one direction indicates that the magnitudes in the other directions be small. It can be seen that the largest value in V^T for SF_6 flow rate (the (3,3) element in above V^T) maps through the minimum singular value, indicating that flow rate has a little effect on any of the outputs, since the minimum singular value is very small relative to the other singular values. It is likely that the relative insensitivity of our system to SF_6 flow rate is due in part to the fact that the reactor is operated in a region of very low loading (only a small part of electrode is covered by chips with the bulk of the plasma). Based on above analysis, the suitable control loop pairings can be determined by equation (5.3-7): [F] -- Pressure, [SF_x] -- SF_6 flow rate, [E/p] -- RF power. These pairings are stable based on Niederlinski stability criterion [97].

5.4 Decoupling Multivariable Control Strategy

5.4.1 Design of a Structural Compensator

The SVD can be used to design structural compensators [96] to minimize control loop interactions for the plasma etching process. Consider the static system shown in Figure 5.04. An input compensator, V, and an output compensator, U^T, can be added as shown in Figure 5.05(a). Since V^TV and $U^TU = I$ and Σ is a diagonal matrix, then the structured inputs (u^*) and outputs (y^*) form a naturally decoupled system (Figure 5.05 (b)). The gain between u_i^* and y_i^* is σ_i.

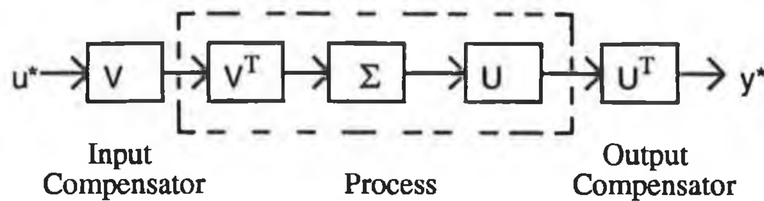

(a) Input and Output Compensation

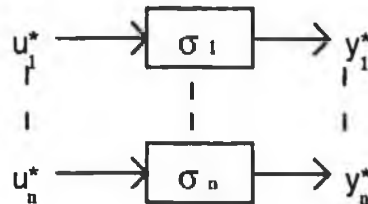

(b) Naturally Decoupled System

Figure 5.05 SVD Structural Compensation

The purpose of the structural compensation design is to create structured inputs and outputs that are non-interacting in the steady state with compensators that are insensitive to measurement and manipulated variable error. From an implementation point of view, it is more desirable to operate on the actual process inputs and outputs. Consider the block diagram for a plasma etching control system

with input and output compensators (D_i and D_o) shown in Figure 5.06 (a) and rearranged in (b), where the actual process inputs and outputs are operated on by the control system.

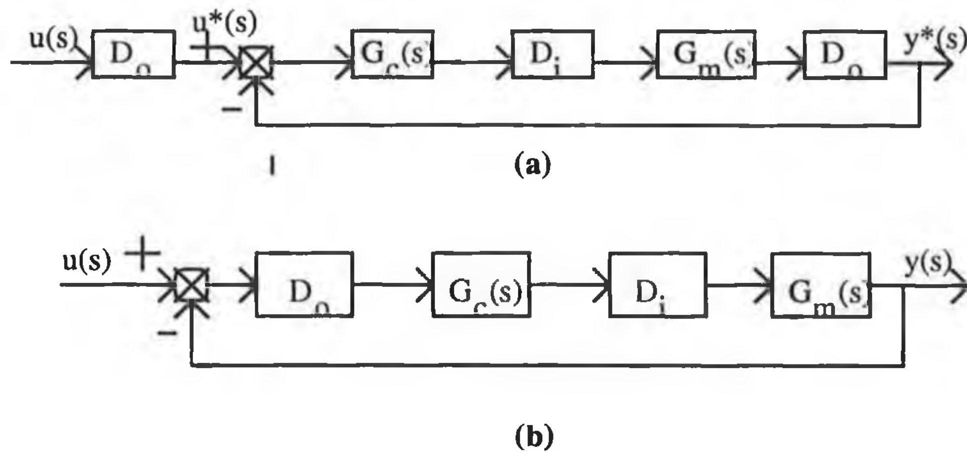

Figure 5.06 Rearrangement of Block Diagram for System with Input and Output Compensation

Then $D_i = V_R$ and $D_o = U_R^T$, where V_R and U_R are the real approximations to $V(j\omega)$ and $U(j\omega)$ respectively. The multivariable control structure for plasma etching can be designed by making use of SVD pairing single-loop controllers with a structural compensation. The resulting input and output compensator for system (5.3-2) based on steady state decomposition are shown as follows

$$\text{Input Compensator} = \begin{bmatrix} 0.4897 & -0.4445 & -0.7501 \\ -0.7433 & -0.6626 & -0.0927 \\ 0.4559 & -0.6028 & 0.6548 \end{bmatrix};$$

$$\text{Output Compensator} = \begin{bmatrix} 0.1280 & -0.0222 & -0.9915 \\ -0.6298 & -0.7741 & -0.0640 \\ 0.7661 & -0.6327 & 0.1131 \end{bmatrix};$$

Both of the compensators are needed to break the plasma etching control scheme into non-interacting loops in steady state.

5.4.2 Set-point Compensation and Disturbance Analysis

SVD has been used by Morari [100][107] to assess the operability characteristics of a chemical process plant. This technique is also employed to plasma etching process in our work. The general term operability is used to describe "the ability of the plant to perform satisfactorily under conditions different from the nominal design conditions". The particular term resilience is defined as "a fast and smooth changeover and recovery from process disturbances". The SVD is an important norm bounding technique to analyse static and dynamic resilience, because relevant information pertaining to disturbance directions is obtained. The analysis is based on the open loop plant model, because of the following insights [100]: Any controller provides an approximate inverse of the plant transfer function matrix; Closed loop control quality is limited by system invertibility.

Consider the model,

$$y(s) = G(s)u(s) + d(s) \qquad \textbf{(5.4.2-1)}$$

where y(s) is output, G(s)u(s) is the regression model (4.3.1-1) (in Chapter 4), d(s) is the system disturbance. If the outputs are perfectly controlled, then

$$u(s) = -G^{-1}d(s) ; \qquad \textbf{(5.4.2-2)}$$

For the steady state case, the SVD of G(0) is

$$G = U \Sigma V^T ; \qquad \textbf{(5.4.2-3)}$$

since $V^TV = I$, $U^TU = I$, and Σ is a diagonal matrix of singular values σ_i, with $\sigma_1 \geq \sigma_2 \geq \cdots \geq \sigma_n > 0.0$, we find

$$u = -V \Sigma^{-1} V^T d ; \qquad \textbf{(5.4.2-4)}$$

Then the "best" direction for the disturbance vector, d, is

$d = U_1$;

which results in a manipulated variable vector

$u = V_1$;

and

$$\frac{\|u\|}{\|d\|} = \frac{1}{\sigma_i} ;$$

The largest disturbance can be tolerated along the left singular vector, associated with the largest singular value.

As an example, consider a setpoint change as a disturbance. The "best" setpoint direction is
$y = U_1$;

and the "worst" setpoint direction is
$y = U_n$;

This is used for the plasma etching process to control the setpoint change using the decoupling multivariable control strategy. The set-point compensator can also be designed by SVD. It has been found that it is a good policy to scale all input and output variables to the range -2 to 2. The magnitude of the disturbance to the plasma etching process caused by the multivariable interactions can be illustrated by calculation of the disturbance in silicon etch rate occurring during the transients, which will be discussed later.

5.4.3 Controller Tuning

The control strategy used for the SF_6/Ar plasma etching process is SVD pairings with steady state structurally compensated MIMO decoupling control, as discussed in the previous sections. The closed-loop transfer function for this scheme, shown in Figure 5.07 is

$$Y = (I + G_c D_o G D_i)^{-1}(G_c D_o G D_i u_d + G_d d) \; ; \qquad \textbf{(5.4.3-1)}$$

where

Output variables $Y = [\, y_1 \;\; y_2 \;\; y_3 \,]$;
Input variables $u_d = [u_{d1} \;\; u_{d2} \;\; u_{d3}\,]$;
SISO Controllers $G_c = \mathrm{diag}\,(g_{11c} \;\; g_{22c} \;\; g_{33c})$;
Disturbance input $d = [d_1 \;\; d_2 \;\; d_3\,]$;
Disturbance $G_d = [g_{d1} \;\; g_{d2} \;\; g_{d3}\,]$;
Output compensator $D_o = [d_{o1} \;\; d_{o2} \;\; d_{o3}\,]$;
Input compensator $D_i = [d_{i1} \;\; d_{i2} \;\; d_{i3}\,]$;
Plasma etching process transfer function G has been described in Equations (4.3.1-1) and (5.3-2). The I is an identity matrix.

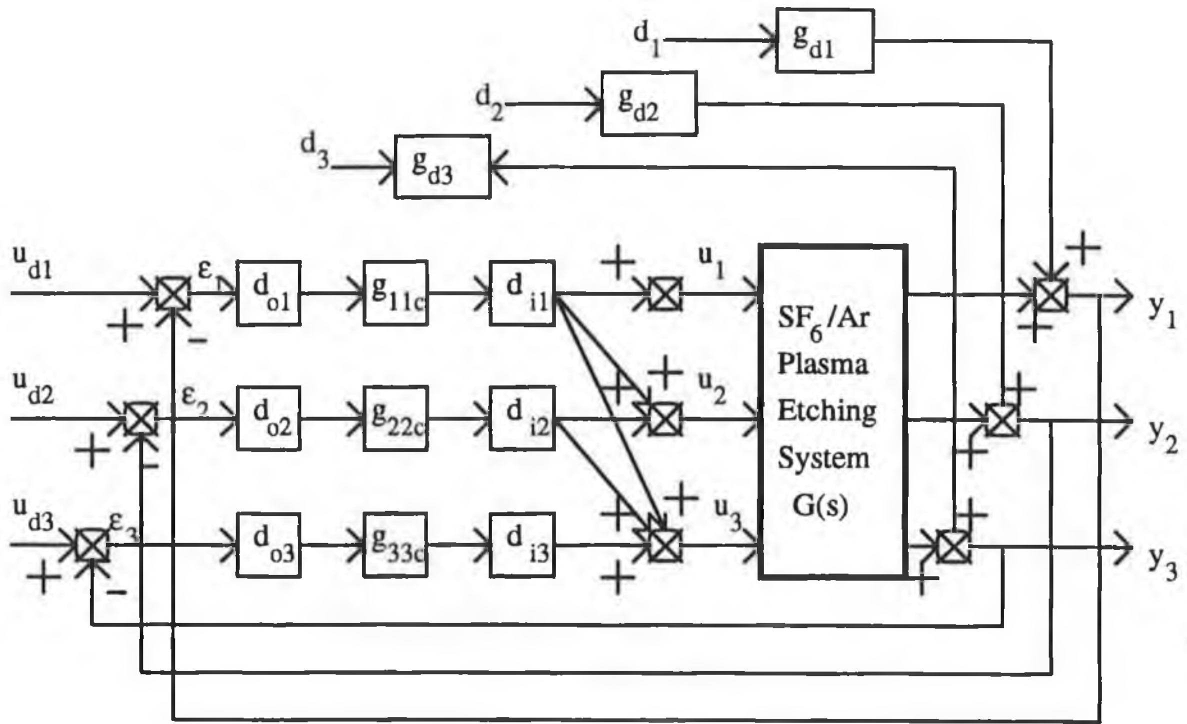

Figure 5.07 SVD Pairing with Structurally Compensated Decoupling MIMO Controller Structure for the SF_6/Ar Plasma Etching System

As discussed in section 5.4.1, if the structural compensation is done perfectly, then

$$D_oGD_i = \text{diag } G(s) ; \tag{5.4.3-2}$$

The closed-loop system transfer function (5.4.3-1) would take the form

$$Y = (I + G_c \text{ diag } G)^{-1}(G_c \text{ diag}G\, u_d + G_d d) ; \tag{5.4.3-3}$$

The initial parameters are tuned using the PI IMC technique [100]. The single-loop controllers are $G_c(s)=\text{diag}(g_{ijc})$ [102]. The low order transfer function model has been estimated from the scaled steady state model. For the first-order plant with step inputs and disturbances, the tuning constants are

$$K_c = \frac{\tau}{K\lambda} \quad \text{and } \tau_I = \tau ; \tag{5.4.3-4}$$

where

K_c, τ_I are the PI tuning constants

K, τ are the steady state gain and time constant of the first-order plant transfer function.
λ is the IMC filter constant = the closed-loop time constant.

Using PI IMC tuning rules, if we neglect disturbances for the moment, the closed loop transfer function (5.4.3-3) becomes

$$Y = \frac{1}{\lambda s + 1} ; \qquad \textbf{(5.4.3-5)}$$

IMC tuning constants for a structurally compensated MIMO system provide controller settings which produce a first-order closed-loop transfer function with a time constant equal to λ and no offset. The gains and time constants used in this analysis are taken from the regression model presented in Chapter 4. According to Morari, et al.[100], λ should be greater than 0.1τ for the first-order systems with dead time. τ is the time constant here. This is generally a good specification for any process since it is not realistic to specify a control system which forces the process to respond 10 times faster than the open-loop case especially for the plasma etching system. λ is initially set to 0.5τ to provide closed-loop response 2 times faster than the open-loop response. Table 5.1 lists the initial tuning constants used for the SF_6/Ar plasma etching process.

The selection of set points for the manipulated variables is in terms of the process variables. The correlations from the regression analysis discussed earlier are used for this purpose.

Table 5.1 IMC Tuning Constants for the Structurally Compensated MIMO Control of the SF_6/Ar plasma etching process.

	[F] -- Pressure	$[SF_X]$ -- SF_6 flow rate	[E/p] -- RF power density
λ	0.20	0.20	0.075
K_c	4.10	9.41	5.50
τ_I	0.40	0.40	0.15

5.5 Simulation Results and Discussion

The low order transfer function model can be estimated from the scaled steady state model based on singular value analysis. The singular value is plotted in Figure 5.08, over the frequency range of interests. The MIMO SVD pairings can be designed using condition number based on singular values.

Figures 5.09, 5.10 and 5.11 show the closed loop responses obtained when the set points of process variables [F], $[SF_X]$, [E/p] are unit step changed, for SVD pairings with the structural compensated MIMO and conventional control of SF_6/Ar plasma etching system, respectively. Figures 5.12 and 5.13 illustrate the effects of 15% increases in RF power density and SF_6 feed flow rate, for SVD pairings with structural compensated MIMO and PI conventional controllers.

The response for the structurally compensated MIMO scheme are typically much faster than the conventional scheme. The dynamic response of the conventionally controlled system is much more dependent on the direction of the forcing and for a step change that is closely aligned with the best disturbance direction [100]. For the same degree of robustness, the performance of the structurally compensated MIMO strategy is much better than the conventional control scheme.

5.6 Performance Variable Analysis

Control system having been demonstrated for SF_6/Ar plasma etching system, it is still necessary to find criteria for choosing set points for the process variables based on performance quantities. The correlations between them studied in Chapter 4 are used for this purpose. These equations are scaled and linearized as in the manipulated/process variable analysis presented in section 5.3. The resulting steady state gain matrix is shown

$$\begin{bmatrix} \text{Si Etch Rate} \\ \\ \text{Si Uniformity} \\ \\ \text{Si Anisotropy} \end{bmatrix} = \begin{bmatrix} 0.800 & 0.050 & -0.030 \\ 0.030 & 1.200 & -0.080 \\ 0.000 & -0.05 & 1.150 \end{bmatrix} \cdot \begin{bmatrix} E/p \\ [SF_x] \\ [F] \end{bmatrix} ; \qquad \textbf{(5.6-1)}$$

SVD analysis is run on this matrix to determine the natural process/performance variable pairings.

$$U = \begin{bmatrix} 0.1004 & -0.0292 & 0.9945 \\ 0.8274 & -0.5527 & -0.0998 \\ -0.5526 & -0.8329 & 0.0313 \end{bmatrix} ;$$

$$\Sigma = \begin{bmatrix} 1.2487 & 0 & 0 \\ 0 & 1.1058 & 0 \\ 0 & 0 & 0.7963 \end{bmatrix} ;$$

$$V^T = \begin{bmatrix} 0.0842 & -0.0361 & 0.9958 \\ 0.8212 & -0.5635 & -0.0899 \\ -0.5643 & -0.8254 & 0.0177 \end{bmatrix} ;$$

The suggested process/performance variable pairings for SF_6/Ar system are: [F] -- Si etch anisotropy, [SF_x] -- Si uniformity, [E/p] -- Si etch rate. The SVD analysis shows which performance variables are most strongly affected by changes in the process variables and these, then, would be most effective when used in process design.

The main use of the SF_6/Ar plasma etching system is to etch silicon, usually in non-critical etching situations where anisotropy is not as necessary but fast uniform etching of silicon is important [5][55]. Being able to specify silicon anisotropy is not very useful in this situation, due to the fact that anisotropy is not critical to the process and that our correlation for anisotropy is poor. The specification of silicon etching uniformity would be more desirable for this etch. The ability to specify silicon etch rate as well as silicon dioxide etch rate is important in this process so that

silicon can be etched quickly, although the SF_6/Ar plasma etching system is employed primarily to etch silicon and SiO_2 etching is not used at the moment. In fact, once the process variable set points are determined, the values of the other performance variables are fixed by the steady-state model relationships.

The control system presented in this chapter could be improved through the use of additional process variables, although it is likely that the measurement of these variables would have to be intrusive to the etching reactor. Specifically, the direct measurement of electron density and the electron energy distribution would be of use in specifying both anisotropy and uniformity.

5.7 Conclusions

Though the simplified dynamic models may not describe the actual plasma etching process as closely as more rigorous dynamic models, there are several important reasons why one might use these models for the control of the real process: The simulation times are much shorter; the important dynamics are also included in the simplified models; only a few parameters need to be specified for a simulation; one of the most important purposes of dynamic simulation is to see how a control system responds to various disturbances and changes in operating conditions. These effects can be identified using the simplified models.

The singular value decomposition yields a system that is non-interacting in the steady state, with compensators that are insensitive to measurement and manipulated variable error, because the plasma etching process vectors of the matrix compensators are orthonormal. We have found that SVD dynamic interaction analysis rarely changes the variable pairing that is obtained from a steady state analysis. Dynamic interaction analysis methods are most useful for determining when a MVSISO strategy is insufficient and a multivariable strategy must be used. This is a logical first step in the control system synthesis and design process. Once one has gone to the trouble of obtaining a dynamic process model, little additional effort is required to perform a much more complete analysis of the feedback control system. Efficient computer-aided-design techniques utilising interactive graphics exist for closed loop stability and performance analysis.

The control system engineer should use process insight to obtain bounds on the process uncertainty. It is well known that good closed loop properties at the plant output do not assure good properties at the plant input. So we cannot consider the effects of output uncertainty only. These will be discussed in next chapter.

A singular value sensitivity technique with a structural compensator has been found to be particularly effective in tuning controllers for simplified decoupling multivariable control of the plasma etching process, though structural compensation may form right half plane zeros (which are known to make control more difficult) since transfer functions are basically being added and subtracted. This particular problem exists with any decoupling type of techniques.

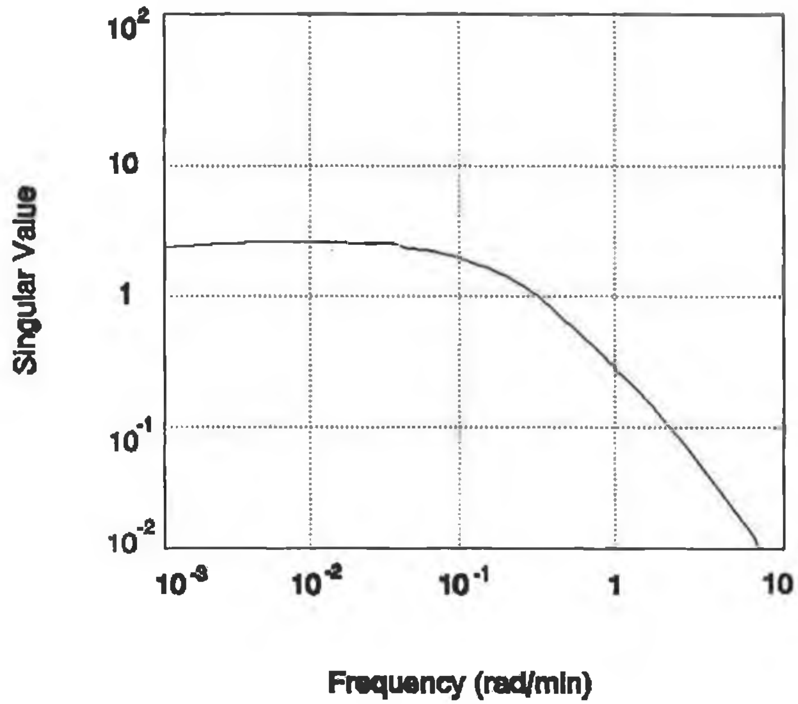

Figure 5.08 Maximum Singular Values for Structurally Compensated Plasma Etching System

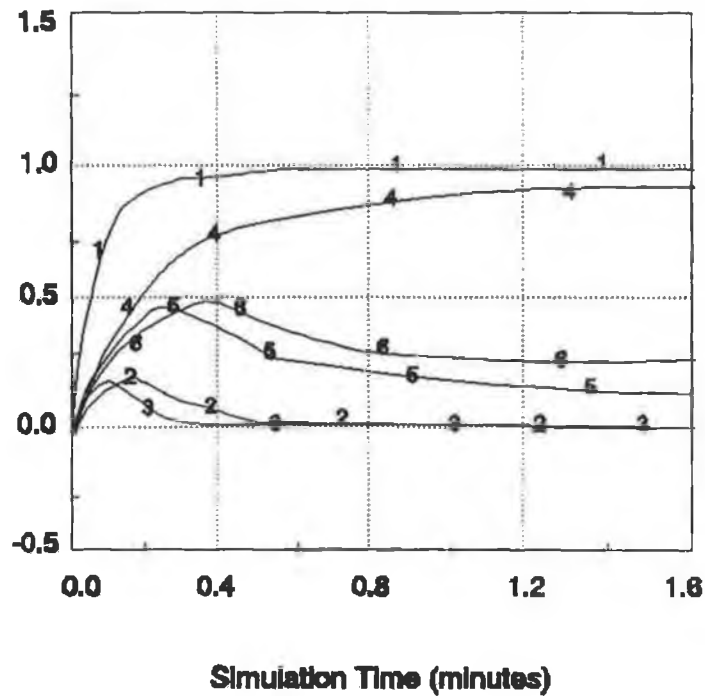

Figure 5.09 SF_6/Ar Plasma Etching System Closed Loop Response to Step Change in [F]. 1,4=[F]; 2,5=[SF_x]; 3,6=[E/p]

1,2,3 —— SVD Pairings with Structurally Compensated MIMO Control System;
4,5,6 —— Conventional Control

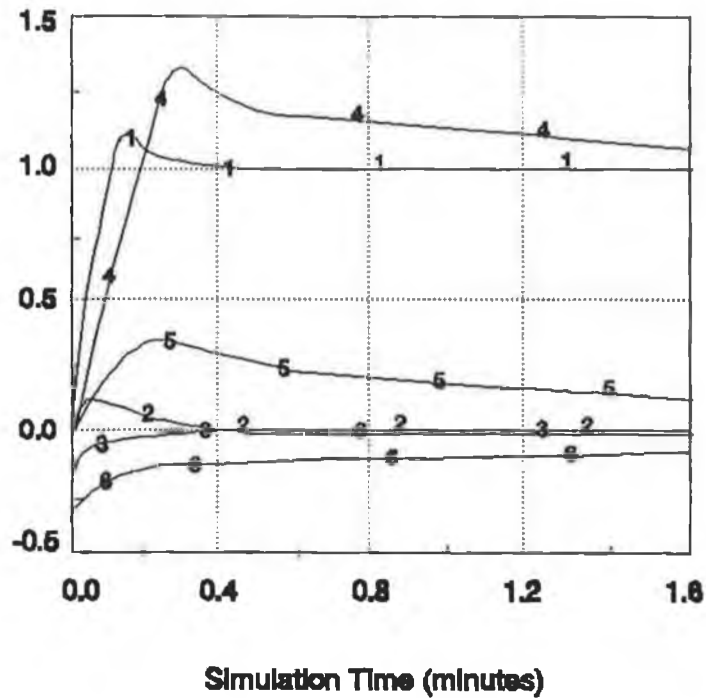

Figure 5.10 SF$_6$/Ar Plasma Etching System Closed Loop Response to Step Change in [SF$_x$]. 1,4=[F]; 2,5=[SF$_x$]; 3,6=[E/p]

1,2,3 —— SVD Pairings with Structurally Compensated MIMO Control System;
4,5,6 —— Conventional Control

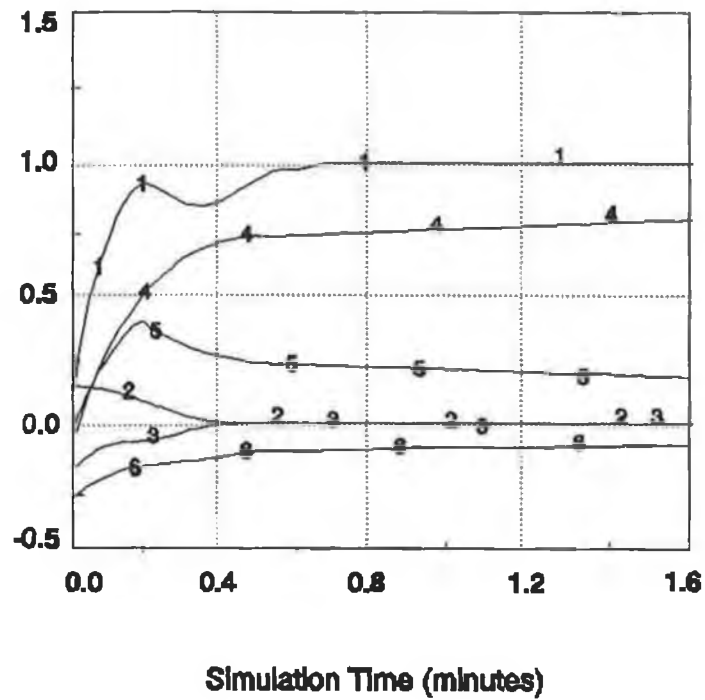

Figure 5.11 SF_6/Ar Plasma Etching System Closed Loop Response to Step Change in [E/p]. 1,4=[F]; 2,5=[SF_x]; 3,6=[E/p]

1,2,3 —— SVD Pairings with Structurally Compensated MIMO Control System;
4,5,6 —— Conventional Control

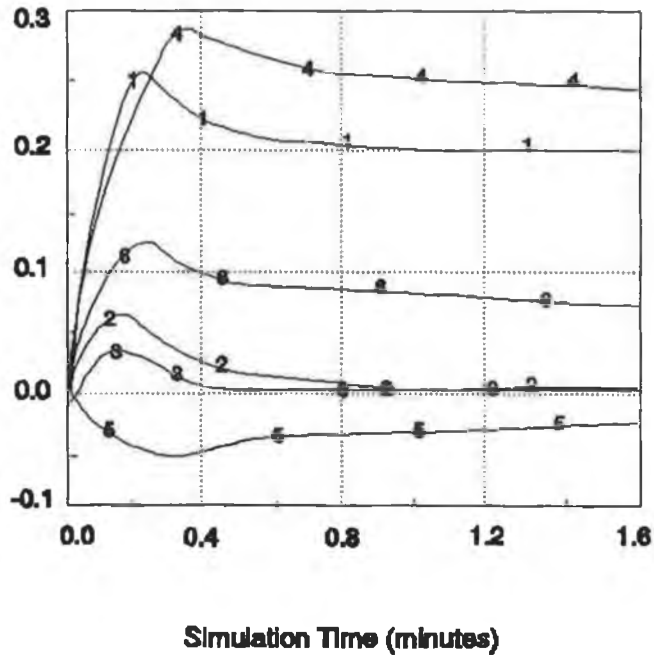

Figure 5.12 SF_6/Ar Plasma Etching System Closed Loop Response for a 15% Increase in RF Power Density. 1,4=[F]; 2,5=[SF_x]; 3,6=[E/p]

1,2,3 —— SVD Pairings with Structurally Compensated MIMO Control System;
4,5,6 —— Conventional Control

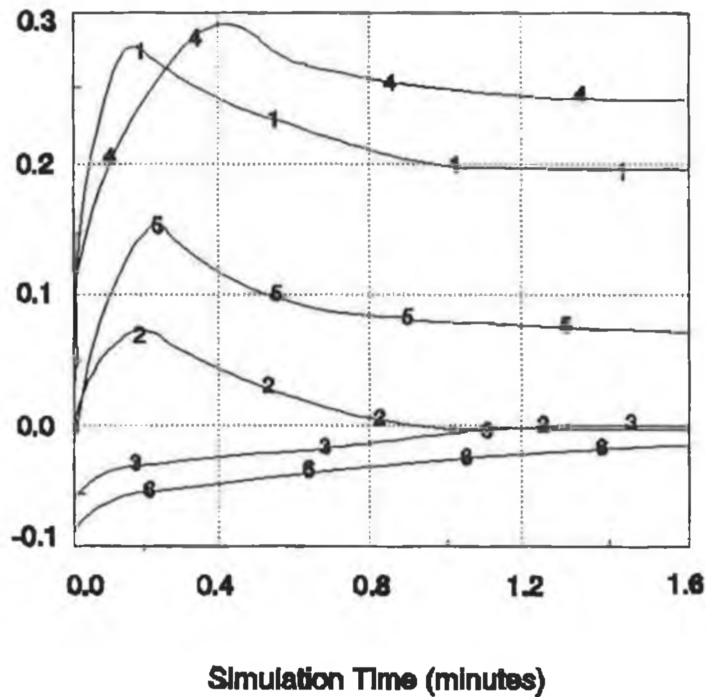

Figure 5.13 SF_6/Ar Plasma Etching System Closed Loop Response for a 15% Increase in SF_6 Flow Rate. 1,4=[F]; 2,5=[SF_x]; 3,6=[E/p]

1,2,3 —— SVD Pairings with Structurally Compensated MIMO Control System;
4,5,6 —— Conventional Control

CHAPTER 6 ROBUST MULTIVARIABLE CONTROL SYSTEM DESIGN

6.1 Introduction

Frequency response control system design techniques have been used for single input-single output (SISO) systems for decades. Early attempts at developing multivariable frequency response techniques were concerned with designing compensators that yielded a diagonally dominant system. Standard SISO techniques could then be used for control systems design. An alternative approach operated on the full multivariable system by extending SISO stability conditions to the multivariable case. Concurrently, developments in computer-aided-graphics gave the control systems engineer the proper tools for quick, accurate interactive control systems design, using judicious amounts of engineering judgement. However, it has only been in the past decade that methods have been developed to rigorously account for the effect of model uncertainty on the design of multivariable control systems. Also, much of the work in academia has previously been based on the assumption that the process being controlled was linear and perfectly modelled. Historically there have been little published work on real-time control of highly non-linear industrial plasma etching processes.

Control system design using linear techniques is based on models that approximate the dynamic behaviour of a physical system. As might be expected, deviation between the model dynamics and the actual system dynamics often exists. Additionally, you may find that during a product's life cycle, system dynamics vary enough to cause concern about system performance or stability. Such scenarios require a controller capable of satisfactory performance in the face of uncertainties. Controllers that behave well in the presence of model variations or uncertainties are termed "robust". The real problem in robust multivariable feedback control system design is to synthesise a control law which maintains system response and error signals to within specified tolerances despite the effects of uncertainty in the system. Uncertainty may take many forms, but among the most significant are noise/disturbance signals and transfer function modelling errors. Another source of uncertainty is unmodelled non-linear dynamics.

The purpose of this chapter is to apply some of the robust multivariable control schemes to plasma etching process control system design in the presence of uncertainty. The desirable properties of multivariable feedback control systems will be reviewed. Initial work involves robust stability with respect to unstructured uncertainty, that is, that a control system will remain stable for any plant perturbation less than a given norm. This gives control system designers a tool with which to trade-off stability and performance. A problem with this technique is that the worst case may not occur for a particular plasma etching process. This can result in a conservative control system design. Also, the case of multiple perturbations is not addressed with unstructured uncertainty procedures. This led to the development of structured uncertainty techniques, which give the designer the ability to provide designs with better performance, for a given uncertainty norm. The robust multivariable control system analysis based on structured uncertainties of inputs and outputs have then been formulated as a "block diagonal bounded perturbation" problem (BDBP) [100]. The solution to this problem involves the use of structured singular value (SSV) that is a generalisation of the singular value decomposition, which is found very useful for robust multivariable control analysis. The robust stability and robust performance properties in the presence of structured process uncertainty and disturbances are discussed for the SF_6/Argon etching system.

In this Chapter, practical design and analysis methods for the robust multivariable control of the SF_6/Argon plasma etching process of Si and SiO_2 based on structured uncertainties at the process' inputs and outputs are presented. The model uncertainty due to process non linearity is highly structured in this process. The initial multivariable control systems are designed by using SVD pairings with input and output structural compensators and conventional control schemes respectively (Chapter 5). Results presented in this work show that both of the control strategies satisfy these robustness requirements, but the robust stability of conventional control is worse for multiplicative input uncertainties and structurally compensated scheme is less sensitive to input perturbations.

6.2 Desirable Multivariable Feedback Properties

The purpose of this section is to outline desirable feedback properties in terms of matrix norms. The relationship of these properties to the model uncertainty issue

will be discussed in the next section. The matrix norm used is the spectral (maximum singular value) norm. A good general reference is Hung and Macfarlane [118]. Consider the multivariable control system shown in Figure 6.01.

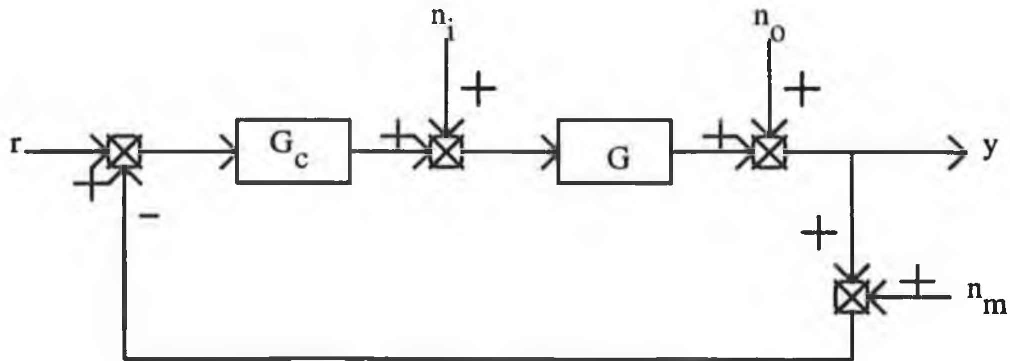

Figure 6.01 General Multivariable Feedback Control System

The following relationship can be found :

$$y(s) = [I + G(s)G_c(s)]^{-1}G(s)G_c(s)r(s) + [I + G(s)G_c(s)]^{-1}G(s)n_i(s) + [I+G(s)G_c(s)]^{-1}n_o(s) - [I + G(s)G_c(s)]^{-1}G(s)G_c(s)n_m(s) \; ; \quad \textbf{(6.2-1)}$$

6.2.1 Setpoint Tracking

For good setpoint tracking $\frac{\|y(s)\|}{\|r(s)\|} \approx 1.0$. Define

$$R(s) = [I + G(s)G_c(s)]^{-1}G(s)G_c(s) \; ; \quad \textbf{(6.2-2)}$$

Then for good setpoint tracking we desire

$$\sigma^*(R(s)) \approx \sigma^*(R(s)) \approx 1.0 \; ; \quad \textbf{(6.2-3)}$$

where σ^* is the maximum singular value of R(s) over the relevant frequency range (low frequencies).

6.2.2 Measurement Noise Rejection

For good measurement noise rejection, $\frac{\|y(s)\|}{\|n_m(s)\|} \approx 0.0$. We then desire

$\sigma^*(R(s)) \approx 1.0$; **(6.2-4)**

over the relevant frequency range for measurement noise. We see immediately that the control system must be designed to have good setpoint tracking properties, yet adequate measurement noise rejection - two conflicting requirements. Generally, we are concerned about setpoint tracking at low frequencies (near steady state), while measurement noise is normally a high frequency problem. This suggests that R(s) should be designed as a low pass filter. The limit to tight high frequency control is model uncertainty.

6.2.3 Disturbance Rejection

Let $n_i(s)$ and $n_o(s)$ represent input and output process noise (disturbances), respectively. For good disturbance rejection, $\frac{\|y(s)\|}{\|n_i(s)\|} \approx \frac{\|y(s)\|}{\|n_o(s)\|} \approx 0.0$. Defining

$T(s) = I + G(s)G_c(s) \equiv$ Return Difference Matrix **(6.2-5)**

then we desire

$\sigma^*(T^{-1}(s)) \approx 0.0$; **(6.2-6)**

for output disturbance rejection and

$\sigma^*(T^{-1}(s)\, G(s)) \approx 0.0$; **(6.2-7)**

for input disturbance rejection. Since G(s) is the process transfer function matrix, $T^{-1}(s)$ is the only matrix determined by the control system design procedure.

Some equations relating the desirable characteristics of multivariable feedback systems have been cited. In the next section the equation for robust stability and performance of multivariable systems with model uncertainty will be discussed.

6.3 Multivariable Control System Analysis Based on Unstructured Uncertainty

Initial robust multivariable control system design methods are based on the assumption that the model uncertainty is unstructured, i.e. only a maximum magnitude bound on the error is available. This section will cover these unstructured techniques. Many of the examples presented in the literatures are purely mathematical examples, not representing any physical process. An example of an early study using unstructured uncertainty was presented by Stein and Doyle [109]. A special issue of IEEE Transactions on Automatic Control contained several relevant articles [116][112][114][115][119]. First, it is important to have an understanding of the forms for expressing model uncertainty.

6.3.1 Characterisation of Uncertainty

Multivariable process uncertainty can be represented by several forms as shown in Figure 6.02: (a) Additive, (b) Multiplicative output, (c) Multiplicative input, (d) Output division, (e) Input division, and (f) Feedback uncertainty. The relationships between the nominal process $G_m(s)$, the actual process $G_p(s)$, and the error matrix L(s) are shown in Table 6.1. A model uncertainty expressed in one form is easily expressed in any of the other forms. For example, a process with additive uncertainty $L_a(s)$ can be expressed as an output uncertainty by the following transformation : $L_o(s) = L_a(s)G_m^{-1}(s)$. The two most commonly used error characterisations are the multiplicative output and input forms [110][113]. The additive error characterisation was used by Arkun [113] in their Robust Nyquist Array approach. The division and feedback uncertainty characterisations have been mentioned by Lehtomaki, et al [116].

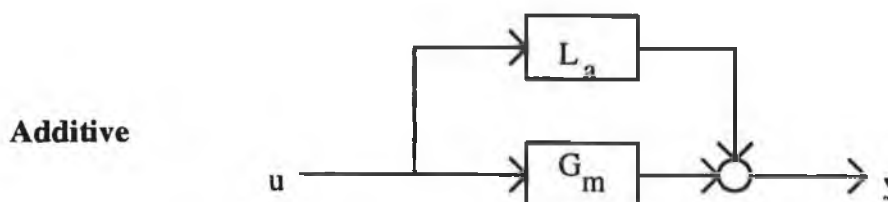

Multiplicative Output

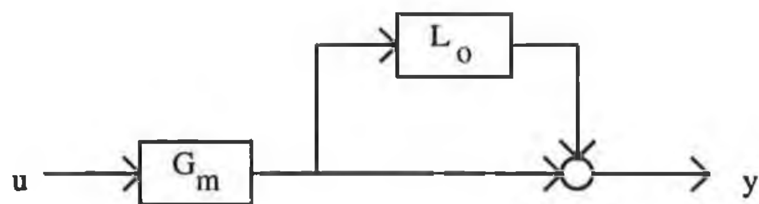

Multiplicative Input

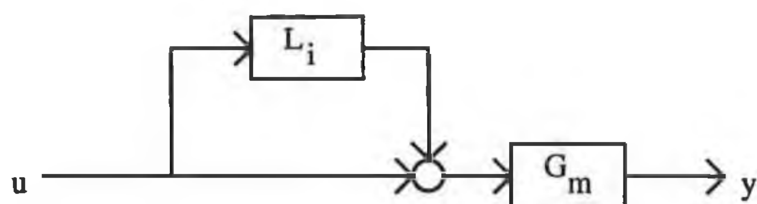

Output Division

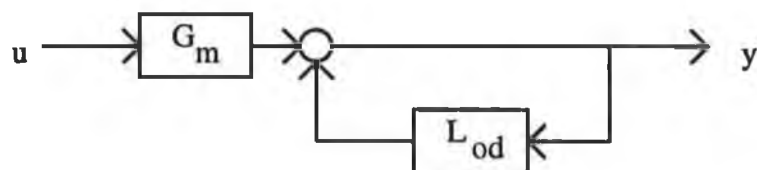

Input Division

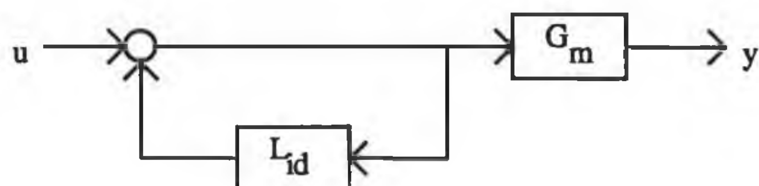

Feedback

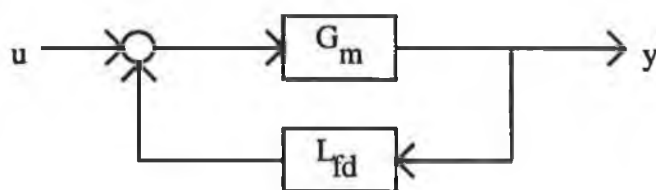

Figure 6.02 Process Uncertainty Relationships

Table 6.1 Process Uncertainty Relationships

Additive	$G_p(s) = G_m(s) + L_a(s)$
Multiplicative Output	$G_p(s) = (I + L_o(s))\ G_m(s)$
Multiplicative Input	$G_p(s) = G_m(s)\ (I + L_i(s))$
Output Division	$G_p(s) = (I - L_od(s))^{-1}\ G_m(s)$
Input Division	$Gp(s) = G_m(s)\ (I - L_id(s))^{-1}$
Feedback	$Gp(s) = (I - G_m(s)L_{fb}(s))^{-1}\ G_m(s)$

The term unstructured uncertainty is used to indicate that the only information available about the error matrix, L(s), is an upper bound on its magnitude. That is

$$l(s) > \sigma^*(L(s)); \qquad \textbf{(6.3-1)}$$

where l is a positive scalar uncertainty, σ^* is a maximum singular value. This representation of uncertainty is generally adequate at higher frequencies, due to unmodelled dynamics. The error matrix could be structured at lower frequencies. The case of structured uncertainties will be covered in section 6.4. The next section is based on an unstructured uncertainty characterisation.

6.3.2 Robustness with Respect to Stability

Assume the nominal closed loop system $[I+G_m(s)G_c(s)]^{-1}G_m(s)G_c(s)$ is stable. The closed loop system is stable for all $L_o(s)$ with $l_o(s) \geq \sigma^*(L(s))$ if and only if all of the models contain the same number of unstable poles as the nominal model and [110]

$$\sigma^*(I + (G_m(j\omega)G_c(j\omega))^{-1}) > l_o(\omega) ; \tag{6.3-2}$$

This is equivalent to the following (the dependence of frequency will be omitted for convenience)

$$\sigma^*(I + (G_mG_c)^{-1}G_mG_c) < 1.0/l_o(\omega) ; \tag{6.3-3}$$

Since $\sigma^*(A) = 1.0/\sigma^*(A^{-1})$. The type of plots for the equivalent expressions are shown in Figure 6.03. Note that equations (6.3-2) and (6.3-3) are based on an output multiplicative perturbation. The corresponding relationships for an input multiplicative perturbation are

$$\sigma^*(I + (G_cG_m)^{-1}) > l_i(\omega) ; \tag{6.3-4}$$

and

$$\sigma^*(I + (G_cG_m)^{-1}G_cG_m) < 1.0/l_i(\omega) ; \tag{6.3-5}$$

It should be emphasised that it is not necessary to have information regarding the error bounds $l_o(\omega)$ and $l_i(\omega)$ in order to tune the controllers for increased robustness. This is because, for a given plant, robustness margins are increased when the minimum singular values of the operators in equations (6.3-2) and (6.3-4) are increased, regardless of the actual error bounds.

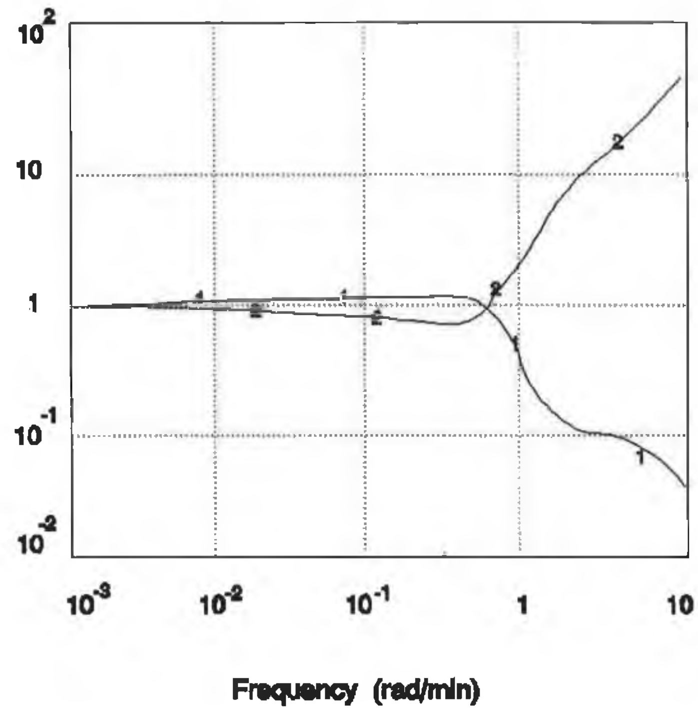

Figure 6.03 Equivalent Plots for Robust Stability with Respect to Output Perturbations

$$1 — \sigma^{*}(I + (G_m(j\omega)G_c(j\omega))^{-1})$$
$$2 — \sigma^{*}((I + G_mG_c)^{-1}G_mG_c)$$

6.3.3 Robustness with Respect to Performance

Arkun, et al [117] have considered a process control system to be robust with respect to performance if for all possible plants. $G_p(s)$, the closed loop system is less sensitive to modelling errors than the equivalent open loop feed forward system. Palazoglu and Arkun [113] have shown that the following inequality quarantines this robustness.

$$\sigma^*(I + G_mG_c)-1.0 \geq 1.0/(\sigma^*[I + (G_mG_c)^{-1}] - l_o(\omega)) \; ; \qquad \textbf{(6.3-6)}$$

The equivalent relationship for input multiplicative uncertainty is

$$\sigma^*(I + G_cG_m)-1.0 \geq 1.0/(\sigma^*[I + (G_cG_m)^{-1}] - l(\omega)) \; ; \qquad \textbf{(6.3-7)}$$

The left side of equations (6.3-6, 7) can be viewed as a performance margin, while the denominator of the right hand side is the stability margin.

6.3.4 Applications of Unstructured Uncertainty

The development of robust multivariable analysis techniques based on unstructured uncertainty is a critical first step towards the development of a more general robust analysis procedure. The advantage is that little information concerning the process uncertainty is needed. Indeed, the tuning procedure based on maximising the operators in equations (6.3-2, 4) are useful even if no bound on the error magnitude is known.

The two major disadvantages of the unstructured uncertainty methods are: (1) no knowledge of the structure of the model error is used, and (2) only one type of uncertainty (e.g. multiplicative output) can be considered at a time. The first disadvantage can lead to conservative designs since equations (6.3-2,4) are only sufficient conditions for stability under output and input perturbations, respectively. There may exist many plants where equations (6.3-2,4) are not satisfied, yet the system are stable. The second disadvantage can not guarantee the stability of systems subject to multiple perturbations.

Consider the SF_6/Ar plasma etching steady state model (in Chapter 5, equation (5.3-2)) and a nominal plant model

$$G_m(s) = \begin{bmatrix} \frac{0.70}{0.40S+1} & 0.0 & 0.0 \\ 0.0 & \frac{1.0}{0.40S+1} & 0.0 \\ 0.0 & 0.0 & \frac{0.65}{0.40S+1} \end{bmatrix}; \qquad \textbf{(6.3-8)}$$

The tuning parameter for this system is determined by using IMC-PID tuning rules presented in Chapter 5 (see Table 5.1). The output uncertainty bound (Eqn.(6.3-2) for the plasma etching system based on the experimental assumptions is shown in Figure 6.04. The minimum $\sigma^* = 0.90$ at 0.50 rad/min. The error bound is $l_o = \sigma^*(L_o) = 0.9$ for the model (5.3-2). The transient response curves shown in Figure 6.05 indicate that the system is stable. This illustrates that, not only is the magnitude of the modelling error important, the structure of the error is important as well.

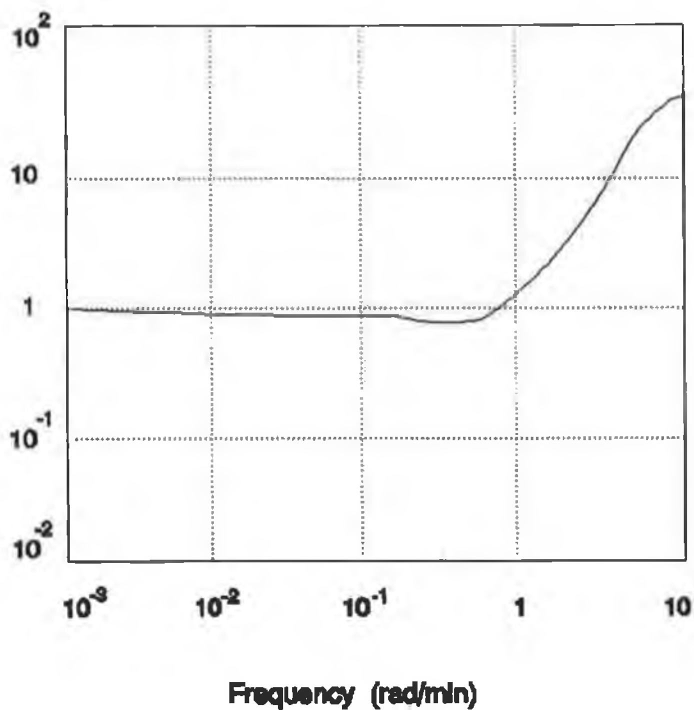

Figure 6.04 Output Uncertainty Bound (Equa.(6.3-2)) for the Plasma Etching System

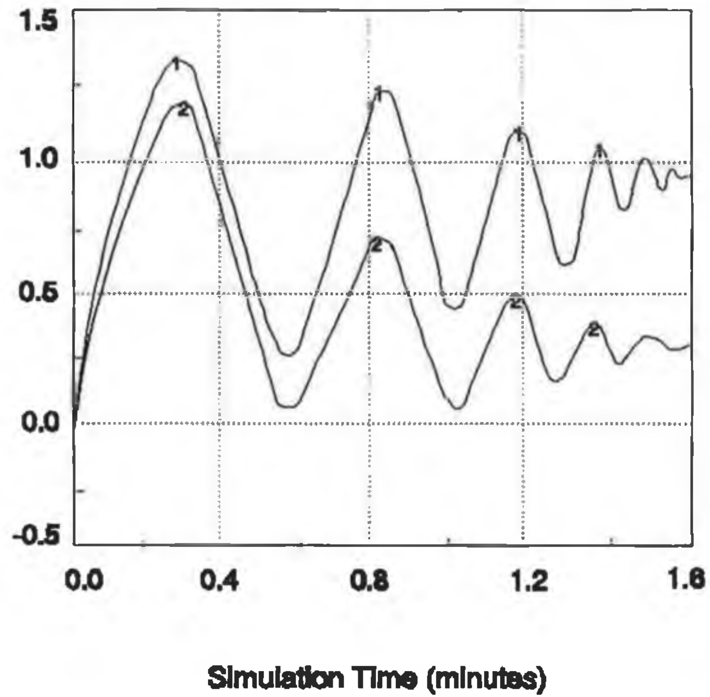

Figure 6.05 Transient Response for SF_6/Ar Plasma Etching System Model

1 = Plasma Etching System Model
2 = Nominal Plant Model

6.4 Multivariable Control System Analysis Based on Structured Uncertainty

The development of analysis methods utilising knowledge of the structure of the process uncertainty is an area of active research interest. Freudenberg, et al [120] presented an analysis procedure based on singular value sensitivities. Their methods can handle structured plant perturbations as well as detect the sensitivity of a feedback system due to simultaneous input and output perturbations. Lehtomaki, et al [121] proposed a method that utilises a partial characterisation of the structure of the modelling error.

Doyle, et al [100][101] have formulated the structured uncertainty as a "block diagonal bounded perturbation" (BDBP) problem. The solution to this problem involves the structured singular value (SSV), which is a generalisation of the singular value decomposition. Doyle [100] has also developed a procedure to synthesise a control system that minimised the SSV for a particular BDBP problem. Morari and Doyle [100] have presented a tutorial that discussed the potential for structured uncertainty analysis in chemical process control.

The SSV method has been found very useful for plasma etching process control, since the model uncertainty due to the non-linear behaviour is highly structured. The next section will introduce the SSV technique, which will be applied to SF_6/Ar plasma etching process control.

6.4.1 The Block Diagonal Bounded Perturbation Problem

Doyle [101] considered the problem of an interconnected linear system with multiple independent norm-bounded perturbations. He noted that, by rearranging the system, it is always possible to isolate the perturbations as a single large block diagonal perturbation. Consider the simple example of a feedback control system with input and output multiplicative uncertainty, shown in Figure 6.06.

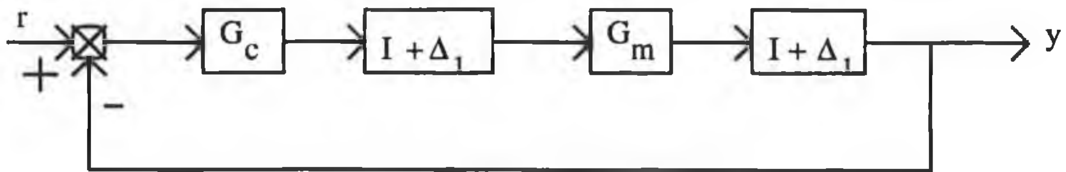

Figure 6.06 Feedback Control System with Input and Output Multiplicative Perturbations

This can be equivalently expressed in the form of Figure 6.07 and rearranged in Figure 6.08.

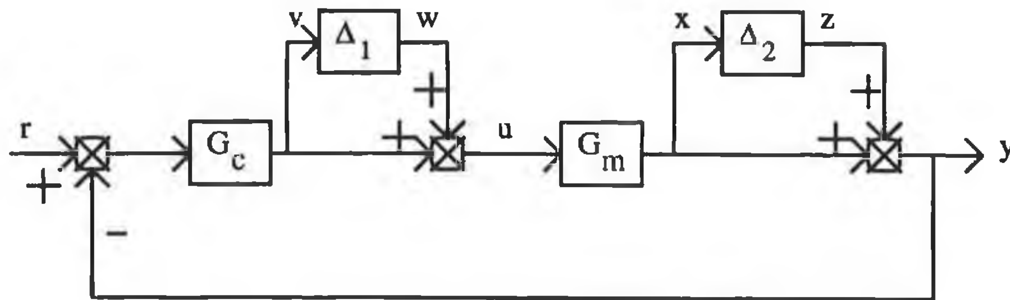

Figure 6.07 Equivalent Representation of Figure 6.06

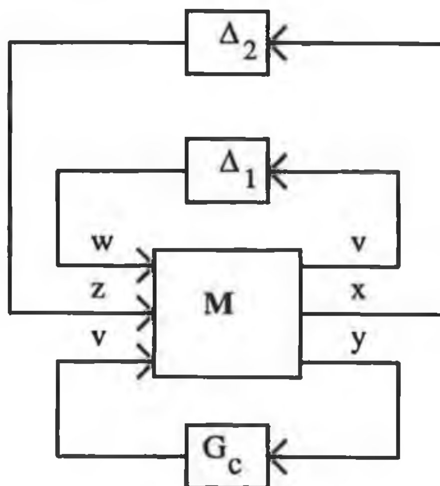

Figure 6.08 Rearrangement of Figure 6.07

The following input-output relationship can be written

$$\begin{bmatrix} v \\ x \\ y \end{bmatrix} = M \begin{bmatrix} w \\ z \\ v \end{bmatrix} \quad ; \qquad \textbf{(6.4-1)}$$

where

$$M = \begin{bmatrix} 0 & 0 & I \\ G_m & 0 & G_m \\ G_m & I & G_m \end{bmatrix} \quad ; \qquad \textbf{(6.4-2)}$$

Finally, G_c can be absorbed into M to obtain the F matrix shown in Figure 6.09.

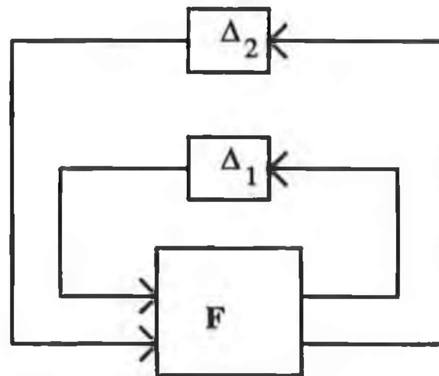

Figure 6.09 The Block Diagonal Bounded Perturbation Representation

This is the form that Doyle [101] termed the BDBP problem. The following relationships should be noted

$$\Delta = \begin{bmatrix} \Delta_1 & 0 \\ 0 & \Delta_2 \end{bmatrix} \quad ; \qquad \textbf{(6.4-3)}$$

and

$$F = \begin{bmatrix} -(I + G_cG_m)^{-1}G_cG_m & -(I + G_cG_m)^{-1}G_c \\ (I + G_mG_c)^{-1}G_m & -(I + G_mG_c)^{-1}G_mG_c \end{bmatrix} \quad ; \qquad \textbf{(6.4-4)}$$

Δ is the block diagonal perturbation matrix, containing the full perturbation matrices Δ_1 and Δ_2. The unstructured analysis approach discussed in the previous section would treat the input and output uncertainties independently, or treat the Δ matrix as a full (unstructured) uncertainty matrix. Doyle [100] has shown that the bounds obtained in each case are virtually useless. The procedure that he developed to solve the problem is known as the structured singular value (SSV), μ.

6.4.2 General Development of the Structured Singular Value

The development of SSV method has been studied by Doyle[100][101] and Fan [122] amongst others. The brief description will be given in this section. Consider a structure, such as that shown in Figure 6.09, composed of m blocks. The set of block sizes can be represented by

$$K = \{ k_1, \cdots, k_m \} \; ; \qquad \textbf{(6.4-5)}$$

where k_i is a positive integer. A family of diagonal matrices is represented by

$$D = \{ \text{block diag}(d_1 I_1, \cdots, d_m I_m) \mid d_i \in (0, \infty) \} \; ; \qquad \textbf{(6.4-6)}$$

A family of block unitary matrices is represented by

$$u = \{ \text{block diag}(U_1, \cdots, U_m) \} \; ; \qquad \textbf{(6.4-7)}$$

The set of block diagonal norm bounded perturbation matrices is

$$X_\delta = \{ \text{block diag}(\Delta_1 \cdots, \Delta_m) \mid \Delta_i \in C^{k_i \times k_i}, \sigma^*(\Delta_i) \leq \delta \} \; ; \qquad \textbf{(6.4-8)}$$

Δ_i is a $k_i \times k_i$ complex matrix.

The SSV of a complex n x n matrix F with respect to block structure K is defined as the positive number μ having the property that

$$\det(I + F\Delta) \neq 0 \;\; \text{for all } \Delta \in X_\delta \; ; \qquad \textbf{(6.4-9)}$$

if and only if

$$\delta\mu(F) < 1 \; ; \qquad \textbf{(6.4-10)}$$

In other words, $\mu(F)$ is 0 if there is no Δ in X_∞ such that $\det(I + F\Delta) = 0$. and

$$(\min_{\Delta \in X_\infty} \{ \sigma^*(\Delta) \mid \det (I + F\Delta) = 0 \})^{-1} \text{ otherwise.}$$

For all $u \in \bar{u}$,

$$\mu(F) = \mu(Fu) = \mu(uF) \; ; \qquad \textbf{(6.4-11)}$$

and for all $D \in \bar{D}$,

$$\mu(F) = \mu(DFD^{-1}) \; ; \qquad \textbf{(6.4-12)}$$

The following expressions can be used to calculate the SSV

$$\mu(F) = \max_{u \in \bar{u}} \rho(Fu) = \max_{u \in \bar{u}} \rho(uF) \; ; \qquad \textbf{(6.4-13)}$$

For block structure no larger than 3.

$$\mu(F) = \inf_{D \in D} \sigma^*(DFD^{-1}) \; ; \qquad \textbf{(6.4-14)}$$

while, in general

$$\mu(F) \leq \inf_{D \in D} \sigma^*(DFD^{-1}) \; ;$$

The optimisation in Equation (6.4-13) is not used because it has non global maxima. Equation (6.4-14) is recommended because it has no local minimum that is not global. The calculation of Equation (6.4-14) will be discussed in the following section.

6.4.3 Characterisation and Computation of SSV

Doyle, et al [101], Grosdidier and P.M.Morari [123] have developed the tools to compute a generalised gradient for the SSV, so that descent directions could be computed for Equation (6.4-14). Fan [122] developed a very efficient technique that decomposed the problem into several "smooth" optimisation problems. His algorithm always completed successfully for block-structures of size no larger than 3, and often did for block-structure of larger size.

Suppose that the assumptions of Equations (6.4-11,12) are satisfied. Note that an m block matrix requires m-1 optimisation variables ($d_1, \cdots\cdots, d_{m-1}$). We have options to calculate the spectral radius and spectral norm since

$$\rho(F) \leq \mu(F) \leq \sigma^*(F) ; \qquad \textbf{(6.4-15)}$$

The computation of μ can be performed directly on commercially available software, such as Matlab μ-Analysis and Synthesis Toolbox.

6.5 A General Framework for Multivariable Control System Design Under Uncertainty

In a previous section we presented Doyles's original development of BDBP problem and illustrated the technique with input and output uncertainty, but with no disturbances or setpoint changes. In this section we will present a more general formulation for multivariable control system design under uncertainty [100][101[122][123].

Consider the general diagram shown in Figure 6.10. This formulation is completely general and will allow us to incorporate performance as well as stability conditions.

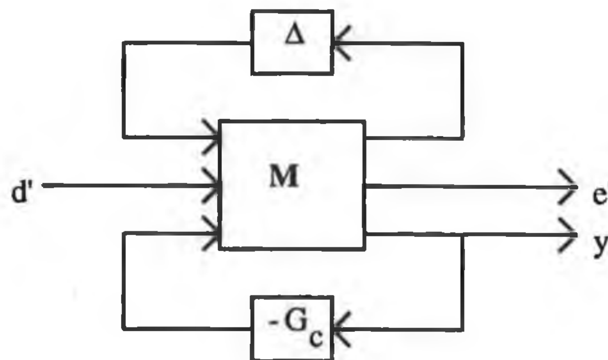

Figure 6.10 General BDBP Diagram

The matrix M includes not only information concerning the nominal plant, $G_m(s)$, but also weighting matrices that are associated with uncertainty and performance specifications. Δ is a norm bounded perturbation matrix.

$\Delta = \text{diag}(\Delta_i)$;

M is weighted so that the singular value,

$\sigma^*(\Delta_i) \leq 1.0$;

M is also weighted so that the possible process disturbance d' occurs on a unit ball and e' will remain inside the unit ball when the performance is acceptable [101].

The controller, G_c, can be absorbed into the structure as shown in Figure 6.11, so that we may analyse the closed loop properties.

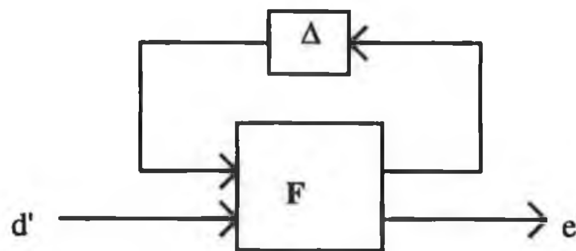

Figure 6.11 General BDBP Diagram with Control Absorbed Into the Structure

The properties that we are interested in are: nominal performance, robust stability, and robust performance. It is implicity assumed that the nominal feedback system is stable.

6.5.1 Nominal Performance

For the nominal model, $\Delta = 0$, and we require the weighted error, e', to be unit bounded for unit norm bounded weighted disturbances, d'.

$$\| e' \| < 1.0 \text{ for } \| d' \| < 1.0 \; ; \qquad \textbf{(6.5-1)}$$

This requires

$$\sup_{\omega \geq 0.0} \sigma^*(F_{22}(j\omega)) < 1.0 \; ; \qquad \textbf{(6.5-2)}$$

6.5.2 Robust Stability

Since the block diagonal perturbation matrix is defined to be unit norm bounded, the condition for robust stability is

$$\sup_{\omega \geq 0.0} \sigma^*(F_{11}(j\omega)) < 1.0 \; ; \qquad \textbf{(6.5-3)}$$

6.5.3 Robust Performance

For robust performance, the weighted error is unit norm bounded for unit norm bounded disturbances and structured perturbations. This condition is

$$\sup_{\omega \geq 0.0} \mu(F(j\omega)) < 1.0 \; ; \qquad \textbf{(6.5-4)}$$

Recall that the block diagonal structure is required to calculate μ.

6.6 Robust Multivariable Plasma Etching Control Based on Structured Uncertainty

Great progress has been made in the development of methods for robust stability and performance of systems subject to disturbances and structured perturbations. What has been lacking is relevant practical applications of the method. Few practical applications of rigorous analysis procedures have been presented particularly in plasma etching process control. Plasma etching is a very non-linear process that is traditionally controlled with linear strategies. This section addresses

the issue of process uncertainty due the inherently non-linear nature of plasma etching. It will shown that the uncertainties are highly structured. The following control strategies will be compared: SVD pairings with a structured compensated MIMO and conventional control.

The plasma etching model representing the nominal operating point is presented in equations (5.3-2) and (6.3-8). The matrix Σ in the SVD analysis reveals the fact that the SF_6 flow rate has only a small effect on the dynamics (Chapter 5). After removing SF_6 flow rate as a manipulated variable from equation (5.3-2), system is then analyzed using SVD technique to determine that the process variable $[SF_x]$ to be eliminated. Thus, the simplified model G(s) is

$$\begin{bmatrix} [F] \\ \\ [E/p] \end{bmatrix} = \begin{bmatrix} \dfrac{0.70}{0.40S+1} & \dfrac{0.20}{0.20S+1} \\ \\ \dfrac{0.50}{0.40S+1} & \dfrac{0.65}{0.15S+1} \end{bmatrix} \cdot \begin{bmatrix} \text{Chamber Pressure} \\ \\ \text{RF Power Density} \end{bmatrix} ; \qquad \textbf{(6.6-1)}$$

The nominal operating conditions are shown in Table 2.5. Consider the operating region to consist of the transfer function relationships for the plants within $\Delta x_1 = \pm\ 0.01 W/cm^2$ (RF power density), $\Delta x_2 = \pm\ 5.00$ mtorr (chamber pressure) fraction of the nominal operating point. We can consider the perturbed plant to be a function of the two process variables, that is, $G(s, \Delta x_1, \Delta x_2)$ represents the plant over the operating region.

We assume that there is an unstructured 15% steady state uncertainty in the RF power density and chamber pressure, keeping SF_6 flow rate constant, and that these errors increase as a function of frequency. We then noted that this unstructured input uncertainty becomes a structured output uncertainty, because of the multiplication with the nominal process plant. The structured formulation is used through the rest of the analysis. The maximum input and output multiplicative uncertainties are shown in Figure 6.12. These uncertainty magnitudes are calculated by

$$l_m(s) = \sup_{\Delta x_1, \Delta x_2} \sigma^*(L(s)) ; \qquad \textbf{(6.6-2)}$$

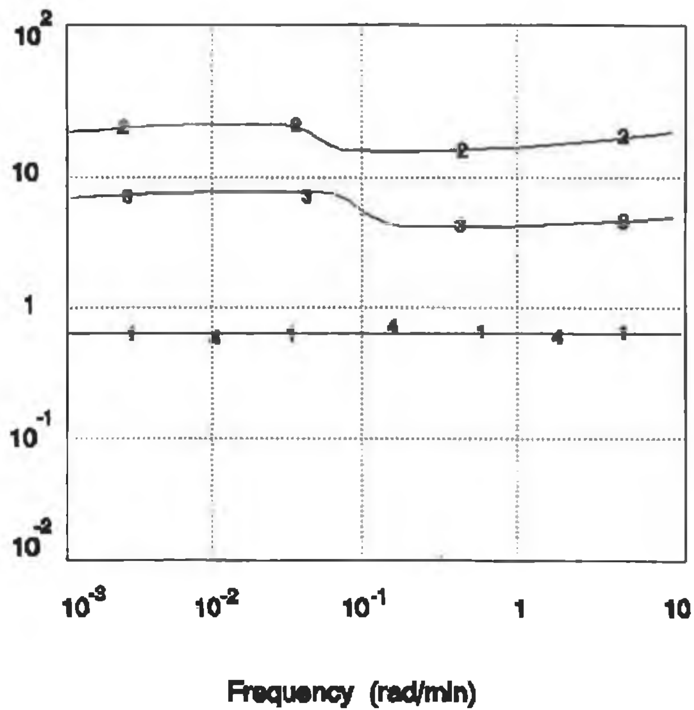

Figure 6.12 Input and Output Multiplicative Uncertainties
1,4 = Output l_o; 2,3 = Input l_i.

1,2 = for Conventional Control
3,4 = for Structurally Compensated MIMO Control

where $L_o = (G_p - G_m)G_m^{-1}$ for output uncertainty and $L_i = G_m^{-1}(G_p - G_m)$ for input uncertainty (Table 6.1). G_p is the real plasma etching plant model (Equation (4.3.1-1)), G_m is nominal plant model.

For our control schemes, we assume there is a very strong correlation between the process gains of each element of the perturbed plant. Let l_{aij} represent the uncertainty in the i, j element of the process gain matrix $G_p(s)$. We find that

$$l_{a21} \approx -l_{a11} \; ; \qquad (6.6\text{-}3)$$
$$l_{a12} \approx -l_{a11} \; ; \qquad (6.6\text{-}4)$$
$$l_{a22} \approx l_{a11} \; ; \qquad (6.6\text{-}5)$$

Therefore the gain matrix uncertainty can be represented primarily by the uncertainty in one element. Assume that l_{a11} provides an exact relationship between the perturbed process and nominal plant model.

$$g_{p11} = g_{m11} + l_{a11} \; ;$$

The following relationships are then predicted from Equations (6.6-3 - 5) (* - denotes that the terms are predicted)

$$g_{p12}^* = g_{m12} - l_{a11} \; ;$$
$$g_{p21}^* = g_{m21} - l_{a11} \; ;$$
$$g_{p22}^* = g_{m22} + l_{a11} \; ;$$

The additional uncertainty between the predicted terms and actual terms can be calculated in the following fashion

$$l_{p12} = g_{p12} - g_{p12}^* \; ;$$
$$l_{p21} = g_{p21} - g_{p21}^* \; ;$$
$$l_{p22} = g_{p22} - g_{p22}^* \; ;$$

Define the following weighting matrices

$$w_1 = \max |l_{p11}| \; ;$$
$$w_2 = \max |l_{p12}| \; ;$$
$$w_3 = \max |l_{p21}| \; ;$$
$$w_4 = \max |l_{p22}| \; ;$$

Then we can develop the block diagram shown in Figure 6.13.

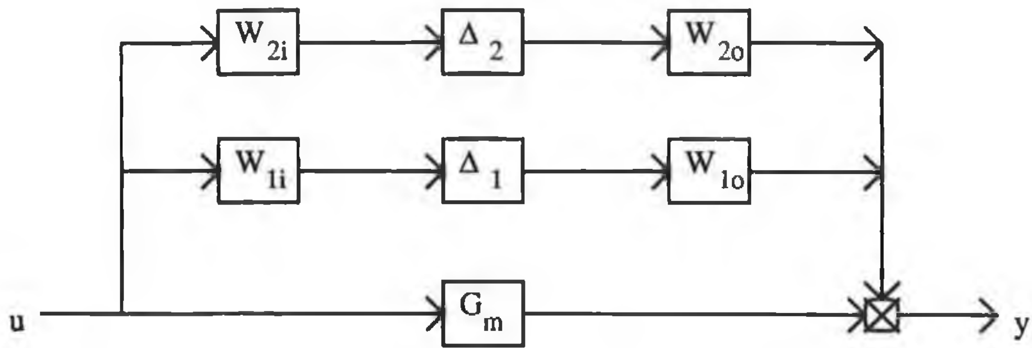

Figure 6.13 Additive Process Uncertainty Characterisation for Plasma Etching Process Control

The following relationships can be found (recall that $\| \Delta_i \| < 1.0$)

$$W_{1o} = \begin{bmatrix} -w_1 \\ w_1 \end{bmatrix} ;$$

$$W_{1i} = [-1 \quad -1] ;$$

$$W_{2o} = \begin{bmatrix} 1 & 0 \\ 0 & 1 \end{bmatrix} ;$$

$$W_{2i} = \begin{bmatrix} 0 & w_2 \\ w_3 & w_4 \end{bmatrix} ;$$

In this case the values of the weighting factors are

$$w_1 = \frac{0.550}{0.40S + 1} ;$$

$$w_2 = \frac{0.070}{0.20S + 1} ;$$

$$w_3 = \frac{0.220}{0.40S + 1} ;$$

$$w_4 = \frac{0.390}{0.15S + 1} ;$$

The block diagonal perturbation structure can be designed as shown in Figure 6.08. The M matrix is

$$M = \begin{bmatrix} 0 & 0 & W_{1i} \\ 0 & 0 & W_{2i} \\ W_{1o} & W_{2o} & G_m \end{bmatrix} \quad ; \qquad \textbf{(6.6-6)}$$

When the controller, G_C, is absorbed into the structure, as shown in Figure 6.09. The following relationship can be derived

$$F_{ij} = M_{ij} - M_{i3}G_c(I + M_{33}G_c)^{-1}M_{3j} \quad ; \qquad \textbf{(6.6-7)}$$

Then we require : $\mu(F) \leq 1.0$ for $\omega \geq 0$ for robust stability.

6.7 Simulation Results and Discussion

Initial tuning parameters are determined using the MIMO IMC-PI tuning rules (Chapter 5). The robust tuning parameters shown in Table 6.2 are determined by iteratively changing the constants until the robust stability is satisfied.

The maximum singular value and μ, which is the inverse of minimum perturbation that will destabilize system, with the conventional and SVD pairing with structurally compensated MIMO control schemes are plotted in Figure 6.14. As shown in this figure, robust performance with respect to uncertainties and performance weightings peaks at a value of $\mu \leq 1.02$. This value does not exceed unity to a significant degree indicating both of controllers achieves robust performance. The input and output uncertainty bounds are shown in Figure 6.15 and 6.16 respectively. The perturbation response of μ-synthesis designed controller for the plasma etching nominal plant is shown in Figure 6.17, which is the same as Figure 5.13, because the uncertainty bounds assumed here are within our working ranges. Both of the control schemes satisfy the robust stability for multiplicative input uncertainties. There exists an input perturbation of less than 20% that will cause system instability. The results illustrates that, not only is the magnitude of the modelling error important, the structure of the error is important as well.

Table 6.2 Robust Tuning Parameters for Plasma Etching System

	Controller G_{c1} ([F] -- Pressure pairing)			Controller G_{c2} ([E/p] -- RF power density pairing)		
Methods ↓	λ_1	K_{c1}	τ_{I1}	λ_2	K_{c2}	τ_{I2}
Conventional Control	0.80	4.90	0.50	0.95	5.80	0.60
Structurally Compensated MVSISO Control	0.30	3.10	0.50	0.40	10.5	0.50

6.8 Conclusions

The structured singular value (SSV), which is a generalisation of regular concept of singular value decomposition (SVD) in the sense that it reduces SVD for the trivial structure, is used as an analysis tool to design controllers that are robustly stable to these structured perturbations. Unstructured uncertainty analysis is used to determine the control system sensitivities to unstructured perturbations, which are due to the inadequate representation of process dynamics with a simple first order and dead time model. The structural compensation method has allowed us to make effective use of the inherent internal structure of the process system.

$\mu(F)$ can be obtained as the solution of several smooth optimisation problems which do not involve any eigenvalues or singular value computation. This technique has been found very useful for plasma etching process, since the model uncertainty due to the non-linear behaviour is highly structured. We believe that it is important to try and tune the different control strategies for the same degree of robustness. The performance requirements can then be used to assess the value of each strategy.

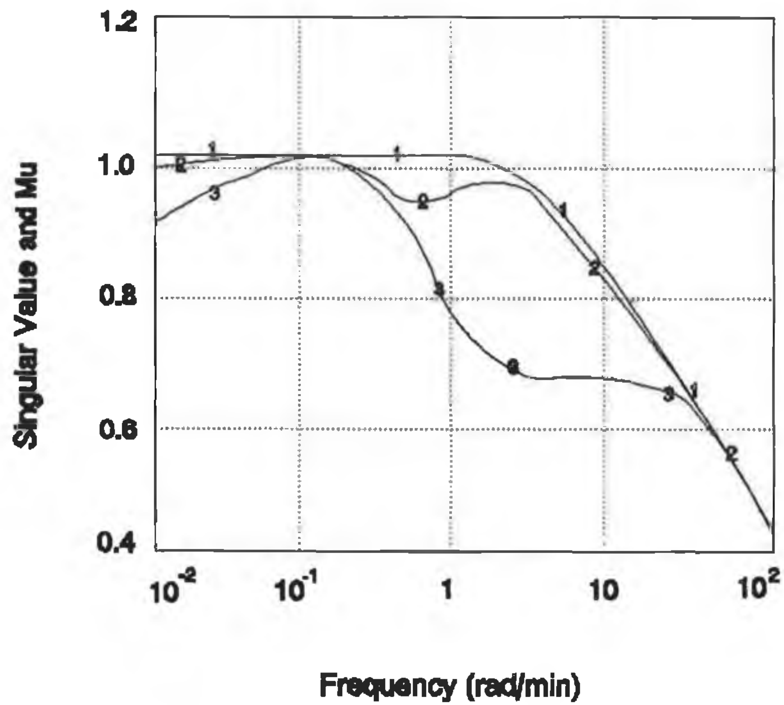

Figure 6.14 Maximum Singular Value and μ with Structurally Compensated MIMO and Conventional Controllers

1 = Maximum Singular Value
2 = Structurally Compensated MIMO Controller
3 = Conventional Control

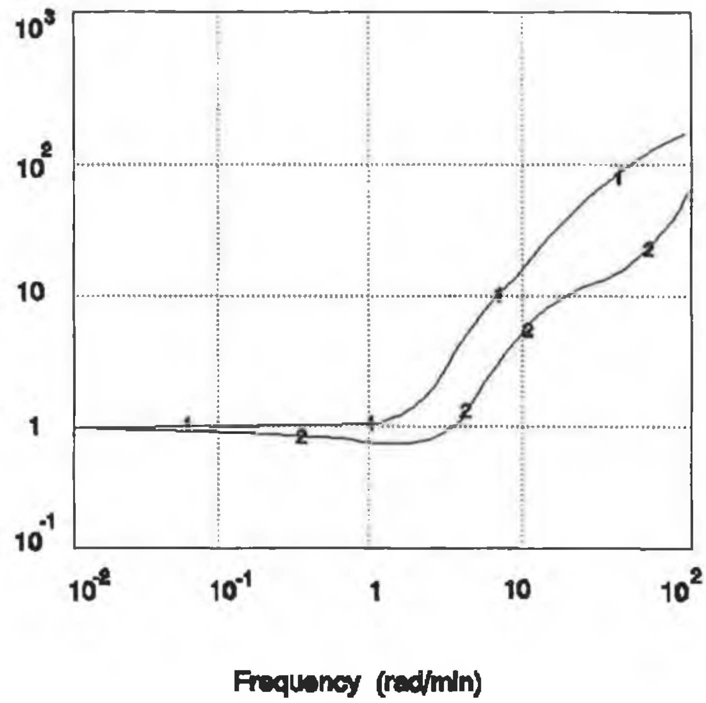

Figure 6.15 Input Uncertainty Bound for the Plasma Etching System

1 = Structurally Compensated MIMO
2 = Conventional Control

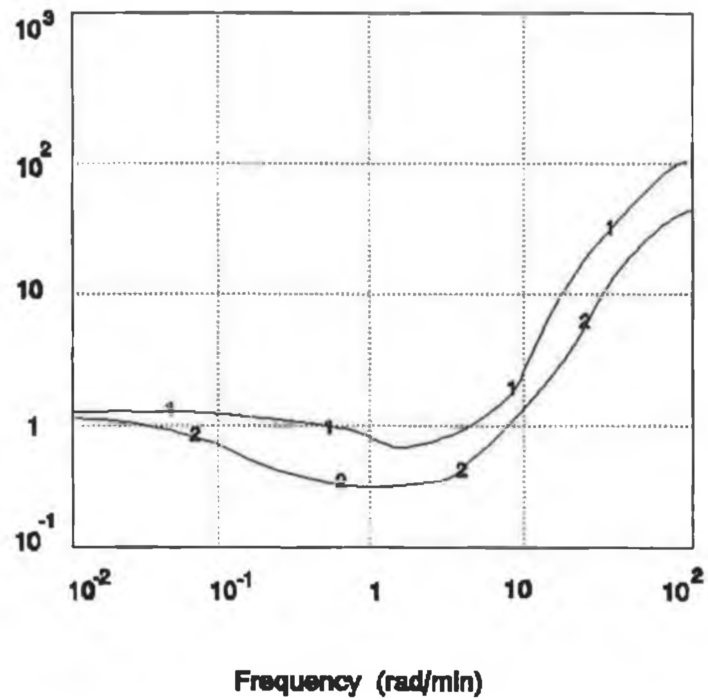

Figure 6.16 Output Uncertainty Bound for the Plasma Etching System

1 = Structurally Compensated MIMO
2 = Conventional Control

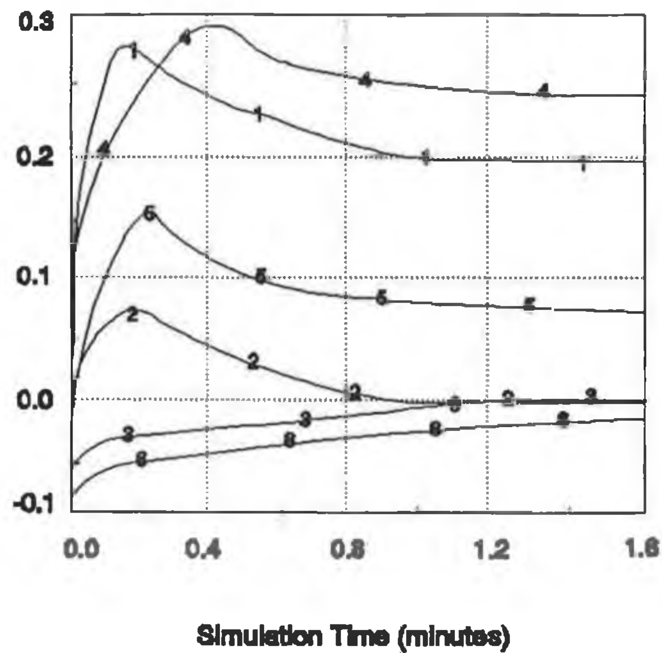

Figure 6.17 Perturbation Responses of the Two Controllers for the Plasma Etching Plant with Uncertainties

1 = Structurally Compensated MIMO
2 = Conventional Control

CHAPTER 7 CONCLUSIONS AND RECOMMENDATIONS

7.1 Conclusions

This research has examined comprehensive reactor modelling, regression modelling, response surface methodology, and control system analysis applied to a plasma etching process. It has been shown that, through response surface methodology, a rational means for process development and specification is available. In addition, we have introduced a concept of feedback control of the process variables, allowing more precise control of the process. Through a steady state analysis of the system combined with a qualitative understanding of the dynamics present in the system, we have demonstrated a methodology for both selecting variable pairings and determining the need for multivariable control on the process under study.

In this dissertation, the chemical and physical mechanisms of plasma etching are described. A parallel plate etcher has been employed to the work. A theoretical comprehensive reactor model is investigated for plasma etching of silicon and SiO_2 with SF_6/Argon. This plasma reactor model is based on conservation of the elemental species participating in the plasma, and elementary gas phase and surface reactions have been included in the model. The conservation equation and boundary conditions are studied. The theoretical predictions show the effects of operating conditions, such as pressure, RF power density, SF_6 gas flow rate and electrode spacing, on the etch rate distribution. Variations in these variables and parameters have been theoretically and experimentally investigated over a limited parameter space to obtain their effects on the etch rates, uniformities etc.

Generally, more uniform etching is achieved by increasing the gas pressure and decreasing the electric discharge power. The success of this overall model with particular emphasis on the comprehensive modelling of the plasma etching depends on accurate knowledge of fundamental electron collision cross sections, some of which are not known and difficult to determine experimentally. Additional information concerning electron density distribution, electric field distribution, and surface recombination probability is needed for a more detailed modelling. The

incorporation of such models with similar modules which describe the plasma and surface chemistry show promise in predictively modelling plasma processes. The development of a predictive model has the potential to improve our ability to provide a basis for further regression modelling studies for the purposes of process control and optimisation.

Pertinent process variables are identified and the above-mentioned regression modelling and control system development strategies are successfully applied to the SF_6/Ar etch system. Regression modelling and response surface methodology are used to develop a steady state model relating manipulated variables to both process and performance variables for this system. The correlations between process and performance variables are found to be important in process specification, yielding a steady state gain matrix for these variables which could later be used to identify which performance variables should be used to specify set points for the process variables during process development. Optical emission spectroscopy and laser interferometry are shown to be an effective tool in plasma etching, both in process development and in process control. These techniques are used to measure several of the process variables and on-line etching rate respectively in a non-intrusive fashion with this approach we gain insight into the dynamics of these variables, and are enable in monitoring these variables in the feedback control system developed for SF_6/Ar etch process under study.

We have shown that, using only steady state information from the etch system, process control strategies can be developed for this process. Using the technique of singular value decomposition (SVD) applied to the steady state gain matrices developed from regression analysis, variable pairings are recommended for the SF_6/Ar etch system. SVD analysis is shown to be effective in identifying system interactions in the recommended pairings which require the application of multivariable control schemes. SVD applied to the process/performance variable correlations yields information as to which of the performance variables should be used in the specification of set points for the etch system process variables. A singular value sensitivity technique with a structural compensator has been found to be particularly effective in tuning controllers for simplified decoupling multivariable control, though structural compensation may form right half plane zeros (causing inverse response) since transfer functions are basically being added and subtracted. This particular problem exists with any decoupling type of techniques [97].

An especially interesting study involves the robustness analysis of the plasma etching process. The control system engineer should use process insight to obtain bounds on the process uncertainty. It is well known that good closed loop properties at the plant output do not assure good properties at the plant input. Both of the effects of input and output uncertainties should be considered for robust control system design. The structured singular value (SSV), μ, is used in this work as an analysis tool to design controllers that are robustly stable to these structured perturbations. For the same degree of robustness, the stability and performance of the structurally compensated MIMO method is much better than that of the conventional control strategy. We believe that it is important to try and tune the different control strategies for the same degree of robustness. The performance requirements can then be used to assess the value of each strategy.

Several conclusions are drawn from the experimental work performed during this research. It is felt that the measurement of other process variables, such as electron density and electron energy distribution, would be beneficial for control of etching process. This may require the use of intrusive measurement techniques, but the potential gain may outweigh the difficulties in implementation.

7.2 Recommendations for Further Work

This work presented in this dissertation forms the groundwork for a great deal of additional work and these are in consequence many opportunities because more precise measurements of the structure and composition of the plasma have not been made. Based on this study, it is found that the optimisation of current plasma etching process is limited by the interdependence of plasma parameters. For example, in most RF systems, as the RF power is raised to increase the plasma density, the bias is also increase according to a functional dependence determined by the reactor geometry, pressure, and gas flow rates. The following possible facts could influence the experimental data and simulation results obtained from this study:

(1) The limitation of the diagnostic technologies, such as optical emission spectroscopy, are the availability of absolute concentration measurements for the

species in the plasma. The operating conditions are reduced to their minimal working areas so that the etch rates can be monitored on-line by laser interferometry. Actual set points of process operating conditions are much higher in order to make the etching process time constant shorter.

(2) Plasma environments are very complicated and many of the surface processes occurring in them are hard to investigate thoroughly. Moreover, the basic parameters which are important in a given condition are not available yet. For example, most of the rate constants for radicals recombination on the surface are not available.

(3) The gas flow calculation could influence the density gradients on the flow development due to a temperature difference between the gas phase and electrode surface.

The overall regression analysis methods have been used in some chemical processes, but little used for microelectronics processes. The main problem is that the dynamics of etch processes are very fast and very hard to know. Only non-intrusive and intrusive on-line measurement techniques could be employed to measure the important process variables, which would be beneficial for control of the etching process. The fit of the quadratic model for some of the process and performance variables is less than satisfactory, particularly in the modelling of etch anisotropy. The approach to this problem could be in the measurement of anisotropy. Actinometry techniques could be employed.

The identification of the critical structural properties of a plasma etching process has been based on one of the simplified dynamic models available in this work. It is believed that the majority of the important effects are adequately determined using these models, but this should be verified by the analysis of more complex models. A Neural Network technique could be applied to develop more precise models and controllers.

There remains a wide open area for applications of H_∞ design techniques, that allow one to consider stability and performance simultaneously. One particularly interesting area involves systems with extra degrees of freedom in the manipulated variables. SSV theory assumes that the uncertainty block, Δ, is complex. In reality, at low frequencies the uncertainty is primarily real, so conservative designs may result. Methods need to be developed to account for this. This is also important for the case when Δ represents real parameter variations, such as rate constants, electron

density and electron energy distribution, etc. The use of SSV analysis allows the establishment of limitations to feedback control of a plasma etching process using linear system theory. It is a logical first step. A logical next step may be to develop a non-linear feedback type of strategy, such as global linearization techniques, to exactly characterise the uncertainty. An important point is that an unstructured uncertainty at one point in a control loop diagram can become structured at another point.

APPENDIX I. REVIEW OF PUBLISHED MODELS

This appendix contains a table summarising several models published in the literature. These models vary in complexity and ideas about the representation of the plasma physics, homogeneous reactions, surface reactions, and profile evolution. Although this table does not include every model cited in the literature, it is very thorough and should provide the reader with a sufficient background. The figure below defines the dimensions referenced in the table.

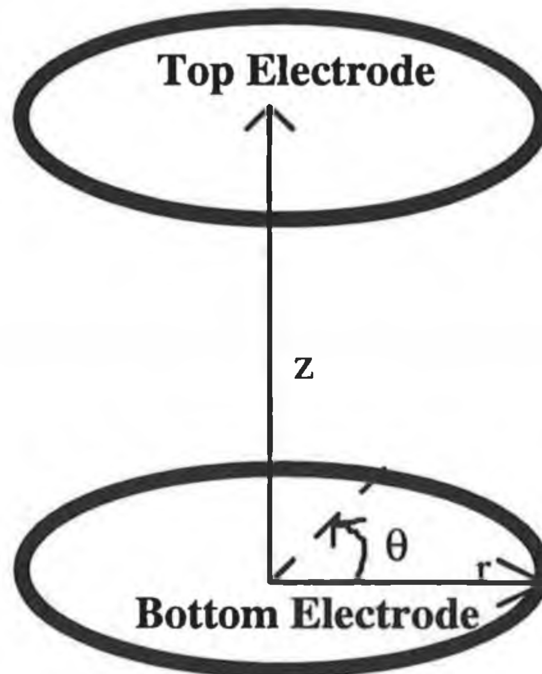

Figure I.1 Dimension Representation

Table I.1 Summary of Models Presented in Literature

Author	System[1]	Comments[2;3;4]
Mogab (1977) [31]	Etching of Si with CF_4/O_2	CSTR reactor model Simplified kinetics No gaseous expansion Chemical etching
Turban, et al. (1981) [128]	Etching of Si with CF_4 Radial and tubular reactors	CSTR reactor model Simplified kinetics Chemical etching No gaseous expansion
Kushner (1982a) [129]	C_nF_m/O_2 and C_nF_m/H_2 Etching Si and SiO_2	Etching by ions and neutrals Detailed homogeneous kinetics Flawed reactor model Plasma discharge model
Chen (1983) [130]	Si deposition with SiH_4 Tubular and radial flow	Two-dimensional (r,z) axisymmetric (mass) model No gaseous expansion Chemical deposition Simplified kinetics

Tachibana, et al. (1984) [131]	Deposition with CH_4	CSTR reactor Detailed homogeneous kinetics with neutral and ionic species No gaseous expansion Chemical deposition
Edelson & Flamm (1984) [132]	CF_4 etching of Si Tubular reactor	Detailed homogeneous Kinetics Includes ions in gas phase, but etching by neutrals only Plug Flow reactor model No gaseous expansion Many parameters Sensitivity Analysis to find significant reactions
Srinivasan, et al. (1985) [133]	Etching of polymers in CF_4/O_2	CSTR model Chemical etching Boltzmann equation for electron energy distribution (commercial package JILA) -used to find rate constants for reactions involving electrons Kinetics from Kushner for reactions not involving electron, plus additional reactions Model includes ions and neutrals

Dalvie, et al. (1986) [134]	Si etching with CF_4	Two-dimensional (r,z) axisymmetric mass, momentum, and heat transfer model No gaseous expansion No heat generated by reactions Simplified kinetics from reduced set found by Edelson and Flamm (1984) Langmuir-Hinshelwood kinetics for etching by Edelson and Flamm (1984)
Plumb & Ryan (1986 [135]	CF_4/O_2 Kinetics Tubular Reactor	Detailed homogeneous kinetics Plug Flow Reactor No gaseous expansion Analysis for Reduced Reaction Set
Ryan & Plum (1986) [136]	Etching of Si in CF_4 Tubular Reactor	Detailed homogeneous kinetics (from above model) Si etch model from Edelson and Flamm (1984)
Venkatesan, et al. (1987) [137]	Silicon etching in CF_4	1-Dimension (r) mass model approximation of 2-D- (effective diffusivity) Simplified kinetics of Dalvie and Jensen (Edelson and Flamm) Langmuir-Hinshelwood kinetics No gaseous expansion

Zawaideh & Kim (1987, 1988) [138][139]	Generalised Etching Model	Includes Plasma model Assumed normal ion incidence Physical Sputtering Chemical etching Enhanced chemical etching Many heterogeneous kinetic constants, values nor sources given Langmuir-Hinshelwood Kinetics No gas phase Kinetics: neutral flux proportional to total gas pressure in 1987 Kinetics for CF_4 in 1988 (coefficients mainly from Edelson and Flamm, no CF_2) Reactor model similar to CSTR Does not explain anisotropy model, only given results
Dalvie and Jensen (1988) [140]	CF_4/O_2 etching of Si	Two-dimensional (r,z) axisymmetric transport (mass and momentum) model Detailed chemical kinetics (Based on Plumb and Ryan,1986) Chemical etch rate Also 1-dimensional dispersion (mass) model
Lii, et al. (1988)	Silicon etching with SF_6	CSTR model with no flow, only reactive loss Simplified kinetics No gaseous expansion Chemical etch rate

Yoo and Dixon (1989) [141]	Silicon nitride deposition from $SiH_4/NH_3/N_2$ with rotating susceptor	2-dimensional (r,z) mass, heat, and momentum model No gaseous expansion No heat of reaction Simplified kinetics (includes no "loss" except for deposition) Surface deposition includes dissociation of radicals liberating hydrogen
Economou, et al. (1989) [142]	O_2 etching of Silver Oxide	Two-dimensional (r,z) axisymmetric transport (continuity and Navier-Stokes) model Simplified chemical kinetics Chemical etching and "Damaged Site" chemical etching:ions generate damaged sites No gaseous expansion
Yamaguchi, et al. (1989) [143]	Si deposition from SiH_4 DC Discharge Tubular Reactor	Plasma Model Two-Dimensional Mass Continuity Only averaged to 1-D (r) No gaseous expansion Simplified kinetics Chemical deposition only

Kline, et al. (1989) [144]	Carbon films deposited from CH_4 2 MHz discharge in Tubular Reactor	Monte Carlo discharge simulator Plug flow model No gaseous expansion in model; results "corrected" for expansion (no detailed) Detailed gas phase kinetics Deposition by neutrals and ions, but not ion-enhanced
Cleland and Hess (1989) [145]	N_2O RF discharge	CSTR with specie specific volumes No gaseous expansion Includes wall recombination
Werner, et al. (1989) [146]	Aluminium etching with Cl_2 and $AlCl_3$ Hexode Reactor	3-dimensional model (r,z,θ) of mass, Navier-Stokes, and heat-transfer using PHOENICS Fluid-Flow-Simulator
Schoenborn, et al. (1989) [147]	Silicon etching in CF_4/O_2	Used CSTR, but never give details of reactor model Gas-phase kinetics of Plumb and Ryan (1986) Chemical etching by F (Ryan and Plumb, 1986) and F_2; atomic oxygen turns SiF(s) into Si(s) and F (gas)

Venkatesan, et al (1989) [148]	Silicon etching with NF_3	Dynamic 2-dimensional (r,z) mass model No gaseous expansion assumed for 2-D Simplified kinetics Chemical etching Also 1-dimension (r) dispersion (mass) model with gaseous expansion
Kobayashi, et al. (1989) [149]	Aluminium etching with Cl	2-dimensional (r,z) axisymmetric heat, mass, and momentum Gaseous expansion due to temperature only Simplified kinetics Chemical etching
Kao and Stenger (1990) [150]	Si etching with CF_4/O_2	Simplified kinetics Chemical etching 2-dimensional (r,θ) mass transfer model, averaged across z No gaseous expansion
Dalvie and Jensen (1990a) [151]	Si etching with CF_4/O_2 Similar to traditional radial flow reactor	2-dimensional (r,z) axisymmetric mass, momentum model Kinetics based on reduced set of Plumb and Ryan (1986), augmented with recombination reactions including wall recombination Langmuir-Hinshelwood kinetics (surface oxidation and CF_x coverage)

Park and Economou (1990a) [152]	Polymer etching with O_2 pulsed and nonpulsed discharges Variable velocity inlets	2-dimensional (r,z) axisymmetric mass, momentum model No gaseous expansion Simplified kinetics, includes wall recombination Chemical etching
Park and Economou (1990b) [153]	Si deposition with SiH_4 pulsed and nonpulsed with/without recycle tubular reactor	One-dimensional (axial) dispersion (mass) model, Simplified kinetics Chemical deposition No gaseous expansion Also CSTR model for pulsed
Park and Economou (1990c) [154]	Si etching with CF_4 Pulsed and nonpulsed discharges	2-dimensional (r,z) axisymmetric mass, momentum, and energy model Kinetics of reduced set of Ryan and Plumb (1986) Gaseous expansion due to temperature only Chemical etching using Langmuir Hinshelwood kinetics (Edelson and Flamm, 1984; Dalvie, et al., 1986) One-dimensional (r) dispersion (mass) model for pulsed

Thorsness and Britten (1990) [155]	Showerhead reactor Napthalene substrate Air used as gas No plasma	2-dimensional (r,z) mass and momentum model of single jet impinging substrate No kinetic model due to no kinetics Evaporation included
Venkatesan, et al. (1990) [156]	Silicon etching in CF_4/H_2 and CF_4/O_2	CF_4/O_2 kinetics reduced set of Plumb and Ryan plus homogenous F recombination Langmuir-Hinshelwood Kinetics (Edelson and Flamm) CF_4/H_2 of Ryan and Plumb and additional reactions (partly Kushner)

1. All reactors are RF radical-flow with planar diodes unless otherwise stated.

2. Simplified kinetics indicates that the kinetic representation was a lumped reaction set, with lumped coefficients estimated or regressed

3. In order for the pressure to remain constant, the gas must expand (non constant density) if the number of moles changes due to reactions. Several models assume negligible change in moles, resulting in constant density.

4. Unless explicably stated, only neutrals were included in models.

APPENDIX II. DERIVATION OF FINITE ELEMENT EQUATIONS

II.1 Introduction

For a detailed introduction to the Finite Element Method (FEM), refer to any one of two treatises [82][157] on the subject. A brief outline of the method is presented below. The general form of the equations being solved here is that of a second order, non-linear differential equation in two dimensions:

$$\nabla^2 u(x) + f(u(x) = 0 \; ; \qquad \textbf{(II.1-1)}$$

where u(x) is the function of interest, e.g., species concentration, defined on a finite domain with appropriate boundary conditions, x is the spatial co-ordinate vector, and f(u) is the collective non-linear part of the equation which may contain first order derivatives of u. Eqn. (II.1-1) may be written in the form of a weighted residual, the integral of which over the 2-D domain Ω is required to be zero:

$$R_i = \int_\Omega (\nabla^2 u(x) + f(u(x))w_i \, d\Omega = 0 \; ; \qquad \textbf{(II.1-2)}$$

where R_i is the residual, and w_i is the weighting function. The application of Green's theorem reduces the order of the second derivative in the equation:

$$R_i = \int_\Omega [(\nabla u \nabla w_i) - f(u)w_i]d\Omega - \int_\Gamma w_i n \nabla u \, d\Gamma = 0 \; ; \qquad \textbf{(II.1-3)}$$

where Γ is the boundary of the 2-D domain, n is the normal vector to the boundary. The form of the boundary integral in Eqn. (II.1-3) is ideally suited for the application of the flux boundary conditions, which are added on to the bulk residual terms. The Dirichlet boundary conditions require the replacement of the residual equation in question with the assignment of the boundary value in its place.

The FEM consists of expanding the unknown function, u, in terms of a finite set of known basis functions and the corresponding unknown coefficients:

$$u = \sum_{j=1}^{N} u_j \phi_j \;; \qquad \textbf{(II.1-4)}$$

$$\nabla u = \sum_{j=1}^{N} u_j \nabla \phi_j \;; \qquad \textbf{(II.1-5)}$$

where ϕ_j is j^{th} member of the set of N basis functions, and $u_j(x)$ is the unknown coefficient. If the weighting function, w_i, is the basis function, ϕ_i, the method is called the Galerkin Finite Element Method (GFEM). By this transformation, the problem then consists of finding the set of N u_j's. Substitution of Eqn.(II.1-4) and (II.1-5) into Eqn. (II.1-3), and integrating numerically over the domain then yields a set of N non-linear algebraic equations for the N u_j's. These non-linear equations are solved in a Newton-Raphson iteration loop.

II.2 Conservation Equations

The relevant residual equations has been listed for the continuity [157], r momentum balance, z momentum balance, and the stream function equations used for the generation of the streamline plots. Therefore, only the equations resulting from the transformation of the individual species balance equations are listed here. The gradient of the flux of any species i is equal to the net rate of production of i [158]:

$$\nabla N_i = r_i \;; \qquad \textbf{(II.2-1)}$$

where N_i is the flux of i and r_i is the net rate of production of i by chemical reaction. When the flux N_i is written as the sum of the diffusive flux and the convective flux, Eqn. (3.4-4) (Chapter 3) is obtained. In vector form:

$$\nabla(\rho\omega_i v) - \nabla(\rho D_{im} \nabla \omega_i) - r_i = 0 \;; \qquad \textbf{(II.2-2)}$$

where ρ is the mass density, v is the velocity from the momentum balance, ω_i is the unknown mass fraction of species i, D_{im} is the multicomponent diffusivity of species i. For a full discussion of Eqn. (II.2-2), refer to Chapter 3.

This equation is transformed by the method outlined in section II.1. The resulting residual equation is:

$$R_{ij} = \int_{\Omega} [\nabla(\rho\omega_i v) - \nabla(\rho D_{im}\nabla\omega_i) - r_i]\,\phi_j\, d\Omega \;; \tag{II.2-3}$$

where R_{ij} is the residual for the ith species on the jth node, Ω is the 2-D axisymmetric domain, and ϕ_j's are biquadratic finite element basis functions. Application of Green's theorem yields:

$$R_{ij} = \int_{\Omega} [\nabla(\rho\omega_i i v)\phi_j + \nabla\phi_j(\rho D_{im}\nabla\omega_i) - r_i\phi_j] d\Omega - \int_{\Gamma} [\phi_j n(\rho D_{im}\nabla\omega_i)] d\Gamma \;; \tag{II.2-4}$$

Ignoring the boundary term for the moment, the first part of Eqn. (II.2-4) is expanded in terms of the scalar components:

$$R_{ij} = \int_{\Omega} [\phi_j v_r \frac{\partial}{\partial r}(\rho\omega_i) + \phi_j v_z \frac{\partial}{\partial z}(\rho\omega_i) + \frac{\phi_j \rho\omega_i}{r}\frac{\partial}{\partial r}(r v_r) + \phi_j \rho\omega_i \frac{\partial}{\partial z}(v_z)$$
$$+ \rho D_{im}\{(\frac{\partial\phi_j}{\partial r})(\frac{\partial\omega_i}{\partial r}) + (\frac{\partial\phi_j}{\partial z})(\frac{\partial\omega_i}{\partial z})\} - r_i\phi_j]\, r\, dr dz \;; \tag{II.2-5}$$

This equation is non-dimensionalized using the following definitions:

Dimensionless radial co-ordinate $\xi = \frac{r}{R_o}$; (II.2-6)

Dimensionless axial co-ordinate $\eta = \frac{z}{Z_o}$; (II.2-7)

Dimensionless r velocity $u_r = \frac{v_r}{V_o}$; (II.2-8)

Dimensionless z velocity $u_z = \frac{v_z}{V_o}$; (II.2-9)

Dimensionless density $\rho_u = \frac{\rho}{\rho_o}$; (II.2-10)

Radial Peclet number $$Pe_r = \frac{V_o R_o}{D_{im}} \;; \qquad \text{(II.2-11)}$$

Axial Peclet number $$Pe_z = \frac{V_o Z_o}{D_{im}} \;; \qquad \text{(II.2-12)}$$

where the subscript o signifies inlet conditions. The dimensionless equation then reads:

$$R_{ij} = \int_\Omega [\frac{\phi_j Pe_r}{\rho_u} \{u_r \frac{\partial}{\partial \xi}(\rho_u \omega_i) + \frac{\rho_u \omega_i}{\xi} \frac{\partial}{\partial \xi}(\xi u_r)\} + \frac{\phi_j Pe_z R_o^2}{\rho_u Z_o^2}\{u_z \frac{\partial}{\partial \eta}(\rho_u \omega_i)$$
$$+ \rho_u \omega_i \frac{\partial u_z}{\partial \eta}\} + (\frac{\partial \phi_j}{\partial \xi})(\frac{\partial \omega_i}{\partial \xi}) + \frac{R_o^2}{Z_o^2}(\frac{\partial \phi_j}{\partial \eta})(\frac{\partial \omega_i}{\partial \eta}) - \frac{R_o^2 \phi_j r_i}{\rho D_{im}}] \, \xi \, d\xi \, d\eta \;;$$

(II.2-13)

Substituting for ω_i in terms of the basis function expansion (Eqn (II.1-4) and (II.1-5):

$$\omega_i = \sum_{k=1}^{N} \omega_{ik} \phi_k \;; \qquad \text{(II.2-14)}$$

$$\frac{\partial \omega_i}{\partial \xi} = \sum_{k=1}^{N} \omega_{ik} \frac{\partial \phi_k}{\partial \xi} \;; \qquad \text{(II.2-15)}$$

$$\frac{\partial \omega_i}{\partial \eta} = \sum_{k=1}^{N} \omega_{ik} \frac{\partial \phi_k}{\partial \eta} \;; \qquad \text{(II.2-16)}$$

the final residual equation is obtained:

$$R_{ij} = \sum_{k=1}^{N} \int_\Omega [\frac{\phi_j Pe_r \omega_{ik}}{\rho_u}\{u_r \frac{\partial}{\partial \xi}(\rho_u \phi_k) + \frac{\rho_u \phi_k}{\xi} \frac{\partial}{\partial \xi}(\xi u_r)\} + \frac{\phi_j Pe_z R_o^2 \omega_{ik}}{\rho_u Z_o^2}\{u_z \frac{\partial}{\partial \eta}(\rho_u \phi_k)$$
$$+ \rho_u \phi_k \frac{\partial u_z}{\partial \eta}\} + \omega_{ik}(\frac{\partial \phi_j}{\partial \xi})(\frac{\partial \phi_k}{\partial \xi}) + \frac{R_o^2}{Z_o^2}(\frac{\partial \phi_j}{\partial \eta})(\frac{\partial \phi_k}{\partial \eta}) - \frac{R_o^2 \phi_j r_i}{\rho D_{im}}] \, \xi \, d\xi \, d\eta \;;$$

(II.2-17)

The last term on the rhs of Eqn (II.2-17) corresponds to the reactions undergone by species i, or the net rate of depletion of species i by chemical reaction. In order for the reaction term to be dimensionless, r_i must have the units $((\frac{gm}{cm^3 s})$. The reaction terms are shown below for the case of depletion ($-r_i > 0$) for the first and second order reactions, which cover the gas phase reactions included in the model. Thus,

$$\text{first order reaction} \quad -r_i = k(\frac{1}{s})c(\frac{mole}{mole})x_i M_i(\frac{gm}{mole}) \ ; \qquad \textbf{(II.2-18)}$$

$$\text{second order reaction} \quad -r_i = k(\frac{cm^3}{s})N_A(\frac{1}{mole})c^2(\frac{mole^2}{cm^6})x_i^2 M_i(\frac{gm}{mole}) \ ; \textbf{(II.2-19)}$$

$$\text{electron impact reaction} \quad -r_i = k(\frac{cm^3}{s})n_e(\frac{1}{cm^3})c(\frac{mole}{cm^3})x_i M_i(\frac{gm}{mole}) \ ; \quad \textbf{(II.2-20)}$$

where k is the rate constant, c is the molar gas density by the ideal gas law, x_i is the mole fraction of species i, M_i is the molecular weight of species i, N_A is Avogadro's number, n_e is the electron density. For detailed discussions of these quantities, see Chapter 3.

II.3 Boundary Conditions

Eqn. (II.2-4) consists of two parts, one being a "bulk" domain term which includes the gas phase phenomena described in section II.2, the other being the "boundary" or surface term. The surface term is non-dimensionalized similarly to the bulk term. Since the detailed form of the equation is different for each individual surface orientation, the results are not presented here. Rather, the general method of the application of the boundary conditions is presented.

The term in question from Eqn. (II.2-4) is

$$R_{ij} = -\int_{\Gamma} [\phi_j n(\rho D_{im} \nabla \omega_i)\, d\Gamma \ ; \qquad \textbf{(II.3-1)}$$

where Γ is the boundary, n is the normal vector to the boundary, and the rest of the terms are as before. The boundary conditions are applied by substituting appropriately for the diffusive flux term in parentheses in the integral. Thus for those species which do not react at the surface, the diffusive flux is identically zero and the residual is not altered. For those species which do react, the flux is given by the rate of surface reaction.

The rate of surface depletion for first order surface reactions is:

$$-R_i^s = k(\frac{cm}{s})c(\frac{mole}{cm^3})x_i M_i(\frac{gm}{mole}) = (\pm)\rho D_{im}\nabla\omega_i \; ; \tag{II.3-2}$$

where the sign of the diffusive flux depends on the surface orientation. At the inlet, the diffusive flux is also affected by the rate of convection in to the reactor:

$$(\pm)\rho D_{im}\nabla\omega_i = R_i^s + \rho V_o(x_i - x_{io}) \; ; \tag{II.3-3}$$

where V_o is the inlet velocity, x_i is the inlet mole fraction of species i, and x_{io} is the feed mole fraction of species i. By these substitutions, the appropriate boundary residual terms are added to the bulk terms.

II.4 Solution of Equations

The unknowns in Eqn. (II.2-17) are the ω_{ik}'s which are the coefficients of the basis functions. These are solved for by solving the vector equation:

$$R_{ij} = 0 \; ; \tag{II.4-1}$$

in a Newton-Raphson iteration loop by supplying an initial guess for the vector ω_{ik}. Thus the update at each $(n+1)^{th}$ iteration is given by:

$$\omega_{ik}^{(n+1)} = \omega_{ik}^{(n)} - [\frac{\partial R_{ij}}{\partial \omega_{ik}}]^{-1} R_{ij}^{(n)} \; ; \tag{II.4-2}$$

where the Jacobian matrix $[\frac{\partial R_{ij}}{\partial \omega_{ik}}]$ is calculated at every iteration. Due to storage costs associated with large matrix inversions, a frontal matrix solver due to Hood

[159] was used. The iteration was continued until the update of the solution vector changed the solution by less than a pre-determined amount.

A problem encountered frequently in Newton-Raphson iteration methods is that the initial guess must be within a certain "domain of convergence" for the iteration to converge to a true solution. In practice, this meant that moving from one set of process parameters to another involved very small step sizes in order to obtain converged solutions. This part of the procedure was the most tedious and costly part of the computations.

APPENDIX III. RELATED ISSUES OF STRUCTURED SINGULAR VALUE DECOMPOSITION

III.1 Introduction

As the largest singular value of a square matrix is in fact its structured singular value with respect to the trivial structure (i.e., no structure), the question arises as to whether some kind of structured singular value decomposition can be meaningfully defined. Such a decomposition, besides its intrinsic conceptual interest, may shed new light into the question of the numerical evaluation of the structured singular value. In next section, we present a few ideas and results that we hope will lead to such a decomposition.

Recall that, in the definition of the structured singular value, the uncertainty matrix Δ is taken from the set X_∞ [101]. As a natural extension, it is interesting to consider the structured singular value defined under more restrictive forms of the set X_σ. For instance, consider the structure
$K = (k_1, k_2, k_3, k_4)$
and suppose $k_1=k_2$ and $k_3=k_4$. Then, by definition [111],

$$X_\sigma = \{\text{block diag}(\Delta_1, \Delta_2, \Delta_3, \Delta_4) \mid \Delta_i \in C^{ki \times ki}, \sigma^*(\Delta_i) \leq \sigma\} \; ; \qquad \textbf{(III.1-1)}$$

and the structured singular value is defined correspondingly. Suppose that physical considerations indicate that the uncertainties Δ_1 and Δ_2 are always identical, and so are Δ_3 and Δ_4. This new quantity has been referred to as the structured singular value with repeated blocks (SSVWRB) if X_σ contains at least two identical blocks [101][111]. The SSVWRB is quite different from the structured singular value and much less is known about it. It is shown in [101][111] that the spectral radius of a matrix is in fact a special case of the SSVWRB with respect to such a structure, with scalar blocks.

As another variation of the structured singular value, which has a lot of interest in application [100], corresponds to the set X_σ of the form

$$X_\delta = \{\text{block diag}(\Delta_1, \Delta_2, \Delta_3, \Delta_4) \mid \Delta_i \in IR^{ki \times ki}, \sigma^*(\Delta_i) \leq \sigma\} \; ; \qquad \textbf{(III.1-2)}$$

This corresponding structured singular value has been referred to as the structured value with real scalar uncertainties (SSVWRSU).

III.2 Structured Singular Value Decomposition

For the trivial structure K=(n), it follows from [122] that

$$(p_0(M)) \qquad \mu(M) = \max_{x \in C^n} \{\|Mx\| \mid \|x\| = 1\} \; ; \qquad \textbf{(III.2-1)}$$

so that the structured singular value of M is nothing but its largest singular value. Any maximizer for (III.2-1) is then a right singular vector associated with the largest singular value. In fact, it is easily checked that a point x is a right (resp. left) singular vector for M if, and only if, it is a stationary point for $p_0(M)$ (resp. $p_0(M^H)$) [more precisely, a point that satisfies the la grange necessary conditions of optimality for $\max_{x \in C^n} \{\|Mx\|^2 \mid \|x\|^2 = 1\}$ (resp. $\max_{x \in C^n} \{\|M^H x\|^2 \mid \|x\|^2 = 1\}$). It is thus of interest to nvestigate whether the stationary points (or some stationary points) of p(M) (resp. $p(M^H)$) exhibit properties that would qualify them as structured singular vectors in some kind of structured singular value decomposition (SSVD). Desirable properties includes:

(1) SSVD should reduce to SVD for the trivial structure,

(2) the structured singular value (maximum and minimum in (III.2-1)) should both be part of SSVD.

(3) SSVD should be in some sense unique, for any given square matrix and structure.

Such an investigation is the purpose of this section.

Theorem below gives, under a certain condition on (M, K), a structured singular value decomposition for M. The condition is as follows.

Condition III.2.1. (M, K) is such that exist n CRSSV's (candidate right structured singular vector) for M, x_1, ..., x_n , such that, for $i \neq j$, x_i and x_j are (M, K) - orthogonal.

Suppose Condition III.2.1 holds, Then

$$M = U^{-H} S V^{-1} \; ; \qquad \textbf{(III.2-2)}$$

where

$$V = [x_1 \; .... \; x_n] \; ;$$
$$U = [y_1 \; .... \; y_n] \; ;$$

x_i is a CRSSV for M and y_i is the CLSSV (candidate left structured singular vector) associated with x_i

$$S = \text{diag}\{\frac{\mu_i}{\xi_i}\} \; ;$$
$$\xi_i = \left\| \Gamma_{x_i}^2 x_i \right\| = \left\| \Gamma_{y_i}^2 y_i \right\| \; ;$$
$$\mu_i = \| M x_i \| = \left\| M^H y_i \right\| \; ;$$

The proof has been given in [122].

In relation with Condition III.2.1, the following questions are of interest:

(a) Can we find some matrix M_o and structure K such that, for any matrix M in the neighbourhood of M_o, Condition III.2.1 holds ?

(b) Suppose that (a) is true. Is it also true that, for any matrix M and structure K, Condition III.2.1 holds ?

(c) Suppose that (a) or (b) is true. Is the decomposition unique ?

(d) Suppose that (a) is true but (b) is not. How to characterise matrix M and structure K such that condition III.2.1 holds ?

Numerical experiments suggest that the answer to question (a) is affirmative. Question (b) to (d) are still open. Concerning the desirable features listed at the beginning of this section, the first one is clearly present, and numerical experiments suggest that the other two are present as well.

III.3 Example

Given a complex n x n matrix M, express the singular value decomposition of M as

$$M = [U_1 U_2] \Sigma [V_1 V_2]^H ;$$

where U_1, $V_1 \in C^{n \times r}$ with r the multiplicity of $\sigma^*(M)$ and $[U_1\ U_2]$, $[V_1\ V_2]$ are unitary. Define

$$\nabla_2 = \{z \in IR^{m-1} \mid z_i = v^H H_i v\ ,\ v \in C^r\ ,\ \| v \| = 1\} ;$$

where

$$H_i = \frac{1}{2}(U_1^H M_i V_1 + V_1^H M_i U_1) ;$$

and

$$M_i = P_i M - M P_i ;$$

We will employ the following two facts [111].

Fact III.1 $\inf_{D \in d} \sigma^*(DMD^{-1}) = \sigma^*(M)$ if, and only if, $o \in \nabla_2$.

Fact III.2 $\mu(M) = \sigma^*(M)$ if, and only if, $0 \in \nabla_2$.

The example to $\mu(M) = \inf_{D \in d} (DMD^{-1})$ is as follows. Let

$$M = \begin{bmatrix} a & 0 \\ ab & ab \\ ab & abj \\ (1-2a^2)^{1/2} & -\frac{a^2(1+j)}{2(1-2a^2)^{1/2}} \end{bmatrix} \begin{bmatrix} 0 & a \\ ab & -ab \\ ab & -abj \\ \frac{a^2(1-j)}{2(1-2a^2)^{1/2}} & (1-2a^2)^{1/2} \end{bmatrix} ;$$

and

$$K = (1,1,1,1) ;$$

where $a = [1 - (1/3)^{1/2}]^{1/2}$, $b = 1/(2^{1/2})$ and j is the square root of -1. One obtains

$$H_1 = a^2 \begin{bmatrix} 1 & 0 \\ 0 & -1 \end{bmatrix}, H_2 = a^2 \begin{bmatrix} 0 & 1 \\ 1 & 0 \end{bmatrix}, H_3 = a^2 \begin{bmatrix} 0 & -j \\ -j & 0 \end{bmatrix} ;$$

and it is easy to check that ∇_2 is a circle with radius a^2 centred at origin. Thus, by Facts III.1 and III.2, we have

$$\inf_{D \in d} \sigma^*(DMD^{-1}) = \sigma^*(M) \neq \mu(M) ;$$

Following is an example of structured singular value decomposition. Let

$$M = \begin{bmatrix} 1.1 & 3.1 & -4.1 \\ 5.1 & -1.0 & -6.1 \\ 3.0 & 2.1 & 9.0 \end{bmatrix};$$

and the structure K=(1,1,1). Then Condition III.2.1 holds and

$$U = \begin{bmatrix} 0.1809396861 & -0.7759545640 & -0.7448144424 \\ 0.1522280420 & -0.4783544300 & 0.6438459868 \\ -0.971641628 & -0.4111831149 & 0.1752535069 \end{bmatrix};$$

$$V = \begin{bmatrix} -0.1845551031 & -0.6667118691 & 0.5367804248 \\ -0.4511663600 & -0.7073078120 & -0.8431099313 \\ -0.8731485152 & 0.2349700889 & 0.0321312834 \end{bmatrix};$$

$$S = \begin{bmatrix} \frac{10.71919740}{1.052121069} & 0 & 0 \\ 0 & \frac{5.833726410}{1.050091668} & 0 \\ 0 & 0 & \frac{4.014529000}{1.054556558} \end{bmatrix};$$

APPENDIX IV CHARACTERIZATION OF STRAY IMPEDANCE

The best method to estimate the plasma impedance is to measure the voltage and current at the powered electrode, however the closest place for these measurements is at the electrical feed-through cable. At higher frequencies the feedthrough cable and the connection used for the voltage measurements create a significant capacitance and inductance which become significant at low plasma impedance. The impedance of the chamber, in the absence of a discharge and under atmospheric pressure, should be measured in order to estimate the stray impedance. The description of the equipment used for these measurements have been presented in Chapter 2.

Measurements of stray impedance have been conducted and the impedance, $Z=(|V|/|I|)\cos\theta$, obtained from the measured voltage and current waveforms, is listed in Table IV.1 under various electrode spacings. The impedance of the chamber, with two electrodes touching, is nearly inductive. The line inductance and resistance can be obtained from

$$Z = R + L\omega \quad \textbf{(A.IV-1)}$$

Run 1 and 2 give L of 441nH and R of 3.26Ω. For the case of separated electrodes (d > 0.5 cm), the impedance of the whole system is dominated by the capacitance of the two electrodes.

$$C_{total} = C_{electrode} + C_{stray} \quad \textbf{(A.IV-2)}$$

The stray capacitance, C_{stray}, is constant and the electrode capacitance, $C_{electrode}$, depends on the electrode spacing. For the parallel electrodes spacing, the electrode capacitance is

$$C_{electrode} = \varepsilon_o A_{eff} / d \quad \textbf{(A.IV-3)}$$

where ε_o is the dielectric constant, A_{eff} is the effective electrode area and d is the electrode spacing. $\varepsilon_o A_{eff} = 66.1345$. Substituting equation (A.IV-3) into (A.IV-2), the total capacitance is

$$C_{total} = C_{stray} + \varepsilon_o A_{eff} / d \qquad \textbf{(A.IV-4)}$$

The measured C_{total} at 13.56MHz is shown in Table IV.1. The stray capacitance is obtained from the intercept, and is equal to 447.55pF. The analogue circuit model, as shown in Figure 2.03, with the calculated stray impedance, can be used to obtain the plasma impedance.

Table A.IV.1 Impedance measurements of the chamber without discharge

Run	Electrode Spacing (cm)	V (volt)	I (amp)	θ (degree)	C_{total} (pF)
1	0.0	58.8	1.535	87.0	
2	0.0	46.4	1.201	85.0	
3	0.5	247.0	12.22	-91.5	582.30
4	0.7	231.5	10.60	-89.4	539.81
5	1.0	216.0	9.34	-90.0	509.78
6	1.2	207.0	8.80	-90.0	501.19
7	1.5	206.5	8.70	-90.1	496.69
8	2.0	196.0	7.98	-90.0	480.00
9	2.5	196.0	7.92	-90.0	475.17
10	3.0	195.0	7.76	-90.0	469.15

The total capacitance is : $C_{total} = 447.552 + 66.1345 \times (1/d)$.

REFERENCES

[1] Vossen, John L., Werner Kern, "Thin Film Processes", RCA Laboratories, David Sarnoff Research Center, Princeton, New Jersey. Academic Press, Inc. New York. ISBN 0-12-728250-5, 1978.

[2] Bell, A.T., "Fundamentals of Plasma Chemistry" in Techniques and Applications of Plasma Chemistry, Hollahan and Bell, ed., Wiley, New York (1974)

[3] Einspruch, N.G. and Brown, D.M., "VLSI Electronics : Microstructure Science," Vol. 8, "Plasma Processing for VLSI", Academic Press, Inc. New York, 1984.

[4] Emile Pfender, Stan Veprek, "Plasma Chemistry and Plasma Processing", Vol.12, No.4, Plenum Press. New York and London. 1992.

[5] Sawin, H.H. and Reif, L.R., "Plasma Processing for Microelectronic Fabrication: Plasma Deposition, Etching, and Sputtering of Thin Films for VLSI", Special Summer Program 10.61s, MIT, 1986.

[6] Leahy., M.F., in "Plasma Process", J.Dielman, R.G.Frieser, and G.S.Mathad, Editors, p.176, The Electrochemical Society Soft bound Proceedings Series, PV82-6, Pennington, NJ(1982)

[7] Sze,S.M., "VLSI Technology", McGraw-Hill, Inc., New York, 1983.

[8] Chang, R.P.H, B. Abeles, " Plasma Synthesis and Etching of Electronic Materials", Materials Research Society symposia proceedings; Volume 38, 1985.

[9] Langmuir, I., "The Interaction of Electron and Positive Ions Space Charges in Cathode Sheaths ", Physical Review, USA, 33,954 (1929)

[10] Irving, S.M., Lemons,K.E., and Bobos,G.E., "Gas Plasma Vapour Etching Process", U.S. Patent 3615956 (1971)

[11] Chapman, B., "Glow Discharge Processes", John Wiley & Sons, New York (1980)

[12] Adams,A.C., and Capio, C.D., "Edge Profiles in the Plasma Etching of Polycrystalline Silicon", Journal of Electrochemical Society, 123, 366,USA,(1981)

[13] Beinvogl,W., and Hasler,B., "Reactive Ion Etching of Polysilicon and Tantalum", Solid State Technology, 26(4), 125(1983).

[14] Mieth,M., and Barker,A., "Anisotropic Plasma Etching Using SF_6 and $CFCl_3$", Journal of Vacuum Science Technology, A1, 629 (1983).

[15] Mieth,M., and Barker,A., "Plasma Etching Using SF_6 and Chlorine Gases", Semiconductor International, May, 1984, pp222.

[16] D'Agostino R.,and Flamm, D.L., "Plasma Etching of Si and SiO_2 in SF_6 - O_2 Mixtures", Journal of Applied Physics, 52, 162 (1981)

[17] Korman,C.S., Chow,T.P., and Bower,D.H., "Etching Characteristics of Polysilicon, SiO_2 and $MoSi_2$ and NF_3 and SF_6 Plasma", Solid State Technology, 26(1), 115(1983)

[18] Parrens, P., "Anisotropic and Selective Reactive Ion Etching of Polysilicon Using SF_6", Journal of Vacuum Science Technology, 19,1403 (1981)

[19] Toyoda,H., Tobinaga,M., and Komiya,H., "Frequency Effect on Material Selectivity in Gas Plasma Etching in Planar Type Reactor", Japan Journal of Applied Physics, 20, 681 (1981).

[20] Light,R.W., and Bell,H.B., "Profile Control of Polysilicon Lines with SF_6/O_2 Plasma Etch Process", Journal of Electrochemical Society, 130, 1567 (1983)

[21] Thompson, B.E., and Sawin,H.H., "Polysilicon Etching in SF_6 RF Discharges", Journal of Electrochemical Society, 133, 1887 (1986)

[22] Pinto, R., Ramanathan,K.V., and Babu,R.S., "Reactive Ion Etching in SF_6 Gas Mixtures", Journal of Electrochemical Society,134,165 (1987)

[23] Agostino,R.D., Colaprico,V., and Cramarossa,F., "The Use of Actinometer Gases in Optical Diagnostics of Plasma Etching Mixtures: SF_6 - O_2", Plasma Chemistry and Plasma Processing, 1, 365 (1981)

[24] Horiike, Y., and Shibagake,M., " A New Chemical Dry Etching", Japan J.Publhing Company, Amsterdam (1967)

[25] McTaggart, F.K., "Plasma Chemistry in Electrical Discharges ", Elserier Publishing Company, Amsterdam (1967).

[26] Heinecke, R.A.H., "Control of Relative Etch Rates of SiO_2 and Si in Plasma Solid State Electronics, 18, 1146(1975).

[27] Coburn, J.W., and Winters, H.F., "Mechanisms in Plasma Etching", Journal of Vacuum Science Technology, 15, 327(1978)

[28] Mogab,C.J., Adams,A.C., and Flamm,D.L., "Plasma Etching of Si and SiO_2-the Effect of Oxygen Additions to CF_4 Plasma", Journal Applied Physics, 49, 3796 (1978)

[29] Kawata,H., Murata,K., and Nagami,K., "Spatial Dependence of the Optical Emission Intensities from $CF_4 + O_2$ Plasma", Journal Vacuum Science Technology, B4, 6 (1986)

[30] Kawata,H., Takao,Y., Murata,K., and Nagami,K., "Optical Emission Spectroscopy of $CF_4 + O_2$ Plasma Using a New Technique", Plasma Chemistry and Plasma Processing, 8,189 (1988).

[31] Mogab,C.J., "The loading Effect in Plasma Etching ", Journal of Electrochemical Society, 124, 1262 (1977).

[32] Lee,Y.H., and Chen,M.M., "Silicon Doping Effects in Reactive Plasma Etching", Journal of Vacuum Science Technology, B4, 468 (1986)

[33] Winters,H.F., and Haarer,D., "Influence of Doping on the Etching of Silicon(111)", Physics Review, B36, 6613(1987)

[34] Winters, H.F., and Coburn,J.W., "The Etching of Silicon with XeF_2 Vapor", Applied Physics Letters, 34,70(1979)

[35] Coburn,J.W., and Winters,H.F., "Ion and Electron Assisted Gas-Surface Chemistry an Important Effect in Plasma Etching", Journal of Applied Physics,50,3189(1979).

[36] Coburn,J.W., and Winters,H.F., "Plasma Etching- a Discussion of Mechanisms", Journal of Vacuum Science Technology, 16, 391 (1979)

[37] Winters,H.F., "The Role of Chemisorption in Plasma Etching ", Journal of Applied Physics, 49,5165 (1978)

[38] Tu,Y., Chuang,T.J., and Winters,H.F., "Chemical Sputtering of Fluorinated Silicon", Physics Review, B23, 823 (1981).

[39] Box,G.E.P., Hunter,W.G., and Hunter, J.S.,"Statistics for Experimenters:An Introduction to Design, Data Analysis, and Model Building",John Wiley and Sons, New York, 1978.

[40] Box, G.E.P. and Draper, N.R., "Empirical Model-Building and Response Surfaces", John Wiley and Sons, New York, 1987.

[41] Hartley, H.O., "Smallest composite designs for quadratic response surfaces", Biometrics, 15(4), 611 (1959).

[42] Hamel,C.J., "The Evaluation of a Single-Step Lift-Off Process using the Method of Response Surface Analysis", 1981 Symposium on VLSI Technology, IEEE Electron Devices Society, IEEE Cat No. 81-CH-1711,10 (1981).

[43] Bergeron, S.F. and Duncan, B.F., "Controlled Anisotropic Etching of Polysilicon", Solid State Technology, 25(8), 98(1982).

[44] Riley, P.E., "Development of a Highly Uniform Silicon Dioxide Etching Process Using Response Surface Methodology", Electrochemical Society Journal, 133(9), 1971 (1986).

[45] Fior, G.O., Giffen, L.N., and Palmer, W.W., "High-Selectivity, Silicon Dioxide Dry Etching Process", Solid State Technology, 31(4), 109(1988).

[46] Daniel, D.W., Bloom, R., and Reece, J.E., "Identifying an Etch Process Window Using Response Surface Methodology", Solid State Technology, 117 (1988).

[47] Mocella, M.T., Jenkins,M.W., Sawin,H.H., and Allen,K.D., "Parametric Characterisation of Plasma Etching Processes", Materials Research Society Symposium Series, 38, 227 (1985).

[48] Sawin, H.H., "A Review of Plasma Processing Fundamentals", Solid State Technology, 28, 211 (1985).

[49] Allen,K.D. and Sawin,H.H.,"The plasma etching of polysilicon with CF_3Cl/Argon discharges: II. Modelling of ion bombardment energy distributions", Electrochemical Society Journal, 133(11), 2326(1986).

[50] Allen,K.D., Sawin,H.H., and Yokozeki,A., "The plasma etching of polysilicon with CF_3Cl/Argon discharges:III. Modelling of etching rate and directionality", Electrochemical Society Journal, 133(11), 2331(1986).

[51] Allen,K.D., Sawin,H.H., and Mocella,M.T., and Jenkins, M.W., "The plasma etching of polysilicon with CF_3Cl/Argon discharges:I. Parametric Modeling and Impedance Analysis", Electrochemical Society Journal, 133(11), 2315(1986).

[52] Gevelber,M.A., Wargo,M.J., and Stephanopoulos,G., "Advanced control design considerations for the Czochralski process", Journal of Crystal Growth, 85, 256 (1987)

[53] Atherton,R.W., "Automation of IC Manufacturing : Control Problems", Semiconductor International, 5, 218 (1986)

[54] Jensen,K.F., "Control problems in microelectronic processing", Third International Conference on Chemical Process Control, Asilomar, CA, 1986.

[55] Mclaughlin,K.J., et al, "Development of Techniques for Real-time Monitoring and Control in Plasma Etching", 1990 Proceedings of American Control Conference. Vol. 1 of 3, pp.101, USA, 1990.

[56] Barna,G..G., "Expert systems and process control in plasma etching: SEMICON West, 1986.

[57] Bresnock, F.J. and Stumpf, Th., "Implementation of adaptive process control to a dry etching process", Journal of Vacuum Science and Technology, 20(4), 1027, 1982.

[58] Selwyn, G.S., "Optical Diagnostic Techniques for RIE", Proceedings of the 6th Symposium on Plasma Processing, ECS national meeting, San Diego, CA, 1984.

[59] Coburn,J., and Chen,M., "Optical Emission Spectroscopy of Reactive Plasmas: A Method for Correlating Emission Intensities to Reactive Particle Density", Journal of Applied Physics, 51, 3134(1980).

[60] SOFIE DIGITWIN Instruments Menu, 1991, France.

[61] Roosmalen, A.J.V., "Review : Dry Etching of Silicon Oxide", Vacuum, 34(3-4), 429, 1984.

[62] Fortuno, G., "Study of Reactive Ion Etching of Si and SiO_2 for CF_xCl_{4-x} Gases", Plasma Chemistry and Plasma Processing, 8(1), 19, 1988.

[63] Danner, D.A., Petrillo, E.J., and Polcari, M.R., "Mechanistic Study of CCl_2F_2/O_2 RIE for Bipolar Trench Isolation", Mat. Res. Soc. Symp. Proc., Vol. 68, 15, 1986

[64] Box, G.E.P. and Wilson, K.B., "On the Experimental Attainment of Optimum Conditions", Journal of the Royal Statistical Society, B13, 1(1951).

[65] Roosmalen A.J.V., "Plasma Parameter Estimation from RF Impedance Measurements in A Dry Etching System", Appl. Phys. Lett. 42(5), 1 March 1983.

[66] Van,A.J., Van den Hoek, W.G.M., and Keller,H., "Electrical Properties of Planar RF Discharges for Dry Etching", Journal of Applied Physics, 58, 653 (1985)

[67] Thompson,B.E., and Sawin,H.H., "Polysilicon Etching in SF_6 RF Discharges", Journal of Electrochemical Society, 133, 1887 (1986)

[68] Bletzinger,P., and Flemming,M.J., "Impedance Characteristics of an RF Parallel Plate Discharge and the Validity of a Simple Circuit Model", Journal of Applied Physics, 62,4688 (1987)

[69] Yoshizawa,T., Sakai,Y., Tagashira,H., and Sakamoto,S., "Boltzmann Equation Analysis of the Electron Swarm Development in SF_6", Journal of Physics D: Applied Physics, 12, 1839 (1979)

[70] Chambers,A.A., Davies,S.V., etc, "Etching of Phosphorous Doped Polysilicon Films", Semiconductor International, pp.66, January (1988)

[71] Kline,L.E., "Electron and Chemical Kinetics in the Low Pressure RF Discharge Etching of Silicon in SF_6", IEEE Transaction of Plasma Science, PS-14, 145 (1986)

[72] Hargis,P.J., and Greenberg,K.E., "Pulsed-ultraviolet Laser Raman ` of Plasma Processing Discharges", Applied Physics Letter, 53, 1809 (1988)

[73] Tan,L., "Modelling and Simulation of Plasma Etching on Si and SiO_2 with SF_6/Ar", Research Report, 02/EE/92, Dublin City University, 1992.

[74] Eisele, K. M., "SF_6, a Preferable Etchant for Plasma Etching Silicon", Journal of Electrochemical Society, 128, 123 (1981)

[75] Jenkins,M.W. and Mocella,M.T., etc, "The Modelling of Plasma Etching Processes Using Response Surface Methodology", Solid State Technology, (4), 175 (1986)

[76] Ryan,K.R., and Plumb,I.C., "Gas-Phase Combination Reactions of SF_6 with F in Plasma of SF_6", Plasma Chemistry and Plasma Processing, 8, 281 (1988)

[77] Flamm, D.L., Donnelly,V.M., and Mucha,J.A., "The Reaction of Fluorine Atoms with Silicon", Journal of Applied Physics, 52, 3633 (1981)

[78] Wagner, J.J. and Brand,W.W., "DC Plasma Etching of Silicon by Sulfur Hexafluoride. Mass Spectrometric Study of the Discharge Products", Plasma Chemistry and Plasma Processing, 1, 201 (1981)

[79] Tang, C.C. and Hess,D.W., "Tungston Etching in CF_4 and SF_6 Discharges", Journal of Electrochemical Society, 131, 115 (1984)

[80] Nordine,P.C., and Legrange,J.D., "Heterogeneous Fluorine Atom Recombination/Reaction on Several Materials of Construction", AIAA Journal, 14, 644(1976)

[81] Ninimiya,K., Suzuki,K., and Nishimatsu,S., "Titration Method for Measuring Fluorine Atom Concentration in Microwave Plasma Etching", Japanese Journal of Applied Physics, 22, 139 (1983)

[82] Press,W.H., Flannery,B.P., etc, "Numerical Recipes in C", Cambridge University Press, New York (1990)

[83] Mahi,B., Arnal,Y., and Pomot,C., "The Etching of Silicon in Diluted SF_6 Plasma: Correlation between the Flux of Incident Species and the Etching Kinetics", Journal of Vacuum Science Technology, B5, 657 (1987)

[84] Takagi, T.,"Ion-surface Interaction during Thin Film Deposition", Journal of Vacuum Science Technology, A2, 382 (1984)

[85] Pelletier, J., "A Model for the Halogen-based Plasma Etching of Silicon", Journal of Physics , D 20, 858 (1987)

[86] Mlynko,W.E., and Hess,D.W., "Electrical Characterization of RF Glow Discharges Using An Operating Impedance Bridge", Journal of Vacuum Science Technology, A3, 499 (1985)

[87] Hargis,P.J., and Greenberg,K.E.,"Pulsed-ultraviolet Laser Raman Diagnostics of Plasma Processing Discharges", Applied Physics Letter, 53, 1809 (1988)

[88] Economou,D.J., and Pomot,C., "A Mathematical Model for a Parallel Plate Plasma Etching Reactor", Journal of Electrochemical Society, 135, 2786 (1988)

[89] Zarowin, C.B., Horwath, R.S., "Control of Plasma Etch Profiles with Plasma Sheath Electric Field and RF Power Density", "Plasma Synthesis and Etching of Electronic Materials", editors, Chang, R.P.H., Abeles B., Materials Research Society symposia proceedings. 1985.

[90] Kleinbaum,D.G., Kupper,L.L., and Muller,K.E., "Applied Regression Analysis and Other Multivariable Methods", by PWS-KENT Publishing Company, 1988. ISBN 0-87150-123-6.

[91] Seborg, D.E., Edgar, T.F., and Mellichamp, D.A., "Process Dynamics and Control", John Wiley and Sons, New York, 1989.

[92] Coburn, J.W. and Chen, M., "Dependence of F atom density on pressure and flow rate in CF_4 glow discharges as determined by emission spectroscopy", Journal of Vacuum Science and Technology, 18(2), 353 (1981).

[93] Shanmugan,K.S. and Breipohl,A.M., "RANDOM SIGNALS :DETECTION, ESTIMATION AND DATA ANALYSIS", by John Wiley & Sons, Inc., Canada, 1988. ISBN 0-471-81555-1.

[94] Lii, Y.J. and Jorne J., " Plasma Etching of Silicon in SF_6 -Experimental and Reactor Modeling Studies", Journal of the Electrochemical Society", 1990 V.137, PT.11, pp.3633-3639.

[95] Ryskamp, C.J., "Explicit vs Implicit Decoupling in Distillation Control", Chemical Process Control II, pp 361-375. Engineering Foundation, 1982. USA.

[96] Lau, H., Alvarez J. and Jensen K.F., "Design of Control Structures by Singular Value Analysis", AIChE J. 31(3):427-439, 1985.

[97] Niederlinski, A., "A Heuristic Approach to the Design of Linear Multivariable Interacting Control Systems", Automatica 7:691, 1981.

[98] Bequette, B.W., and Edgar,T.F., "Selection of Process Measurements in Distillation Column Control to Minimize Multivariable Interactions", 1986 AIChE Annual Meeting, San Francisco, CA.

[99] Palazoglu,A. and Arkun.,Y., " Impact of Modeling Decisions on the Robustness of Tubular Reactors", Proc. of A.C.C., pp.25-30.,1986

[100] Morari, M. and Doyle,J.C., "A Unifying Framework for Control System Design Under Uncertainty and Its Implications for Chemical Process Control", In

M.Morari and T.J.McAvoy (editors), *Chemical Process Control.* CACHE, Elsevier, New York, 1986.

[101] Doyle,J.C., "Structured Uncertainty in Control System Design", *Proceedings of the 24th IEEE Conference on Decision and Control,* pp.260-265, Dec., 1986.

[102] Ray, W.H., "Advanced Process Control", McGraw-Hill Book Company, 1981. USA.

[103] Klema, V.C. and Laub, A.J., "The Singular Value Decomposition : Its Computation and Some Applications", IEEE Transactions on Automatic Control, AC-25(2), 164, 1980.

[104] Bonvin, D. and Mellichamp.,D.A., "A Generalised Structural Dominance Method for the Analysis of Large-Scale Systems", Int. J. Control, 35:807, 1982.

[105] Grosdidier, P. and Morari.,M., "Interaction Measures for Systems Under Decentralised Control", Automatica 22(3):309-319, 1986a.

[106] Downs, J.J. and Moore,C.F., "Steady state Gain Analysis for Azeotropic Distillation", Proc. J.A..C.C. :WP-7C, 1981.

[107] Morari, M., Grimm,W., Oglesby,M.J., and Prosser.,I.D., "Design of Resilient Processing Plants - VII. Design of Energy Management Systems for Unstable Reactors - New Insight", Chem. Eng. Sci., 40(2):187-198, 1985

[108] Maciejowski, J.M., " Multivariable Feedback Design", Cambridge University and Pembroke College, Cambridge. 1989.

[109] Stein, G. and Doyle.,J.C., "Singular Values and Feedback: Design Examples", In Proc. of the 1987 Allerton Conference on Communication, Control and Computing, p.p.461-470.

[110] Dolye, J.C. and Stein,G., "Multivariable Feedback Design: Concepts for a Classical/Modern Synthesis", IEEE Trans. on Auto. Control AC-26(1):4-16, 1981.

[111] Doyle, J.C., Wall,J.E., and Stein,G., "Performance and Robustness Analysis for Structured Uncertainty", Proc. 21st IEEE Conf. on Decision and Control, p.p. 629-636, 1982.

[112] Safonov, M.G., Laub,A.J., and Hartmann,G.L., "Feedback Properties of Multivariable Systems: The Role and Use of the Return Difference Matrix", IEEE Trans. on Auto. Control AC-26(1):47-65, 1981.

[113] Palazoglu, A. and Arkun,Y., "Robust Tuning of Process Control Systems Using Singular Values and Their Sensitivities", Chem. Eng. Commun. 37:315-331, 1985.

[114] Postlethwaite, I., Edmunds,J.M.,and MacFarlane,A.G.J., "Principle Gains and Principle Phases in the Analysis of Linear Multivariable Feedback Systems", IEEE Trans. on Auto. Control AC-26(1):32-46, 1981.

[115] Cruz,J.B., Freudenberg,J.S., and Looze,D.P., "A Relationship Between Sensitivity and Stability of Multivariable Feedback Systems", IEEE Trans. on Auto. Control AC-26(1):66-74, 1981.

[116] Lehtomaki,N.A., Castanon,D., etc, "Robustness Tests Utilizing the Structure of Modelling Error", In Proceedings of the 1981 CDC, p.p. 1173-1190.

[117] Arkun,Y.,B., etc, "Robustness Analysis of Process Control Systems. A Case Study of Decoupling Control in Distillation", Ind. Eng. Chem. Process Des. Dev. 23(1): 93-101, 1984

[118] Hung,Y.S. and MacFarlane,A.G.J., "Multivariable Feedback: A Quasi-Classical Approach", Springer Verlag, New York, 1983.

[119] Palazoglu,A. and Owens,S.E., "Impact of Modelling Decisions on the Robustness of Tubular Reactors", In Procs. of A.C.C., p.p., 25-30, 1986

[120] Freudenberg,J.S., and Looze,D.P., "Relations Between Properties of Multivariable Feedback Systems at Different Loop-Breaking Points: Part II", In Procs. of the 1986 ACC, p.p. 771-776, 1986.

[121] Lehtomaki, N.A., Castanon,D.A., etc, "Robustness and Modelling Error Characterization", IEEE Trans. on auto. Control AC-29(3):212-220, 1984.

[122] Fan,M.K.H., "An Algorithm to Compute the Structured Singular Value", Technical Report TR-86-8, Systems Research Center, University of Maryland, 1987.

[123] Grosdidier, P. and Morari,M., "The Mu Interaction Measure", to appear in Ind. Eng. Chem. Fund., 1986b.

[124] Friedland,B., "Control System Design - An Introduction to State-Space Methods", McGraw-Hill, 1987.

[125] Hariharan,S.I., and Moulden,T.H., "Numerical methods for partial differential equations", The University of Tennessee Space Institute, 1986. ISBN 0-470-20377-3 (USA only).

[126] Howell T., "Non-linear Time Series - A Dynamical System Approach", Clarendon Press Oxford, 1990.

[127] Noye, J., "Numerical Solutions of Partial Differential Equations", Proceedings of 1981 Conference on the Numerical Solutions of Partial Differential Equations held at Queen's College, Melbourne University, Australia.

[128] Turban, G., Pasquereau, J., Rapeaux, M., Catherine, Y., and Grolleau, B., "Decomposition and Recombination of CF_4 in Plasma Etching", paper presented at Third Symposium on Plasma Processing-The Electrochemical Society, (1981)

[129] Kushner, M.J., "A Kinetic Study of the Plasma-Etching Process. I. A model for the etching of Si and SiO_2 in C_nF_m/H_2 and C_nF_m/O_2 plasmas", J. Appl. Phys., 53(4), 2923 (1982a).

[130] Chen, I., "Mass Transfer Analyses of the Plasma Deposition Process", Thin Solid Films, 101, 41(1983)

[131] Tachinana, K., Nishida, M., Harima, H., and Urano, Y., "Diagnostics and Modelling of a Methane Plasma Used in the Chemical Vapour Deposition of Amorphous Carbon Films", J.Phys. D: Appl. Phys., 17, 1727 (1984).

[132] Edelson, D. and Flamm, D.L., "Computer Simulation of a CF_4 Plasma Etching Silicon", J.Appl: Phys., 56(5), 1522 (1984)

[133] Srinivasan, V., Sivasubramanian,M.S., and Babu,S.V., "Simulation of Plasma Reactors: Etch Rate of Polymers", Symp. Proc. 7th Int. Symp. Plasma Chem., Vol 4, 1405 (1985)

[134] Dalvie,M., Jensen,K.F., and Graves,D.B., "Modelling of Reactors for Plasma Processing I: Silicon Etching by CF_4 in a Radial Flow Reactor", Chem. Eng. Sci., 41(4), 653 (1986)

[135] Plumb, I.C. and Ryan, K.R., "A Model of the Chemical Processes Occurring in CF_4/O_2 Discharges Used in Plasma Etching", Plasma Chem. Plasma Proc., -6(3), 205 (1986)

[136] Ryan,K.R. and Plumb,I.C., "Gas-Phase Reaction of CF_3 and CF_2 with Hydrogen Atoms: Their Significance in Plasma Processing", Plasma Chem. and Plasma Proc., 4(3), 141 (1986)

[137] Venkatesan, S.P., Trachtenberg, I., and Edgar, T., "Effect of Flow Direction on Etch Uniformity in Parallel-Plate (Radial Flow) Isothermal Plasma Reactors", J. of Electrochem. Soc., 134(12), 3194 (1987)

[138] Zawaideh,E., and Kim,N.S., "A Plasma Etching Model Based on a Generalised Transport Approach", J.Appl. Phys., 62(6), 2498 (1987)

[139] Zawaideh,E., and Kim, N.S., "A Generalised Plasma Etching Model", J.Appl. Phys., 64(8), 4199 (1988)

[140] Dalvie, M. and Jensen,K.F., "Spatially Resolved Studies of CF_4/O_2 Plasma Etching of Silicon", Paper 39D, Extended Abstracts, 1988 AIChE Annual Meeting, Washington DC, Nov. 27-Dec. (1988)

[141] Yoo,C.-s. and Dixon,A.G., "Plasma Deposition of Silicon Nitride Films in a Radical-Flow Reactor", AIChE Journal, 35(6), 995 (1989)

[142] Economou, D.J. and Alkire, R.C., "A Time-Average Model of the RF Plasma Sheath", J. of Electrochem. Soc., 135(2), 756 (1989)

[143] Yamaguchi,Y., Sumiyama, A., Hattori, R.-i., Morokuma, Y., and Makabe, T., "A Model of Amorphous Silicon Deposition in DC Glow Discharge in Silane", Plasma Dev. Appl., 505 (1989)

[144] Kline, L.E., Partlow, W.D., and Bies, W.E., "Electron and Chemical Kinetics in Methane RF Glow-Discharge Deposition Plasmas", J.Appl. Phys., 65(1), 70 (1989)

[145] Cleland, T.A., and Hess, D.W., "Diagnostics and Modeling of N_2O RF Glow Discharges", J. of Electrochem. Soc., 136(10), 3103 (1989)

[146] Werner,C., Ulacia,J.I., and Howell,S., "Numerical Simulation of Gas Flow and Chemical Reactions in Semiconductor Processing Equipment", paper 6-3, conference unknown.

[147] Schoenborn,P., Patrick,R., and Baltes,H.P., "Numerical Simulation of a CF_4/O_2 Plasma and Correlation with Spectroscopic and Etch Rate Data", J. of Electrochem. Soc., 136(1), 199 (1989)

[148] Vankatesan,S.P., Trachtenberg,I. and Edgar,T., "On the Dynamics of an Isothermal Radial-Flow Plasma Etcher", J.Electrochem. Soc., 136(9), 2532 (1989)

[149] Kobayashi,J., Nakazato,N., and Hiratsuka,K., "Numerical Simulation for Gas Flow and Mass Transfer in a Dry Etching Chamber", J. of Electrochem. Soc., 136(6), 1781 (1989)

[150] Kao,A.S. and Stenger,H.G., "Analysis of Nonuniformities in the Plasma Etching of Silicon with CF_4/O_2 ", J. of Electrochem. Soc., 137(3), 954 (1990)]

[151] Dalvie,M., and Jensen,K.F., "Combined Experimental and Modeling Study of Spatial Effects in Plasma Etching: CF_4/O_2 Etching of Silicon", J. Electrochem. Soc., 137(4), 1062 (1990a)

[152] Park,S.K. and Economou,D.J., "Numerical Simulation of a Single-Wafer Isothermal Plasma Etching Reactor", J.Electrochem. Soc., 137(8), 2624 (1990a)

[153] Park,S.K. and Economou,D.J., "Analysis of a Pulsed-Plasma Chemical Vapor Deposition Reactor with Recycle", J. Electrochem. Soc., 137(7), 2103 (1990b)

[154] Park,S.K. and Economou,D.J., "A Mathematical Model for Etching of Silicon Using CF_4 in a Radial Flow Plasma Reactor", J.Electrochem. Soc. 137(9), (1990c)

[155] Thorsness, C.B. and Britten, J.A., "Influence of Finite Jets on Mass Transfer in Radio-Flow, Multijet CVD Reactors", AIChE Journal, 36(5), 801 (1990)

[156] Venkatesan, S.P., Trachtenberg, I. and Edgar, T., "Modeling of Silicon Etching in CF_4/O_2 and CF_4/H_2 Plasmas", J. Electrochem. Soc., 137(7), 2280 (1990)

[157] Lapidus,L. and Pinder,G.F., "Numerical Solution of Partial Differential Equations in Engineering and Science", John Wiley and Sons (1982).

[158] Bird,R.B., Stewart,W.S., and Lightfood,E.N., "Transport Phenomena", John Wiley and Sons. (1980)

[159] Hood, P., "Frontal solution program for unsymmetric matrices", Int. J. Num. Methods Eng. 10(2), p.379-399 (1986)

[160] Smith,R.S., Doyle,J.C., Morari,M., and Skjellum,A., "A case study using μ: laboratory process control problem", Proc. IFAC Congress, 1987.

[161] Laughlin,D.L., Rivera,D.E., and Morari,M., "Smith predictor design for robust performance", Int. J. Control, vol. 46, no.2, 1987.

[162] Spyros, G.T., "Applied control: current trends and modern methodologies", Marcel Dekker, Inc., New York, 1993.